Vol. 59 JULY, 1955 No. 7

THE JOURNAL OF PHYSICAL CHEMISTRY

(Registered in U. S. Patent Office)

THE JOURNAL OF PHYSICAL CHEMISTRY

(Registered in U. S. Patent Office)

Published monthly by the American Chemical Society at 20th and Northampton Sts., Easton, Pa.

Entered as second-class matter at the Post Office at Easton, Pennsylvania.

The *Journal of Physical Chemistry* is devoted to the publication of selected symposia in the broad field of physical chemistry and to other contributed papers.

Manuscripts originating in the British Isles, Europe and Africa should be sent to F. C. Tompkins, The Faraday Society, 6 Gray's Inn Square, London W. C. 1, England.

Manuscripts originating elsewhere should be sent to W. Albert Noyes, Jr., Department of Chemistry, University of Rochester, Rochester 3, N. Y.

Correspondence regarding accepted copy, proofs and reprints should be directed to Assistant Editor, Allen D. Bliss, Department of Chemistry, Simmons College, 300 The Fenway, Boston 15, Mass.

Business Office: Alden H. Emery, Executive Secretary, American Chemical Society, 1155 Sixteenth St., N. W., Washington 6, D. C.

Advertising Office: Reinhold Publishing Corporation, 430 Park Avenue, New York 22, N. Y.

Articles must be submitted in duplicate, typed and double spaced. They should have at the beginning a brief Abstract, in no case exceeding 300 words. Original drawings should accompany the manuscript. Lettering at the sides of graphs (black on white or blue) may be pencilled in, and will be typeset. Figures and tables should be held to a minimum consistent with adequate presentation of information. Photographs will not be printed on glossy paper except by special arrangement. All footnotes and references to the literature should be numbered consecutively and placed in the manuscript at the proper places. Initials of authors referred to in citations should be given. Nomenclature should conform to that used in *Chemical Abstracts*, mathematical characters marked for italic, Greek letters carefully made or annotated, and subscripts and superscripts clearly shown. Articles should be written as briefly as possible consistent with clarity and should avoid historical background unnecessary for specialists.

Symposium papers should be sent in all cases to Secretaries of Divisions sponsoring the symposium, who will be responsible for their transmittal to the Editor. The Secretary of the Division by agreement with the Editor will specify a time after which symposium papers cannot be accepted. The Editor reserves the right to refuse to publish symposium articles, for valid scientific reasons. Each symposium paper may not exceed four printed pages (about sixteen double spaced typewritten pages) in length except by prior arrangement with the Editor.

Remittances and orders for subscriptions and for single copies, notices of changes of address and new professional connections, and claims for missing numbers should be sent to the American Chemical Society, 1155 Sixteenth St., N. W., Washington 6, D. C. Changes of address for the *Journal of Physical Chemistry* must be received on or before the 30th of the preceding month.

Claims for missing numbers will not be allowed (1) if received more than sixty days from date of issue (because of delivery hazards, no claims can be honored from subscribers in Central Europe, Asia, or Pacific Islands other than Hawaii), (2) if loss was due to failure of notice of change of address to be received before the date specified in the preceding paragraph, or (3) if the reason for the claim is "missing from files."

Subscription Rates: to members of the American Chemical Society, $8.00 for 1 year, $15.00 for 2 years, $22.00 for 3 years; to non-members, $10.00 for 1 year, $18.00 for 2 years, $26.00 for 3 years. Postage free to countries in the Pan American Union; Canada, $0.40; all other countries, $1.20. $12.50 per volume, foreign postage $1.20, Canadian postage $0.40; special rates for A.C.S. members supplied on request. Single copies, current volume, $1.00; foreign postage, $0.15; Canadian postage $0.05. Back issue rates (starting with Vol. 56): $15.00 per volume, foreign postage $1.20, Canadian, $0.40; $1.50 per issue, foreign postage $0.15, Canadian postage $0.05.

The American Chemical Society and the Editors of the *Journal of Physical Chemistry* assume no responsibility for the statements and opinions advanced by contributors to THIS JOURNAL.

The American Chemical Society also publishes *Journal of the American Chemical Society, Chemical Abstracts, Industrial and Engineering Chemistry, Chemical and Engineering News, Analytical Chemistry*, and *Journal of Agricultural and Food Chemistry*. Rates on request.

THE JOURNAL OF
PHYSICAL CHEMISTRY

(Registered in U. S. Patent Office) (Copyright, 1955, by the American Chemical Society)

VOLUME 59 JULY 22, 1955 NUMBER 7

PRESEPARATION PHENOMENA AND MICROCOACERVATION

BY FUMIO OOSAWA

Department of Physics, Faculty of Science, Nagoya University, Nagoya, Japan

Received July 8, 1954

The preseparation phenomena of solutions are discussed. With the aid of some numerical examples it is pointed out that solutions of high molecular weight substances often show marked preseparation. This is probably one of the reasons why microcoacervation is easily observed in these solutions. The changes in size distribution and in the total volume of the second phase were investigated by Frenkel's method.

The pretransition phenomena, which in general take place before the macroscopic phase transition, have been treated theoretically by several authors; the precondensation of gases and premelting of solids have been dealt with.[1,2] In this paper we have discussed the preseparation phenomena of solutions using for the most part a method similar to that employed by Frenkel in the theory of precondensation.[1] It was found that in solutions of high molecular weight substances the preseparation is sometimes large enough to be observed owing to the characteristics of these solutions. The feature of the phase separation in them is changed; for instance, the macroscopic separation point deviates from that which would be expected if only the equilibrium between the macroscopic phases were taken into consideration.

Preseparation can be regarded as a concentration fluctuation.[3,4] Under ordinary conditions the concentration in a small volume of the solution fluctuates only within the neighborhood of the average concentration. However, near the separation point the fluctuation to the second phase cannot be disregarded. It is well known that near the critical mixing point of a solution the concentration fluctuation, like the density fluctuation of a gas near the critical point,[3,5] becomes very large because of the infinitely small value of the second order derivatives of the free energy. In this discussion it is pointed out that solutions of high molecular weight substances, even in the region far from the critical mixing point, show a large concentration fluctuation to the second phase before phase separation occurs. Indeed, the large fluctuation of these solutions has been studied by many authors, but their discussions have been limited to the fluctuation in the neighborhood of the average concentration.[4,6]

Preseparation is related to the microcoacervation seen in biocolloids or high polymer solutions.[7] Microcoacervation is a complicated state, which is regarded in most cases as transient or metastable. Preseparation, however, might be regarded as an ideal case of equilibrium microcoacervation.

Heterophase Fluctuation.—As the simplest case, we shall consider a two-component solution with the solubility curve shown in Fig. 1*a*. When the temperature T is decreased, the solution of the concentration c_0 separates into two phases at the temperature T_0. The ratio θ of the total volume of the second phase to that of the whole solution changes with T as shown by the curve (APB) in Fig. 2. In certain cases, however, owing to preseparation small volumes of the second phase may be formed in the first phase before macroscopic

(1) J. Frenkel, *J. Chem. Phys.*, **7**, 200, 538 (1939); "Kinetic Theory of Liquids," Oxford, 1946, Chap. 7; W. Band, *J. Chem. Phys.*, **7**, 324, 927 (1936).

(2) J. E. Mayer and M. G. Mayer, "Statistical Mechanics," John Wiley & Sons, Inc., New York, N. Y., 1940, Chap. 13 and 14; W. G. McMillan and J. E. Mayer, *J. Chem. Phys.*, **13**, 276 (1945).

(3) M. V. Smoluchovski, *Ann. Physik*, **25**, 205 (1903); A. Einstein, *ibid.*, **33**, 1275 (1910).

(4) P. Debye, *J. Appl. Phys.*, **15**, 338 (1944); THIS JOURNAL, **51**, 18 (1947).

(5) O. K. Rice, *J. Chem. Phys.*, **15**, 314 (1947); R. W. Rowden and O. K. Rice, *ibid.*, **19**, 1423 (1951); M. J. Klein and L. Tisza, *Phys. Rev.*, **76**, 1961 (1949).

(6) H. C. Brinkmann and J. J. Hermans, *J. Chem. Phys.*, **17**, 574 (1949); J. G. Kirkwood and R. J. Goldberg, *ibid.*, **18**, 54 (1950).

(7) A. Dobry, *J. chim. phys.*, **35**, 387 (1938); **36**, 102, 296 (1939); H. G. Bungenberg de Jong, *Kolloid Z.*, **79**, 334 (1937); **80**, 221 (1938), "Colloid Science," edited by H. R. Kruyt, Elsevier Press, Inc., Houston, Texas, 1949, Vol. II, Chap. 8; J. Th. Overbeek, Vol. I, Chap. 7.

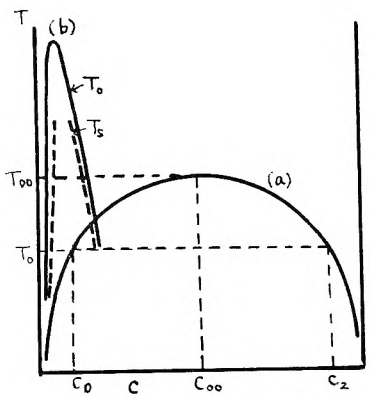

Fig. 1.—Solubility curves.

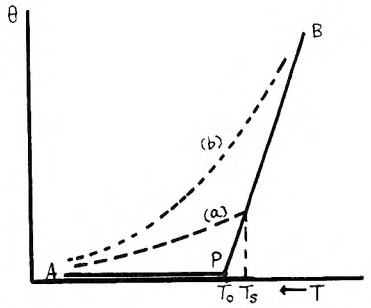

Fig. 2.—The relations between θ and T.

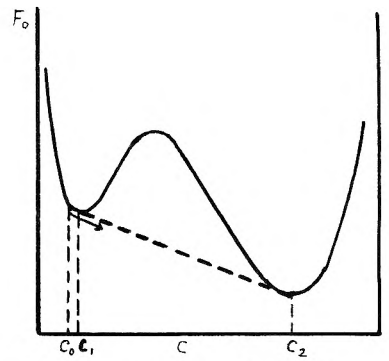

Fig. 3.—The relation between F_0 and c_0, and the fluctuation to heterogeneous states.

separation and θ may be observed as shown by curve (a) in Fig. 2.

The relation between c_0 (g./ml.) and the free energy F_0 (per ml.) of the solution at temperatures lower than the critical mixing temperature T_∞ is illustrated in Fig. 3. As already mentioned, when c_0 is far from the concentration range between c_1 and c_2 or when T is sufficiently higher than T_c, the concentration c in the small volume v fluctuates only in the neighborhood of c_0. The probability of such a fluctuation is given by[3,4]

$$\exp\left(-{}^1/_2 v(\partial^2(F_0/kT)/\partial c_0^2)(c - c_0)^2\right) \qquad (1)$$

When c_0 approaches c_1, or when T approaches T_0, the fluctuation to the heterogeneous state represented by the dotted line in Fig. 3 occurs. If c in v becomes larger than c_1, the solution in v becomes heterogeneous. The probability of such a fluctuation is easily calculated. As a special case, the probability that v as a whole forms the second phase of the concentration c_2 is

$$\exp\left(-v(\partial^2(F_0/kT)/\partial c_0^2)(c_1 - c_0)(c_2 - c_1)\right) \qquad (2)$$

which may be rewritten as

$$\exp\left(-vN_0(\partial(P_0/RT)/\partial c_0)(c_2 - c_1) \times (\partial \ln c_1/\partial T_0)(T - T_0)\right) \qquad (3)$$

where P_0 is the osmotic pressure, N_0 the Avogadro number, and $(\partial c_1/\partial T_0)$ the gradient of the solubility curve at T_0. If c_0 is small

$$\partial(P_0/RT)/\partial c_0 = 1/M + 2A_2 c_0 + \ldots \qquad (4)$$

M is the molecular weight of the solute and A_2 the second virial coefficient. If the value of (3) is not much smaller than unity, in other words, if $(T - T_0)$ is small enough to satisfy this condition, the small volumes of the second phase produced in the solution will be sufficient to be observable. In solutions of high molecular weight substances this condition is comparatively easily satisfied because of the following characteristics: (*i*) $\partial(P_0/RT)/\partial c_0$ is small because of large M. (In the neighborhood of T_0, A_2 is negative and therefore $\partial(P_0/RT)/\partial c_0$ is in general smaller than $1/M$.) (*ii*) In solutions of high molecular weight substances, especially of linear high polymers or of fibrous proteins, the concentration of the second phase is small. This means that the solubility curves are not symmetrical (Fig. 1b) and the difference $(c_2 - c_1)$ is small even in the region far from the critical mixing point (T_∞, c_∞). That this dissymmetry is characteristic of solutions of linear and large molecules has been shown theoretically.[8] The solubility curves of most solutions of low molecular weight substances have no great dissymmetry and $(c_2 - c_1)$ is large except in the region of the critical point.

For example, given the solution of a high molecular weight substance, in which $M = 10^5$, $c_2 - c_1 = 3 \times 10^{-2}$, $\partial \ln c_1/\partial T_0 = 0.2$, and $v = 10^{-15}$, (3) $= \exp(-40(T - T_0))$. When $T - T_0 = 1/10$, (3) $= 5 \times 10^{-2}$. Then it should be possible by regulation of the temperature to make the value of (3) large enough for observable preseparation.

On the other hand, if we have the solution of a low molecular weight substance, in which $M = 50$, $c_2 - c_1 = 0.5$, $\partial \ln c_1/\partial T_0 = 0.2$, and $v = 10^{-15}$, (3) $= \exp(-10^5(T - T_0))$. Even if much smaller values of v are assumed, (3) is still so small that the conditions necessary for observable preseparation cannot be satisfied.

Size Distribution of Particles of the Second Phase and Change of Their Total Volume.—In the last section it was shown that in some cases the preseparation or the fluctuation to the second phase is not negligible even in the region far from the critical mixing point. In these cases the fluctuation of the solution in v to a homogeneous state of a concentration between c_1 and c_2 is still negligible. For example, if $M = 10^5$, $v = 10^{-15}$ and $(c - c_0) = 5 \times 10^{-3}$, the probability of this fluctuation (1) is $\exp(-10^2)$; if $(c - c_0) = 10^{-2}$, (1) $= \exp(-6 \times 10^2)$. Although the actual probability is somewhat larger than (1), it is still negligible. The difference between the preseparation under discussion and the fluctuation which occurs near the critical mixing point is made clear by this fact. In the latter case it is impossible to define two coexisting phases distinctly; in the present case, however, this definition is both permissible and possible. Thus the preseparation state may be considered as a mixture of two phases, the concentrations of which are nearly equal to c_0 $(\cong c_1)$ and equal to c_2, respectively. The second phase is suspended as many small particles of various sizes and shapes. The concentration in them is uniform (c_2) and the free energy of the

(8) P. J. Flory, *J. Chem. Phys.*, **10**, 51 (1942); **12**, 425 (1944); **13**, 453 (1945); "Principles of Polymer Chemistry," Cornell Univ. Press, Ithaca, N. Y., 1953, Chap. 12.

particle of volume v may be written as $vF_0(c_2) + \sigma_v$. When v is large, the correction term σ_v, being positive, is approximately proportional to the surface area of the particle. Of course there may be small fluctuation in the solution which cannot be treated as a phase. This situation is understandable, when the particles are compared with the clusters in the condensation theory.[2] The large clusters correspond to the particles of the second phase; *i.e.*, the contribution to the cluster integrals from the particles of concentration c_2 is overwhelmingly large. The smallest clusters are included in the theory of the macroscopic homogeneous phase or in F_0. Although the clusters of intermediate size should not be so simply treated, we shall temporarily apply to them the expression of the free energy developed for the larger clusters; their σ_v values may be relatively large.[1]

The volume v_0, in which one solute molecule (and some solvent molecules) are contained, is taken as the unit volume of the second phase. When small particles of various sizes l_{v_0} (l is an integer) are suspended in the solution, the free energy of the whole solution is written as

$$F(c_0,n_1) = VF_0(c_0) + V\Delta F + \sum_l n_l\sigma_l - TS(n_l) \quad (5)$$

where

$$\Delta F = {}^1/_2(\partial^2F_0/\partial c_0^2)(2(c_2 - c_1)(c_1 - c_0)\,\theta + (c_2 - c_1)^2\theta^2)$$

and

$$\theta = \sum_l \ln_l v_0/V$$

n_l denotes the number of particles of the size lv_0, σ_1 their surface free energy, and $S(n_l)$ the mixing entropy of all particles. In deriving the above equations, the effect of the fluctuations to the second phase on the whole solution has been taken into consideration up to the order of θ^2. When $\theta \ll 1$, $S(n_l)$ may be expressed as

$$S(n_l) = -k\left(\sum_l n_l \ln\left(n_l/\left(n_0 + \sum_l n_l\right)\right) + n_0 \ln\left(n_0/\left(n_0 + \sum_l n_l\right)\right)\right) \quad (6)$$

where n_0 is the number of solute molecules in the first phase. From these equations the equilibrium values of n_l are given by

$$n_l = n_0 \exp\left(-\delta(\theta - \theta_0)l - (\sigma_1/kT)\right) \quad (7)$$

where

$$\delta = v_0N_0(\partial(P/RT)/\partial c_0)(c_2 - c_1)^2/c_0$$

$$\theta_0 = (c_0 - c_1)/(c_2 - c_1)$$

$$\theta/(1 - \theta) = (c_0/c_2)\int_{l_0}^{\infty} l \exp\left(-\delta(\theta - \theta_0)l - (\sigma_1/kT)\right) dl \quad (8)$$

l_0v_0 means the volume of the smallest particles. These equations are valid only when the integral in (8) converges, *i.e.*, when $\delta(\theta - \theta_0) > 0$. If $T > T_0$, this condition is always satisfied, because $\theta_0 < 0$. When $T < T_0$, θ_0, corresponding to the curve (PB) in Fig. 2, becomes positive. Then at T_s, determined by the equation

$$\theta_0(T_s)/(1 - \theta_0(T_s)) = (c_0/c_2)\int_{l_0}^{\infty} l \exp\left(-(\sigma_l/kT_s)\right) dl \quad (9)$$

$\theta(T_s)$ must become equal to $\theta_0(T_s)$ and curve (a) intersects curve (PB) in Fig. 2. Above T_s, the change of n_l and θ with T can be traced by (7) and (8), and n_l evidently decreases with increasing l. Below T_s, according to (7), n_l increases with l for large l and (8) diverges; this means that the macroscopic second phase is formed and $\theta(T)$ must coincide with $\theta_0(T)$, as shown in Fig. 2. Thus T_s is just the macroscopic separation temperature observed and $(T_0 - T_s) = \theta(T_s)(c_2 - c_1)(\partial \ln c_1/\partial T_0)/c_1$.[9]

A theory of solutions, which dealt with every possible configuration and distribution of all molecules, would include the preseparation state and would give the true separation temperature T_s directly. However, the T_0 predicted by most theories[10] deviates from T_s as shown in Fig. 1,[11] because homogeneity is assumed except for the influence of small clusters and the large heterogeneity is neglected.

If the surface tension between the two phases is not too small, the particles of the second phase can show no large deviation from the spherical shape and σ_l will be proportional to $l^{2/3}$, *i.e.*, $\sigma_l = \sigma_0 l^{2/3}$. Obviously $\theta(T_s)$ increases with decreasing σ_0/kT_s. When two regular solutions, the concentrations of which are c_1 and c_2, are in contact, the excess energy due to the contacting surface, σ, is approximately given by[12]

$$\sigma/kT = N'(1/z')(1/\rho^2)(c_2 - c_1)^2\Delta H/RT \quad (10)$$

N' is the total number of solute and solvent molecules on the surface, z' a number between 2 and 4, and ρ the density of the solute. ΔH, which denotes the heat of mixing of one mole of solute with the solvent at infinite dilution, is positive for partially immiscible solutions. The actual surface tension is probably less than this because of rearrangement of molecules at the boundary.

For solutions of low molecular weight substances, in which $\Delta H/RT = 2$ and $(c_2 - c_1) = 0.5$, the surface tension calculated by (10) is of the order of 1–10 dynes/cm. In this case σ_v/kT is so large that $\theta(T_s)$ becomes negligible; *e.g.*, σ_v/kT is about 30 to 300 even for a very small particle of $v = 10^{-19}$. In solutions of high molecular weight substances $(c_2 - c_1)$ is much smaller and $\Delta H/RT$ also is less. According to the theory of regular solutions of low molecular weight substances, $\Delta H/RT \cong 2$ at the critical mixing point.[10] Smaller critical values of $\Delta H/RT$ have been found for solutions of high molecular weight substances.[13] This is due to the

(9) In the general case of multi-component systems, if similar approximations are used, $\delta(\theta - \theta_0)l$ in (7) may be replaced by $\sum_i\sum_j v(\partial^2F_0/\partial c_{i1}\partial c_{j1})(c_{i2} - c_{i1})(c_{j2} - c_{j1})(\theta - \theta_0)$ for sufficiently large v and the behavior of θ will be similar to that described above; c_i is the concentration of the i-th component and the suffixes 1 and 2 represent the two phases, respectively.

(10) For example, the theory of regular solutions and the theory of high polymer solutions based upon the lattice model; ref. 8; R. H. Fowler and E. A. Guggenheim, "Statistical Thermodynamics," Cambridge, 1939, Chap. 8, etc.

(11) It is remarkable that the deviation of the solubility curve is always inward.

(12) This expression is applicable to linear high polymer solutions if the monomer is used as the unit for defining N', and ΔH.

(13) The simple theory for linear high polymers gives a value of $^1/_2$ or less and even smaller values have been found experimentally.[8]

fact that in the case of large M, as soon as A_2 becomes negative, $\partial(P_0/RT)/\partial c_0$ becomes negative. Thus, if $\Delta H/RT = {}^1/_2$ and $(c_2 - c_1) = 2 \times 10^{-2}$ ($c_1 = 10^{-3}$, $c_2 = 2 \times 10^{-2}$), the surface tension is of the order of 10^{-3} dynes/cm. and σ_v/kT of a particle of the diameter 10^{-5} cm. is of the order of 10. $\theta(T_s)$ can be calculated from the approximate formula

$$\theta(T_s)/(1 - \theta(T_s)) = (c_0/c_2) \int_{l_0}^{\infty} l \exp\left(-(\sigma_0/kT_s)l^{2/3}\right) dl \quad (11)$$

Then if $M = 10^5$ ($v_0 = 10^{-17}$), $\sigma = 3 \times 10^{-3}$ dynes/cm., and $l_0 = 5$, $\theta(T_s)$ is about 5×10^{-3} [14]; *i.e.*, the particles of the second phase larger than $l_0 v_0$ occupy 0.5% of the total volume of the solution. Even when T is a little apart from T_s, $\theta(T)$ is still large, because in these solutions $\delta\theta_0$ is small as shown in the last section. Hence preseparation is often observable in the solutions of high molecular weight substances and their characteristics discussed above may account in part for the fact that microcoacervation is easily seen in them. Similar conclusions are obtained with regard to phase separation by precipitants.

In the case of the very small surface tension the right-hand side of (9) approaches unity. In that event T_s cannot be found and a discontinuous macroscopic phase separation is not observed (Fig. 2b). Figure 1 shows that with an increase in T_0, $(c_2 - c_1)$ and consequently σ_0/kT are decreased; if in the example cited for solutions of high molecular weight substances $(c_2 - c_1)$ becomes smaller than 10^{-2}, macroscopic separation does not occur. Even in this case the solution may be regarded as a mixture of the two phases, because the fluctuation to homogeneous states between c_1 and c_2 is still negligible. At such temperatures, therefore, the submicroscopic second phase grows continuously throughout the concentration change.[15] When T_0 approaches more closely to T_∞, the solution can no longer be regarded as a mixture of the two phases and the fluctuation takes place over a wide range of concentrations.[3,5]

Preseparation influences the osmotic pressure and turbidity. The true osmotic pressure P, which is smaller than P_0, can be derived from F of (5) instead of F_0 by differentiation. The following approximate relations are obtained

$$(P_0 - P)/P_0 = (c_2/c_0)(1/(1 - \theta)) = \left(\sum_l \ln_l\right)/n_0 \quad (12)$$

$$P(c_0, T_s)/RT = c_1/M + A_2c_1^2 + \ldots = P_0(c_1, T_s)/RT \quad (13)$$

The turbidity of the solution τ is inversely proportional to $\partial(P/RT)/\partial c_0$ and is larger than τ_0, the turbidity of the imaginary homogeneous solution derived from $\partial(P_0/RT)/\partial c_0$. The relative increment is written as[16]

$$(\tau - \tau_0)/\tau_0 = (\partial((P_0 - P)/RT)/\partial c_0)/(\partial(P/RT)/\partial c_0) = \left(\sum_l l^2 n_l\right)/n_0 \quad (14)$$

If the particles of the second phase are regarded as associated solute molecules, the molecular weights of which are lM, the same expression with (14) is obtained.[6,17] For a solution of the high molecular weight substance with the same numerical values as the example in the preceding section, $(\tau - \tau_0)/\tau_0$ at T_s, calculated by similar approximations with (11), was found to be of the order of unity.[18] The increase of the turbidity near the separation point can be predicted from the simple theories of F_0 due to the decrease of $\partial(P_0/RT)/\partial c_0$,[8,19] but the present discussion concludes the additional anomalous increase due to preseparation.[20]

(14) θ thus obtained contains only the contribution from the configuration corresponding to the second phase, although for very small l or lv_0 the fluctuation to the state between c_1 and c_2 is not always negligible.

(15) The range of temperature in which this occurs may be related to the range between the two critical temperatures T_m and T_c in the theory of condensation.[2,5] (According to the approximations used here, however, the osmotic pressure changes continuously throughout the concentration change.) Since of course the idea of suspended particles is not applicable to this case, it will be discussed elsewhere on the basis of the lattice model of solutions.

(16) τ in (14) is the turbidity at the scattering angle of zero or that determined with light of very long wave length. The turbidity at a finite angle is useful for the determination of the average size and shape of particles; however, in the present case, where the particles are polydisperse, the analysis is difficult; ref. 4, 6, 17.

(17) G. Mie, *Ann. Physik*, **25**, 377 (1908); B. Zimm, *J. Chem. Phys.*, **16**, 1093, 1099 (1948).

(18) The weight average value of l, $\langle l \rangle = (\Sigma_l l^2 n_l)/(\Sigma_l l n_l) = ((\tau - \tau_0)/\tau_0)(P_0/(P_0 - P))$, is calculated from (11), (7) and (14); the numerical values, however, have no rigorous meaning because of the rough approximations employed, especially of those concerning small particles. The fact that in solutions of high molecular weight substances calculated values of $\langle l \rangle$ can be considerably larger than l_0 suggests the important role of large particles in them.

(19) P. Debye and F. Bueche, *J. Chem. Phys.*, **18**, 1423 (1950).

(20) In solutions of multi-component solvents the selective absorption of the solvent by the solute may be another cause of the anomalous turbidity.[21] However, if the relation between the refractive indices of components makes this interpretation impossible, the anomalous turbidity must be attributed to preseparation.

(21) R. H. Ewart, C. P. Roe, P. Debye and J. R. McCartney, *J. Chem. Phys.*, **14**, 687 (1946).

THE VAPOR PRESSURE OF MERCURY AT 250–360°

BY F. H. SPEDDING AND J. L. DYE

Contribution No. 375 from the Institute for Atomic Research and Department of Chemistry,[1] *Iowa State College, Ames, Iowa*

Received September 3, 1954

The vapor pressure of mercury was measured with a new-design isoteniscope in the region 250 to 360°. The vapor pressure fits the equation $\log_{10} P = 10.59901 - 3335.027/\theta - 0.865372 \log_{10} \theta$ (1), in which $\theta = 273.160 + t$, with t in °C. (Int.)

This Laboratory is currently engaged in the determination of some thermodynamic properties of rare earth–metal solutions. In the course of this study it was desired to measure the vapor pressure of mercury. The necessary apparatus was constructed for this purpose, and included a new type of isoteniscope, and a thermostat bath which controlled the temperature of a molten salt bath to ±0.005° between 225 and 400°.

In order to determine the accuracy attainable with this apparatus, the vapor pressure of pure mercury was measured at a number of temperatures between 250 and 360°. The design of the isoteniscope used in this research is being modified at present to make the instrument more rugged. The values obtained for the vapor pressure of mercury were more self-consistent than any data previously reported, but the least-squares expression agrees very well with the values found by other investigators.

Apparatus.—The isoteniscope, Fig. 1, was constructed of Pyrex glass. The pressure-sensitive element was a 0.2 mm. thick glass diaphragm made in a glass-blower's lathe from a section of 45 mm. tubing. The platinum contacts were connected through a relay system to solenoid valves which automatically regulated the pressure above the diaphragm to within about 5 mm. of the pressure in the system. The pressure of the system was determined more accurately by manually adjusting the pressure above the diaphragm until the "break" point was just reached. The external pressure was then measured with a manometer and cathetometer system accurate to ±0.05 mm. The isoteniscope was constructed so that even with a vacuum in the system it required several millimeters of pressure above the diaphragm to reach the "break" point. This was called the zero correction and was subtracted from all readings. The zero correction was determined at various temperatures by a calibration run prior to the actual run with mercury. The correction changed by about 1 mm. from room temperatures to 300°.

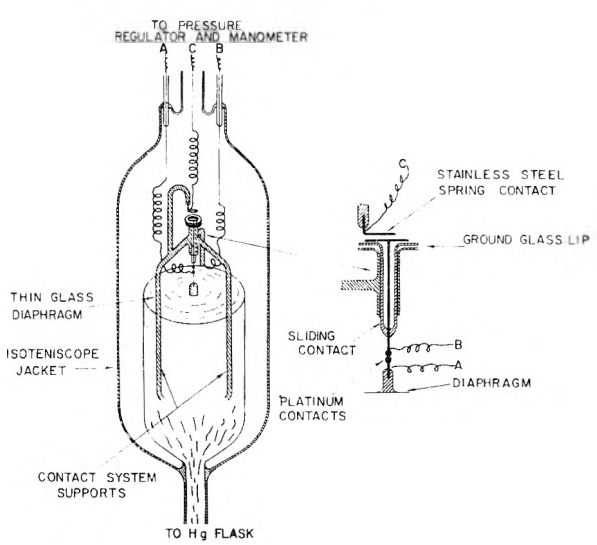

Fig. 1.—Isoteniscope.

A 25-ml. flask was connected to the isoteniscope and also to a vacuum system. A number of sealed glass tips which could be broken by "magnetic hammers" were included to connect the Hg flask with the vacuum system. This is especially important when the vapor pressure of an amalgam instead of pure Hg is being measured, because the composition of the amalgam can be changed by distilling Hg out of the system without opening the system to the atmosphere.

The thermostat bath and control circuit are shown diagrammatically in Fig. 2. Two elements, each about 100 ft. in length, were wound together around the steel core, one of #18 "Chromel A" wire for the heating current, and the other of #20 "Hytempco" wire for a resistance element. The windings were separated from each other and the steel core by $^3/_{16}$ in. porcelain fish spine insulators strung on the wires.

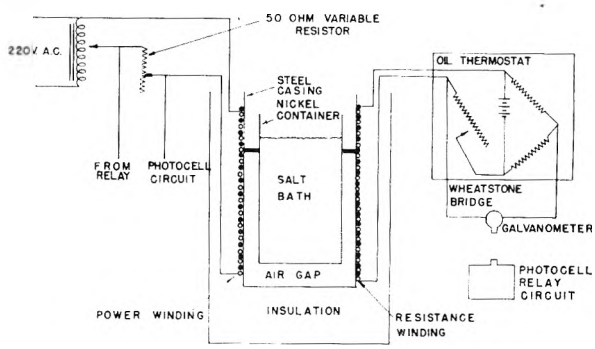

Fig. 2.—Thermostatic bath and control circuit.

The resistance winding was balanced at any desired bath temperature in a Wheatstone bridge circuit, thermostated in oil at 25°. Any unbalance of the bridge resulting from heating or cooling of the resistance winding of the furnace was detected by a galvanometer whose beam activated a photocell relay circuit. When closed, this relay circuit shunted out a variable resistor in the power circuit, thus increasing the power input to the bath. Although the temperature of the air gap in the thermostat may have fluctuated because of the cycling, the large heat capacity of the salt-bath compared to the air gap prevented the salt-bath from exhibiting variations in temperature due to the cycling. As a result of the stable control circuit and the large heat capacity of the salt-bath, the temperature of the bath was constant within ±0.005° for several hours and ±0.01° for much longer periods.

The thermostat was mounted on an elevator which permitted it to be raised and lowered. The isoteniscope system remained fixed in position, with the source of heat being raised to it. The inner container of the thermostat was made of nickel sheet, and contained a salt-bath mixture of $NaNO_3$ and KNO_3. The salt-bath was stirred vigorously with a mechanical stirrer, so that no temperature gradients were observed. The temperature of the bath was measured to ±0.001° with a platinum resistance thermometer calibrated by the National Bureau of Standards and encased in a close-fitting, thin nickel sheath. The thermometer used had a "δ" value of 1.4919. Nickel was used as a construction material so that molten chloride baths could also be employed; however, with a nitrate bath, stainless steel would have been satisfactory.

(1) Work was performed in the Ames Laboratory of the Atomic Energy Commission.

Experimental

The mercury used in this research was first specially purified. Chemically pure, triple-distilled mercury was washed several times each with (1) a solution of dilute $Hg_2(NO_3)_2$, (2) dilute HNO_3, (3) distilled water, by dropping the mercury in a fine stream through a long column containing the wash solution. The mercury was then vacuum-dried, filtered several times through a pin-hole in filter paper, and finally twice distilled in a stream of air as recommended by Hulett.[2]

About 80 g. of the purified mercury was introduced into the flask in the isoteniscope system and degassed under a vacuum of about 5×10^{-6} mm. The degassing was aided by distilling nearly half of the mercury out of the system. The glass tube from the flask to the vacuum system was then sealed off under vacuum, the temperature of the system was brought to the desired value, and the null pressure read on the manometer in the external system. The temperature of the bath remained constant to $\pm 0.005°$ for at least 10 minutes before making a reading of the pressure and at least three independent readings of the pressure were made. The data represent values from two completely independent determinations.

Results and Discussion

The vapor pressure of mercury was measured at a number of temperatures and the data were fitted to an equation of the type

$$\log_{10} P = A + B/T + C \log_{10} T$$

by a least-squares method. Since the major experimental error is the determination of the pressure (as indicated by the fact that the deviations were about ± 0.10 mm. independent of temperature), the least-squares treatment was carried out assuming error in P only, and included a weighting factor so that the equation for $\log P$ rather than P could be used. If this factor were not used, the low pressure values would be given much more importance than is justifiable.

The resulting equation leads to a normal boiling point of 356.575° which is 0.005° below the currently accepted value of 356.580°.[3]

If the latter value is adopted as a fourth fixed point for the platinum resistance thermometer a temperature correction of about 0.005° is necessary. The least-squares equation which then results is

$$\log P = 10.59901 - \frac{3335.027}{\theta} - 0.865372 \log_{10} \theta \quad (1)$$

in which $\theta = 273.160 + t$ with t in °C. (cor.).

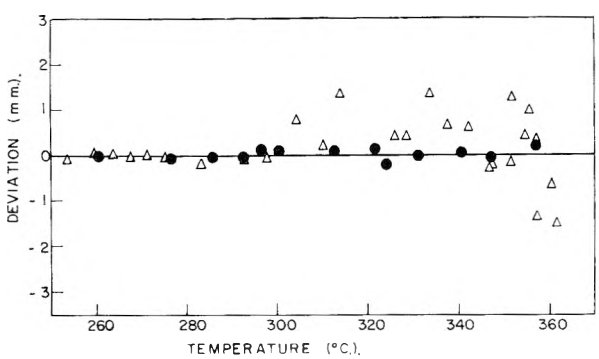

Fig. 3.—Deviations of measured vapor pressure from empirical formulas: ●, this Laboratory—deviations from least-square equation 1; △, Smith and Menzies deviations from their own equation 2.

(2) G. A. Hulett, *Phys. Rev.*, **21**, 288 (1905); **33**, 307 (1911).

(3) J. A. Beattie, B. E. Blaisdell and J. Kaminsky, *Proc. Am. Acad. Arts Sci.*, **71**, 375 (1937).

The measured vapor pressures and the deviations from equation 1 are given in Table I.

TABLE I

THE VAPOR PRESSURE OF MERCURY FROM 260 TO 360°

Av. deviation—0.08_7 mm.

t (°C.)	p (mm.)	Dev. (mm.) Obsd.-Calcd.
260.650	97.9_9	0.00
276.632	145.0_4	−0.08
285.767	179.6_7	−0.09
291.539	205.1_5	+0.12
292.561	209.7_5	−0.05
300.426	249.7_2	+0.09
312.828	325.4_5	+0.02
321.555	389.4_2	+0.11
324.067	409.4_4	−0.22
331.102	470.9_8	−0.04
340.700	566.8_1	+0.03
347.068	638.6_3	−0.09
357.059	766.7_5	+0.19

An interesting fact emerged from the least-squares treatment of the data. This is that A, B and C can be simultaneously varied in an appropriate way by relatively large amounts with little change in the calculated pressures. For example the two formulas

$$\log_{10} P = 10.68074 - \frac{3342.364}{\theta} - 0.890032 \log_{10} \theta$$

and

$$\log_{10} P = 10.51828 - \frac{3327.690}{\theta} - 0.840712 \log_{10} \theta$$

both give values of P which differ from those given by (1) by less than 0.10 mm. over the entire range of temperatures used. However, if A is changed from 10.59901 to 10.59906 without changing B and C, the calculated pressure near the boiling point changes by 0.10 mm. Obviously, one must use formulas of this type with caution outside of the range of experimental measurements.

The most self-consistent values previously measured over this temperature range are those of Smith and Menzies[4] which were corrected to the present temperature scale (but using only the usual three calibration points) by Menzies[5] in 1927. These data were found by Menzies to fit the equation

$$\log_{10} P = 9.957094 - \frac{3283.90}{\theta'} - 0.66524 \log_{10} \theta' \quad (2)$$

in which $\theta' = 273.100 + t'$ and P is in mm. The deviations of the present measurements from equation 1 and of the measurements of Smith and Menzies from equation 2 are shown in Fig. 3. It is seen that the data of this Laboratory are more self-consistent, due largely to better temperature control.

Douglas, Ball and Ginnings,[6] in a very complete work on the thermodynamic properties of mercury recalculated the temperatures of Smith and Menzies employing a cubic equation for the thermometer resistance taking the boiling point of mercury

(4) A. Smith and A. W. C. Menzies, *J. Am. Chem. Soc.*, **32**, 1434 (1910).

(5) A. W. C. Menzies, *Z. physik. Chem.*, **130**, 90 (1927).

(6) T. B. Douglas, A. F. Ball and D. C. Ginnings, *J. Research Natl. Bur. Standards*, **46**, 334 (1951).

found by Smith and Menzies as a fourth fixed point for thermometer calibration. In addition these authors have calculated the vapor pressure of mercury from thermal measurements on the liquid and estimates of the second virial coefficient of the vapor. Their results are given by their equation 35.

Epstein and Powers[7] obtained an expression for the vapor pressure of mercury utilizing all available thermodynamic measurements which is intended to be valid from the triple point to the critical point.

Beattie, Blaisdell and Kaminsky[3] measured the vapor pressure of mercury very accurately in the range 660 to 860 mm. and with these measurements fixed the boiling point as 356.580°.

The vapor pressures calculated from the expressions of the five investigators mentioned have been tabulated for rounded values of temperature from 250 to 360° in Table II. The values of Smith and Menzies are for the corrected temperature given by Douglas, Ball and Ginnings.[6]

It is seen that the agreement between various investigators is quite good. All expressions must of course give the same value at the normal boiling point. The very close agreement of Douglas, Ball and Ginnings with the data of Smith and Menzies is due in part to the fact that the value chosen for the second virial coefficient of the vapor in the former calculations was adopted partly because of the close agreement with measured vapor pressures. The differences generally are too small to be ascribed any significance.

(7) L. F. Epstein and M. D. Powers, AECU-1640, Sept. 1951.

TABLE II

THE VAPOR PRESSURE OF MERCURY IN MM. AT ROUNDED TEMPERATURES ACCORDING TO VARIOUS INVESTIGATORS

t (°C.)	S and D.	B., B. and K.	S. and M.	D., B. and G.	E. and P.
250	74.41		74.49	74.50	74.35
260	96.40		96.47	96.48	96.30
270	123.66		123.73	123.73	123.52
280	157.17		157.23	157.23	156.97
290	198.02		198.05	198.05	197.76
300	247.41		247.41	247.41	247.08
310	306.68		306.66	306.65	306.32
320	377.32		377.28	377.27	376.93
330	460.94		460.89	460.87	460.56
340	559.30		559.25	559.22	558.98
350	674.28	674.26	674.26	674.24	674.12
360	870.95	808.00	807.97	807.99	808.03

KINETICS OF THE REACTION BETWEEN o-CHLORONITROBENZENE AND ETHANOLAMINE

BY PHILIP L. GORDON,[1] T. A. ALFREY, JR.,[2] AND ERNEST I. BECKER[3]

Contribution from the Chemical Laboratories of the Polytechnic Institute of Brooklyn, Brooklyn, N. Y.

Received September 8, 1954

The reaction between o-chloronitrobenzene and ethanolamine has been studied. The high rate of reaction, the more negative $\Delta S^{\circ}\ddagger$ and the smaller E_a compared with the lower rates, less negative $\Delta S^{\circ}\ddagger$ and the larger E_a for n-butylamine are evidence for a cyclic mechanism. In accord with this mechanism also is the fact that a mixture of ethylamine and ethanol —in which the functional groups are on separate molecules—reacts more slowly than ethanolamine. Thus, the reaction with ethanolamine is depicted as going through a cyclic transition state in which the amino group is attacking the carbon holding chlorine while simultaneously the hydroxyl group is solvating the chlorine atom. At low concentrations phenol accelerates the reaction; at higher concentration it decelerates the reaction. This effect is that expected for a substance more electrophilic than the alcohol, but which can effectively remove amine from solution by neutralization.

Introduction

During the investigation of a number of organic bases as dehydrochlorinating agents for polymeric materials, such as polyvinylidene chloride and polyvinyl chloride, it was observed that ethanolamine was uniquely effective.[4] In fact, its efficiency was ultimately exploited by the development of an analytical procedure for chlorine in copolymers of vinylidene chloride.[4] Tests on a number of aromatic molecules with reactive halogens demonstrated that among these, also, ethanolamine was an effective reagent for displacing the halogen. It thus became the purpose of this investigation to determine the cause of the effectiveness of ethanolamine in displacing chloride from aromatic molecules.

The reaction selected for study was that between ethanolamine and o-chloronitrobenzene. The product, N-(2′-nitrophenyl)-ethanolamine had already been characterized.[5-7] Using larger excesses of ethanolamine and a temperature range of 57–82°, the described product could be obtained in 95% yield, indicating the suitability of these conditions for the kinetic study. The course of this investigation was patterned after Swain's study of the displacement reaction of trityl chloride in which kinetic evidence for the termolecular mechanism was established.[8]

Experimental

Starting Materials.—o-Chloronitrobenzene (E. K. White Label grade) was recrystallized from petroleum ether twice to a pale yellow solid, m.p. 31.5°. Ethanolamine, ethylamine, n-butylamine, pyridine, methanol, ethanol, isopropyl alcohol, n-hexanol, 2-butoxyethanol and n-butyl ether were

(1) Taken from the Dissertation presented to the Graduate Faculty of the Polytechnic Institute of Brooklyn in partial fulfillment of the requirements for the degree of Doctor of Philosophy, 1953.

(2) Dow Chemical Company, Midland, Michigan.

(3) To whom inquiries concerning this publication should be sent.

(4) P. L. Gordon and G. Dolgin, M.S. theses, Polytechnic Institute of Brooklyn, 1948.

(5) P. Karrer, E. Schlittler, K. Pfaehler and F. Benz, *Helv. Chim. Acta*, **17**, 1516 (1934).

(6) C. B. Kremer, *J. Am. Chem. Soc.*, **59**, 1681 (1937).

(7) C. B. Kremer, *ibid.*, **61**, 1223 (1939).

(8) C. G. Swain, *ibid.*, **70**, 1119 (1948).

highest purity, commercially available compounds, which were dried and distilled before use taking heart cuts which were checked to agree with the literature values. Dioxane was a specially purified, anhydrous material, m.p. 10.5°. Phenol was recrystallized from petroleum ether, m.p. 43.0°. β-Methoxyethylamine was obtained from a 70% aqueous solution by azeotropic removal of the water with benzene and twice distilling the amine. The heart cut, b.p. 94°, was used for the experiments.

Procedure.—The reactions were run in a Precision Scientific Company constant temperature bath with a rated and measured accuracy of ±0.05°. The first run was made using 2.0 g. of *o*-chloronitrobenzene and 98 g. of ethanolamine. The reactants were weighed into a 500-ml. erlenmeyer flask with a ground glass stopper. After allowing the flask containing the ethanolamine to come to 57.0° in the constant temperature bath, the *o*-chloronitrobenzene was added. The stopper was sealed with tape and the contents were swirled in the bath to effect rapid solution. The mixture was maintained at 57.0° for eight hours. Ten-gram samples were pipetted at timed intervals into 150 ml. of cold water. After acidification, the chloride content was determined gravimetrically as silver chloride.

In order to determine whether the reaction rate was affected by possible traces of moisture in the reagents or solvents, the reaction was repeated using 0.5, 1.0 and 2.0% of water based on the weight of ethanolamine. No significant difference in rate was observed for any of these concentrations.

The kinetic determinations using varying concentrations of 2-butoxyethanol were performed in the same manner. In the case of the methanol series, the use of ground glass stoppered flasks was unsatisfactory due to the volatility of the methanol. For this series sealed test-tubes were simultaneously placed in the bath and individually withdrawn at timed intervals. Cooling the tubes in ice and water served to stop the reaction before opening them. The same analytical procedure was used. This method was used for all subsequent kinetic studies.

Results and Discussion

In all cases the reaction was found to be first order in *o*-chloronitrobenzene by standard techniques,[9] as was to be expected with one of the reactants in large excess. For the reaction using varying quantities of 2-butoxyethanol the data are shown in Table I; for the methanol series in Table II; for the additional series of solvents in Table III.

TABLE I

TABULATION OF RATE CONSTANTS FOR THE REACTION BETWEEN *o*-CHLORONITROBENZENE AND ETHANOLAMINE IN VARYING CONCENTRATIONS OF 2-BUTOXYETHANOL AT 57.0°

o-Chloronitrobenzene, mole/l.	Ethanolamine, mole/l.	2-Butoxyethanol, mole/l.	Rate constants, $k \times 10^7$
0.0636	16.28	...	675.0
.0636	8.2	3.72	146.1
.0636	4.1	5.61	38.0
.0636	2.05	6.55	16.25
.1272	1.02	7.00	6.09
.1272	0.515	7.25	2.96

TABLE II

TABULATION OF RATE CONSTANTS FOR THE REACTION BETWEEN *o*-CHLORONITROBENZENE AND ETHANOLAMINE IN VARYING CONCENTRATIONS OF METHANOL AT 57.0°

o-Chloronitrobenzene, mole/l.	Ethanolamine, mole/l.	Methanol, mole/l.	Rate constants, $k \times 10^7$
0.0636	16.25	...	675.0
.0636	12.27	6.0	166.0
.0636	8.20	12.24	40.2
.0636	4.10	18.0	10.3
.1272	2.05	21.6	2.87
.1272	1.008	22.85	1.66

(9) A. G. Worthing and J. Geffner, "Treatment of Experimental Data," John Wiley and Sons, Inc., New York, N. Y., 1943, Chapter III.

TABLE III

TABULATION OF RATE CONSTANTS FOR THE REACTION BETWEEN *o*-CHLORONITROBENZENE AND ETHANOLAMINE IN VARIOUS SOLVENTS AT 57.0°

o-Chloronitrobenzene, 0.1272 mole/l.; ethanolamine, 2.05 mole/l.

Solvent	Concn., mole/l.	Rate constant, $k \times 10^7$
Methanol	21.6	2.87
Ethanol	14.82	6.22
Isopropyl alcohol	11.7	9.24
2-Butoxyethanol	6.55	16.25
Methanol	10.8	8.6
2-Butoxyethanol	3.36	
Hexanol	3.5	13.7
2-Butoxyethanol	3.36	
Dioxane	10.26	42.8
Dioxane	5.13	21.2
2-Butoxyethanol	3.36	
n-Butyl ether	2.94	18.4
2-Butoxyethanol	3.36	
Pyridine	10.84	32.6

Comparison of the data of Tables I and II shows that at fixed concentrations of *o*-chloronitrobenzene and ethanolamine, the rate is slower with the larger molar concentration of methanol. This is taken to mean that the larger concentration of added hydroxyl groups has slowed the reaction. That this decrease in rate is probably not due to the ether function of 2-butoxyethanol is shown by comparison with the reaction in dioxane (Table III) in which the rate is faster than for the hydroxylic solvents. With these facts as a guide, an empirical equation was devised which took into account the concentration of ethanolamine and also the inhibiting effect of the hydroxylic solvents.

$$k = \frac{[\text{Ethanolamine}]}{a + b\,[\text{Solvent}]^2} \qquad (1)$$

where

k = experimental first-order rate constant in sec.$^{-1}$
$[\ ]$ = concentrations in mole l.$^{-1}$
a = constant for no solvent in mole sec. l.$^{-1}$
b = constant for the solvent in l. sec. mole^{-1}

The constants were determined as follows: with no solvent Equation 1 becomes

$$k = \frac{[\text{Ethanolamine}]}{a} \qquad (2)$$

thus permitting the evaluation of a directly from the experimental data. Using the value of a so obtained, 2.42×10^{-5} mole/sec. l.$^{-1}$. Equation 1 was then used for evaluating b in each experiment in the 2-butoxyethanol series and in the methanol series. The results are given in Table IV. The small average deviations, about 6%, validate equation 1 for these series.

It is now possible to examine a mechanism for the reaction. The reaction is first order in *o*-chloronitrobenzene, the reactant in minimum quantity, and depends to an inverse second power

TABLE IV

Measured values, $k = 10^7$	$b \times 10^{-4}$	Calcd. values for $k \times 10^7$ using av. value for b = 2.61×10^4	%
2-Butoxyethanol series			
146	2.28	137	6.0
38	2.68	38.7	1.8
16.25	2.42	15.2	6.4
6.09	2.87	6.4	6.5
2.97	2.83	3.18	7.0
Av. dev. for this series = 5.8%			
Methanol series[a]			
166	1.38	174	4.6
40.2	1.20	38.9	3.3
10.3	1.17	9.52	7.5
2.87	1.48	3.24	9.6
1.50	1.26	1.45	3.3
Av. dev. for this series = 5.66%			

[a] Calculated values for $k \times 10^7$ using average value for $b = 1.28 \times 10^4$.

on the concentration of solvent. Of a number of mechanisms consistent with these facts is the following: One molecule of ethanolamine reacts with one molecule of *o*-chloronitrobenzene. As the nucleophilic group ($-NH_2$) attacks the carbon to which the chlorine is attached, there is a simultaneous solvating attack on the chlorine by the electrophilic group ($-OH$). The accompanying diagram depicts the cyclic transition inferred.

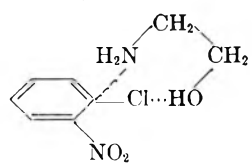

This treatment is, thus, a cyclic adaptation of the termolecular, or concerted, displacement mechanism of Swain[10] and corresponds to his Type D reaction in his illustrations for the different possibilities for concerted displacements.

The introduction of a hydroxylic solvent, such as methanol or 2-butoxyethanol, inhibits the reaction. Hydrogen bonding to both the chlorine atom and to the ethanolamine is consistent with the inverse square dependence on the concentration of solvent. The inhibition results from disturbance of the favorable juxtaposition of groups in the cyclic transition state. The effect of added alcohols may be found in their probable different acidities or in their different structures which may interfere with hydrogen bonding. Swain and Brown[11a] have previously put forth a cyclic mechanism to account for the unique effectiveness of 2-hydroxypyridine on the mutarotation of tetramethylglucose in benzene.

With equation 1 as a guide, an interpretation of the significance of a and b may be made. The constant a is a function of the ethanolamine, which in this case is also the electrophilic reagent. The value for this constant is unaffected by the solvent used in the reaction, and if the interpretation of the mechanism is feasible, can be used as a relative value for the inhibiting effect of the solvent. From the equation the value of b is directly proportional to the inhibiting effect of the polar solvent.

The series of kinetic runs made with the different solvents gave results which fitted this hypothesis. Based on the interpretation above it would be predicted that for longer carbon chains attached to the OH group in an alcohol, *i.e.*, the lower the molar concentration of OH, there would be less inhibition and a higher rate for a comparable mixture of reactants. The data of Table III bear out this contention.

The use of ether-type solvents, such as dioxane or *n*-butyl ether, instead of alcohols, also resulted in higher reaction rates between *o*-chloronitrobenzene and ethanolamine. When solvent mixtures were used, the rates were roughly equal to the average of the values for the two solvents taken separately.

The next portion of this investigation was concerned with the effect of phenol on the reaction rate. On the basis of the postulated mechanism for the present reaction, and Swain's work on the effect of phenol on the solvolysis of trityl chloride in methanol, it was possible to predict the behavior of phenol when added to a mixture of *o*-chloronitrobenzene and ethanolamine in methanol. Swain[8] had shown that phenol solvates halogen more efficiently than carbon and also that the complexing tendency between phenol and methanol is negligible Therefore, the addition of phenol to the reaction mixture should set up a concerted displacement according to the following diagram. Analogously, for the reaction of *o*-chloronitrobenzene and ethanolamine the initial effect of phenol should be an acceleration of the rate of reaction. As the concentration is increased, the acid–base reaction between the phenol and ethanolamine should effectively reduce the concentration of ethanolamine, and beyond some optimum point, the rate of reaction should decrease.

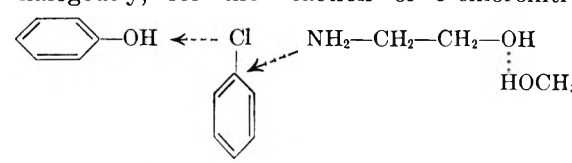

The results of the series of kinetic studies on the effect of phenol on the reaction between *o*-chloronitrobenzene and ethanolamine, substantiated these predictions. The data are given in Table V, and

TABLE V

TABULATION OF RATE CONSTANTS FOR THE REACTION BETWEEN *o*-CHLORONITROBENZENE AND ETHANOLAMINE IN METHANOL WITH VARYING CONCENTRATIONS OF PHENOL

o-chloronitrobenzene, 0.1272 mole/l.; ethanolamine, 2.05 mole/l.

Phenol, mole/l.	Methanol, mole/l.	Rate constant, $k \times 10^7$
...	21.60	2.87
0.0695	21.55	4.67
0.1390	21.48	7.58
0.2770	21.35	8.95
0.5560	21.18	5.71
1.1100	20.62	1.85

(10) C. G. Swain, *J. Am. Chem. Soc.*, **72**, 4578 (1950).

(11) (a) C. G. Swain and J. F. Brown, Jr., *ibid.*, **74**, 2534 (1952); (b) **74**, 2538 (1952).

the plot of rate constants against concentration of phenol in Fig. 1 clearly shows a maximum of $k = 8.9 \times 10^{-7}$ sec.$^{-1}$ with 0.255 molar phenol.

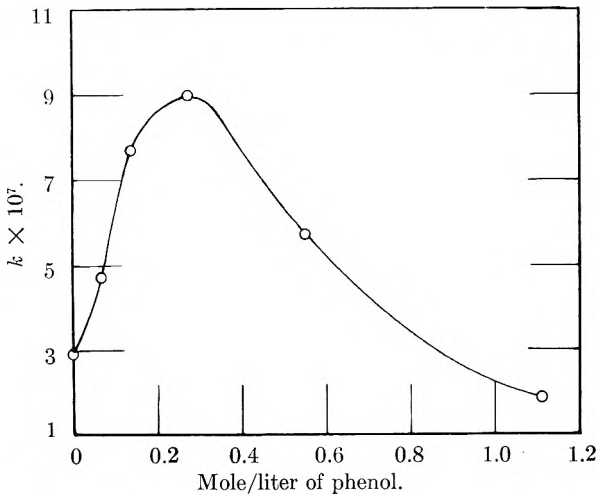

Fig. 1.—Effect of concentration of phenol on the rate constant for the reaction between *o*-chloronitrobenzene and ethanolamine at 57°.

This reaction would be expected to be first order in *o*-chloronitrobenzene, first order in phenol, and first order in the complex formed by ethanolamine and methanol. However, since the complexing reaction is undoubtedly reversible, a simple termolecular rate equation would not suffice in this case. An attempt was made here to fit an equation to the data.

A further test for a cyclic mechanism is based on the absolute rate equation 3 of Eyring. In this treatment the entropy of activation is examined. A high negative value for $\Delta S^{\circ}\ddagger$ indicates the loss of a number of degrees of freedom in proceeding from the reactants to the transition state, which is consistent with a cyclic transition state. A recent example of this reasoning is that of Foster, *et al.*,[12] in their investigation of the energy of activation and the entropy of activation in the rearrangement of three-carbon systems.

In order to apply this treatment, it was necessary to obtain the activation energy for the reaction between *o*-chloronitrobenzene and ethanolamine, and also for the reaction between *o*-chloronitrobenzene and *n*-butylamine. Since a cyclic intermediate could not be involved in the case of *n*-butylamine, a sizeably larger $\Delta S^{\circ}\ddagger$ for the ethanolamine reaction over that for the *n*-butylamine reaction should indicate a cyclic intermediate for the ethanolamine case.

The activation energies for the two reactions were obtained from the slopes of the plots of log k *versus* $1/T \times 10^5$ from the data in Tables VIII and IX. The values of k at various temperatures were determined from the data in Tables VI and VII. For the reaction with ethanolamine $E_a = 9.41$ kcal. mole^{-1}; for the reaction with *n*-butylamine, $E_a = 18.0$ kcal. mole^{-1}. The low activation energy for the ethanolamine reaction is another point in favor of the termolecular mechanism of Swain.[8]

The entropies of activation, $\Delta S^{\circ}\ddagger$, were calculated from the Eyring rate equation, assuming κ (kappa) to be unity

$$k = \frac{\kappa k T}{h} e^{\Delta S^{\circ}\ddagger/R} e^{-\Delta H^{\circ}\ddagger/RT} \qquad (3)$$

κ = transmission coefficient, assumed to be unity
k = first-order reaction rate constant
k = Boltzmann constant, 1.3805×10^{-16} erg deg.$^{-1}$
T = temperature in °K.
h = Planck's constant, 6.626×10^{-27} erg sec.
$\Delta H^{\circ}\ddagger$ = heat of activation
$S^{\circ}\ddagger$ = entropy of activation

(12) G. E. Foster, A. C. Cope and F. Daniels, *J. Am. Chem. Soc.*, **69**, 1893 (1947).

TABLE VI

EFFECT OF THE VARIATION OF TEMPERATURE ON THE RATE OF REACTION BETWEEN *o*-CHLORONITROBENZENE AND ETHANOLAMINE

o-Chloronitrobenzene (*a*), 0.0636 mole/l.; ethanolamine 16.25 mole/l.

Reaction time, hr.	Chlorine removed, %	Reaction time, hr.	Chlorine removed, %	Reaction time, hr.	Chlorine removed, %
Temp., 57°		Temp., 76°		Temp., 82°	
0.5	12.85	0.75	36.8	0.75	56.3
2.0	41.1	1.5	68.0	1.0	67.7
2.75	49.5	2.0	71.5	1.5	76.1
3.5	58.8	2.5	79.6	2.5	93.0
4.5	67.7	2.75	82.5	3.12	94.1
5.5	75.1	3.5	89.0		
$k = 6.75 \times 10^{-5}$		$k = 17.2 \times 10^{-5}$		$k = 21.8 \times 10^{-5}$	

TABLE VII

EFFECT OF THE VARIATION OF TEMPERATURE ON THE RATE OF REACTION BETWEEN *o*-CHLORONITROBENZENE AND *n*-BUTYLAMINE

o-Chloronitrobenzene (*a*), 0.0636, mole/l.; *n*-butylamine 10.02 mole/l.

Reaction time, hr.	Chlorine removed, %	Reaction time, hr.	Chlorine removed, %	Reaction time, hr.	Chlorine removed, %
Temp., 57°		Temp., 68°		Temp., 76°	
3.0	22.1	1.0	20.5	1.0	40.2
5.0	33.6	3.0	45.4	2.0	59.3
8.5	49.9	5.0	64.3	3.0	69.0
10.0	54.6	8.0	78.0	4.5	82.6
13.5	66.1	16.0	98.6	8.0	95.2
16.0	71.8				
$k = 2.27 \times 10^{-5}$		$k = 5.26 \times 10^{-5}$		$k = 9.18 \times 10^{-5}$	

TABLE VIII

TABULATION OF RATE CONSTANTS FOR THE REACTION BETWEEN *o*-CHLORONITROBENZENE AND ETHANOLAMINE AT VARYING TEMPERATURES

Temp., °K.	$1/T \times 10^5$	Rate constant, $k \times 10^5$	log k
330.2	302.8	6.75	−4.171
349.2	216.4	17.2	−3.765
355.2	281.5	21.8	−3.662

TABLE IX

TABULATION OF RATE CONSTANTS FOR THE REACTION BETWEEN *o*-CHLORONITROBENZENE AND *n*-BUTYLAMINE AT VARYING TEMPERATURES

Temp., °K.	$1/T \times 10^{5a}$	Rate constant $k \times 10^5$	Log k
330.2	302.8	2.27	−4.645
341.2	293.1	5.26	−4.280
349.2	286.4	9.18	−4.037

[a] T is absolute temperature.

Thus, for the ethanolamine reaction, in which $\Delta H^{\circ\ddagger} = 8.75$ kcal./mole^{-1}, $\Delta S^{\circ\ddagger} = -51.3$ e.u. and for the reaction with *n*-butylamine, $\Delta S^{\circ\ddagger} = -27.5$ e.u.

These results definitely show a greater loss of degrees of freedom on going to the transition state for the reaction between *o*-chloronitrobenzene and ethanolamine as against the reaction with *n*-butylamine. This loss of additional degrees of freedom for an analogous reaction is strong evidence for a cyclic transition state.

In order to provide further evidence for the cyclic transition state, a study was made in which the ordinary type of termolecular reaction would take place, that is, a reaction in which the nucleophilic and electrophilic groups were in different molecules. This was accomplished by using ethylamine and ethanol in equimolecular proportions and adding *o*-chloronitrobenzene in dioxane at 57.0°. The rate constants for this series are given in Table X. The rate constant for this reaction was found to be 12.87×10^{-7} sec.$^{-1}$, approximately one-third the rate for a comparable reaction with ethanolamine. A more rapid rate would be expected for the cyclic mechanism, since each time the nucleophilic group attacked, the electrophilic group would be in position to aid in the reaction. β-Methoxyethylamine was treated with *o*-chloronitrobenzene in dioxane at 57.0°. The data for these runs are presented in Table XI. The rate constant for this reaction was found to be 7.82×10^{-7} sec.$^{-1}$ as against 42.8×10^{-7} sec.$^{-1}$ for the reaction between ethanolamine and *o*-chloronitrobenzene in dioxane, using the same molar proportions. This demonstrated that when the actively functioning hydroxyl group in ethanolamine is converted to a relatively inactive ether, the compound acts like a monofunctional reagent.

TABLE X

RATE OF REACTION BETWEEN *o*-CHLORONITROBENZENE AND ETHYLAMINE IN ETHANOL AND DIOXANE AT 57.0°

o-Chloronitrobenzene, 0.1272 mole/l.; ethylamine, 2.05; ethanol, 2.05; dioxane, 8.04.

Reaction time, hr.	Chlorine removed, %	Reaction time, hr.	Chlorine removed, %
8	4.9	34	16.4
15	8.1	48	22.0
22	11.5	54	23.7

$k = 12.82 \times 10^{-7}$ sec.$^{-1}$

TABLE XI

RATE OF REACTION BETWEEN *o*-CHLORONITROBENZENE AND β-METHOXYETHYLAMINE IN DIOXANE AT 57.0°

o-Chloronitrobenzene, 0.1272 mole/l.; β-methoxyethylamine, 2.05; dioxane, 10.49.

Reaction time, hr.	Chlorine removed, %	Reaction time, hr.	Chlorine removed, %
8	3.4	34	10.4
15	5.8	48	13.3
22	7.5	54	14.4

$k = 7.82 \times 10^{-7}$

Conclusions

(1) The reaction between ethanolamine and *o*-chloronitrobenzene is of the nucleophilic displacement type, and the product is an almost quantitative yield of N-(2′-nitrophenyl)-ethanolamine, when the reaction is run at temperatures between 57 and 82° in a large excess of ethanolamine.

(2) The reaction is inhibited by alcohols and ethers.

(3) For the concentration of reactants used in these determinations, the over-all reaction rate was first order in all cases.

(4) The mechanism of the reaction between ethanolamine and *o*-chloronitrobenzene was interpreted as involving a cyclic intermediate in which the amino group of the ethanolamine is the nucleophilic group and the hydroxyl group of the same molecule is the electrophilic group.

(5) In hydroxylic solvents, the reaction was found to be first order in *o*-chloronitrobenzene and first order in ethanolamine, with an inverse second order dependence on solvent, in accordance with the rate equation

$$k = \frac{[\text{Ethanolamine}]}{a + b\,[\text{Solvent}]^2}$$

The inhibiting action of the solvent was tentatively related to its hydrogen-bonding capacity.

(6) The addition of phenol to the reaction mixture of ethanolamine, *o*-chloronitrobenzene and methanol was found to increase the rate of reaction initially and then to decrease it when the effective concentration of ethanolamine was reduced by acid–base reaction with the phenol.

(7) The energy of activation for the reaction between *o*-chloronitrobenzene and ethanolamine was found to be 9.4 kcal. mole^{-1} and for the reaction with *n*-butylamine it was 18.0 kcal. mole^{-1}. The entropy of activation for the ethanolamine reaction was −51.3 and −27.5 e.u. for the *n*-butylamine reaction. These figures are in accord with the argument for a cyclic transition state complex.

(8) With a mixture of ethylamine and ethanol in place of ethanolamine in the reaction with *o*-chloronitrobenzene the rate was one-third as fast as that obtained with ethanolamine, providing further evidence for the cyclic mechanism. When the hydroxyl group of the ethanolamine was replaced by methoxyl, the rate of reaction dropped to approximately one-sixtieth of a comparable ethanolamine reaction.

Acknowledgment.—The authors wish here to express their deep appreciation to Professor J. Steigman for a number of critical discussions and to the American Waterproofing Corporation in whose laboratories this work was carried out.

ADSORPTION STUDIES ON METALS. IV. THE PHYSICAL ADSORPTION OF ARGON ON OXIDE-COATED AND REDUCED NICKEL

BY A. C. ZETTLEMOYER, YUNG-FANG YU AND J. J. CHESSICK

Contribution from the Surface Chemistry Laboratory, Lehigh University, Bethlehem, Pa.

Received October 28, 1954

Isotherms for the adsorption of argon on oxide-coated nickel powder and on this sample after each of several reductions with dry hydrogen at 350° were determined at −195 to −183°. Equilibrium functions, isosteric heats of adsorption and integral molar entropy values were calculated. These data show a marked difference in the surface nature of the unreduced and reduced samples. However, the adsorption behavior of argon on the reduced samples was similar above monolayer coverage. In this region of adsorption the only effect of reductions at high temperature was to cause an increase in particle size due to sintering without markedly changing the surface nature of the reduced metal powder. The equilibrium function and isosteric heat data indicate that both the unreduced and reduced samples were heterogeneous. Adsorption sites of higher energy as well as a wider distribution of sites characterized the unreduced samples. Stronger cooperative effects leading to an increase in heat values and a subsequent maximum monolayer coverage was found for argon adsorption on the reduced sample. On the basis of experimental and calculated integral entropy values, a model of localized adsorption on a heterogeneous surface without adsorbate interactions explains the adsorption of argon on the unreduced and reduced sample. This model is probably not valid beyond $\theta = 0.5$ for the unreduced sample and beyond the relatively low value of $\theta = 0.2$ for the reduced sample; above these θ values lateral interaction set in. At very low coverages on both samples the heterogeneous nature of the surfaces was evident from the low molar entropy values S_s and small configurational entropy contribution.

Introduction

Gas adsorption techniques were employed in this Laboratory to study the surface heterogeneity of molybdenum metal.[1] A thick oxide film was formed on the molybdenum surface after exposure to moist air during storage. Reduction of this polymolecular oxide film by high temperature treatment with dry hydrogen increased the surface roughness or physical surface heterogeneity. After successive heatings in the presence of hydrogen a lower limit of surface area was reached. For a further understanding of metallic surface properties, this work has been extended to nickel.

Through the development of adsorption thermodynamics and its application to various adsorption systems in the last decade, it is now well established that thermodynamic functions are very useful for characterizing the properties of adsorbed films. However, because of the complexity of the different existing forces and the wide differences in surfaces, it is helpful to investigate more than one function before reaching final conclusions. A sharp initial drop of the isosteric heat with increasing surface coverage is generally attributed to the surface heterogeneity. Following Hill's[2] statistical development, the entropy of the adsorbed phase could be evaluated, which serves as a parameter for defining a surface. Furthermore, Morrison and Drain[3] were able to calculate the configurational and non-configurational entropy values of systems consisting of a heterogeneous surface. Recently, Graham[4] has introduced the equilibrium constant of a localized adsorption system for characterizing a surface. Very little work has been done with the last method. In the present work the conclusions from this free energy function are compared to those of isosteric heats and entropies.

Experimental

Materials and Apparatus.—The nickel sample furnished by the International Nickel Company had a reported purity when first prepared greater than 99%, and a particle size range from 2 to 25 μ. The sample was passed through a 400 mesh sieve before use to remove large particles.

High purity tank argon and helium were used. The argon was further purified by passage through fine copper gauze heated to 500° and dried with magnesium perchlorate. Helium was purified by passage through a charcoal trap immersed in liquid nitrogen.

Tank hydrogen, 99.8% pure, was passed slowly through a Baker Deoxo Unit, containing a palladium catalyst, and then through a drying train consisting of two magnesium perchlorate driers, a phosphorus pentoxide tube and a cold trap immersed in liquid nitrogen. Previous work in this Laboratory showed that water diffused into the reduction system if rubber connections were used. Therefore, the reduction system was of all-glass construction with Tygon tubing connections.

An Orr type[5] apparatus was used. Apiezon B oil which had a very low vapor pressure and did not dissolve measurable amounts of the gases studied was used in the manometers. Pressures as low as 0.005 cm. were measured with this oil. However, the height of the manometer restricted pressure measurements to about 5 cm. To increase the range of the manometer, a back pressure was applied to the vacuum side of the manometer for pressures greater than 5 cm. In this way, adsorption pressures as high as 20 cm. were obtained.

It was shown previously[6] that samples with an area as low as 0.5 m.^{2} could be studied with precision with this apparatus. Nevertheless, in this investigation sufficiently large samples were taken so that the total area ranged from 3 to 7 m.^{2}.

Pretreatment of Samples.—The unreduced, polycrystalline samples were first washed with absolute alcohol to remove any organic film. They were then degassed at room temperature for at least 12 hours to an ultimate pressure below 10^{-5} mm. before adsorption measurements were made.

Reductions of the surface oxide which had formed on the nickel powders on exposure to moist air during storage,[1] were carried out at 350°. The hydrogen after thorough drying was passed slowly through the samples at atmospheric pressure. The reduction times are listed in Table I. Two nickel samples which differed slightly in area but were obtained from the same batch were studied. The first sample was subjected to four reductions. After each reduction the sample was degassed at 25° to 10^{-5} mm. for 6 hours, then argon adsorption isotherms were determined at −195°. The second sample was studied primarily to substantiate the results found with the first sample as well as to obtain some additional data for the adsorption of argon at −183 and −195°. After the desired adsorption measurements were made, the samples were again subjected to hydrogen treatment at 350°. Since the reduced nickel was never

(1) F. H. Healey, J. J. Chessick and A. C. Zettlemoyer, THIS JOURNAL, **57**, 178 (1953).

(2) T. L. Hill, *J. Chem. Phys.*, **17**, 520 (1949).

(3) J. M. Drain and J. A. Morrison, *Trans. Faraday Soc.*, **48**, 316 (1952).

(4) D. Graham, THIS JOURNAL, **57**, 665 (1953).

(5) W. J. C. Orr, *Proc. Roy. Soc. (London)*, **173A**, 349 (1939).

(6) J. J. Chessick, Ph.D. Thesis, Lehigh University, 1952.

exposed to any gas except non-reactive helium and argon after the first reduction, the second and subsequent hydrogen treatments were not strictly reductions. Rather they were conducted to allow a study of the change of the surface properties of the metal as sintering progressed; they are labeled reductions merely as a convenience.

No effort was made to remove sorbed hydrogen from the reduced samples by degassing at elevated temperatures, since the primary objective of this investigation was to characterize two different surfaces—the oxide-coated and that produced by reduction—by gas adsorption methods. However, to determine the effect of this sorbed hydrogen on the reduced samples on the adsorption of argon, a separate sample was reduced under the usual conditions and degassed at 350° for 3 hours. Large amounts of hydrogen were evolved. Isotherms reduced to unit surface area for this sample and other samples which were reduced but not degassed at high temperature were found to coincide exactly above monolayer coverage indicating that in this region the argon adsorption was independent of any hydrogen presorbed. Beeck[7] also found that the adsorption of krypton on nickel films was independent of hydrogen presorbed in his sample

Procedure.—One of the often unrecognized difficulties in adsorption studies at low temperatures is the slow attainment of equilibrium at small adsorption pressures. Spurious rates or heat curves have been shown to result when insufficient time has been allowed for equilibrium.[6,8] To accelerate thermal equilibrium in the low pressure region, it was found expedient to precool the sample in the presence of helium at the adsorption temperature for 2 or 3 hours before adsorption measurements were made. The system was then degassed for 30 minutes at the adsorption temperature and argon adsorption measurements begun. As a result of precooling, equilibrium at pressures below 0.1 mm. was attained within 15 minutes; however, at least 1 hr. was allowed for equilibrium to be reached in the low pressure region.

Results and Discussion

Adsorption Isotherms.—Argon adsorption isotherms were measured at −195° on unreduced, oxide-coated nickel and on this sample after each of four successive reductions at 350°. The shapes of the isotherms indicated a marked difference in the behavior of argon adsorbed on the unreduced and reduced powders. Contrariwise, isotherms for argon adsorbed on the reduced nickel samples were found to be very nearly parallel in the region above monolayer coverage although they showed a decrease in the amount adsorbed after each reduction. This decrease, which exponentially approached a limiting value, resulted from a definite increase in particle size of the metal powder due to sintering at the reduction temperature. Confirmation of these initial results was obtained when similar studies were conducted on a new sample of lower initial area but obtained from the same batch of nickel powder. Furthermore, the temperature dependency for adsorption on this second sample was determined at −183 and −195° and isosteric heats of adsorption were calculated.

Some tentative conclusions concerning the natures of the nickel surfaces before and after reduction were possible from a knowledge of the prehistory of the nickel and a visual inspection of these isotherms. First, since the metal was polycrystalline, it was reasonable to assume that the surfaces were heterogeneous. Further, it was concluded that the distributions of adsorption energy sites on the oxide-coated and reduced metal were quite different. Finally, it appeared that while a new type of surface resulted after reduction of the oxide film, the effect on this new surface of sintering at high temperature was to cause a decrease in area without drastically changing its site energy distribution, particularly at higher coverages. Considerable evidence was obtained to substantiate these findings as well as to yield more quantitative information on the nature of these two different surfaces.

Adsorption Isotherms Reduced to Unit Surface Area.—Adsorption in the first layer, whether chemical or physical, depends on two factors: the extent of the surface and the energy of interaction between surface and adsorbate. Brunauer[9] designated the former the "non-specific" factor, the latter the "specific" factor in adsorption. This delineation was, of course, an oversimplification since the interactions between adjacent adsorbed molecules can be an important additional factor. However, if physical adsorption were completely "non-specific," then surface area alone would be controlling and isotherms for a gas adsorbed on all types of surfaces would coincide if volumes adsorbed per unit area were plotted against pressure. This situation would not exist, on the other hand, if surface "specificities" were also important. Isotherms of this nature were developed in order to differentiate between the adsorption behavior of argon on both the unreduced and reduced nickel samples. For this reason a measure of the specific areas of these samples was necessary.

The values for V_m were obtained by the usual BET method and represented the STP volumes of gas required to cover the surface of one gram of sample with one adsorbed layer. The specific areas of the samples were calculated from these V_m values assuming that the adsorbed molecules had the same hexagonal close-packing as in the liquid state.[10] Another method, the "B" point method of obtaining V_m and corresponding area values, was to use the volume adsorbed at the beginning of the linear portion of the Type II isotherms. The results of this latter method were adopted here

TABLE I

ADSORPTION OF ARGON ON NICKEL

Reduction no.	Time, hr.	BET V_m, ml./g.	BET Area, m.²/g.	"B" Point V_m, ml./g.	"B" Point Area, m.²/g.
		Sample 1, −195°			
Unreduced	...	0.195	0.73	0.167	0.63
1	2.0	.168	.63	.155	.58
2	3.5	.119	.45	.113	.43
3	2.5	.107	.40	.103	.39
4	3.0	.100	.38	.098	.37
		Sample 2, −195°			
Unreduced	...	0.154	0.57	0.133	0.50
1	2.5	.117	.44	.112	.42
2	2.0	.100	.37	.098	.37
		Sample 2, −183°			
Unreduced	...	0.152	0.59	0.126	0.49
1	2.5	.122	.47	.107	.42
2	2.0	.104	.40	.095	.37

(7) O. Beeck, "Advances in Catalysis," Vol. II, Academic Press, Inc., New York, N. Y., 1950, p. 160.

(8) F. C. Tompkins, *Trans. Faraday Soc.*, **34**, 1469 (1938).

(9) S. Brunauer, "The Adsorption of Gases and Vapors," Princeton Univ. Press, Princeton, N. J., 1943, p. 329.

(10) Ref. 9, p. 287.

because of the better agreement in area values calculated from V_m values at −183 and −195° obtained by this "B" point method. This agreement is shown in the last column of Table I for sample no. 2.

The isotherms measured for the adsorption of argon on unreduced nickel and on this same sample after each of four, successive, high temperature reductions are shown in Fig. 1. The adsorption values were reduced to unit area; *i.e.*, V/V_m values were plotted against relative pressure. There was no doubt that the "specific" forces whether surface, adsorbate interaction or both were different for argon adsorbed on unreduced and reduced nickel. On the other hand, the coincidence of the four isotherms for the reduced samples, although they differed in area by as much as 36%, strongly suggested that only small changes in these "specific" forces occurred as a result of sintering at the reduction temperature.

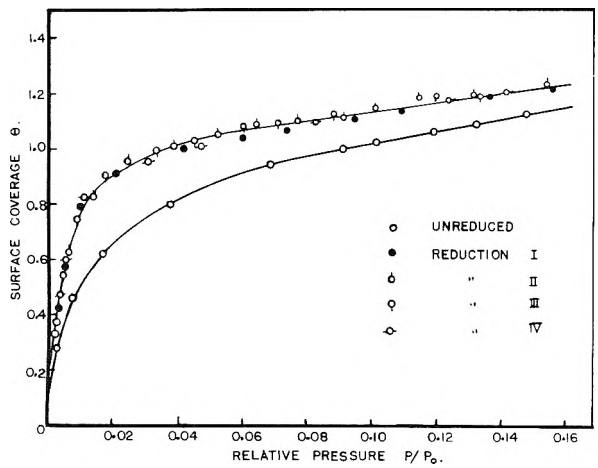

Fig. 1.—Adsorption isotherms of argon on nickel at −195° reduced to unit surface.

Free Energy Change of Adsorption.—Graham[4] developed a simple distribution function which he claimed provides the basis for a sharp classification of physical adsorption in terms of the surface properties of the adsorbent as well as adsorbate interaction. The equilibrium constant for the transfer of one mole of adsorbate from the standard state as a liquid to the adsorbed phase can be written

$$K = \frac{\theta}{(1-\theta)X} \qquad (1)$$

where θ is the fraction of surface covered and X is the relative pressure of the gas in equilibrium with solid. The free energy change is simply given by the relationship

$$-\Delta F^\circ = RT \ln K \qquad (2)$$

and constitutes a measure of the strength of the adsorption bond. In the ideal case involving localized, non-interacting adsorption on a uniform surface, K is a constant. Therefore, deviations of this constant from ideality can furnish information concerning the factors responsible for non-ideality such as lateral interactions between adsorbed molecules and the heterogeneous nature of the surface.

The equilibrium functions for the adsorption of argon on the second sample of the unreduced nickel and for this same sample after each of two successive reductions are shown plotted in Fig. 2 as a function of θ. The shape of the equilibrium function curve for argon adsorbed on the unreduced sample indicate adsorption on a heterogeneous surface. Initial adsorption took place on sites of high energy. Furthermore, these site energies decreased markedly with increasing θ. The equilibrium function was found to be nearly constant between $\theta = 0.5$ to $\theta = 0.8$, the criterion for adsorption on a uniform surface. However, a balance between coöperative adsorption and surface heterogeneity, itself, could be responsible for the constancy of K in this region.

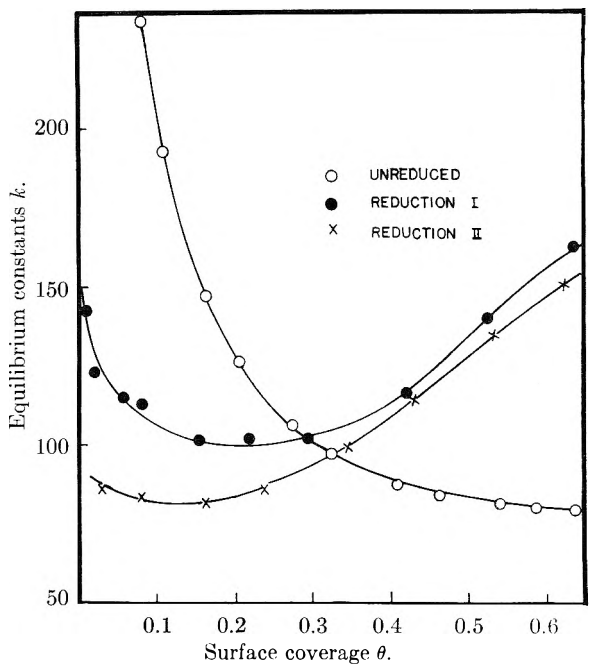

Fig. 2.—Equilibrium constants for argon adsorbed on nickel.

For the two reduced samples, the values of K were about 25 units apart at $\theta = 0.1$ and became nearly equal as θ increased. This initial difference was evidence for the presence of surface heterogeneities at low coverages which tend to disappear as a result of sintering. Generally, it appeared from the much lower K values that the reduced samples were less heterogeneous than the unreduced nickel. Consequently, interactions between adsorbed molecules and a subsequent increase in K began at very low coverages, *ca.* $\theta = 0.2$.

Isosteric Heats of Adsorption.—Isosteric heat values obtained from adsorption measurements on the second nickel sample are plotted in Fig. 3 as a function of the volume adsorbed. The sharp decrease in the heat values at small volumes adsorbed for the unreduced sample was of particular interest. A sharp initial decline in the heat values was found also for the reduced samples but over a smaller range of adsorption. Also, H_0, the heat of adsorption at zero coverage was approximately 1.6 kcal. greater for the unreduced sample than for this same sample after one reduction.

The rise in the heat curve and subsequent maximum near monolayer coverage are attributable to cooperative adsorption on the reduced surfaces. Almost exact coincidence of the heat curves for argon adsorbed on the reduced samples resulted if these values were plotted as a function of surface coverage θ indicative of adsorption on the same type of surface. However, at low values of θ the heats of adsorption were less after the second reduction. The equilibrium function and isosteric heat data indicate that both the unreduced and reduced nickel samples were heterogeneous and that these surface heterogeneities strongly influenced adsorption in the region of small θ for the reduced samples and to higher values of coverage for the unreduced nickel. Furthermore, the surface heterogeneities on the reduced samples tended to smooth out as a result of sintering at the high temperature employed in the reduction.

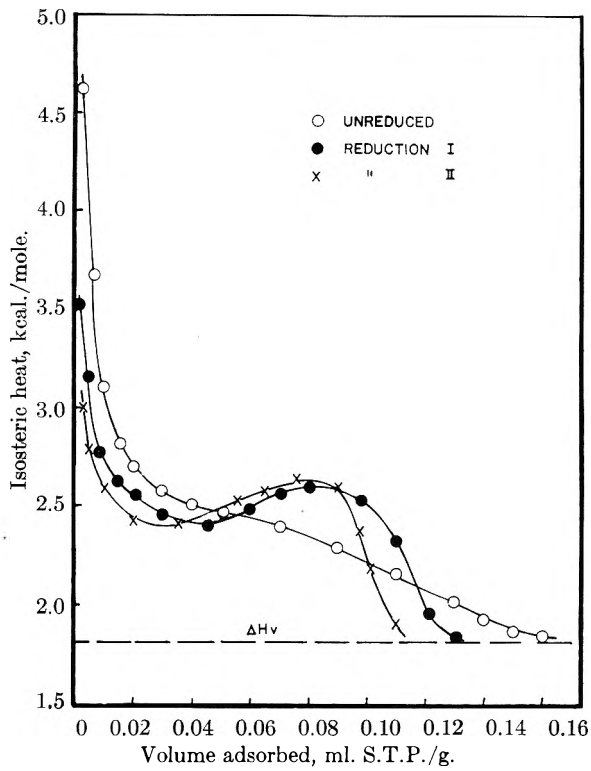

Fig. 3.—Isosteric heats of adsorption of argon on nickel.

Absolute Entropy of the Adsorbed Phase.—Hill[2] showed that for a model of localized adsorption on a heterogeneous surface without adsorbate interactions the configurational entropy at temperature T is given by the equation

$$S_c = k \ln \prod_i \frac{B_i!}{N_i!(B_i - N_i)!} \qquad (3)$$

where B_i represents the sities of energy i and N_i the number of molecules adsorbed on the B_i sites. The maximum possible configurational entropy S_m (T infinite) is expressed by the relationship

$$S_m = k \ln \frac{B!}{N!(B - N)!} \qquad (4)$$

and is independent of the distribution of site energies on the surface. S_m also gives the configurational entropy on a uniform surface. Drain and Morrison[3] carried out the arduous calculations necessary to obtain the configurational entropy from equation 3 as well as the non-configurational entropy for the adsorption of argon on rutile at 85°K. A knowledge of the site energy distribution for argon adsorbed on this solid at 0°K. was essential to their calculations and this in turn was obtained from calorimetric measurements of the heat capacities of adsorbed argon films down to very low temperatures. These heat capacity measurements probably represent the only method presently available to obtain a distribution function at 0°K. where the surface sites fill strictly in order of their energies.

Since it was impossible to obtain a proper distribution function for the argon–nickel systems studied here, the rigorous calculations of the type outlined by Hill could not be carried out. However on the basis of the model of localized adsorption on a heterogeneous surface, the integral molar configurational entropy is represented reasonably well by the equation

$$S_c = \frac{\pi^2}{3} \times R \times \frac{\mathrm{d} \ln V}{\mathrm{d} \ln p} \qquad (5)$$

This expression 5 is accurate for a site energy distribution wide compared to RT and should not be in error by more than 20% even for a homogeneous surface below monolayer coverage.[3]

In Fig. 4 the experimental molar entropies, S_s, for argon adsorbed on unreduced nickel and this sample after one reduction are plotted as a function of surface coverage, θ. The general shapes of the two curves are similar; *i.e.*, both show an increase in entropy with increasing adsorption in the range of low θ values and then remain little changed as coverage increases. The absence of high entropy values in the region of small θ was surprising for this adsorbate at this temperature and suggested that adsorption here took place on very heterogeneous portions of the surfaces with small contributions to the total entropy due to configurational effects and particularly so for the unreduced sample.

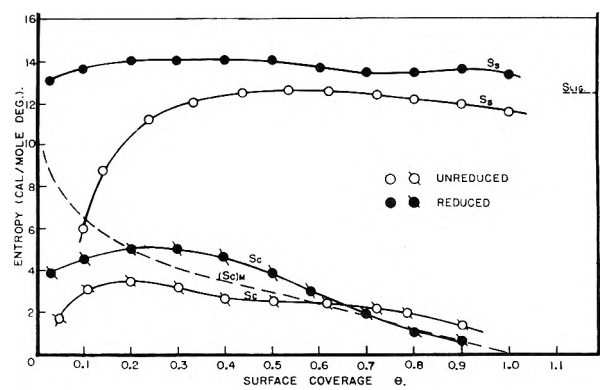

Fig. 4.—Molar and configurational entropies of argon on nickel.

For localized adsorption on a heterogeneous surface, configurational entropies calculated from equation 5 should be valid for the argon–nickel systems up to the point where cooperative adsorption began. Calculated configurational entropy

values for both nickel surfaces are compared in Fig. 4. These values were one to two entropy units lower for the unreduced surface and supported the contention based on previous data that this unreduced surface was the most heterogeneous of the two types studied. Furthermore, the configurational entropies for both surfaces tended toward zero as $\theta \rightarrow 0$, a fact already deduced from the shapes of the integral entropy curves at low θ.

The calculated S_c curves increased with increasing coverage and eventually exceeded the maximum possible configurational entropy, S_m. For the reduced sample, this took place at $\theta \sim 0.2$ and undoubtedly was evidence for the onset of adsorbate interactions at unusually low coverages. The equations developed by Hill[2] to treat adsorption on a heterogeneous surface with nearest neighbor interaction were too complex to treat mathematically even if a proper distribution function had been available. Thus it was likely that a model of localized adsorption on a heterogeneous surface without adsorbate interaction was not valid beyond $\theta = 0.2$ and $\theta = 0.5$ for the reduced and unreduced surfaces, respectively.

In the presence of interactions a division into a non-configurational and configurational entropy becomes arbitrary. Thus, it is difficult to interpret the essentially constant entropy values at higher coverages. These values are very near the entropy of liquid argon for both samples.

Acknowledgment.—The authors gratefully acknowledge the financial support provided by the Office of Naval Research, Project NR-057-186, Contract N8onr-74300.

SOME MEASUREMENTS OF DIFFUSION IN LIQUIDS

BY PIN CHANG AND C. R. WILKE

Division of Chemical Engineering, University of California, Berkeley, Calif.

Received November 26, 1954

Diffusion coefficients for iodine and toluene in a series of saturated hydrocarbons and for benzoic, acetic and formic acids in a number of organic solvents are reported. Data were obtained by the diaphragm cell method.

Introduction

At the present time diffusion in liquids is not fully understood. Besides inadequate theoretical description of the liquid state, insufficiency of experimental data has constituted one main difficulty in its investigation. Not all the data in the literature are sufficiently accurate, and some pertain to relatively high concentrations of the solute thereby requiring a knowledge of activity coefficients for interpretation. In addition there has been more extensive study of the diffusion of various solutes in a given solvent than of a single solute in various solvents. The latter is desirable for consideration of the role of solvent properties. This investigation was undertaken to provide additional data for dilute solutions to serve as a possible basis for the development of improved correlations of liquid diffusion.

Experimental

A. Solvents Used.—All solvents except normal hydrocarbons were of C.P. grade and were used without further purification.

The normal hydrocarbons were first passed through a silica gel column, and then distilled. The portion of distillate having a boiling point within one degree of the boiling point of the pure substance was recovered for use in the diffusion studies. The viscosities of the normal hydrocarbons were measured with an Ostwald viscosimeter. Their viscosities are compared with those reported in Timmermans[1] as follows.

Solvent	Viscosity of solvent used at 25°, C.p.	Viscosity of pure solvents at 25° reported in Timmermans
n-Decane	0.860	0.853
n-Dodecane	1.416	1.353
n-Heptane	0.384	0.389
n-Hexane	0.304	0.294
n-Octane	0.509	0.508
n-Tetradecane	2.12	...

(1) T. Timmermans, "Physico-chemical Constants of Pure Organic Compounds," Elsevier Publishing Co., Inc., New York, N. Y.

It is seen that except for *n*-dodecane and *n*-hexane viscosity values agree very closely with those reported in the literature.

B. Apparatus.—The diaphragm cell method was used for measurement and its principles and technique have been described previously.[2] The diaphragms had a pore diameter of two to five microns so that stirring had no detectable effect on the transport within the diaphragms. Each of the cells consisted of a vertical glass diaphragm approximately 3 mm. in thickness and 5 cm. in diameter separating the cell into two compartments having a volume of 80–100 ml. each. Short iron rods encased in glass were placed in each compartment to be operated as magnetic stirrers. Magnets were located suitably beneath the cells on pulleys which were rotated by a variable speed belt drive. This arrangement provided adequate stirring to maintain uniform concentrations in each compartment. The entire apparatus was built into an air-bath containing eight rotating magnets capable of simultaneous operation of four cells. Bath temperature was controlled to ±0.1°.

C. Procedure.—In treating the diffusion experiment the standard equation[2] was used

$$\log_{10} \frac{\Delta C_i}{\Delta C_f} = \beta' D_i t \qquad (1)$$

where

β' = the cell constant
D_i = the integral diffusion coefficient
t = time during an experiment
ΔC_i and ΔC_f = the initial and final concentration differences

Equation 1 is based on the assumption of concentration-independent diffusion coefficients and quasi steady-state conditions. Therefore the diffusion coefficient obtained is an integral diffusion coefficient. The cell constant, β', has to be determined with a standard substance whose diffusion coefficient is known as a function of concentration. For this purpose, 0.1 N KCl aqueous solution was used. For the diffusion of 0.1 N KCl solution in water until concentrations in the two compartments are, respectively, 0.075 and 0.025 N the integral diffusion coefficient is 1.870×10^{-5} cm.²/sec. at 25°[3] and 2.093×10^{-5} cm.²/sec. at 30°. The value at 30° is based on diffusion data obtained partly from Harned and Nuttall[3] and partly from the extrapolation by theory of Onsager and Fuoss.[3] Since

(2) A. R. Gordon, *N. Y. Acad. Sci.*, **46**, 285 (1945).

(3) H. S. Harned and R. L. Nuttall, *ibid.*, **51**, 781 (1949).

diffusion data of KCl up to 0.1 N solution at 4 and 25° and the existing data at 30° agree well with the theory, the values obtained by extrapolation were expected to be correct within their experimental error. This was evidenced by agreement between the values of cell constant obtained at 25 and 30°.

For a measurement, the solutions were kept at constant temperature in a water-bath. Either concentrated or dilute solution was charged into one compartment and application of vacuum to the other compartment enabled the solution to wet and fill up the glass diaphragm completely. This compartment was then filled. The other compartment was similarly filled with the other solution, and preliminary diffusion started in order to obtain a continuous concentration gradient of solute across the diaphragm. For estimating the time necessary to do so the following rule[2] was used

$$\frac{Dt}{L^2} = 1.2$$

where

t = time required
D = diffusion coefficient of the solute
L = effective length of the diaphragm

After sufficient time had elapsed, the solution in each compartment was replaced by fresh solutions and the normal diffusion period started. The normal diffusion period usually required a few days. At the end of the experiments, samples were withdrawn from each compartment for analysis. General practice was to run the experiment long enough so as to make $\log_e (\Delta C_i)/(\Delta C_f)$ larger than 1.2. In this case 1% error in titration would give about 4% error in diffusion coefficient.

D. Analyses.—The analyses of solute concentrations were performed by titration with a microburet graduated to 0.02 ml. Standard solution of sodium thiosulfate of concentration 0.05 N was used for analysis of iodine, and 0.1 N standard solution of sodium hydroxide was used for the analysis of the acids with phenolphthalein as indicator. The reproducibility of this titration was usually ±0.15%. For the determination of potassium chloride concentration, standard silver nitrate solution was used. The error in the value of the diffusion coefficient introduced by the titration was found to depend on the time of the experiment. It was important to titrate solutions in one run with the same standard solution so that the error in standardization of the solution, if any, would be cancelled out, producing no effect on the value of diffusion coefficients.

The analysis for toluene in normal hydrocarbons was made by means of a Beckman spectrophotometer. The extinction coefficients were determined and found to obey Beer's law. However, these extinction coefficients may not be those for the pure substances, for although the solvents had been refined, there was no proof that they were chemically pure. The diffusion coefficient was considered to be independent of the extinction coefficients as long as Beer's law was obeyed. Values of extinction coefficients for the solvents used are shown in Table I. The reproducibility of the spectrophotometric reading is within 1.5%.

TABLE I

EXTINCTION COEFFICIENTS OF TOLUENE IN NORMAL HYDROCARBONS

Solvent	Temp., °C.	Wave length, Å.	Molal extinction coefficient
n-Hexane	23.5	2600	185.0 ± 0.8
		2620	206.8 ± .7
n-Heptane	23.5	2600	109.7 ± .1
		2620	112.8 ± .2
n-Decane	23.5	2600	105.2 ± .4
		2620	106.3 ± .1
n-Dodecane	23.5	2600	148.2 ± .5
		2620	166.4 ± .6

E. Reliability of the Method for Measurements Used in This Investigation.—The reliability of the present method of measurement was examined by the following measures:

1. Calibration of the diaphragm cells at 25 and 30°, using data of Harned and Nuttall[3] for potassium chloride, gives reproducible cell constants. Furthermore, the measurement of diffusion coefficient of potassium chloride at 50.9° gave a value of 3.18×10^{-5} cm.²/sec. in agreement with the extrapolated value from the data of Harned and Nuttall at 25 and 30° (Table II).

TABLE II

DIFFUSION OF 0.1 N KCl INTO WATER

Temp., °C.	$D \times 10^5$, cm.²/sec.
25	1.870 (Harned and Nuttall)
30	2.093 (Harned and Nuttall)
50.9	3.18 (This research)
50.9	3.20 (Extrapolated value)

2. Measurement of the diffusion coefficient of hydrochloric acid at initial concentrations of 0.07 N and zero at 30° yielded a value of 3.40×10^{-5} cm.²/sec. Interpolation of data of James and Gordon[4] at 25 and 35° gave a value of 3.30×10^{-5} cm.²/sec. On the other hand, Falinski's datum[5] of 0.1 N HCl diffusing into water at 16° is also higher than the interpolated value from Gordon's data (Table III).

TABLE III

DIFFUSION OF 0.07 N HCl INTO WATER

	Diffusion coefficient, $D \times 10^5$ cm.²/sec.		
Temp., °C.	This research	Interpolation from Gordon	Falinsk
30	3.40	3.30	...
16	...	2.39	2.52

3. Measurement of diffusion coefficient of iodine in bromobenzene at 30° yielded 1.394×10^{-5} cm.²/sec. while the extrapolated value from Miller's data[6] came out to be 1.39×10^{-5} cm.²/sec.—in excellent agreement. Diffusion of iodine in carbon tetrachloride was also measured at 30° and compared with Miller's data. Table IV shows that the present values at mean concentrations of 0.0501 and 0.0921 N at 30° are, respectively, 1.58×10^{-5} and 1.51×10^{-5} cm.²/sec. compared with an extrapolated value of 1.53×10^{-5} cm.²/sec. from Miller's data for diffusion from 0.095 N to zero concentration in his apparatus. Since Miller used a different method of measurement, this integral coefficient would not correspond exactly to one obtained in this study with initial concentrations of 0.095 N and zero.

TABLE IV

DIFFUSION OF IODINE IN CCl_4

	$D \times 10^5$ cm.²/sec.		
Temp., °C.	This research	Miller	Av. concn., N
30	1.58	...	0.0501
	1.50	...	0.0921
		1.53	0.048

Results

Data for diffusion of benzoic acid, acetic acid, formic acid cinnamic acid, toluene and iodine are tabulated in Tables V through X. The reproducibility of data depended upon the duration of the experiment and the technique of titration. The acids and iodine were titrated by standard solutions with a microburet calibrated to 0.02 of a milliliter. Usually three milliliters of standard solutions were required to titrate a sample of larger volume, and it was possible to read the buret to 0.01 milliliter. The reproducibility was therefore within 0.3%. For the diffusion measurement, the values of $\Delta C_i/\Delta C_f$ were usually around 1.4. Since the diffusion coefficients depended on the logarith-

(4) W. A. James and A. R. Gordon, *J. Chem. Phys.*, **7**, 963 (1939).
(5) M. Falinski, *Compt. rend.*, **218**, 754 (1944).
(6) C. C. Miller, *Proc. Roy. Soc.* (*London*), **106**, 724 (1924).

TABLE V

DIFFUSION OF BENZOIC ACID

Solvent	Temp., °C.	$D \times 10^5$, cm.²/sec.	Viscosity of solvent $\eta \times 10^2$, poise	Initial cell compartment concn., g. mole/l.		$D\eta/T \times 10^{10}$
Carbon tetrachloride	14.8	0.78	1.048	0.07389	0	2.82
	25.0	0.91	0.907	.07227	0	2.76
	40.5	1.17	.732	.07216	0	2.74
Benzene	15.0	1.17	.696	.09060	0	2.83
	25.0	1.38	.503	.09061	0	2.79
	40.0	1.76	.497	.09052	0	2.78
Toluene	16.0	1.29	.620	.03195	0	2.76
	25.0	1.49	.552	.03195	0	2.77
	40.0	1.85	.471	.03018	0	2.78
Acetone	13.2	2.37	.342	.05089	0	2.82
	25.0	2.62	.312	.05099	0	2.75
	40.0	3.05	.268	.05088	0	2.73
Ethylene glycol	25.0	0.043 (±10%)	17.33	.05933	0	2.49
	50.0	0.18 (±10%)	6.62	.06048	0	3.77

TABLE VI

DIFFUSION OF ACETIC ACID[a]

Solvent	Temp., °C.	Diffusion coefficient $D \times 10^5$, cm.²/sec.	Viscosity of solvent $\eta \times 10^2$, poise	$D\eta/T \times 10^{10}$
Carbon tetrachloride	6.5	1.15	1.201	4.94
	14.8	1.27	1.052	4.63
	25.0	1.49	0.907	4.53
	40.0	1.78	.736	4.18
Benzene	25.0	2.09	.603	4.22
	5.9	1.58	.817	4.62
Toluene	25.0	2.26	.552	4.19
	15.0	1.90	.620	4.10
	6.8	1.66	.701	4.16
Acetone	40.0	4.04	.268	3.45
	25.0	3.31	.312	3.46
	15.0	2.92	.337	3.41
Ethylene glycol	15.0	0.039 (±10%)	26.09	3.5
	25.0	0.13 (±10%)	17.33	7.4
	30.0	0.20 (±10%)	13.35	8.8

[a] Initial cell compartment concentrations approximately 0.003 and 0 mole fraction.

TABLE VII

DIFFUSION OF CINNAMIC ACID

Solvent	Temp., °C.	$D \times 10^5$, cm.²/sec.	Viscosity of solvent $\eta \times 10^2$, poise	Initial cell compartment concn., g. mole/l.		$D\eta/T \times 10^{10}$
Carbon tetrachloride	25	0.76	0.907	0.03501	0	2.30
Benzene	25	1.12	.599	.03922	0	2.25
Toluene	25	1.18	.552	.03230	0	2.18
Acetone	25	2.41	.312	.04915	0	2.52

TABLE VIII

DIFFUSION OF TOLUENE

Solvent	Temp., °C.	$D \times 10^5$, cm.²/sec.	Viscosity of solvent $\eta \times 10^2$, poise	$D\eta/T \times 10^{10}$
n-Hexane	25.0	4.21	0.304	4.13
n-Heptane	25.0	3.72	0.384	4.80
n-Decane	25.0	2.09	0.860	6.04
n-Dodecane	25.0	1.38	1.416	6.54
n-Tetradecane	25.0	1.02	2.120	7.23
n-Heptane	6.9	2.95	0.469	4.94
	40.0	4.33	0.333	4.60

TABLE IX

DIFFUSION OF FORMIC ACID[a]

Solvent	Temp., °C.	Diffusion coefficient $D \times 10^5$, cm.²/sec.	Viscosity of solvent $\eta \times 10^2$, poise	$D\eta/T \times 10^{10}$
Carbon tetrachloride	8.5	1.61	1.163	6.65
	25.0	1.89	0.907	5.74
	15.0	1.67	1.048	6.08
Benzene	6.2	1.99	0.815	5.81
	13.9	2.31	.712	5.72
	25.0	2.28	.603	5.21
Toluene	6.2	2.28	.706	5.77
	14.1	2.46	.635	5.44
	25.0	2.65	.552	4.90
Acetone	25.0	3.77	.312	3.94
	13.5	3.27	.346	3.95
	6.5	3.13	.370	4.14
Ethylene glycol	25.0	0.094 (±10%)	17.33	5.5
	50.0	0.22 (±10%)	6.62	4.4

[a] Initial cell compartment concentrations approximately 0.003 and 0 mole fraction.

TABLE X

DIFFUSION OF IODINE IN VARIOUS ORGANIC SOLVENTS

Solvent	Temp., °C.	$D \times 10^5$, cm.²/sec.	Viscosity of solvent $\eta \times 10^2$, poise	Initial cell compartment concn., g. mole/g.		$D\eta/T \times 10^{10}$
n-Tetradecane	25	0.96	2.120	0.007745	0	6.81
n-Octane	15	2.43	0.579	0.04220	0	4.89
	25	2.76	0.508	.04210	0	4.71
	40	3.22	0.417	.04231	0	4.29
n-Hexane	25	4.24	0.304	.05600	0	4.31
Cyclohexane	15	1.54	1.056	.06389	0	5.65
	30	1.92	0.820	.06334	0	5.21
	40	2.30	0.703	.06383	0	5.17
Methylcyclohexane	40	2.71	0.549	.04422	0	4.74
	30	2.30	0.639	.04421	0	4.86
Ethyl alcohol	40	1.77	0.821	.1164	0	4.65
	25	1.32	1.065	.1165	0	4.71
Bromobenzene	30	1.39	0.985	.03043	0	4.53
Carbon tetrachloride	30	1.63	0.839	.01450[a]		4.57
		1.61		.03622[a]		
		1.58		.05005[a]		
				.09205[a]		

[a] Average concentration over both compartments during the diffusion measurement.

mic values of $\Delta C_i/\Delta C_f$, a reproducibility within 1.5% frequently was obtained, in fact, within 1% in many measurements.

For diffusion in very viscous solutions, for example the diffusion of acids in ethylene glycol, the data were not expected to be accurate because of the slow diffusion rate and resulting small contration changes during an experiment. They were expected to be good within 20%, however.

The diffusion of toluene at 25° in various normal hydrocarbons was studied. Analyses by the Beckman spectrophotometer were reproducible to within 1.5%. With a value of $\Delta C_i/\Delta C_f$ equal to 1.5, this reproducibility should give an accuracy of ±2% for the diffusion coefficient. No duplicate runs were made in normal hydrocarbons because of the limited amount of solvents.

Discussion

Data were taken at various temperatures for most of the systems. It was of particular interest to examine the group $D\eta/T$ which according to both the Stokes–Einstein equation and the Eyring theory should be essentially independent of temperature.[7]

The $D\eta/T$ groups for benzoic acid diffusion in carbon tetrachloride, benzene, toluene and acetone do not vary by more than 5% over a fairly wide range of temperature. Benzoic acid has an anomalous behavior in ethylene glycol, as shown by the appreciable change of $D\eta/T$ with temperature (Table V). This does not seem to be attributable to inaccuracy of the results as mentioned in the preceding section. However, it is not surprising in view of the complicated hydrogen bonding structure in ethylene glycol which may change in character with temperature.

Except for the systems of acetic acid in acetone and toluene and formic acid in acetone, formic acid and acetic acid do not give constant values of $D\eta/T$. This is possibly due to some complication from molecular association of formic and acetic acids.

In an adjunct paper[8] the authors have examined a large body of data and proposed an empirical equation for estimation of diffusion coefficients

$$D = 7.4 \times 10^{-10} \frac{T(xM)^{1/2}}{\eta V^{0.6}} \qquad (2)$$

where

D = diffusion coefficient, cm.²/sec.
T = temperature, °K.
M = solvent molecular weight
η = solution viscosity, poise
V = solute molar volume, cc./g. mole

The molar volume of the solute at its normal boiling point is estimated by the atomic contributions of Le Bas[9,10] for complex molecules. x is an association parameter for the solvent having a value of 1.0 for unassociated liquids and values of 2.6, 1.9 and 1.5 for water, methanol and ethanol, respectively. Although this equation has no quantitative theoretical basis it represents a large body of data with an average deviation of about 10%.

Figure 1 shows experimental data for diffusion of acetic and benzoic acids in several solvents plotted according to equation 2. Practically all the data fall within 10% of the correlation line indicating that satisfactory results are obtained assuming the acids to be in monomeric form.

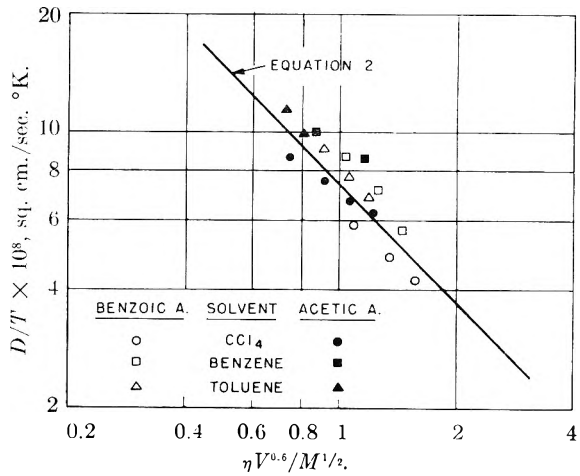

Fig. 1.—Diffusion of organic acids.

The diffusion rate of formic acid in ethylene glycol is lower than that of acetic acid, whereas the converse is true in other solvents. This is evidently due to the formation of ester. In the determination of the formic acid by titration with sodium hydroxide solution, a few drops of the latter, which is expected to be much less than the quantity required to neutralize the acid, suffice to turn the solution red with phenolphthalein, the color vanishing in about 30 seconds. This indicates that only a small fraction of the formic acid remains as formic acid in equilibrium with the ester.

Comparison of data in Tables X and XI indicates that diffusion of iodine in saturated hydrocarbons gives considerably higher values of $D\eta/T$ than diffusion in aromatic hydrocarbons of similar molecular weight. This is in agreement with the concept of complex formation in iodine–aromatic hydrocarbon systems as postulated by Benesi and

TABLE XI

DIFFUSION OF IODINE IN AROMATIC HYDROCARBONS

Solvent	Temp., °C.	$D\eta/T \times 10^{10}$	Densities of solvents	Viscosity $\eta \times 10^2$, poise
Benzene[a]	8.86	4.38	...	0.765
	19.91	4.29	0.888	.648
Toluene[a]	8.66	3.98	...	.675
	19.91	3.93	0.878	.588
m-Xylene[a]	8.90	3.74	...	.745
	19.91	3.74	0.872	.649
Benzene[b]	25.0	4.33	...	.605
Toluene[b]	25.0	3.99	...	.559
m-Xylene[b]	25.0	3.73	...	.589
Mesitylene[b]	25.0	3.39	...	.681

[a] C. C. Miller, *Proc. Roy. Soc. (London)*, **106**, 724 (1924).
[b] B. R. Hammond and R. H. Stokes, *Trans. Faraday Soc.*, **49**, 886 (1953).

(7) C. R. Wilke, *Chem. Eng. Prog.*, **45**, 219 (1949).
(8) C. R. Wilke and Pin Chang, presented at New York meeting, American Institute of Chemical Engineers, December, 1954.
(9) Perry, "Chemical Engineers' Handbook," McGraw-Hill Book Co., Inc., New York, N. Y., 1950.
(10) J. H. Arnold, *Ind. Eng. Chem.*, **22**, 109 (1930).

Hildebrand[11] and previously suggested to be a factor in iodine diffusion by Hammond and Stokes.[12]

From the foregoing discussion it is evident that a further theoretical approach is needed which adequately accounts for specific interactions of solvent and solute molecules to serve as a basis for improvement of empirical relations such as equation 2. Although not entirely satisfactory, the assumption of constancy in $D\eta/T$ appears to provide a fair representation of the temperature dependence. Equation 2 is considered to be useful as a first approximation for engineering design and certain other purposes for which moderate precision may be sufficient.

Acknowledgment.—Assistance of Research Corporation through a grant-in-aid is gratefully acknowledged.

(11) H. A. Benesi and J. H. Hildebrand, *J. Am. Chem. Soc.*, **71**, 2703-2707 (1949).

(12) H. R. Hammond and R. H. Stokes, *Trans. Faraday Soc.*, **49**, 886 (1953).

THE KINETICS OF DISPLACEMENT REACTIONS INVOLVING METAL COMPLEXES OF ETHYLENEDIAMINETETRAACETIC ACID

BY K. BRIL, S. BRIL AND P. KRUMHOLZ

Contribution from the Research Laboratory of Orquima S.A. São Paulo, Brasil

Received January 11, 1955

The kinetics of the reversible exchange reaction $PbY^{=} + Zn^{++} \rightleftarrows ZnY^{=} + Pb^{++}$ has been studied in acetate buffered solutions, at an ionic strength of one, at 25°, by means of the polarographic method using the streaming mercury electrode. The exchange proceeds *via* at least three simultaneous reaction paths. The proton-catalyzed reaction path is discussed on the basis of the "stationary state approximation." The equilibrium constant of the exchange reaction calculated from the kinetic measurements is in a very good numerical agreement with the value of this constant as determined by the usual equilibrium measurements.

Displacement reactions of the general type[1]

$$Me_{(1)} + Me_{(2)}Y \rightleftarrows Me_{(2)} + Me_{(1)}Y \qquad (1)$$

where Y represents the tetravalent anion of ethylenediaminetetraacetic acid (= Enta), are measurably slow processes.[2-10] Schwarzenbach and colleagues[7] studied in detail the kinetics of the reaction between copper(II) salts and the cadmium–Enta complex. They found that this apparently simple reaction proceeds actually *via* four different reaction paths

$$Cu + \begin{bmatrix} CdY \\ \uparrow\downarrow \\ CdYH \\ \uparrow\downarrow \\ Cd + YH \\ \uparrow\downarrow \\ Cd + YH_2 \end{bmatrix} \begin{matrix} \rightleftarrows Cd + CuY \\ \\ \rightleftarrows Cd + CuY + H \\ \\ \rightleftarrows Cd + CuY + H \\ \\ \rightleftarrows Cd + CuY + 2H \end{matrix} \qquad (2)$$

The reactions enclosed in the parentheses are assumed to be in a "quasi-equilibrium state" during the over-all exchange process.

Long and colleagues studied the kinetics of the exchange reaction 1 between radioactive iron(III) perchlorate and the iron(III) Enta complex.[6] They found the acid induced dissociation of the complex to be the "rate-determining step" of this exchange in acid solutions.

It seemed to us interesting to investigate further the mechanism of the exchange reaction 1 and in particular to examine how far the "quasi-equilibrium" hypothesis is justified. For this purpose it is desirable to choose a system where both the forward and the reverse reaction 1 can be conveniently measured.[11] The system

$$ZnY + Pb \rightleftarrows PbY + Zn \qquad (3)$$

was found convenient for such study, and the results obtained are reported.

The polarographic technique using the streaming mercury electrode as an indicator electrode of the progress of the reaction was applied throughout this work.

Experimental Part

Materials.—The preparation and the standardization of the Enta disodium salt, zinc nitrate and lead nitrate solutions were described in a previous communication.[8] The solutions of the metal–Enta complexes contained an excess of 0.5% of uncomplexed metal. The *p*H of these solutions was adjusted to about 5.5.

Apparatus.—The jet electrode arrangement, as well as the auxiliary equipment were described in a previous communication.[8] For the kinetic measurements a simple time registering device was used. Instead of taking galvanometer readings at given time intervals, the time intervals between suitably chosen galvanometer readings were determined. A disk of cardboard about 8 cm. in diameter is fixed on the axis of an electric clock. When making a galvanometer reading, one pushes down an ink writing pointer (fixed upon a flexible arm), which leaves a mark on the paper. This device allows the time to be determined with a precision of about 0.2 sec.

(1) In this and in the following equations ionic charges are omitted for the sake of simplicity.

(2) F. A. Long, S. Jones and M. Burke, Brookhaven Conference Report 2, Upton, N. Y., December 1, 1948.

(3) R. Pribil and E. Vicenova, *Chem. Listy*, **45**, 532 (1951).

(4) G. Schwarzenbach and E. Freitag, *Helv. Chim. Acta*, **34**, 1503 (1951).

(5) C. M. Cook, Jr., and F. A. Long, *J. Am. Chem. Soc.*, **73**, 4119 (1951).

(6) S. S. Jones and F. A. Long, THIS JOURNAL, **56**, 25 (1952).

(7) H. Ackermann and G. Schwarzenbach, *Helv. Chim. Acta*, **35**, 485 (1952).

(8) K. Bril and P. Krumholz, THIS JOURNAL, **57**, 874 (1953).

(9) K. Bril and P. Krumholz, *ibid.*, **58**, 339 (1954).

(10) G. Schwarzenbach, R. Gut and G. Anderegg, *Helv. Chim. Acta*, **37**, 937 (1954).

(11) In the system studied by Ackermann and Schwarzenbach,[7] the reverse reaction 1 is almost negligible and enters only as a numerically very small correction term into the over-all rate expression.

Calibrations and Measurements.—All measurements were made at 25 ± 0.1°, at an ionic strength of one adjusted with potassium nitrate. The *p*H of all solutions was maintained by means of an acetate buffer. All solutions were 0.1 *M* in sodium acetate; the concentration of acetic acid varied between 2.5×10^{-3} and 4×10^{-2} *M*.

The reaction progress was followed by measuring the diffusion current of the lead ion at a constant applied potential.

The diffusion current constant of lead (I_d) depends slightly upon the concentrations of both the zinc- and the lead–Enta complex.[8] I_d was determined in the presence of varying lead–Enta concentrations as described in our previous paper.[8] The influence of the zinc–Enta complex upon I_d was accounted for, where necessary, by extrapolating the time–diffusion current plot of the actual kinetic experiment to zero time. I_d was then calculated from the known initial lead concentration and the determined initial diffusion current. All other factors being constant, I_d was found to be constant within 1–2% in the lead concentration range 5×10^{-6} to 5×10^{-4} *M*.

The *p*H of all solutions was measured before and after the kinetic experiment with a precision of about ±0.01 *p*H unit.

For the kinetic measurements 20 ml. of a buffered metal–Enta complex solution was pipetted into the polarographic reaction cell, thermostatized and oxygen removed by passing a stream of pure nitrogen during about 30 min. Then the residual current of the metal-Enta solution was determined and compensated.

Meanwhile the solution containing the competing metal (at the same *p*H and ionic strength), was brought to the same temperature. The air was removed by means of a nitrogen stream introduced through a recalibrated 10-ml. pipet with a cut-off outflow tip. This pipet was used to deliver 10 ml. of the metal solution into the polarographic cell. It was verified that by this operation no measurable amount of oxygen was introduced into the reaction mixture. The outflow time of our pipet was about 1 sec. The mixing was accomplished by means of a rapid nitrogen stream. The mixing time determined by delivering 10 ml. of a solution of lead nitrate into 20 ml. of a lead–Enta solution, was of the order of the galvanometer period, a steady galvanometer reading being obtained after less than 2 sec.[12] Thus the uncertainty concerning the reaction time was also of about 2 sec.

The reaction was followed until equilibrium was reached. From the known initial concentrations, $(\ )_0$, and the observed equilibrium concentration of lead, $(Pb)_e$, the equilibrium constant K_{Zn}^{Pb} was calculated as described in a previous communication.[8] Its value was confirmed in a duplicate experiment in which all components of the reaction were mixed in exactly the same proportions as in the actual kinetic experiment, and the equilibrium concentration of lead measured after several hours standing. The values of K_{Zn}^{Pb} thus obtained agreed within better than 5%. This indicates clearly that no appreciable amount of lead ion was electrolyzed during the kinetic experiment.[8,13]

Experimental Results

The formal kinetics of the reaction 3 were studied first by mixing lead nitrate with the zinc–Enta complex in well buffered solutions containing zinc nitrate and zinc–Enta complex in great excess over lead. Under such conditions the diplacement reaction behaves like a reversible first-order reaction (see ref. 7). The rate expression

$$-\frac{d(Pb)}{dt} = v^+ - v^- = k^+(Pb) - k^-(PbY) \quad (4)$$

may be integrated directly, giving

$$\ln\{(Pb) - (Pb)_e\} = -(k^+ + k^-)t + \ln\{(Pb)_0 - (Pb)_e\} \quad (5)$$

where (Pb), $(Pb)_0$ and $(Pb)_e$ represent, respectively, the actual, initial and equilibrium concentrations of lead.[14] The equilibrium condition

$$k^+(Pb)_e = k^-(PbY)_e = k^-\{(Pb)_0 - (Pb)_e\} \quad (6)$$

makes it possible to calculate both kinetic "constants" k^+ and k^- from rate and equilibrium measurements.

For the graphic evaluation of equation 5 experimental points were used up to 10–20% away from equilibrium. The equilibrium concentration of the lead–Enta complex in the different experiments was equivalent to a 40–60% exchange. Relation 5 was found to be valid, within the experimental error, in the following range of concentrations

$$\begin{aligned} (Pb)_0 &= 1.6 \times 10^{-4}\ M \\ 2 \times 10^{-3}\ M < (ZnY)_0 &< 1.5 \times 10^{-2}\ M \\ 5 \times 10^{-3}\ M < (Zn)_0 &< 3 \times 10^{-2}\ N \\ 5 \times 10^{-7}\ M < [H] &< 1 \times 10^{-5}\ M \end{aligned} \quad (7)$$

For $(Zn)_0 < 10^{-2}$ *M* and $(ZnY)_0 < 5 \times 10^{-3}$ *M* we found

$$K_{Zn}^{Pb} = 2.95 \pm 0.2 \quad (8)$$

However with increasing zinc–Enta complex and zinc concentrations a small but systematic increase of K_{Zn}^{Pb} was observed. This is due to the formation of metal–metal–Enta ion pairs.[8,15]

In the indicated concentration range, k^+ is a linear function of the concentration of the zinc–Enta complex, and up to $[H] = 8 \times 10^{-6}$ *M* a linear function of the hydrogen ion activity[16] (see Fig. 1).

Inspection of Fig. 1 shows that k^+ can be represented according to

$$k^+ = \{k_0^+ + k_{Zn}[H]\}(ZnY) \quad (9)$$

k_{Zn}, as shown in Fig. 2, is a linear function of the reciprocal zinc concentration. For $1/(Zn)_0 = 0$, k^+ is still dependent upon the hydrogen ion activity. This indicates that k_{Zn} contains a term independent of the zinc concentration, so that k_{Zn} can be expressed as

$$k_{Zn} = k_1^+ + k_2^+/(Zn) \quad (10)$$

(12) The jet electrode, as an indicator electrode for kinetic measurements has a definite advantage over the conventional dropping mercury electrode, which makes necessary the use of long period galvanometers. Using the jet electrode in connection with a short-period automatic current–time registering device, it should be possible to follow even much faster reactions than those studied here.

(13) The electrolyzing potential was applied only when galvanometer readings were taken. Thus even for reaction mixtures taking about one hour or more to reach equilibrium, the total electrolysis time was never longer than about 3 minutes.

(14) In this and in the following equations, symbols like (Pb) represent the sum of free (hydrated) and weakly complexed (like $Pb(CH_3COO)_x$ or $Pb(NO_3)_2$) metal ions. The kinetic constants discussed represent therefore the sum of kinetic constants for processes in which those ions take part simultaneously.

(15) The influence of the metal–metal–Enta ion pair formation (see ref. 8) upon the K_{Zn}^{Pb} value is masked here partially by the high nitrate and acetate concentrations as well as the elevated ionic strength. This masking effect was discussed in a previous communication.[8] The comparison of the K_{Zn}^{Pb} value previously reported (= 14.5) and valid at 20°, 1.0 *M* nitrate concentration and in the *absence* of acetate buffer, with our present value of 2.95 indicates clearly that the acetate complexes of lead are more stable than the corresponding complexes of zinc (*cf.* eq. 10, p. 878, ref. 8); see S. Aditya and R. Prasad, *J. Indian Chem. Soc.*, **29**, 169 (1952); **30**, 213, 255 (1953); V. F. Toporova and F. M. Batyrshina, *C. A.*, **44**, 3392 (1950). NOTE: recently Schwarzenbach and colleagues[10] published new values of K_{Me2}^{Me1} for an extensive series of metal–Enta complexes (see for comparison ref. 4 and 8). The values reported are corrected for the influence of MeY–H formation. However, formation of other weak complexes (such as acetates) and(or) ion pairs, was neglected. This is the reason why the discrepancy between our[8] and Schwarzenbach's K_{Me2}^{Me1} values although small remains greater than allowed for by the experimental errors (especially for systems involving the lead ion).

(16) At lower *p*H, terms quadratic in [H] appear in the rate expression in accordance with the findings of Ackermann and Schwarzenbach[7] for the system cadmium–Enta + copper. The present study was limited to a *p*H range within which those terms are numerically negligible.

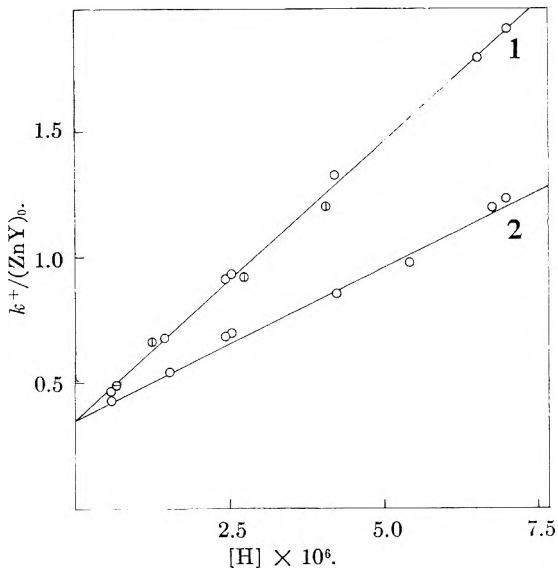

Fig. 1.—$k^+/(ZnY)_0$ as a function of the hydrogen ion activity; ionic strength = 1.0; nitrate solutions; acetate buffer; t = 25°; $(Zn)_0 = 5.45 \times 10^{-3}$ M (curve 1), 10.8×10^{-3} M (curve 2); $(ZnY)_0$ = ⊕, 2.02×10^{-3} M; ⊙, 4.69×10^{-3} M; ⊖, 10.06×10^{-3} M.

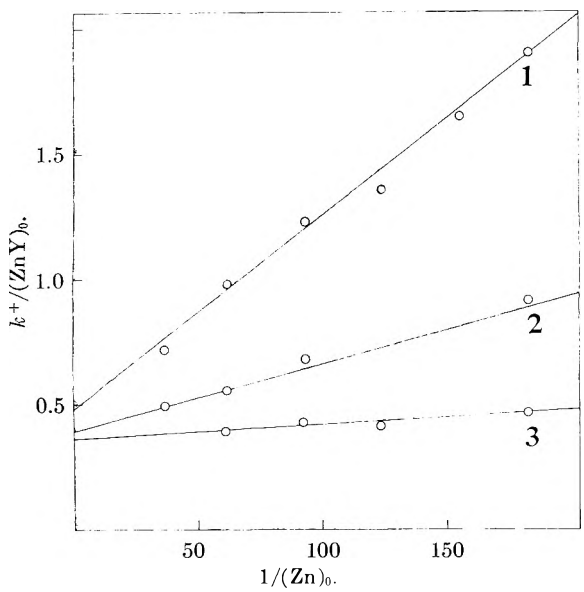

Fig. 2.—$k^+/(ZnY)_0$ as a function of the reciprocal zinc concentration; ionic strength = 1.0; nitrate solutions; acetate buffer; t = 25°; $(ZnY)_0 = 4.7 \times 10^{-3}$ M; pH 5.15 (curve 1), 5.61 (curve 2), 6.24 (curve 3).

The total rate expression for the forward reaction 3 may therefore be represented according to

$$v^+ = \left\{k_0^+ + k_1^+[H] + k_2^+\frac{[H]}{(Zn)}\right\}(Pb)(ZnY) \quad (11)$$

in full analogy with the findings of Ackermann and Schwarzenbach[7] for the reaction between copper nitrate and the cadmium–Enta complex.

The lines in Figs. 1 and 2 have been calculated according to equation 11 using the following numerical values for the constants

$$\begin{aligned} k_0^+ &= 0.34 && \text{moles liter}^{-1}\ \text{sec.}^{-1} \\ k_1^+ &= 2 \times 10^4 && \text{moles liter}^{-1}\ \text{sec.}^{-1} \\ k_2^+ &= 1.1 \times 10^3 && \text{moles liter}^{-1}\ \text{sec.}^{-1} \end{aligned} \quad (12)$$

In the concentration range investigated, experiment and theory agree within about 5% or better.

As already stated, the same set of experiments makes it possible to calculate k^- using relations 5 and 6. Independently, k^- was determined by studying the reaction between the lead–Enta complex and zinc. The "initial velocity method" was used for this study.[17] The uncertainty as to the v_0 value was estimated to about ±10%.

The lead–Enta complex concentration was var-

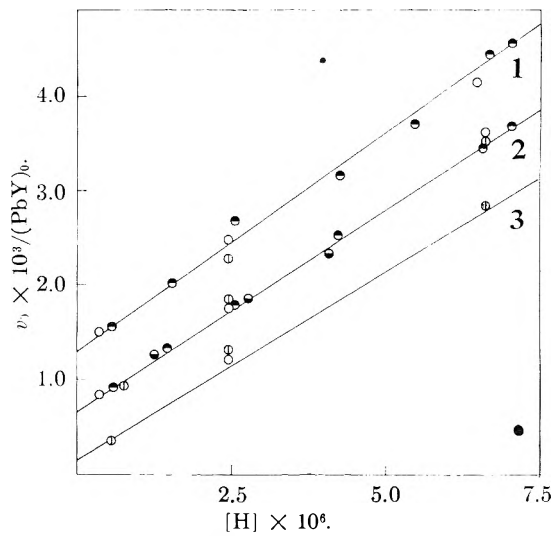

Fig. 3.—k^- as a function of the hydrogen ion activity at different zinc concentrations; ionic strength = 1.0, acetate buffer; t = 25°; $(Zn)_0 = 10.8 \times 10^{-3}$ M (curve 1); 5.45×10^{-3} M (curve 2); 1.32×10^{-3} M (curve 3). Points obtained from initial velocity measurements: ⊙ $(PbY)_0 = 0.101 \times 10^{-3}$ M and ⊕, $(PbY)_0 = 1.01 \times 10^{-3}$ M. Points obtained using relations 5 and 6: ◒, $(ZnY)_0 = 2.02 \times 10^{-3}$ M and ◓, $(ZnY)_0 = 4.69 \times 10^{-3}$ M.

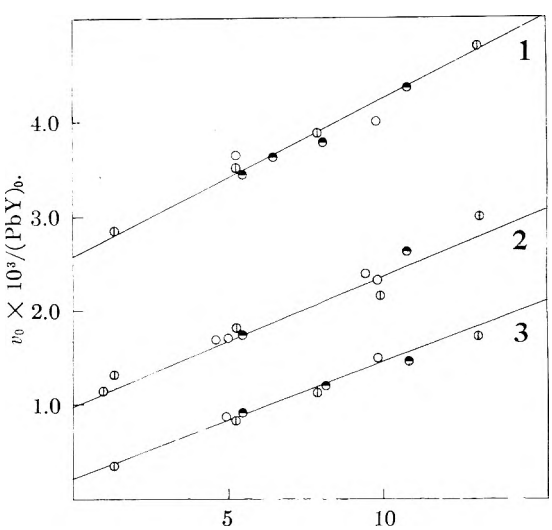

Fig. 4.—k^- as a function of the zinc concentration at different pH, ionic strength = 1.0; nitrate solutions; acetate buffer; t = 25°; pH 5.18 (curve 1), 5.61 (curve 2), 6.24 (curve 3). Points obtained from initial velocity measurements: ⊙, $(PbY)_0 = 0.101 \times 10^{-3}$ M and ⊕, $(PbY)_0 = 1.01 \times 10^{-3}$ M. Points obtained using relations 5 and 6: ◒, $(ZnY)_0 = 2.02 \times 10^{-3}$ M and ◓, $(ZnY)_0 = 4.69 \times 10^{-3}$ M.

(17) The initial velocity $(v)_0$ was determined by the usual extrapolation method of the velocity at time t, to $t = 0$.

ied between 5×10^{-5} M and 10^{-3} M. k^- was found independent, within the experimental error, of both lead–Enta and zinc–Enta concentrations. As shown in Figs. 3 and 4, k^- is proportional to the zinc concentration as well as to the hydrogen ion activity. There is no term in k^- independent of both those concentrations, but, clearly, one term dependent only upon the zinc concentration and a second one dependent only upon the hydrogen ion activity. However the existence of three terms in the rate expression for the forward reaction 3 makes necessary the occurrence of a third term in the rate expression for the reverse reaction. Inspection of Figs. 3 and 4 shows that the dependence of k^- upon the zinc concentration is slightly higher at greater values of the hydrogen ion activity, and *vice versa*. This indicates that the third term might be proportional to the product of both zinc and hydrogen ions concentrations.[18] The rate expression for the reverse reaction 3 could be thus represented by

$$v^- = \{k_0^-(\mathrm{Zn}) + k_1^-[\mathrm{H}](\mathrm{Zn}) + k_2^-[\mathrm{H}]\}(\mathrm{PbY}) \quad (13)$$

The lines drawn in Figs. 3 and 4 have been computed by means of equation 13 using the following values of the constants

$$\begin{aligned} k_0^- &= 0.12 && \text{moles liter}^{-1}\ \text{sec.}^{-1} \\ k_1^- &= 7.1 \times 10^3 && \text{moles liter}^{-1}\ \text{sec.}^{-1} \\ k_2^- &= 3.9 \times 10^2 && \text{moles liter}^{-1}\ \text{sec.}^{-1} \end{aligned} \quad (14)$$

Experimental values of both series of experiments agree within 10% (or better) with those computed according to relations 13 and 14; this agreement is quite satisfactory considering the greater experimental error involved in the determination of k^- as compared with k^+.

Discussion

To be correct the empirical equations 11 and 13 must be thermodynamically consistent. Introducing the condition of equilibrium

$$v_e^+ = v_e^- \quad (15)$$

the Guldberg and Waage equilibrium relation for reaction 3 should result. Grouping the terms according to the microreversibility principle, one finds easily the condition for "thermodynamic compatibility"

$$\frac{k_0^+}{k_0^-} = \frac{k_1^+}{k_1^-} = \frac{k_2^+}{k_2^-} = K_{\mathrm{Zn}}^{\mathrm{Pb}} \quad (16)$$

Experimentally we found: $k_0^+/k_0^- = k_1^+/k_1^- = k_2^+/k_2^- = 2.82$ as compared with the directly determined value of 2.95 ± 0.2. This good agreement confirms the thermodynamic correctness of both experimental rate expressions 11 and 13.

Grouping the terms of relations 11 and 13 according to equation 16 the experimental over-all rate expression for reaction 3 becomes

$$\begin{aligned} v = v^+ + v^- = {} & k_0^+(\mathrm{Pb})(\mathrm{ZnY}) - k_0^-(\mathrm{Zn})(\mathrm{PbY}) + \\ & + k_1^+(\mathrm{Pb})(\mathrm{ZnY})[\mathrm{H}] - k_1^-(\mathrm{Zn})(\mathrm{PbY})[\mathrm{H}] + \\ & + k_2^+\frac{(\mathrm{Pb})(\mathrm{ZnY})[\mathrm{H}]}{(\mathrm{Zn})} - k_2^-(\mathrm{PbY})[\mathrm{H}] \end{aligned} \quad (17)$$

The reaction paths as proposed by Schwarzenbach and Ackermann[7] (see eq. 2) for the exchange reaction between the copper nitrate and the cadmium–Enta complex are compatible with the experimental rate expression 17.

It is most probable that the first term of equation 17 expresses the velocity of the direct exchange reaction according to equation 3.

The second rate term of equation 17 can be correlated with the following reaction path

$$\mathrm{ZnY} + \mathrm{H} \rightleftarrows \mathrm{ZnYH} \quad (18a)$$

$$\mathrm{ZnYH} + \mathrm{Pb} \rightleftarrows \mathrm{PbYH} + \mathrm{Zn} \quad (18b)$$

$$\mathrm{PbYH} \rightleftarrows \mathrm{PbY} + \mathrm{H} \quad (18c)$$

provided that the rates of the dissociation and the formation of the protonated species are very rapid as compared with the rates of the direct and reverse displacement processes 18b. Under these conditions reactions 18a and 18c are in a quasi-equilibrium state, and the kinetic rate expression assumes the form of the second term of equation 17. We feel however that the experimental evidence is not good enough (see Experimental Results) for a quantitative interpretation of this reaction path.

The third rate term of equation 17 can be correlated with the reaction path

$$\mathrm{ZnY} + \mathrm{H} \underset{k_{2a}^-}{\overset{k_{2a}^+}{\rightleftarrows}} \mathrm{Zn} + \mathrm{YH} \quad (19a)$$

$$\mathrm{YH} + \mathrm{Pb} \underset{k_{2b}^-}{\overset{k_{2b}^+}{\rightleftarrows}} \mathrm{PbY} + \mathrm{H} \quad (19b)$$

Assuming reaction 19a to be in a quasi-equilibrium state it can be shown (see ref. 7) that the rate expression corresponding to this reaction path is identical with the third term in equation 17 if

$$k_2^+ = k_{2b}^+ k_{2a}^+/k_{2a}^- \text{ and } k_2^- = k_{2b}^-$$

The validity range of the quasi-equilibrium assumption can be deduced easily by means of the stationary state approximation.[19] Due to the equilibrium position of both series reactions 19, the concentration of HY will remain always very small as compared with the concentrations of all other reaction partners.[20] The stationary state approximation is thus applicable and allows the calculation of the concentration of HY during the over-all exchange process. One finds easily

$$(\mathrm{YH}) = \frac{k_{2a}^+(\mathrm{ZnY}) + k_{2b}^-(\mathrm{PbY})}{k_{2a}^-(\mathrm{Zn}) + k_{2b}^+(\mathrm{Pb})}[\mathrm{H}] = \alpha[\mathrm{H}] \quad (20)$$

Using relation 20 the rate expression for the reaction path 19 becomes

$$-\frac{\mathrm{d(Pb)}}{\mathrm{d}t} = k_{2b}^+(\mathrm{Pb})[\mathrm{H}]\alpha - k_{2b}^-(\mathrm{PbY})[\mathrm{H}] =$$

(18) This conclusion is supported by theoretical considerations as will be shown in the discussion of the experimental results.

(19) The reaction path 19 represents a proton catalysis of reaction 3 and may be treated mathematically as such. See G. M. Schwab, "Katalyse vom Standpunkt der chemischen Kinetik," J. Springer, Berlin, 1931; R. P. Bell, "Acid-Base Catalysis," Clarendon Press, Oxford, 1941. Displacement reactions of this type were treated mathematically by K. H. Herzfeld, *Z. physik. Chem.*, **98**, 161 (1921). For a more rigorous treatment of the stationary state approximation see the papers of Skrabal, *i.e.*, *Monatsh.*, **74**, 293 (1943).

(20) Using the values of the dissociation constants for both PbY and ZnY as determined by Schwarzenbach and colleagues (see ref. 10), and the ionization constants for Enta acid as reported by G. Schwarzenbach and H. Ackermann, *Helv. Chim. Acta*, **30**, 1798 (1947), it is possible to calculate, approximately, the equilibrium constants of both elementary reactions 19a and 19b.

$$\frac{d(Zn)}{dt} = k_{2a}^{+}(ZnY)[H] - k_{2a}^{-}(Zn)[H]\alpha = \frac{k_{2a}^{+}k_{2b}^{+}(ZnY)(Pb) - k_{2a}^{-}k_{2b}^{-}(PbY)(Zn)}{k_{2a}^{-}(Zn) + k_{2b}^{+}(Pb)}[H] \quad (21)$$

Under the condition that

$$k_{2b}^{+}(Pb) << k_{2a}^{-}(Zn) \quad (22)$$

relation 21 assumes the following form

$$-\frac{d(Pb)}{dt} = k_{2b}^{+}\frac{k_{2a}^{+}}{k_{2a}^{-}}(ZnY)(Pb)\frac{[H]}{(Zn)} - k_{2b}^{-}(PbY)[H] \quad (23)$$

which is obviously identical with the third term of the experimentally found equation 17.

We have now to verify whether condition 22 was fulfilled in our experiments. For the reverse reaction 3, studied by the method of initial velocities, the initial lead concentration is zero, or at least very small, so that the condition 22 is satisfactorily fulfilled. In the case of the forward reaction 3 the lead concentration was, in our experiments, at least one-thirtieth that of zinc. Even if the greater stability of the lead–Enta complex, as compared to the zinc–Enta complex ($K_{Zn}^{Pb} \simeq 3$), is due exclusively to a higher rate of formation ($k_{2b}^{+} \simeq 3k_{2a}^{-}$), $k_{2a}^{-}(Zn)$ will still be about 10 times greater than $k_{2b}^{+}(Pb)$. Under the limited precision of our experiments the influence of this term upon the denominator of 21 would fall within the experimental errors.

The formal agreement between the empirical and deduced rate equation for the third reaction path does not constitute a definite proof that the formulated reaction sequence 19 is the only one, or even the most important. It is possible and even probable that this reaction path occurs *via* the protonated complexes, MeY–H, according to the reaction sequence

$$ZnY + H \underset{k_{2c}^{-}}{\overset{k_{2c}^{+}}{\rightleftharpoons}} ZnYH \quad (24a)$$

$$ZnYH \underset{k_{2d}^{-}}{\overset{k_{2d}^{+}}{\rightleftharpoons}} Zn + YH \quad (24b)$$

$$Pb + YH \underset{k_{2e}^{-}}{\overset{k_{2e}^{+}}{\rightleftharpoons}} PbYH \quad (24c)$$

$$PbYH \underset{k_{2f}^{-}}{\overset{k_{2f}^{+}}{\rightleftharpoons}} PbY + H \quad (24d)$$

As long as the stationary state approximation can be applied to the particles ZnYH, PbYH and YH kinetics offer no means of distinguishing between this sequence and 19.[21] It is further possible that not only protons but also undissociated acetic acid reacts with the metal–Enta complexes. This means that reaction 3 could be not only proton, but generally acid catalyzed.

(21) The stationary state approximation gives for the reaction path 24 the following rate expression

$$-\frac{d(Pb)}{dt} = \frac{k_{2c}^{+}k_{2d}^{+}k_{2e}^{+}k_{2f}^{+}(ZnY)(Pb)[H] - k_{2c}^{-}k_{2d}^{-}k_{2e}^{-}k_{2f}^{-}(PbY)(Zn)[H]}{(k_{2e}^{-} + k_{2f}^{+})k_{2c}^{-}k_{2d}^{-}(Zn) + (k_{2c}^{-} + k_{2d}^{+})k_{2e}^{-}k_{2f}^{+}(Pb)}$$

which is identical in form with relation (21).

THE SECOND AND THIRD ORDER INTERACTION OF A MIXTURE OF GASES AND A SURFACE[1]

BY TAKAO KWAN,[2] MARK P. FREEMAN[3,4] AND G. D. HALSEY, JR.

Department of Chemistry, University of Washington, Seattle, Washington

Received January 14, 1955

Expressions are developed for the second and third mixed virial coefficients between a solid and a two-component gas mixture. The apparent volume of a vessel filled with a high surface-area powder is developed as a function of mole fraction of the gas mixture and these coefficients. Numerical evaluation of the constants is made on the basis of a cube-law attraction energy with the surface and hard-sphere repulsion for the gases. Experiments are reported for the systems argon–krypton–alumina, argon–methane–charcoal, and argon–nitrogen–charcoal. The agreement is satisfactory.

Introduction

This paper is an extension of previous work[5–7] on the interaction of a gas and a surface under conditions such that the highest important interactions are between pairs of gas molecules. The experimental method is to measure the apparent volume of the vessel containing the finely divided solid with, in this case, a mixture of gases of known composition. Since the experiments reported here are for mixtures of two gases only, it will suffice to generalize the derivation[7] of the second- and third-order interactions of a single gas to the three component case: that is, surface, gas A, and gas B.

Development of the Virial Expansion.—We shall not repeat the complete derivation of the earlier reference, but only point out the essential differences brought on by the introduction of the second gaseous component. We shall need to consider the following interaction energies: u_i^A and u_j^B, the interaction between the surface and the single molecules of species A and B; u_{ij}^{AA} and u_{kl}^{BB}, the interactions between similar pairs of gas molecules;

(1) Presented at the 127th National Meeting of the American Chemical Society, Cincinnati, Ohio, March 29–April 7, 1955.

(2) The Research Institute for Catalysis, Hokkaido University, Sapporo, Japan. Fullbright Scholar, Visiting Lecturer, University of Washington, 1954–1955. Present address: Frick Chemical Laboratory, Princeton, N. J.

(3) National Science Foundation Predoctoral Fellow, 1954–1955.

(4) Presented in partial fulfillment of the requirements for the degree of Doctor of Philosophy.

(5) W. A. Steele and G. D. Halsey, Jr., *J. Chem. Phys.*, **22**, 979 (1954).

(6) W. A. Steele and G. D. Halsey, Jr., THIS JOURNAL, **59**, 57 (1955).

(7) Mark P. Freeman and G. D. Halsey, Jr., *ibid.*, **59**, 181 (1955).

and u_{ij}^{AB}, the interaction between a dissimilar pair. Given N_A molecules of species A and N_B molecules of B, we must make a summation of these energies to arrive at the total potential energy. This will yield an expression analogous to eq. 1 of our previous paper.

If we now define a set of functions of the form

$$f_i^A = \exp\{-u_i^A/kt\} - 1, \text{ etc.} \quad (1)$$

and

$$f_{jk}^{AB} = \exp\{-u_{jk}^{AB}/kt\} - 1, \text{etc.} \quad (2)$$

we can perform a derivation analogous to but considerably more cumbersome than our earlier one. It leads to the expression for the total pressure for a geometric volume V_{geo} and a temperature T

$$P = NkT\left\{\frac{X_A}{V_{geo}+B_{AS}} + \frac{1-X_A}{V_{geo}+B_{BS}} - N\left[\frac{X_A^2 C_{AAS}}{(V_{geo}+B_{AS})^3} + \frac{(1-X_A)^2 C_{BBS}}{(V_{geo}+B_{BS})^3} + \frac{X_A(1-X_A)C_{ABS}}{(V_{geo}+B_{AS})(V_{geo}+B_{BS})}\left(\frac{1}{V_{geo}+B_{AS}} + \frac{1}{V_{geo}+B_{BS}}\right)\right]\right\} \quad (3)$$

Here, N is the total number of gas molecules of both species, and X_A is the mole fraction of species A. The B_{GS}'s and C_{GGS}'s stand for integrals of the type

$$B_{BS} = \int_{V_{geo}} f_1^B \, d\tau_1^B \quad (4)$$

and

$$C_{ABS} = \iint_{V_{geo}} (1+f_1^A)(1+f_1^B) f_{11}^{AB} \, d\tau_1^A \, d\tau_1^B \quad (5)$$

$$C_{GGS} = \iint_{V_{geo}} (1+f_1^G)(1+f_2^G) f_{12}^{GG} \, d\tau_1^G \, d\tau_2^G \quad (6)$$

where the symbol G stands for either A or B and $d\tau_i^G$ is the differential volume element available to the ith molecule of species G.

For convenience, we write

$$1/V_0 = \frac{X_A}{V_{geo}+B_{AS}} + \frac{1-X_A}{V_{geo}+B_{BS}} \quad (7)$$

We also define C_0 so that

$$C_0/V_0^3 = \frac{X_A^2 C_{AAS}}{(V_{geo}+B_{AS})^3} + \frac{(1-X_A)^2 C_{BBS}}{(V_{geo}+B_{BS})^3} + \frac{X_A(1-X_A)C_{ABS}}{(V_{geo}+B_{AS})(V_{geo}+B_{BS})}\left(\frac{1}{V_{geo}+B_{AS}} + \frac{1}{V_{geo}+B_{BS}}\right) \quad (8)$$

If we now introduce the apparent volume defined as before by the perfect gas law

$$V = NkT/P \quad (9)$$

and substitute into equation 3 using the definitions (7) and (8) we find

$$1/V = (1/V_0) - (C_0/V_0^3)(PV/kT) \quad (10)$$

Notice that at $P = 0$, $V = V_0$. Also

$$\frac{\partial 1/V}{\partial PV} = -C_0/V_0^3 kT \quad (11)$$

At $P = 0$, this expression reduces to

$$\partial V/\partial P|_0 = C_0/kT \quad (12)$$

This is the generalized form of eq. 18 of the previous paper. It remains to show how V_0 and C_0 vary with mole fraction.

Variation of the Intercept and Slope with Mole Fraction.—The variation of the apparent volume extrapolated to zero pressure is given directly by the simple expression defining V_0, eq. 7.

However, the slope C_0/kT is now given by the rather awkward expression

$$C_0/kT = V_0^3/kT\left[\frac{X_A^2 C_{AAS}}{(V_{geo}+B_{AS})^3} + \frac{(1-X_A)^2 C_{BBS}}{(V_{geo}+B_{BS})^3} + \frac{X_A(1-X_A)C_{ABS}}{(V_{geo}+B_{AS})(V_{geo}+B_{BS})}\left(\frac{1}{V_{geo}+B_{AS}} + \frac{1}{V_{geo}+B_{BS}}\right)\right] \quad (13)$$

The functional dependence of slope on X_A is somewhat obscured in this equation owing to the implicit relationship of V_0 with X_A. If it happens that we are studying two gases and the apparent volumes of each of the pure constituents at zero pressure are not too far apart, then we can gain more insight into the functional dependence in (12) by expanding it in terms of

$$\delta = (B_{AS} - B_{BS})/(2V_{geo} + B_{AS} + B_{BS})$$

to yield the result

$$C_0/kT = 1/kT\{[X_A^2 C_{AAS} + (1-X_A)^2 C_{BBS} + 2X_A(1-X_A)C_{ABS}] + 6\delta X_A(1-X_A)[-X_A C_{AAS} + (1-X_A)C_{BBS} + [X_A - (1-X_A)]C_{ABS}] + 0(\delta^2)\} \quad (14)$$

Notice that when δ approaches zero, this expression reduces to the same form as that for the second virial coefficient for a mixture of two gases.[8]

Crude Model for Evaluating the Third Virial Coefficient.—We shall retain the same crude hard sphere model as before.[7] This leaves us but one new parameter to evaluate, C_{ABS}. C_{AAS} and C_{BBS} may be evaluated directly from the parametric representations and tabulations of our previous papers.[5,7]

In the evaluation of C_{ABS} we follow a derivation essentially identical to that for C_{GGS}, but differing in the following respects.

(1) The energies of interaction at the distance of closest approach (ϵ_G^*) are now different for the two atoms.

(2) The distance of closest approach of atoms of different species (D_{AB}) is taken to be $(D_{AA} + D_{BB})/2$.

(3) The unit length is now taken to be D_{AB}.

(3a) (δ_G) is now taken to be D_{GS}/D_{AB}.

(4) The area available for interaction is taken to be the area available to the gas atom with the lesser area as defined in ref. (5). That is, it has been found that when applying this model,[6] different gases will have slightly different available areas of interaction with the solids. This difference probably reflects the imperfection of the model, but if we assume that the model is correct and that more

TABLE I

Adsorbent	Gases	ϵ^* (kcal./mole)	A (m.²/g.)	D_{GS} (Å.)	D_{GG} (Å.)	D_{AB} (Å.)
Alumina	Krypton	3.46	131	1.99	3.61	3.52
	Argon	2.80		1.87	3.42	
Charcoal	Methane	4.64	980	3.30	3.88	3.65
Saran S-85	Argon	3.66		2.90	3.42	
Charcoal	Nitrogen	3.70	1030	2.59	3.68	3.55
Saran S-85	Argon	3.66		2.90	3.42	

(8) See R. H. Fowler and E. A. Guggenheim, "Statistical Thermodynamics," Cambridge University Press, Cambridge, 1952, p. 297, eq. 720.3.

area is available to one species owing to, say, its small size permitting it to penetrate crevices forbidden to the other, we may assign the lesser area to the interaction. Areas and other parameters used in evaluating C_{ABS} are tabulated in Table I.

(5) The limits of integration must be modified to account for the difference in atomic size involved.

It should be mentioned that we are given both D_{AB} and D_{GS} for each gas involved. This is too much information unless different gases interact with different effective planes of interaction in the solid. We shall make this assumption.

With the above restrictions in mind, we can go through a derivation exactly like that for C_{GGS}. Equation 5 becomes

$$C_{ABS} = -\pi A D_{AB}{}^4 \int_{\sigma_A} \exp\left\{\frac{\delta_A^3 \epsilon_A^*}{kT\sigma_A^3}\right\} \left\{\int_{\sigma_B} \exp\left\{\frac{\delta_B^3 \epsilon_B^*}{kT\sigma_B^3}\right\} [1 - (\sigma_A - \sigma_B)^2] d\sigma_A d\sigma_B \quad (15)$$

where σ_B goes from the limits $\sigma_A - 1$ when $\sigma_A - 1 > \delta_B$ and otherwise from δ_B to $\sigma_A + 1$, and σ_A goes from δ_A to $V_{geo}/AD_{AB} \approx \infty$.

This is the expression we integrated, but no general parametric representation is possible in this case for instead of the two parameters we had in the evaluation of C_{GGS}, we now have four parameters which would require a hyperspace representation. C_{ABS} must therefore be re-evaluated for each new situation.

Notice the square bracket in equation 15 is to the first power. A typographical error in our previous paper[7] put a square root sign over the analogous term in eq. 22.

Equation 13 is in such a form that C_{ABS} may be directly evaluated from the experimental results if we know C_{AAS} and C_{BBS}. These in turn may be evaluated from equation 13 when it is expressed for the pure constituents ($X_A = 1, 0$). Alternatively we can of course use the theoretical values of C_{AAS} and C_{BBS}.

It is not easy to find rare gas combinations that cover the situations we felt to be of interest, so that in two of the three cases we used one molecular gas in conjunction with a rare gas. We might expect that when a molecular gas is involved one would get considerably more deviation from the hard sphere behavior assumed by the crude model.

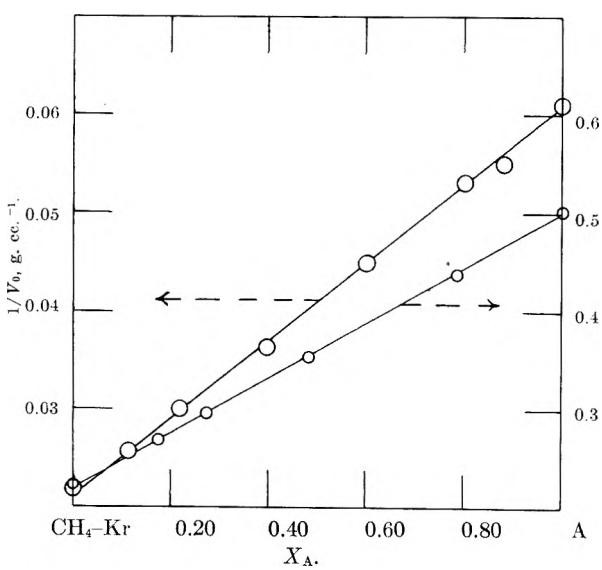

Fig. 1.—Reciprocal intercept *vs.* mole fraction argon for two systems: left, methane–argon–Saran S-85 (32.37°); right, krypton–argon–alumina (−45.20°).

Experimental.—The apparatus has been described previously,[5-7] and the gases and solids used have been described in these same papers.

The only new step involved was that of making the gas mixtures. The gases used were first measured out in a buret and then introduced into a one-liter flask where they were mixed by heating on one side with a small flame. Otherwise the technique was similar to that used previously.[5]

Comparison of Theory with Experiment.—Three systems were investigated: argon and krypton over alumina at −45.20°; argon and methane over Saran charcoal S-85 at 32.37°; and argon and nitrogen over the same charcoal at 0°.

The comparison with theory can be made in two stages. First, the functional dependence of slope and intercept on mole fraction is given rigorously by equations 7 and 11 or 12. Then the values of the "C's" needed for the best fit may be compared with those calculated by the crude theory. Only rough agreement may be expected.

A plot of the reciprocal of the intercept shows the required straight line form as a function of mole fraction (Fig. 1). The values of B_{AS} and B_{BS} have already been shown[5,6] to be in satisfactory accord with the crude model.

In Fig. 2, the experimental slopes for the system argon–methane–charcoal are compared with the best theoretical line as calculated from equation 13, with the C's as adjustable parameters where the C_{GGS}'s are evaluated from 13 applied to the pure constituents. The shape of the curve is correct within experimental error.

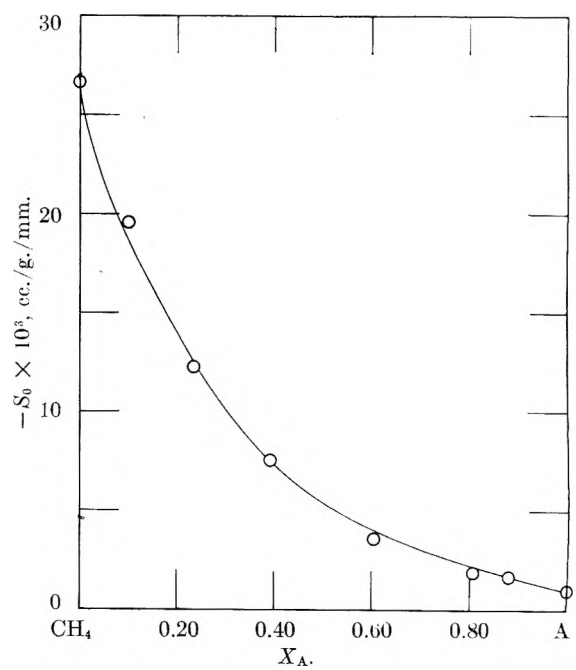

Fig. 2.—Theoretical dependence of slope on mole fraction argon with the parameters adjusted for best fit shown with the experimental slopes for the system methane–argon–Saran S-85 (32.37°).

In Fig. 3, we have plotted the experimental

TABLE II

Adsorbent	Gases	$C_{AAS}/kT \times 10^4$, cc./g./mm. Theo.	Exptl.	$C_{BBS}/kT \times 10^4$, cc./g./mm. Theo.	Exptl.	$C_{ABS}/kT \times 10^4$, cc./g./mm. Theo.	Exptl.
Alumina $T = -45.2°$	A: argon B: krypton	1.01	0.37	13.76	15.46	3.33	4.24
Charcoal Saran S-85 $T = 32.27°$	A: argon B: methane	10.28	9.97	212.0	267.4	41.0	92.6
Charcoal Saran S-85 $T = 0°$	A: argon B: nitrogen	34.0	35.4	49.0	58.6	34.37	50.61

slopes and the theoretical line evaluating all of the C's from the crude model alone for the system Kr–A–alumina. When one bears in mind that there are no adjustable parameters, the agreement is excellent.

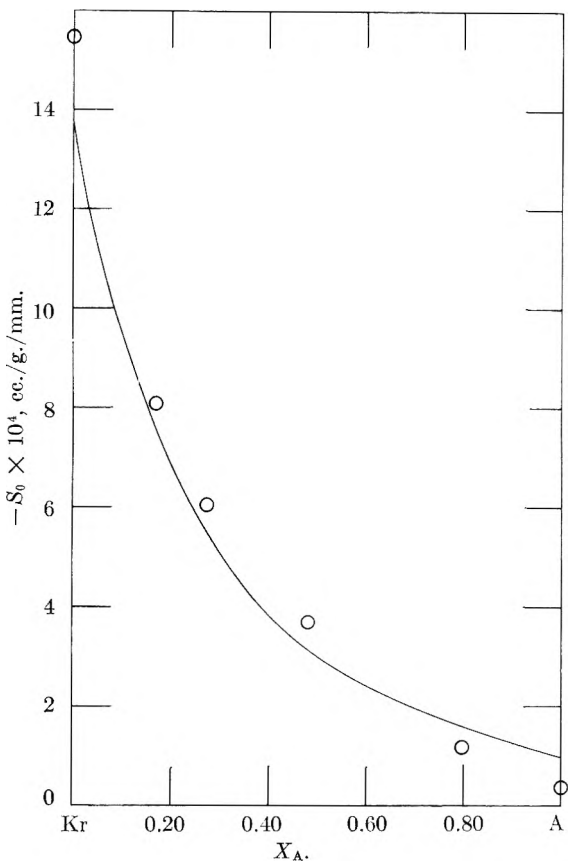

Fig. 3.—Theoretical dependence of slope on mole fraction argon with the parameters evaluated from the crude model shown with the experimental slopes of the system krypton–argon–alumina (−45.20°).

For both the above systems. the one gas, argon, interacts much less strongly with the surface than the second. In the system argon–nitrogen–charcoal the gases interact to about the same degree. In Fig. 4, the crude theory slopes are compared with the raw data. The C_{GGS}'s have been experimentally determined. The limiting slopes for the pure constituents are close enough together to make the experimental error appreciable, but the trend of slope with mole fraction is what is expected. Some curvature in the plots shows that higher order interactions are appreciable at these temperatures. With nitrogen as one component, it is not surprising that some stronger energy sites exist that approach saturation at lower pressures. Nevertheless, the crude theory still seems to be roughly adequate. The calculated and experimental values of the C's are compared in Table II.

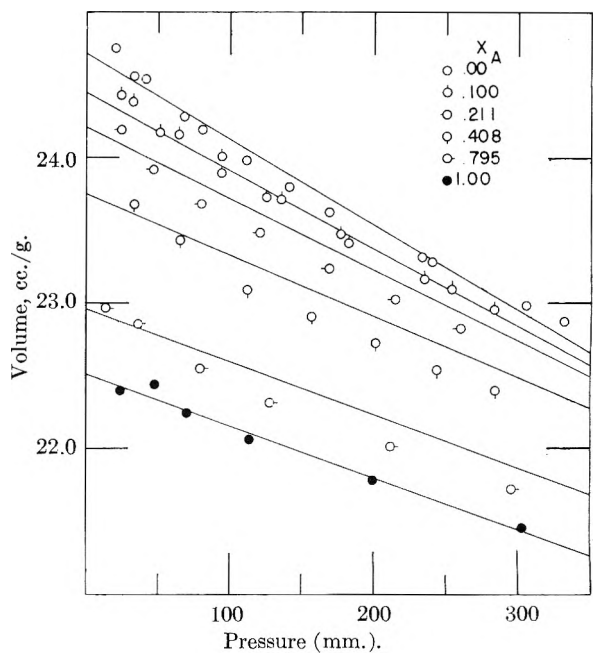

Fig. 4.—Theoretical volume *vs.* pressure lines with the parameter C_{ABS} evaluated from the crude model and intercepts from eq. 7 shown with the raw data for the system nitrogen–argon–Saran S-85 (0°).

Conclusion.—This work constitutes a convenient and rigorous approach to mixed adsorption. We have avoided that term, however, because it implies an arbitrary distinction between the adsorbed phase and the gas phase. By treating the problem from the standpoint of a single gas phase under the influence of a potential energy field, a number of problems (notably analysis of the gas phase) are eliminated or bypassed.

A similar experimental treatment of mixed adsorption has been made by Van der Waarden and Scheffer[9] who studied the adsorption of hydrogen and nitrogen on silica gel. We had originally intended to analyze their data; however, they proved to be unsuitable.

(9) M. Van der Waarden and F. E. C. Scheffer, *Rec. trav. chim.*, **71**, 689 (1952).

THE POLYMORPHISM OF MONO-α-AMINOACYL TRIGLYCERIDES

BY W. FREDERICK HUBER, RUTH DAVIS AND E. S. LUTTON

Contribution from the Research and Development Department of The Procter & Gamble Company, Cincinnati, Ohio

Received January 15, 1955

The polymorphism of a series of symmetrical 2-α-aminoacyl triglycerides and their acetate salts and of two N-acylated 2-α-aminoacyl glycerides is reported. The substitution of an amino group for a hydrogen atom on the α-carbon of the 2-acyl chain causes little change in the type of phase behavior of a triglyceride. The 2-α-aminoacyl triglycerides exhibit m.p. levels and long spacings similar to those of the corresponding 2-acyl triglycerides where the α-aminoacyl and 2-acyl groups contain the same number of carbon atoms. The acetates and N-acylated 2-α-aminoacyl glycerides have no counterpart in conventional glyceride molecules for direct comparisons, but show polymorphic behavior reminiscent of more familiar glycerides.

Previous papers from this Laboratory have reported the polymorphic behavior of various fatty acid glycerides. These studies have been extended to the mono-α-aminoacyl triglycerides.[1] All the compounds discussed here are symmetrical diacid triglycerides of the XYX type in which Y is an α-aminoacyl and X is a saturated C_{12}, C_{16} or C_{18} acyl group. The compounds for which X-ray diffraction and melting characteristics are discussed are 2-alanyl-1,3-dilaurin (LAL), 2-alanyl-1,3-dipalmitin (PAP), its acetate (PAPAc), 2-alanyl-1,3-distearin (SAS), its acetate (SASAc), 2-α-aminobutyryl-1,3-distearin (SBS), 2-valyl-1,3-distearin (SVS), its acetate (SVSAc), 2-α-aminolauroyl - 1,3 - distearin (SL_NS), its acetate (SL_NSAc), and also 2-N-acetylalanyl-1,3-dipalmitin and 2-N-palmitoylalanyl-1,3-dipalmitin. The free-base glycerides exhibit alpha and either a beta or beta prime form, with one compound, SAS, showing sub-alpha in addition to alpha and beta forms. The acetate salts show typical alpha forms with SASAc, like its free base, also exhibiting a sub-alpha state. The higher melting forms of PAPAc and SASAc are beta-prime while those of SVSAc and SL_NSAc, corresponding to no classical glyceride types, are designated as Forms I and II.

2-N-Acetylalanyl-1,3-dipalmitin and 2-N-palmitoylalanyl-1,3-dipalmitin both show alpha forms and two higher-melting forms. The latter do not fit classical types closely except for an intermediate beta-3 form for the first compound.

Experimental

Purification of the Compounds.—The preparation of the mono-α-aminoacyl and acylated mono-α-aminoacyl glycerides has been reported.[1] All compounds were recrystallized just prior to study. The amino acid glyceride acetates were recrystallized by addition of 10 to 20 volumes of petroleum ether to a solution of the compound in 2 to 5 volumes of chloroform containing about 1% of acetic acid. The free bases were prepared as required by washing the acetates in chloroform solution with water at 0°; this was followed by recrystallization from 10 to 20 volumes of ether or petroleum ether at 0° to −20°. All compounds were 95 to 100% pure as indicated by perchloric acid titration of the amino group.

Both 2-N-acetylalanyl-1,3-dipalmitin and 2-N-palmitoylalanyl-1,3-dipalmitin were recrystallized from petroleum ether. Kjeldahl nitrogen analysis indicated the compounds to be 95 and 97% pure, respectively. Titration with perchloric acid indicated both to be 97% pure, based on the presence of no more than 3% unacylated amino groups.

Thermal and X-Ray Diffraction Technique.—Established techniques[2] were used for obtaining m.p. and diffraction data. "Rapid complete m.p.'s" and "regular complete m.p.'s" were determined for each compound, the former for metastable phases, especially alpha, the latter usually for the stable form only. Compounds in melt-filled glass capillaries tended to decompose on repeated thermal treatment; this caused a progressive clouding which greatly hampered observation of melting behavior. By filling the capillaries with powdered sample and sealing before heating, the useful life of the capillaries was prolonged and more precise data could be obtained. All m.p. determinations reported here are on such powder-filled capillaries with the exception of those on 2-alanyldilaurin. Capillaries for the latter compound, due to its low m.p., were liquid-filled and then sealed.

The possible existence of intermediate melting forms was explored as follows. Melted samples in capillaries were held at 1 ± 0.2° below the alpha m.p. for 10 minutes during which time they solidified and then at 1 ± 0.2° above the alpha m.p. where partial melting and resolidification occurred. The process took 10 to 20 minutes for the acetates and 2-N-acetylalanyl- and 2-N-palmitoylalanyl-1,3-dipalmitin. The free bases required a period of several hours. Actually only one form other than alpha (or sub-alpha) was obtained from melt for any of these compounds with the exception of SL_NSAc which showed two.

Flat film X-ray diffraction patterns were made on all polymorphic forms with a General Electric XRD-1 unit employing Cu Kα nickel-filtered radiation and a 0.025 in. pinhole system. Sample-to-film distance was usually 10 cm., with a few patterns being taken at 5 cm. Low-melting phases were kept below their m.p.s. in a small cold-block during exposure.

Thermal and X-ray diffraction data are listed in the following order: compound, polymorphic form: m.p. °C.; long spacing, L.S. (in Å.); short spacings, S.S. (in Å.). Unless indicated otherwise, m.p.'s of metastable forms are rapid c.m.p.s.; m.p.'s. of stable forms are c.m.p.s. Relative intensities of diffraction lines are indicated by (VS) = very strong, (S) = strong, (M) = medium and (W) = weak.

Mono-α-aminoacyl Glycerides: LAL. α-1: 10° (approx.)[3]; L.S. 22.3; S.S. 4.10 (M). β-3 (like): 26.5°[4]; L.S. 39.1; S.S. 4.70 (M), 3.87 (M). **PAP.** α-1: 29.9 ± 0.2°; L.S. 25.6; S.S. 4.09 (M). β-3: 48.2°; L.S. 43.8; S.S. 5.38 (S-), 5.04 (M-), 4.57 (VS), 4.01 (S), 3.83 (S), 3.70 (M-), 3.53 (M), 3.38 (M-). **SAS.** sub-α-1: no m.p.[5]; L.S. 29.2; S.S. 4.15 (S), 3.75 (W). α-1: 40.9 ± 0.1°; L.S. 29.5; S.S. 4.13 (VS). β-3: 56.6°; L.S. 48.1; S.S. 5.34 (M-), 4.56 (S), 3.98 (M), 3.81 (M). **SBS.** α-1: 39.6 ± 0.3°; L.S. 30.5; S.S. 4.14 (S). β′-3: 56.3°; L.S. 55.2; S.S. 4.69 (M-), 4.20 (VS), 3.78 (S). **SVS.** α-1: 37.7 ± 0.2°; L.S. 30.6; S.S. 4.13 (M+). β′-3: 56.5°; L.S. 57.7; S.S. 5.13 (M-), 4.74 (M), 4.21 (VS), 3.80 (S). SL_NS. α-2: 40.3 ± 0.8°[6]; L.S. 47.5; S.S. 4.08 (S). β′-3 (like): 66.8°; L.S. 66.4; S.S. 5.16 (M-), 4.63 (S), 4.19 (VS), 3.91 (S).

Mono-α-aminoacyl Glyceride Acetates: PAPAc. α-1: 32.2 ± 0.4°; L.S. 31.5; S.S. 4.10 (M). β′-3 (like): 85.1°; L.S. 51.4; S.S. 5.11 (W), 4.39 (M-), 4.17 (VS), 4.07 (M),

(1) W. F. Huber, *J. Am. Chem. Soc.*, **77**, 112 (1955).

(2) E. S. Lutton, F. L. Jackson and O. T. Quimby, *ibid.*, **70**, 2441 (1948).

(3) Starts to melt and reclouds.

(4) Obtained from melt only.

(5) The sub-α-1 form, present at 0°, transforms reversibly to the α-1 form below room temperature.

(6) Softening point.

3.80 (M−), 3.60 (M). **SASAc.** sub-α-1: no m.p.[7]; L.S. 34.2; S.S. 4.16 (S), 3.79 (M). α-1: 41.8 ± 0.3°; L.S. 33.3; S.S. 4.08 (S). β′-3 (like): 86.7°; L.S. 55.2; S.S. 5.51 (M+), 4.60 (W), 4.30 (M), 4.15 (S), 4.03 (W), 3.76 (W+), 3.62 (W+). **SVSAc.** α-1: 41.7 ± 0.2°; L.S. 32.5; S.S. 4.10 (S). Form I-3[8]: 75.2 ± 0.3°; L.S. 54.4; S.S. 4.73 (S), 4.25 (W), 3.81 (S). Form II-3: 79.6°; L.S. 55.2; S.S 4.88 (S), 4.17 (S), 3.85 (S), 3.77 (S−). **SL_NSAc.** α-4: 57.4 ± 0.2°; L.S. 93.1; S.S. 4.08 (VS). Form I-2 (4)[9]: 74.5 ± 0.5°; L.S. 44.4 (88.8); S.S. 4.65 (M). Form II-2 (4): 75.9°; L.S. 44.3 (88.6); S.S. 5.93 (W), 4.90 (M−), 4.45 (M+), 4.19 (M−), 3.96 (VS), 3.56 (M−).

Acylated Aminoacyl Glycerides. 2-N-Acetylalanyl-1,3-dipalmitin.—α-1: 32.6 ± 0.2°; L.S. 28.1; S.S. 4.07 (S). β-3 (like)[8]: 62.8 ± 0.3°; L.S. 53.2; S.S. 5.06 (M), 4.55 (S), 4.16 (W), 3.77 (VS), 3.49 (W). Form I-3: 67.7°; L.S. 56.2; S.S. 4.73 (S), 4.17 (VS), 3.95 (M), 3.61 (M−). **2-N-Palmitoylalanyl-1,3-dipalmitin.** α-3: 52.8 ± 0.3°; L.S. 73.1; S.S. 4.14 (VS). Form I-3[8]: 72.0 ± 0.5°; L.S. 67.1; S.S. 5.05 (M),[10] 4.15 (VS), 3.78 (M). Form II-2 (4): 75.2°; L.S. 44.3 (88.6); S.S. 4.63 (M−), 4.15 (S), 3.92 (M), 3.71 (M), 3.56 (W).

Discussion

D,L-α-Aminoacyl Glycerides.—The lowest melting forms of all the mono-α-aminoacyl glycerides studied are α-1, *i.e.*, single-chain-length α-forms with the exception of SL_NS which is α-2. In addition, SAS shows a sub-α-form. Previous experience[11] has shown that symmetrical short-chain 2-acyl 1,3-diglycerides (an XYX type) such as 2-acetyl-, 2-propionyl-, 2-butyryl- and 2-caproyl-1,3-distearin, also exist in α-1 and possibly also sub-α-1 forms. Since the long spacings of the α-forms of the 2-α-aminoacyl glycerides are essentially the same as those of the analogous 2-acyl glycerides, the long chains of the former like those of the latter must be perpendicular to the planes of the end groups. The amino group has little or no effect on the longitudinal dimension of the unit cell. This is illustrated in Fig. 1 which shows a plot of long spacings, with varying chain length of the 2-acyl and 2-α-aminoacyl groups in a series of 1,3-distearoyl triglycerides. Note that the α-long spacings of both series follow practically the same path. The correspondence between the α-form m.p.'s of these 2-α-aminoacyl glycerides and those of the conventional XYX type triglycerides is not as apparent; however, the general trend of the m.p. curves for the two series is the same. This is shown in Fig. 2, the aminoacyl glycerides usually melting 5 to 10° higher.

Comparisons of the long spacings and m.p.'s of the stable forms of the 2-α-aminoacyl-1,3-distearins and the analogous 2-acyl glycerides are also shown in Figs. 1 and 2, respectively. LAL, PAP and SAS all of which contain a 2-alanyl group have β-3 (or β-like) stable forms. SBS,

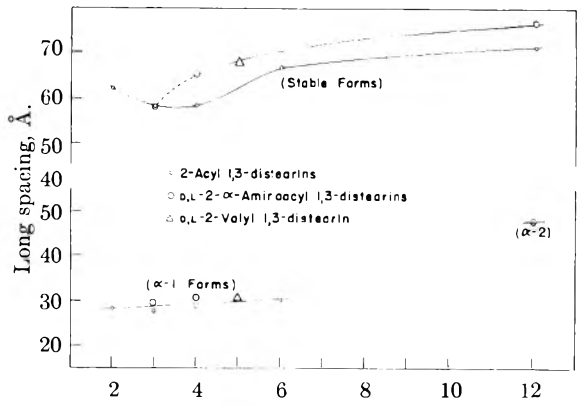

Fig. 1.—Comparison of long spacings of symmetrical distearoyl triglycerides: α and stable forms. (The data for 2-lauroyldistearin are those of T. Malkin and M. L. Meara, *J. Chem. Soc.*, 1141 (1939).)

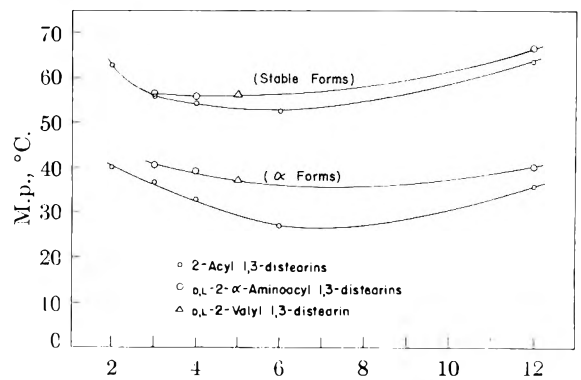

Fig. 2.—Comparison of melting points of symmetrical distearoyl triglycerides: α and stable forms.

SVS and SL_NS which have, in the 2-position, α-aminoacyl groups containing 4 or more carbon atoms, exist in β′-3 (or β′-like) stable forms. The value for the β-stable form of SAS falls on the curve for the β-forms of the 2-acyl-1,3-distearins. Stable forms of the remaining α-aminoacyl-distearins, being β-prime, have values which follow a parallel but slightly higher curve. M.p. agreement is good, differences between corresponding members being only 1 to 3°.

Figure 3 shows the long spacings and Fig. 4 the m.p.'s for the α- and stable forms of the 2-alanyl and corresponding 2-propionyl symmetrical triglycerides in which the fatty acyl group varies from 12 to 18 carbons. It is readily apparent that introduction of the amino group into the 2-acyl chain causes little change in m.p. or type of phase behavior.

The α-forms of the "free bases" transform rather slowly to the stable forms. In the case of the somewhat similarly behaving palmitoyl- and stearoyl-diacetins, mixtures have shown extreme alpha stability,[12] but a 50:50 mixture of the present PAP and SAS was little if any more α-stable than the individual components and after 24 hours was completely transformed to beta.

These results show that the substitution of an amino group on the α-carbon of one acyl group of a

(7) The sub-α-1 form present at 0°, transforms reversibly to the α-1 form below 20°.

(8) Solvent crystallized.

(9) Obtained pure from melt. The rod pellet prepared from solvent crystals appears to be a mixture of forms I and II, with the former predominating.

(10) Diffuse diffraction line.

(11) (a) F. L. Jackson, R. L. Wille and E. S. Lutton, *J. Am. Chem. Soc.*, **73**, 4280 (1951). (b) Heretofore unreported m.p.'s and long spacings of several XYX glycerides are: the lowest melting form of 2-propionyldilaurin 9.8°, 19.2 Å. (α-1); 2-propionyldipalmitin 24.4°, 25.7 Å. (α-1); 2-propionyldistearin 36.9°, 27.6 Å. (α-1), 28.6 Å. (sub α-1) and for the solvent-crystallized forms of 2-propionyldilaurin 24.1°, 37.1 Å. (Form I-3); 2-propionyldipalmitin 46.8°, 44.0 Å. (β-3); 2-propionyldistearin 55.5°, 48.4 Å. (β-3).

(12) F. J. Baur, *J. Am. Oil Chem. Soc.*, **31**, 196 (1954).

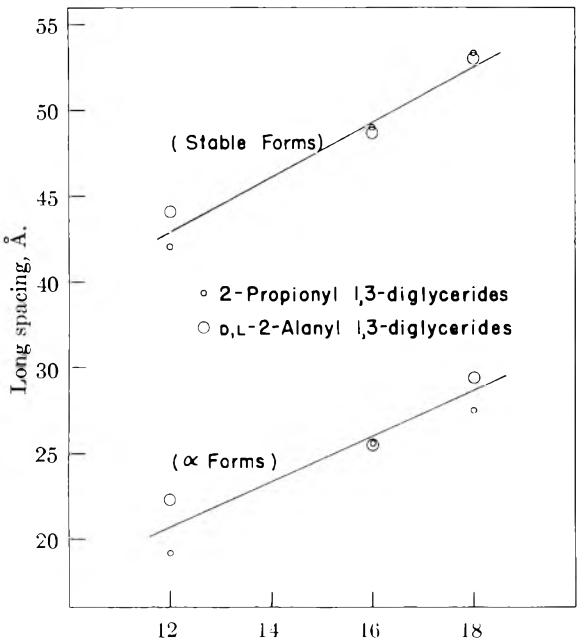

Fig. 3.—Comparison of long spacings of symmetrical triglycerides.

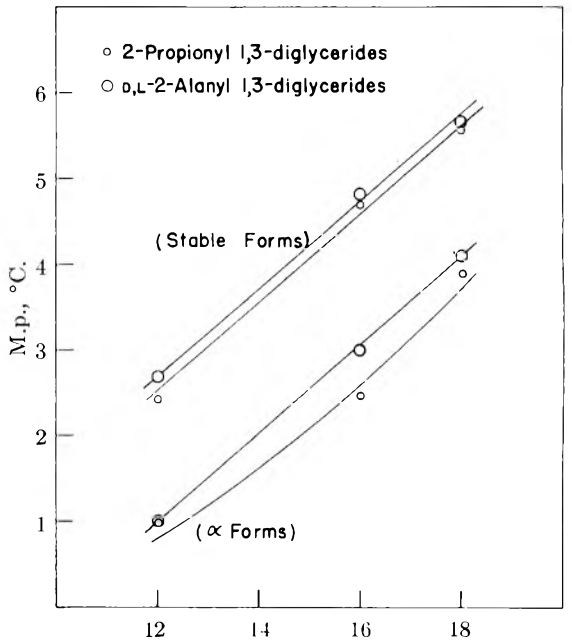

Fig. 4.—Comparison of melting points of symmetrical triglycerides.

triglyceride has little effect on melting properties and the major features of crystal structure.

D,L-α-Aminoacyl Glyceride Acetates.—The 2-alanyl glyceride acetates, PAPAc and SASAc, show α-1 and β-prime-3-like structures. In addition, like its free base, SASAc exhibits a sub-α-1 form. It appears, surprisingly, that as the 2-α-aminoacyl group lengthens, the similarity of the diffraction patterns to those of conventional triglyceride forms diminishes. This is shown for SVSAc and SL_NSAc which have α-1 and (apparently) α-4 forms, respectively. They also show intermediate (from solvent) and stable forms, the diffraction patterns of which do not resemble classical beta or β-prime forms. SVSAc has triple-chain-length intermediate (from solvent) and stable forms which are designated as Form I-3 and Form II-3. Of these compounds only SL_NSAc shows two higher melting forms from melt, which, being either double-or quadruple-chain-length, have been designated as Form I-2 and Form II-2 or 4. Form I, held near its m.p. until partial melting and resolidification has occurred, yields Form II.

Acylated Aminoacyl Glycerides.—The acylated 2-alanyldipalmitins, 2-N-acetylalanyl-1,3-dipalmitin and 2-N-palmitoylalanyl-1,3-dipalmitin, each show three polymorphic forms.

2-N-Acetylalanyl-1,3-dipalmitin has a typical α-1 form, m.p. 32.6°, an intermediate β-3-like structure (from solvent), m.p. 62.8°, and a highest-melting triple-chain-length form designated as Form I-3, m.p. 67.7°. The diffraction data on the intermediate β-3-like structure were obtained on a rod pellet of the crystals from solvent. All attempts to prepare this form from melt gave products melting between 63 and 67.5°, and the X-ray patterns showed evidence of partial transformation of this intermediate form to Form I-3 or transformation accompanied by decomposition.

2-N-Palmitoylalanyl-1,3-dipalmitin has a typical α-3 form, m.p. 52.8°, an intermediate Form I-3 (from solvent), m.p. 72.0°, and a highest melting form designated Form II-2 (or 4), m.p. 75.2°.

Acknowledgment.—The authors wish to express their appreciation to R. H. Lindahl for making the X-ray diffraction patterns used in this paper.

LIQUID–VAPOR EQUILIBRIUM IN MICROSCOPIC CAPILLARIES. II. NON-AQUEOUS SYSTEMS

BY M. FOLMAN AND J. L. SHERESHEFSKY[1]

Contribution from the Physical Chemistry Laboratory, Israel Institute of Technology, Haifa, Israel

Received January 28, 1955

The lowering of the vapor pressure of toluene and isopropyl alcohol over concave surfaces was measured in capillaries 0.8 to 3.0 μ in radius. The determination was based on the principle of equilibrium between the liquid contained in a cone-shaped capillary and the vapor of the same liquid over a solution of a non-volatile solute. The results obtained point out the inapplicability of Kelvin's relation to capillaries of the order concerned. Moreover, it seems that the polarity of the liquid influences the extent of the deviation from the equation. These deviations are explained on basis of assumption of long range forces.

The vapor pressure lowering over curved surfaces is given by Kelvin's relation[2]

$$\ln \frac{P}{P_0} = \pm \frac{2\sigma M}{dRTr} \qquad (1)$$

where P_0 is the vapor pressure over a plane surface; P the vapor pressure over a curved surface of radius of curvature r; d the density; M the molecular weight; σ the surface tension; R the gas constant, and T the absolute temperature. The positive and negative signs apply to convex and concave surfaces, respectively.

For convex surfaces (1) has been verified for radii of curvature of several microns, for water droplets by Goodris and Kulikova,[3] for droplets of dibutyl phthalate by Shereshefsky and Steckler,[4] by Lyalikov[5] for mercury droplets and by La Mer and Gruen,[6] for dioctyl phthalate and oleic acid droplets less than a micron in diameter.

For concave surfaces the experimental results are considerably different from the calculated. Shereshefsky[7] found that the lowering of the vapor pressure in capillaries of 4.05 μ radius is twenty-three fold. On the other hand, Thoma[8] working with capillaries of tenths of a millimeter radius obtained results in agreement with Kelvin's relation. Recently Shereshefsky and Carter,[9] in capillaries 3 to 10 μ in radius, obtained lowerings of the vapor pressure of water 30 to 80 times that calculated.

The present work was undertaken with the view of testing the applicability of the Kelvin relation in cases of concave surfaces of organic liquids, and to observe the influence of polarity on the abnormal effects found by Shereshefsky.

Experimental

1. **Method.**—Similar to the method of Shereshefsky and Carter,[9] the measurements were based on the equilibrium established between the liquid in a cone-shaped capillary and its vapor from a bulk solution of the liquid and a non-volatile solute. The liquid column in a capillary of this shape, when brought in contact with the vapor of the solution, will either increase or decrease in height, depending on the relative vapor pressures of the two parts of the system. In a full capillary, the liquid will evaporate, and the radius of the meniscus will decrease until the vapor pressure over the meniscus will equal the vapor pressure of the solution. After this point is reached, continued contact of the two parts of the system will not affect the position and radius of the meniscus. The latter may be obtained from the relation

$$r \cos \theta = r' \qquad (2)$$

where r and r' are the radii of the meniscus and capillary, respectively, and θ is the contact angle. The vapor pressures of the solutions at the concentrations involved in these experiments were calculated with adequate accuracy from Raoult's law.

2. **Apparatus.**—The apparatus consisted of a high vacuum system, thermostat, vessel containing the capillaries and the solution, a vessel for weighing the solvent, an arrangement for the purification and storage of the solvent and a microscope-cathetometer with a source of light.

The capillaries were prepared from 0.5 mm. Pyrex capillary tubing. The tubing was cleaned with hot concentrated nitric acid and rinsed with redistilled water for several hours. The drawing of the cone-shaped capillaries was carried out in a cross flame produced by two microburners by a twisting motion in two steps. Suitable portions were then selected for calibration and use. The calibration was made on a microscope with a screw micrometer eyepiece of tenfold magnification and an objective with a 44-fold magnification. The micrometer eyepiece was previously calibrated against a stage micrometer consisting of a glass plate with an engraved line one mm. in length and divided into one hundred equal parts.

The capillary diameter was measured at 0.5-mm. intervals starting from the open end. The light used came from a microscope lamp provided with a blue filter. The precision of the measurements was 0.1 μ for radii of 0.7 μ and larger. In order to eliminate capillaries with an elliptical cross section, three calibrations were made at different positions after the rotation of each capillary around its axis. Owing to the fact that the walls of the capillary act as lenses, it was necessary to introduce a correction in order to obtain the real radius. It can be shown that if the thickness of the capillary wall is at least ten times greater than the inner radius, the real radius may be obtained by dividing the apparent radius by the refractive index of the glass.

Eight suitable capillaries were attached to the inner wall of a Pyrex tube 14 mm. in diameter which served as the capillary chamber. They were arranged in four pairs and placed on different levels 30 mm. apart. The attachment of the capillaries was carried out by heating carefully, with a microburner from the outside, the point of the tube opposite the capillary's closed end, until the glass melted slightly. This prevented any possible damage to the capillary.

A 100-cc. bulb attached to the lower end of the capillary chamber served as the solution vessel.

The thermostat was of 250-liters capacity. It included a toluene–mercury thermoregulator, a 400 watt heating element with a variable resistance in series, an electronic relay, a copper coil connected to a refrigerating unit with a circulating pump, and a powerful electrical stirrer. The

(1) Visiting Professor of Physical Chemistry (1950–1952) under sponsorship of U.S.A. State Department.

(2) W. Thomson, *Phil. Mag.*, [4] **42**, 448 (1871).

(3) N. Goodris and L. Kulikova, *J. Russ. Phys. Chem. Soc., Physical Part*, **56**, 167 (1924).

(4) J. L. Shereshefsky and S. Steckler, *J. Chem. Phys.*, **4**, 108 (1936).

(5) K. S. Lyalikov, *Acta Physicochim., U.R.S.S.*, **12**, 42 (1940).

(6) V. L. La Mer and R. Gruen, *Trans. Faraday Soc.*, **48**, 410 (1952).

(7) J. L. Shereshefsky, *J. Am. Chem. Soc.*, **50**, 2966 (1928).

(8) H. Thoma, *Z. Physik*, **64**, 224 (1938).

(9) J. L. Shereshefsky and C. P. Carter, *J. Am. Chem. Soc.*, **72**, 3682 (1950).

TABLE I

TOLUENE DATA AT 20°

Mol. frac.	Kelvin radius, μ	Capillary radii at level of meniscus at equilibrium, μ: Cap. 7	Cap. 16	Cap. 14	Cap. 5	Cap. 17	Cap. 1	Cap. 18	Cap. 2	Obsd./Calcd.
0.00466[b]	0.51	...	1.55	1.60	1.70	2.35	1.50	1.45	1.50	2.9
.00611[a]	.41	1.80	1.80	1.30	full	2.10	1.20	1.20	1.30	3.5
.00611[b]	.41	...	1.20	1.30	1.30	2.20	1.00	1.35	1.30	3.0
.00763[b]	.34	...	1.15	1.30	1.30	1.65	0.95	1.20	1.25	3.5
.00763[a]	.34	...	1.30	1.35	1.30	2.00	1.00	1.10	1.25	3.6
.00900[b]	.28	...	...	1.30	1.35	2.05	1.10	1.05	1.10	4.2
.01080[b]	.23	...	...	1.25	1.30	2.00	1.00	1.00	1.00	4.8
.01174[b]	.21	...	...	1.10	1.25	1.90	0.90	0.95	0.95	4.9
.01174[a]	.21	...	...	1.20	1.30	1.90	0.95	1.00	0.95	5.1
.01375[b]	.18	...	...	1.05	1.20	1.85	0.90	0.90	0.85	5.4

[a] Evaporation. [b] Condensation.

TABLE II

ISOPROPYL ALCOHOL DATA AT 20°

Mol. frac.	Kelvin radius, μ	Capillary radii at level of meniscus at equilibrium, μ: Cap. 14	Cap. 5	Cap. 17	Cap. 1	Cap. 18	Cap. 2	Obsd./Calcd.
0.00342[a,c]	0.39	1.90	2.15	...	2.30	2.50	2.60	5.8
.00342[a,c]	.39	2.00	2.25	...	2.35	2.55	2.65	5.7
.00342[b,c]	.39	1.80	2.10	...	2.20	2.50	2.55	6.0
.00342[b,c]	.39	1.80	2.10	...	2.20	2.60	2.60	5.9
00411[a]	.33	1.70	1.70	...	1.50	1.60	1.80	5.1
.00471[a]	.29	1.60	1.30	...	1.30	1.35	1.60	4.9
.00471[a]	.29	1.50	1.40	...	1.40	1.30	1.50	5.0
.00552[a]	.25	1.55	1.20	1.90	1.35	1.20	1.30	5.3
.00552[a]	.25	1.60	1.30	1.90	1.30	1.25	1.40	5.4
.00663[a]	.20	1.40	1.20	1.70	1.20	1.20	1.30	6.3
.00923[a]	.15	1.30	1.00	1.80	1.25	1.20	1.30	8.0
.01226[b]	.11	0.95	0.95	1.55	1.00	1.00	1.10	9.0
.01226[a]	.11	1.00	1.00	1.65	1.05	1.10	1.20	9.6
.01578[a]	.086	0.95	1.10	1.65	1.10	1.10	1.10	12.6
.01578[a]	.086	0.95	1.00	1.75	1.00	1.05	1.00	11.6

[a] Evaporation. [b] Condensation. [c] Measurements at 25°.

temperature was maintained constant within 0.001 to 0.002° for 24 hours.

The weighing vessel was a glass bulb of 60 cc. with a stopcock. It was connected to the vacuum system by means of a ground glass joint and a three-way stopcock. The vessel for storing pure liquid consisted of two conjugated bulbs attached to the system through a stopcock.

The position of the meniscus was measured by a Gaertner cathetometer that permitted adjustment to 0.01 mm. A fluorescent lamp placed outside the thermostat served as a source of diffuse light.

Dibutyl phthalate was used as the non-volatile solute. It was prepared from an analytical grade sample by double vacuum distillation and collection of the middle fractions. The toluene with which the first series of measurements was carried out was purified from an analytical grade sample by shaking with concentrated sulfuric acid until no brown color appeared, washing with dilute NaOH solution and distilled water, drying over metallic sodium by refluxing for 24 hours and distilling. The isopropyl alcohol, of analytical grade, was twice distilled and dried over calcium oxide under reflux for 24 hours and distilled.

3. Procedure.—A weighed quantity of the solute was introduced into the solution vessel which was then pumped for 24 hours and left under high vacuum for several days. The purified solvent was introduced into the storage vessel, and was freed of dissolved air by vacuum distillation from one bulb to the other and subsequent pumping off of the freed air. The solvent was then transferred to the weighing bulb by distillation *in vacuo*. The bulb was removed and weighed, and after its re-attachment to the system the solvent was transferred by evaporation to the solution vessel. Equilibrium was approached from two directions, by evaporation from full capillaries and by condensation into empty or partially filled capillaries. The positions of the meniscus were measured at intervals of 15 to 30 minutes. The level at which the meniscus remained unchanged for one or two hours was accepted as the equilibrium point.

Results

The contact angles of toluene and isopropyl alcohol as determined macroscopically on glass are zero. To determine the angle in microscopic capillaries a series of microphotographs were taken of capillaries of approximately 10 μ radius and partially filled with the liquid. The menisci were clearly seen and showed that the contact angle was not appreciably different from zero. Figure 1 shows the variation of the radii of the capillaries with the distance from the open end.

The measurements on toluene were carried out at 20°. They were made at seven different concentrations of the solution. Three of the determinations were made both by evaporation and condensation. The results are given in Table I. In column 1 is given the concentration of the solutions in mole fractions, in column 2 the theoretical Kelvin radius, in the remaining columns except the last are given the observed radii of the capillaries at the level of the meniscus at equilibrium, and in the last column is given the ratio of the average observed radius to the calculated one. The results in capillary 17 are not included in the averages.

Good agreement can be observed between the

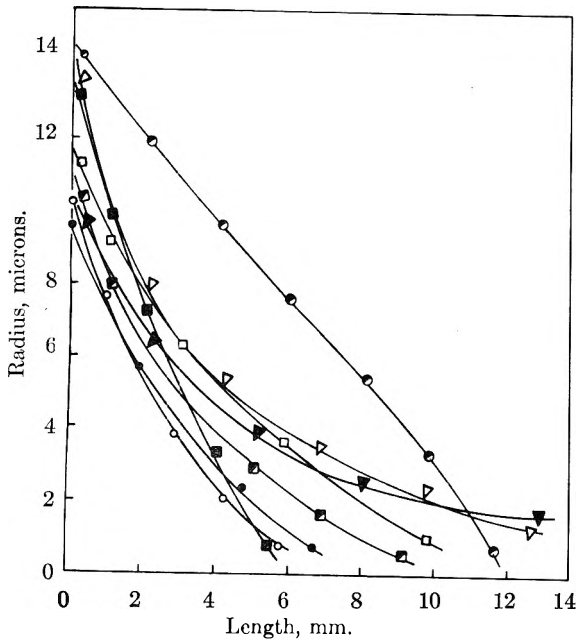

Fig. 1.—Variation of capillary bore: cap. 1, ●; cap. 2 ■; cap. 5, ○; cap. 7, ▲; cap. 14, □; cap. 16, △; cap. 17, ◑; cap. 18, ◩.

results in different capillaries with the exception of capillary 17 which for yet unknown reasons always gave higher results, as compared with the others. There is also good agreement between the values obtained by evaporation and condensation procedures, except for capillaries 7 and 16 at the mole fraction 0.00611. At this concentration the capillaries 7 and 16 gave values which were higher than the average, perhaps, because being the largest capillaries they required a long time to reach equilibrium at this low concentration. These two capillaries were calibrated to 1.7 and 1.1 μ, respectively, and therefore show no data for radii below these. It can be seen from the last column that the ratio r(obs.)/r(calcd.) increases from 2.9 for the lower concentration to 5.4 for the highest concentration.

All measurements on isopropyl alcohol were carried out at 20°, except for the mole fraction 0.00342. For technical reasons, the latter had to be made at 25°. Table II contains the results obtained for ten different concentrations. Here also, good agreement exists between the values for the several capillaries. An exception is capillary 17 which again gave higher values. At low concentrations the spread in the results for the different capillaries is rather great, although the agreement between capillaries on the same level in the capillary vessel is remarkably good. The ratio r(obs.)/r(calcd.) for all capillaries, except no. 17, varies from 4.9 to 12.6.

Discussion

The results of these measurements show that the Kelvin equation cannot be applied in estimating vapor pressure lowering over concave surfaces in microscopic capillaries. Nor can it be applied in estimating pore radii at given vapor pressures as it is done in adsorption analysis. The observed lowering is many times greater than the value

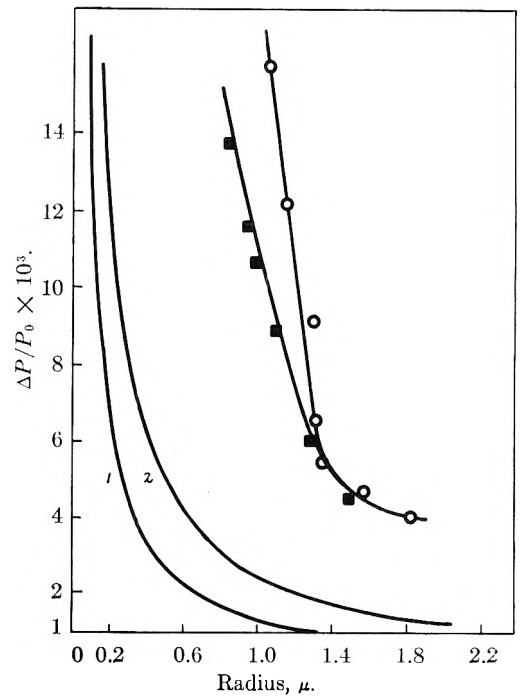

Fig. 2.—Relative vapor pressure lowering. Iscpropyl alcohol: Kelvin 1, measurements ○; toluene: Kelvin 2, measurements ■.

calculated with this equation. Moreover, the effect differs in magnitude with the nature of the liquid. The lowering for isopropyl alcohol was found to be much greater than for toluene, and the results for water reported in the preceding paper[9] show that the effect for the latter is still greater. This effect seems to change with the polarity of the liquid, and increases with increasing dipole moment of the molecule.

It is well known that many physical properties of capillary held liquids are different from those for the bulk liquid. To the literature references given in the preceding paper, describing these anomalies, can be added the observations on the freezing point of capillary condensates,[10-12] the increase in the heat of vaporization,[13] the rise in the critical temperature,[14] and the increase in specific polarization.[15] In so far as density[16,17] and surface tension[18] are concerned, experimental data show values which are very near those of the bulk liquid. Theoretical considerations by Tolman[19] and Hill[20] require that the effect of curvature on surface tension be slight at the curvatures prevailing in these experiments, and become

(10) S. Brunauer, "The Adsorption of Gases and Liquid," Princeton University Press, Princeton, N. J., 1945, p. 444.
(11) J. P. Jones and R. A. Gortner, THIS JOURNAL, **36**, 387 (1932).
(12) M. Shimizu and I. Higuti, *ibid.*, **56**, 198 (1952).
(13) L. F. Gleysteen and V. R. Deitz, *J. Research Natl. Bur. Standards*, **35**, 283 (1935).
(14) W. A. Patrick, W. C. Preston and A. E. Owens, THIS JOURNAL, **29**, 431 (1925).
(15) S. Kurosaki, *ibid.*, **58**, 320 (1954).
(16) E. O. Wiig and A. J. Juhola, *J. Am. Chem. Soc.*, **71**, 561 (1949).
(17) H. L. McDermot and W. G. M. Tuck, *Can. J. Res.*, **28B**, 292 (1950).
(18) L. H. Cohan and G. L. Meyer, *J. Am. Chem. Soc.*, **62**, 2715 (1940).
(19) R. C. Tolman, *J. Chem. Phys.*, **17**, 338 (1949).
(20) T. L. Hill, *J. Am. Chem. Soc.* **72**, 3923 (1950).

appreciable for radii of about ten millimicrons or less. It is of interest to point out that the observation on the specific polarization of the condensed water vapor made by Kurosaki is in good agreement with the observations on the elastic properties of liquid water in microscopic capillaries made by Deryagin.[21] In both instances, the capillary held water behaves as if it were in a solid-like form, resembling ice. These physical properties do not all depend on the curvature of the meniscus, and their abnormal values point to appreciable changes in the state of aggregation of the substances.

No anomalies have been observed in connection with positive curvatures of these magnitudes. Shereshefsky and Steckler,[4] and LaMer and Green[6] have shown that the Kelvin equation is valid for convex surfaces of droplets of various liquids ranging from 1.67 to a fraction of a micron in radius.

Furthermore, the effect observed in the present study is different in nature from that of Kelvin in several respects. Figure 2, in which is illustrated the behavior of the two liquids with respect to the theoretical and to each other, shows that the abnormal relative lowering of the vapor pressure at large capillary radii is approximately the same for both, toluene and isopropyl alcohol, while the Kelvin effect is widely different. As the capillary radius decreases, the curves diverge, with the abnormal relative lowerings of the latter liquid becoming greater. The contrary behavior is observed for the Kelvin curves; they tend to approach each other, and the difference between the relative lowerings tends to decrease with decreasing capillary radius.

These considerations lead us to believe that the abnormal vapor pressure lowering observed in this study and, perhaps, the other abnormal capillary properties, are induced by the capillary walls. Furthermore, the magnitude of the effect and the size of the capillaries in which it is manifested leads us to believe that the forces involved are effective over appreciable distances from the wall. Instances in which forces of long range were observed have been recently gathered and reviewed by Henniker,[22] citing cases where the forces were effective over several thousands ångströms.

This explanation is also supported by the observation made in the present study that the magnitude of the effect is proportional to the total molecular moments of the substances measured in the direction of the electric field. These moments were calculated to be approximately 30 D, for isopropyl alcohol, and 19 D, for toluene. The total moment for the water molecule is approximately the same as for isopropyl alcohol, while the effect is very much greater. The greater effect for water is, perhaps, due to the increased specific polarization observed by Kurosaki.[16]

Another factor supporting the explanation of the effect is the observation of the inverse relation between the effect and the capillary radius. As a wall effect, its magnitude should be proportional to the extent of surface exposed to unit volume of liquid. The ratio of lateral surface to volume in a right cone is given by $3(r^2/h^2 + 1)/r$, where r is the radius of the base and h is the height of the cone. The capillaries used in the present study approximated right cones in which r^2/h^2 was negligible with respect to unity, and in which the lateral area per unit volume was equal to $3/r$. The relative lowering of the vapor pressure was found to vary directly with this ratio.

(21) B. Deryagin, *Z. Physik*, **84**, 657 (1933).

(22) J. L. Henniker, *Rev. Mod. Phys.*, **21**, 322 (1949).

THE INFRARED ABSORPTION SPECTRA OF SOME ANTIBIOTICS IN ANTIMONY TRICHLORIDE SOLUTION[1]

BY J. R. LACHER, J. L. BITNER AND J. D. PARK

University of Colorado, Boulder, Colorado

Received January 19, 1955

It has been found that liquid antimony trichloride is an infrared transmitting solvent for several antibiotics and their hydrochlorides. The spectra of aureomycin, terramycin, tetracycline, aureomycin·HCl and terramycin·HCl are shown for the LiF and NaCl regions. Terramycin and its hydrochloride show new intense bands not given by the other antibiotics. They are probably due to a strongly hydrogen bonded hydroxyl groups.

Recently, much work has been done on the antibiotics, aureomycin, terramycin, tetracycline and their hydrochlorides and hydrates concerning their physiological, physical and chemical properties.[2-11] In conjunction with this work several infrared

(1) This research was supported in part by the Atomic Energy Commission, Contract No. AT(29)-787, Program A.

(2) B. M. Duggar, *Ann. N. Y. Acad. Sci.*, **51**, 177 (1948).

(3) R. W. Broschard, A. C. Dornbush, S. Gordon, B. L. Hutchings, A. R. Kohler, G. Krupka, S. Kushner, D. V. Lefemine and C. Pidacks, *Science*, **109**, 199 (1949).

(4) P. P. Regna, L. A. Solomons, K. Murai, A. E. Timreck, K. J. Brunings and W. A. Lazier, *J. Am. Chem. Soc.*, **73**, 4211 (1951).

(5) J. H. Boothe, J. Morton, H. J. P. Petisi, R. G. Wilkinson and J. H. Williams, *ibid.*, **75**, 4621 (1953).

(6) L. H. Conover, W. T. Moreland, A. R. English, C. R. Stephens and F. J. Pilgrim, *ibid.*, **75**, 4622 (1953).

(7) F. A. Hochstein, C. R. Stephens, L. H. Conover, P. P. Regna, R. Pasternack, P. N. Gordon, F. J. Pilgrim, K. J. Brunings and R. B. Woodward, *ibid.*, **75**, 5455 (1953).

(8) C. R. Stephens, L. H. Conover, R. Pasternack, F. A. Hochstein, W. T. Moreland, P. P. Regna, F. J. Pilgrim, K. J. Brunings and R. B. Woodward, *ibid.*, **75**, 5455 (1953).

(9) J. Robertson, L. Robertson, P. F. Eiland and R. Pepinsky, *ibid.*, **74**, 841 (1952).

(10) J. D. Dunitz and J. H. Robertson, *ibid.*, **74**, 1108 (1952).

(11) R. Pasternack, P. P. Regna, R. L. Wagner, A. Bayley, F. A. Hochstein, P. N. Gordon and K. J. Brunings, *ibid.*, **73**, 2400 (1951).

spectra of these compounds and their degradation products were run in a nujol paste.[4,7] The spectra, in many cases, were of such a nature that few, if any, specific assignments could be made from them. Previously, the infrared spectra of several pyrimidines and amino acids were run in this Laboratory with antimony trichloride as the solvent.[12,13] The effect of the solvent on the position of the fundamental stretching frequencies of the O–H, N–H and C–H groups was determined in conjunction with this work. Acetamide, benzoic acid and phenol were used as the reference compounds, since the positions of these bands are well known for them. It was found that little or no shifting of the above bands occurred. Preliminary work indicated that antimony trichloride was also a suitable solvent for several antibiotics which have naphthalene as the basic ring structure. The present paper describes the results obtained using antimony trichloride solutions of aureomycin, terramycin, tetracycline, aureomycin·HCl and terramycin·HCl.

Experimental Details

A Perkin–Elmer model 12B spectrometer with two monochromators was used. One monochromator was fitted with a LiF prism and covered the spectral region from 1 to 5 μ. The other was fitted with a NaCl prism and extended the region to approximately 12.5 μ. The antimony trichloride was purified by the method previously described.[12]

A "Teflon" cell with silver chloride windows was used for both the LiF and NaCl regions. The body of the cell is made of "Teflon" and is one cm. long with an inside diameter of 2.0 cm. The walls are made rather thick to prevent buckling. A neck of monel metal, fitted with a "Teflon" stopper, is fastened to the body of the cell in order to expedite its filling and emptying. The stopper is necessary to exclude moisture from the filled cell. "Teflon" gaskets were used to ensure a tight seal and to prevent contact between the metal cell clamps and the silver chloride windows. The windows are reduced to free silver if they are allowed to remain in contact with the steel clamps. Since antimony

TABLE I

OBSERVED FREQUENCIES AND ASSIGNMENTS 1 TO 5 μ

Wave length					
Aureomycin	Terramycin	Tetracycline	Aureomycin HCl	Terramycin HCl	Assignment
	1.42	1.44			
	1.52				
	1.91	1.92	1.96	1.91	2ν C=O
2.24	2.24	2.24	2.22	2.23	
		2.26			
2.35	2.34				
2.48	2.48	2.48		2.47	
		2.59			
	2.63	2.65		2.63	
2.75	2.75	2.75	2.76	2.75	1ν OH alcoholic
2.82	2.82	2.81	2.82	2.81	1ν OH
2.91	2.91	2.91	2.91		1ν N–H of NH_2 *asym.*
	2.96			2.96	
3.03	3.02	3.03	3.03		1ν N–H of NH_2 *sym.*
	3.10			3.09	
			3.17	3.17	
3.29	3.21	3.27	3.27	3.23	1ν C–H aromatic
	3.29	3.31			
		3.37	3.39	3.36	1ν C–H aliphatic
				3.42	
	3.54		3.52		
3.58	3.63	3.61			
	4.28			4.28	
	4.30			4.30	

TABLE II

OBSERVED FREQUENCIES AND ASSIGNMENTS 2 TO 12.5 μ

Wave length					
Aureomycin	Terramycin	Tetracycline	Aureomycin HCl	Terramycin HCl	Assignment
2.78	2.77	2.78	2.78	2.78	1ν OH alcoholic
2.83	2.85	2.84	2.84	2.85	1ν OH
2.91	2.94	2.93	2.94		
				3.00	
3.04		3.05	3.07		
	3.13				
3.29	3.24	3.31	3.30	3.24	
		3.24			
	3.40				
3.45	3.44			3.44	
3.60		3.59		3.65	
	4.28			4.29	
				5.71	1ν C=O
6.02	6.00	6.01	6.02	5.96	1ν C=O
	6.17	6.16		6.16	
6.28	6.28	6.28	6.28	6.28	1δ NH_2
6.47		6.47	6.47	6.47	
6.66	6.63	6.65	6.66	6.62	
6.89	6.86	6.89	6.95	6.89	1δ C–H bending of CH_3
	7.06				
7.19		7.19	7.18		
7.28	7.28	7.28	7.30		1ν C–N
7.55	7.50	7.53	7.59	7.56	
7.92	8.05		7.97	7.82	
8.12	8.20	8.09	8.12	8.05	1δ C–H out of plane
8.46	8.48	8.47		8.50	
8.54					
8.80	8.93	8.84	8.86	8.82	
	9.03				
9.27	9.30	9.29	9.29		
9.50		9.54	9.55		OH deform. alcohols
9.72	9.72	9.81		9.67	
10.01	9.97		9.96	10.01	
10.20	10.13	10.20	10.21	10.23	
				10.25	
10.54	10.42				
10.73	10.78	10.75	10.73	10.59	
10.87	10.97		10.88	10.73	
11.10		11.11	11.02	10.97	
11.29			11.16	11.08	
	11.40			11.36	
11.56	11.60	11.59	11.77	11.70	
12.21	12.12	12.20		12.12	
12.41		12.44		12.21	
		12.30			

(12) J. R. Lacher, V. D. Croy, A. Kianpour and J. D. Park, THIS JOURNAL, **58**, 206 (1954).

(13) J. R. Lacher, D. E. Campion and J. D. Park, *Science*, **110**, 300 (1949).

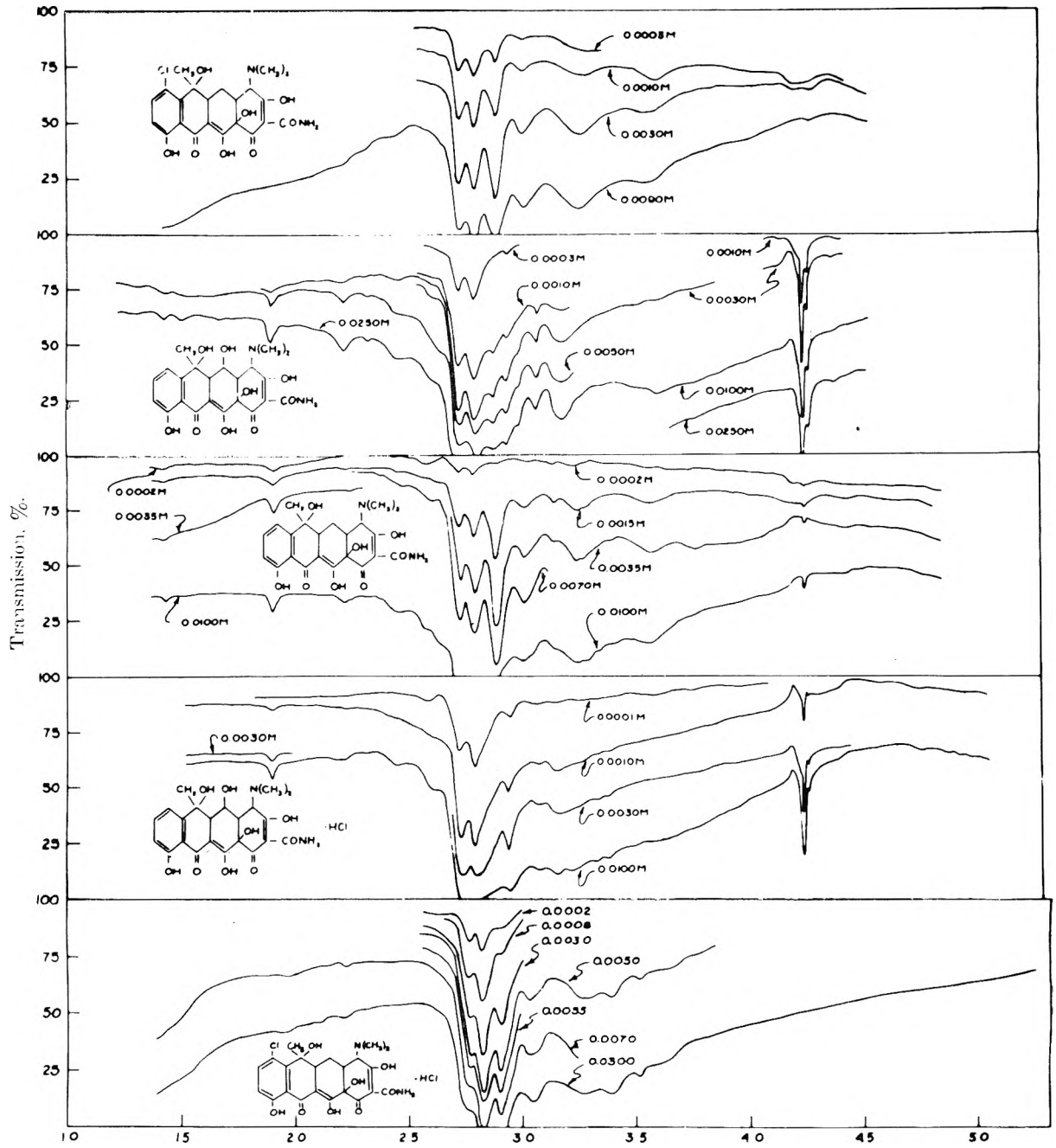

Fig. 1.—Infrared spectra of aureomycin, terramycin, tetracycline, terramycin·HCl, and aureomycin·HCl in molten antimony trichloride; 1.0 cm. cell with silver chloride windows; indicated molar concentrations; temperature 90°; Perkin–Elmer single beam.

trichloride melts at 73.4°, it is necessary to heat the cell. A separate heating unit, which was also used as the cell holder, was used to maintain the cell at approximately 90°.

The aureomycin, terramycin and tetracycline were dried for at least 24 hours in a vacuum drying pistol which employed water as the refluxing fluid. The hydrochlorides of terramycin and aureomycin were dried for 8 hours at approximately 90° in an atmosphere of dry hydrogen chloride. The spectra of the hydrochlorides were observed both before and after being dried. There was no noticeable change.

Results

The spectra of the compounds under consideration were obtained in the 1.0 to 5.0 μ region using a LiF prism and are shown in Fig. 1. The region between 2.0 and 12.0 μ was studied using a NaCl prism and the results shown in Fig. 2. Tables I and II give the wave length of the bands along with a few possible assignments.

The structure and composition of these antibiotics are very similar. They vary only at the two positions indicated by R_1 and R_2 in the structural formula given below. The structural formulas of the individual antibiotics may be obtained by replacing the R's with the atoms indicated below. The numbering system followed is that suggested by P. P. Regna and associates.[7]

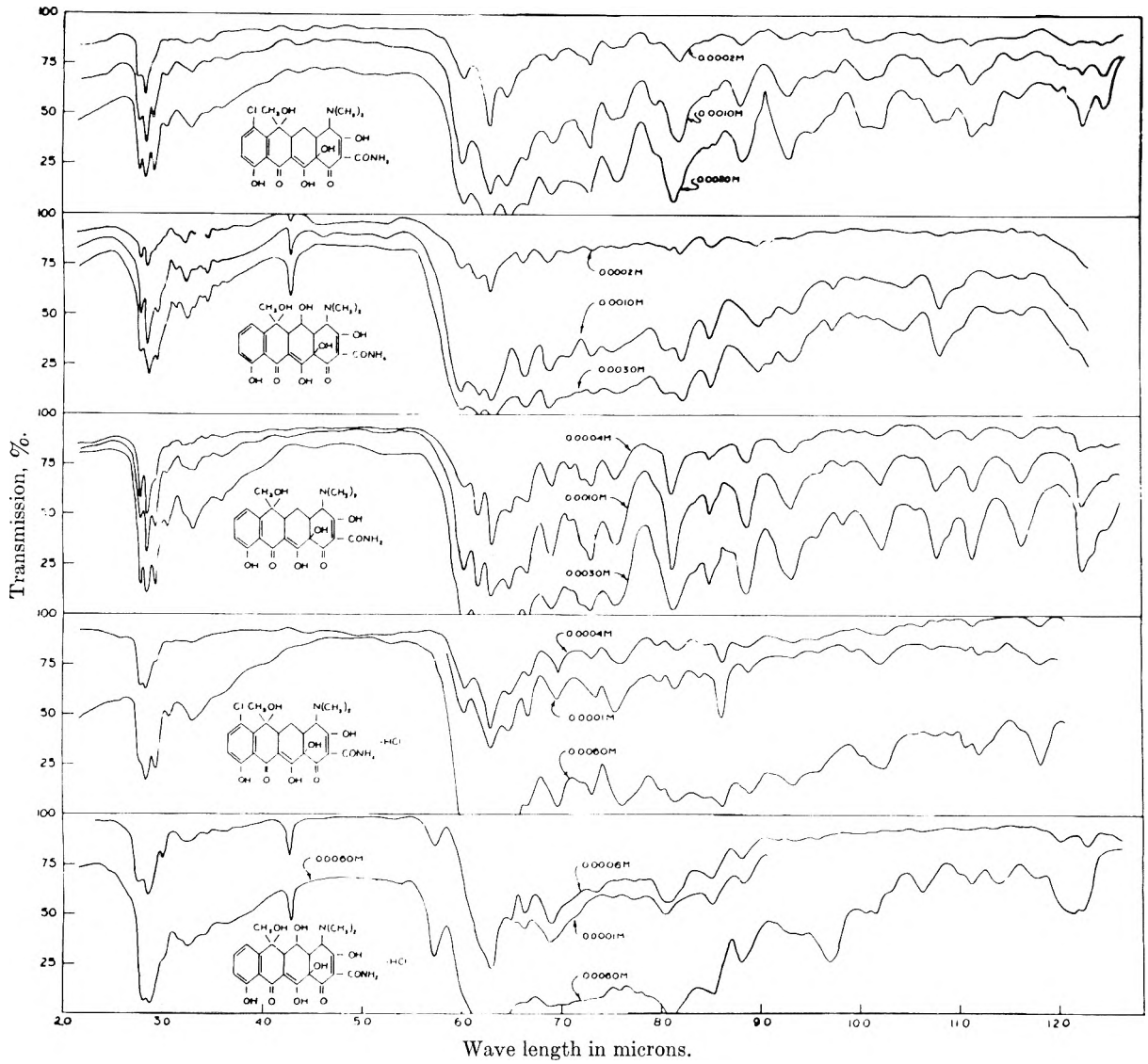

Fig. 2.—Infrared spectra of aureomycin, terramycin, tetracycline, aureomycin·HCl, and terramycin; HCl in molten antimony trichloride; 1.0 cm. cell with silver chloride windows; indicated molar concentrations; temperature 90°: Perkin-Elmer single beam.

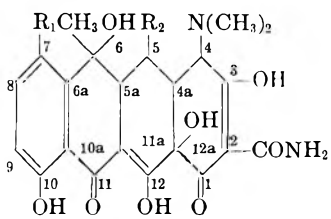

	R_1	R_2
aureomycin	Cl	H
terramycin	H	OH
tetracycline	H	H

A peak at 2.75 and 2.81 μ, present in all the compounds studied, has been attributed to O–H bonds. The position of the bands arising from the fundamental stretching frequencies of the various types of O–H groups has been frequently discussed.[14–22] The band at 2.75 μ may be assigned to the alcoholic O–H groups, such as at position 12a, which are present in these compounds. The second peak, at 2.81 μ, may be due to an O–H group involved in hydrogen bonding, or, to a tautomeric enol system

involving the groups at positions 10, 11 and 12. Hydrogen bonding, as determined by Fisher-Hirschfelder models, can occur between the carbonyl at position 1, the hydroxyl group at position 12 and/or the amide at position 2. The hydroxyl group at position 3 can form hydrogen bonds with the amide at position 2 and/or the dimethylamine group at position 4. In addition, the carbonyl group at position 11 is able to form hydrogen bonds with the hydroxyl groups at positions 10 and 12.

(14) V. D. Croy, Master's Thesis, University of Colorado, 1951.
(15) M. Hunsberger, *J. Am. Chem. Soc.*, **72**, 5626 (1950).
(16) R. E. Richards and H. W. Thompson, *J. Chem. Soc.*, 1248 (1947).
(17) J. J. Fox and A. E. Martin, *Trans. Faraday Soc.*, **36**, 897 (1940).
(18) L. Kellner, *Proc. Roy. Soc. (London)*, **A157**, 110 (1936).
(19) R. E. Richards and H. W. Thompson, *J. Chem. Soc.*, 1260 (1947).
(20) A. M. Buswell, V. Deitz and W. H. Rodebush, *J. Chem. Phys.*, **5**, 501 (1937).
(21) J. J. Fox and A. E. Martin, *Proc. Roy. Soc. (London)*, **A162**, 419 (1937).
(22) R. B. Barnes, L. G. Bonner and E. U. Condon, *J. Chem. Phys.*, **4**, 722 (1936).

The structure of these compounds is conducive to the formation of both systems.[23] P. P. Regna and associates report the presence of three pK_a values for aureomycin·HCl and terramycin·HCl of approximately 3.5, 7.6 and 9.2. On the basis of ultraviolet studies they attribute the pK_a value, 3.5, to the HCl, one to the portion of the structure involving positions 1, 2 and 3, and the last remaining one to the system including positions 10, 10a, 11, 11a and 12. From these pK_a values it appears that the tautomeric enol system competes strongly with several of the possible chelate ring systems in these antibiotics. If this is true, it is quite possible that the peak arising at 2.81 μ is due to the tautomeric enol system. It could then be assumed that the bands arising from hydrogen bonding occur in the 3 to 3.5 μ region, which would account for the high amount of absorption in this region.

With the exception of terramycin·HCl, all the compounds contain an intense peak at 2.91 μ and a second smaller peak at 3.03 μ. These two bands have been assigned to the asymmetrical and symmetrical fundamental stretching frequencies of the NH_2 group. Similar assignments have been made for a number of compounds containing the above group.[14,24-27] The position of the C–H fundamental stretching frequency bands, for both the aromatic and aliphatic C–H groups, has been studied by many workers.[14,18,28-31] The aromatic C–H group band falls in the 3.2–3.3 μ region and that of the methyl group in the 3.4–3.6 μ region. The spectra of the compounds under consideration show bands in the above regions which may be ascribed to the C–H groups present.

Terramycin and its hydrochloride show several bands which are not present in the other antibiotics. These occur at 2.96, 3.10, 4.28 and 4.30 μ. These apparently arise because of the presence of a hydroxyl group in the 5-position. This hydroxyl group is in close proximity to the hydroxyl group at position 6 and the dimethylamine group at position 4. Thus, there is a good possibility of intramolecular hydrogen bonding occurring between the above groups. Although the bands at 2.96 and 3.10 μ occur in the region associated with the hydrogen bonded hydroxyl groups found in many compounds, the bands at 4.28 and 4.30 μ occur in a region associated with only a few strongly hydrogen bonded hydroxyl groups. Rundle and Parasol[32] and Lord and Merrifield[33] have studied the O–H stretching frequencies present in crystalline compounds. Since the O–H $\cdots$ O distances are known, they could empirically correlate the frequency with this bond distance. Using our band at 4.28 and 4.30 μ, their curves give an O-H $\cdots$ O bond distance of about 2.55 Å. The sharpness of the band would suggest that the hydrogen is more or less symmetrically held between the two oxygens. This band could also be attributed to a C$\equiv$N group formed from dehydration of the amide group by the solvent. In this connection it might be noted that the hydrochloride of terramycin does not have the peaks, 2.91 and 3.03 μ, assigned to the N–H fundamental stretching vibrations of the amide group. Unfortunately, terramycin itself, which also gives rise to the peaks at 4.28 and 4.30 μ, has the above two bands which are missing in its hydrochloride. This would, of course, tend to rule out this explanation. A third possibility to be considered is that the solvent interacts with the terramycin and its hydrochloride. P. P. Regna and associates[4] report that terramycin forms a complex with $CaCl_2$ and heavy metal salts. The majority of their experiments were carried out in aqueous solution. An increase in the solubility of the base was noticed in aqueous and alcoholic solutions with the addition of $CaCl_2$. A pK_a shift of almost 2 pK units to the acid side occurs when an alkaline earth or heavy metal salt is present in aqueous solution.

The spectra of the various antibiotics are very similar in the region from approximately 5.7 to 7.5 μ with the greatest variation being shown by terramycin·HCl. The complexity of the spectra reduces the certainty of the assignments made in this region; thus it has only been possible to propose several tentative ones. A strong band occurring in the spectra of aureomycin, terramycin, tetracycline and aureomycin·HCl at about 6.0 μ has been assigned to the carbonyl groups present. The spectrum of terramycin·HCl has a band at 5.71 μ and a shoulder at 5.96 μ; both can be attributed to carbonyl groups. This would indicate that terramycin·HCl, unlike the other antibiotics, has at least one free carbonyl group present when dissolved in molten antimony trichloride. This is a rather common assignment for bands occurring in this region.[24-26,34-36] The band arising at about 6.9 μ in all the compounds under consideration has been assigned to a C–H bending vibration of the methyl groups. I. A. Brownlie[27] and others[12,25,37] have made the same assignment for this band in a wide variety of compounds. It is possible that the bands falling at about 6.2 and 6.6 μ are due to ring vibrations of the phenyl group, and the band at 6.28 μ to a bending vibration of the NH_2 group. The spectra of aureomycin and aureomycin·HCl which contains a Cl, position 7, on the phenyl group, do not contain the band at 6.2 μ.

(23) N. V. Sidgwick, "The Electronic Theory of Valency," Oxford University Press, London, 1927.

(24) D. J. Emery, Master's Thesis, University of Colorado, 1952.

(25) H. M. Randall, *et al.*, "Infrared Determination of Organic Structures," D. Van Nostrand Co., Boston, Mass., 1949.

(26) L. N. Short and H. W. Thompson, *J. Chem. Soc.*, 168 (1952).

(27) I. A. Brownlie, *ibid.*, 3063 (1950).

(28) J. J. Fox and A. E. Martin, *ibid.*, 318 (1939).

(29) R. B. Barnes, *et al.*, "Infrared Spectroscopy," Reinhold Publ. Corp., New York, N. Y., 1944.

(30) A. M. Buswell, W. H. Rodebush and M. F. Roy, *J. Am. Chem. Soc.*, **60**, 2444 (1938).

(31) F. T. Wall and G. W. McMillan, *ibid.*, **62**, 2225 (1940).

(32) R. E. Rundle and Matthew Parasol, *J. Chem. Phys.*, **20**, 1487 (1952).

(33) R. C. Lord and R. E. Merrifield, *ibid.*, **21**, 166 (1953).

(34) M. L. Josien and N. Fuson, *J. Am. Chem. Soc.*, **73**, 478 (1951).

(35) L. Marion, D. A. Ramsay and R. N. Jones, *ibid.*, **73**, 305 (1951).

(36) G. G. Olson, Ph.D. Thesis, University of Colorado, 1951.

(37) G. Herzberg, "Molecular Spectra and Molecular Structures, II. Infrared and Raman Spectra of Polyatomic Molecules," D. Van Nostrand Co., New York, N. Y., 1945.

THE INFRARED ABSORPTION SPECTRA OF SOME SUBSTITUTED PURINES AND PYRIMIDINES IN ANTIMONY TRICHLORIDE SOLUTION[1]

BY J. R. LACHER, J. L. BITNER, D. J. EMERY, M. E. SEFFL AND J. D. PARK

University of Colorado, Boulder, Colorado

Received January 31, 1955

It was previously found that liquid antimony trichloride is a suitable infrared transmitting solvent for several pyrimidines, purines and amino acids. The present work extends the number of pyrimidines and purines studied by this method. The spectra of 24 pyrimidines and purines were studied in the NaCl region. Nineteen of the above purines and pyrimidines were also studied in the LiF region.

The present investigation is a continuation of the work which began several years ago in this Laboratory.[2,3] Many infrared spectral studies have been made of these compounds.[4-10] In

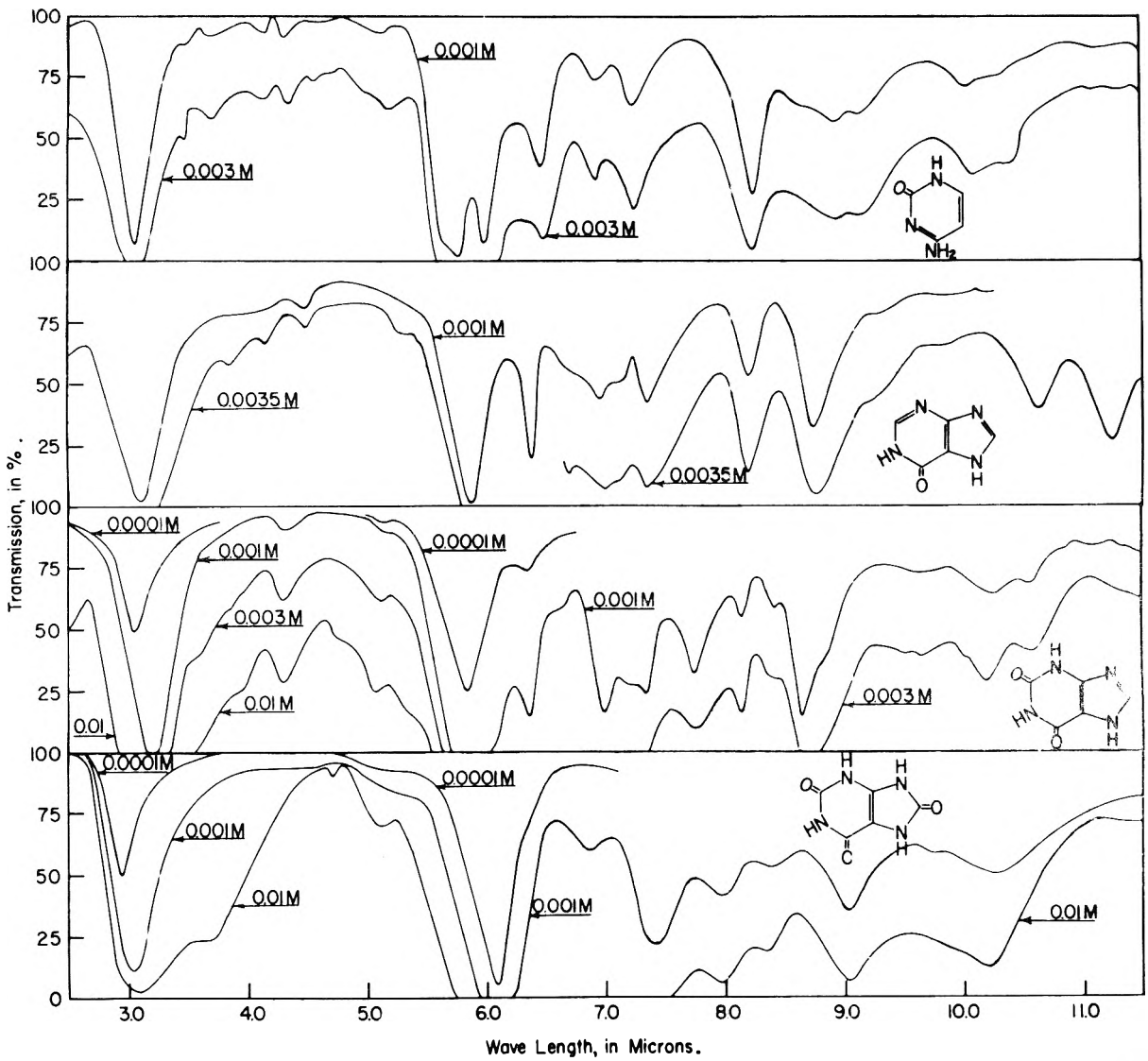

Fig. 1.—Infrared spectra of cytosine, hypoxanthine, xanthine and uric acid in molten antimony trichloride. All spectra in a 5.4 cm. cell with silver chloride windows.

(1) This research was supported in part by the Atomic Energy Commission, Contract No. AT(29)-787, Program A.

(2) J. R. Lacher, D. E. Campion and J. D. Park, *Science*, **110**, 300 (1949).

(3) J. R. Lacher, V. D. Croy, A. Kianpour and J. D. Park, THIS JOURNAL, **58**, 206 (1954).

(4) E. R. Blout and R. C. Mellors, *Science*, **110**, 137 (1949).

(5) E. R. Blout and M. Fields, *J. Am. Chem. Soc.*, **72**, 479 (1950).

(6) E. R. Blout and M. Fields, *Science*, **107**, 252 (1949).

(7) E. R. Blout and M. Fields, *J. Biol. Chem.*, **178**, 335 (1949).

(8) J. A. Brownlie, *J. Chem. Soc.*, 3062 (1950).

(9) M. M. Stimson and M. J. O'Donnell, *J. Am. Chem. Soc.*, **74** 1805 (1952).

(10) L. N. Short and H. W. Thompson, *J. Chem. Soc.*, 168 (1952).

general, this work has been hampered by the lack of a suitable solvent, since a majority of the compounds are insoluble in the solvents usually considered applicable to infrared investigations. Thus the investigations have, on the whole, been restricted to the study of these compounds in the solid state, using nujol paste or perfluorinated kerosene and as solid solutions using KBr as the second component. Previously, it has been shown that antimony trichloride is a satisfactory solvent for a number of difficulty soluble substances.[2,3] The present work has extended the number of pyrimidines studies in the infrared region using this solvent.

Results

The spectra of 24 purines and pyrimidines have been observed in the NaCl region and are shown in Figs. 1, 2, 3, 4, 5 and 6. These are cytosine, uracil, thymine, 6-methyluracil, dihydrothymine, 5-chlorouracil, 6-ethoxyuracil, 6-ethoxy-1-methyluracil, barbituric acid, adenine, hypoxanthine, guanine, xanthine, uric acid, thioadenine, thiocytosine, 2-thiouracil, thiobarbituric acid, 4-amino-2-thiouracil, thiothymine, 6-methyl-2-thiouracil, 6-propyl-2-thiouracil, orotic acid and the potassium salt of orotic acid. In addition, all of the above compounds with the exception of thioadenine, thiobarbituric acid, 4-amino-2-thiouracil, 6-propyl-2-

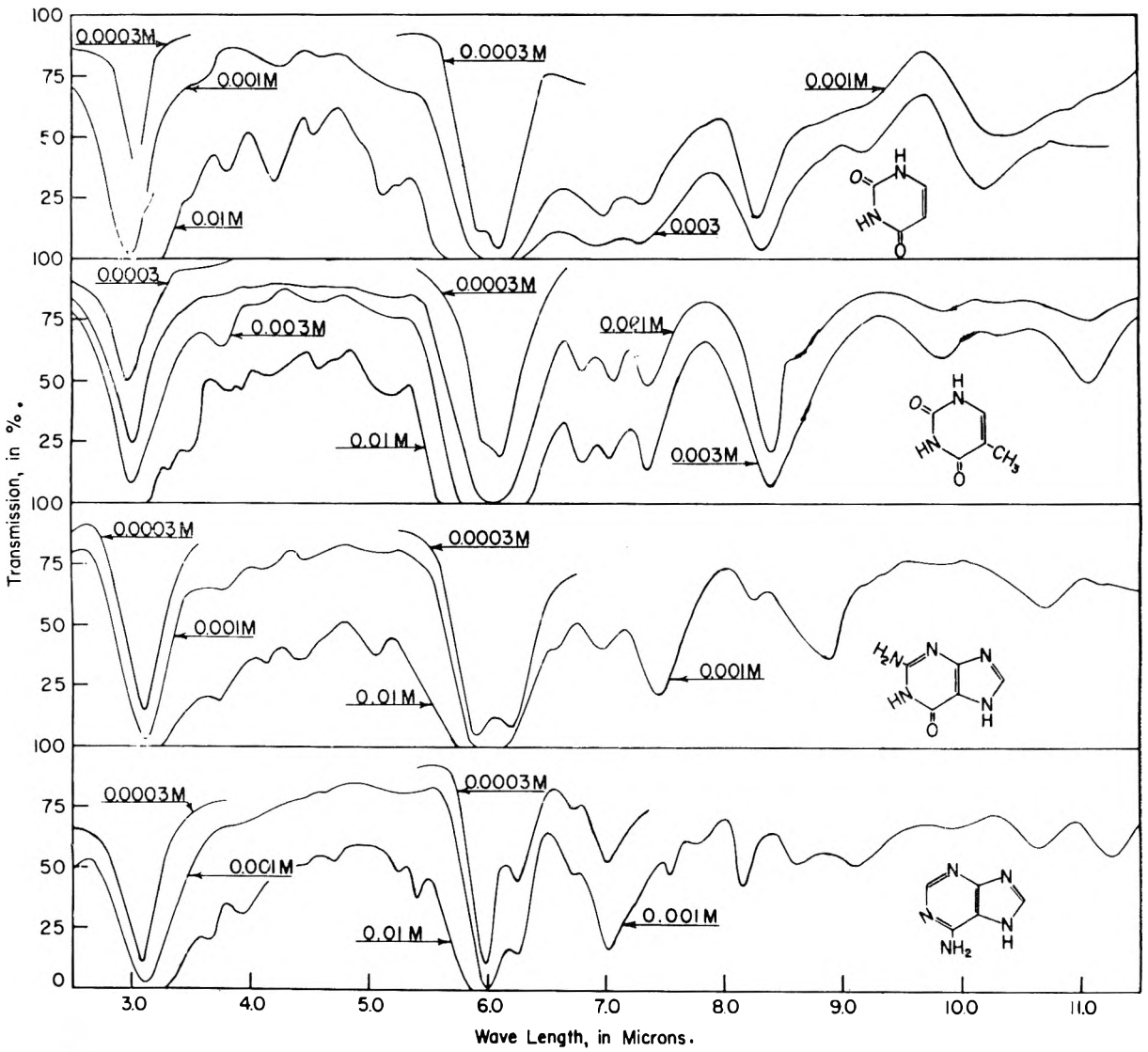

Fig. 2.—Infrared spectra of uracil, thymine, guanine and adenine in molten antimony trichloride. All spectra in 5.4 cm. cell with silver chloride windows.

The experimental procedures involved in these studies have been described previously.[3] thiouracil and the potassium salt of orotic acid were also studied in the LiF region. Their spectra are

shown in Figs. 7, 8, 9, 10 and 11. Tables I and II give the position of peaks which have been assigned in the LiF and NaCl region, respectively.

The LiF region contains the fundamental stretching frequencies of the C–H, O–H, N–H, S–H, etc., groups. These produce, perhaps, the

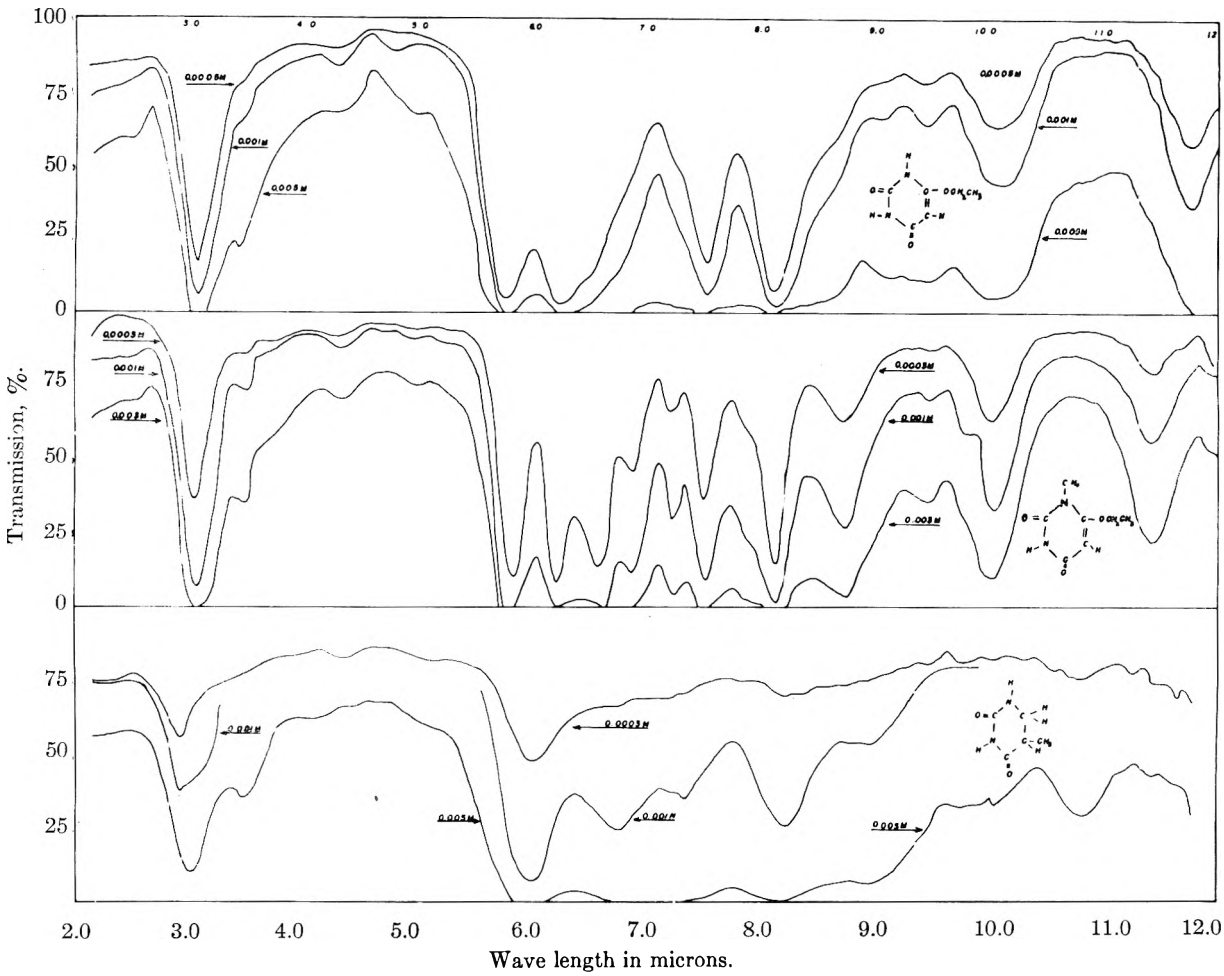

Fig. 3.—Infrared spectra of 6-ethoxyuracil, 6-ethoxy-1-methyluracil and dihydrothymine in molten antimony trichloride. All spectra in 5.4 cm. cell with silver chloride windows.

TABLE I

LiF REGION

	2ν N–H of NH	2ν C–H aromatic	3ν C=O (1) and/or 3ν C=C (2) and/or 3ν C=N (3)	1ν asym. N–H of NH_2	1ν N–H of N–H	1ν C–H aromatic	1ν C–H aliphatic	2δ C–H out of plane
Cytosine	1.53	1.66	...	2.91	2.99	3.24	...	4.09
Uracil	1.52	1.65	1.99	...	2.98	3.21	...	...
Thymine	1.51	1.67	2.00	...	2.98	3.24	3.43	...
							3.47	
							3.52	
6-Methyluracil	1.47	...	...	...	3.00	...	3.50	4.15
Dihydrothymine	1.56	...	1.99	...	2.98	...	3.36	4.15
							3.42	
							3.45	
5-Chlorouracil	1.53	1.65	1.99	...	2.99	3.24	...	4.23
6-Ethoxyuracil	...	...	1.95	...	3.02	3.20	3.36	4.15

TABLE I (*Continued*)

	2ν N–H of NH	2ν C–H aromatic	3ν C=O (1) and/or 3ν C=C (2) and/or 3ν C=N (3)	1ν asym. N–H of NH_2	1ν N–H of N–H	1ν C–H aromatic	1ν C–H aliphatic	2δ C–H out of plane
6-Ethoxy-1-methyl-uracil	...	...	2.03	...	3.03	3.21	...	4.19
Barbituric acid	1.54	...	1.98	...	3.00	...	...	4.11
Adenine	1.52	1.64	2.00	2.88	3.00	3.25	...	...
Hypoxanthine	1.53	1.63	2.03	...	3.03	3.17	...	4.10
Guanine	1.52	1.59	2.01	2.89	2.98	3.19	...	...
Xanthine	1.53	1.64	2.00	...	3.03	3.19	...	...
Uric acid	1.52	...	1.99	...	2.98	...	...	...
Thiocytosine	1.50	1.65	...	2.87	2.97	3.21	..	4.11
Thiouracil	...	...	...	...	3.03	3.21	...	4.15
Thiothymine	...	..	...	...	3.03	3.23	3.40 4.43	4.17
6-Methyl-2-thio-uracil	...	...	...	...	3.03	3.21	3.41 3.45	...
Orotic acid	...	..	...	...	2.98	3.20	...	4.09

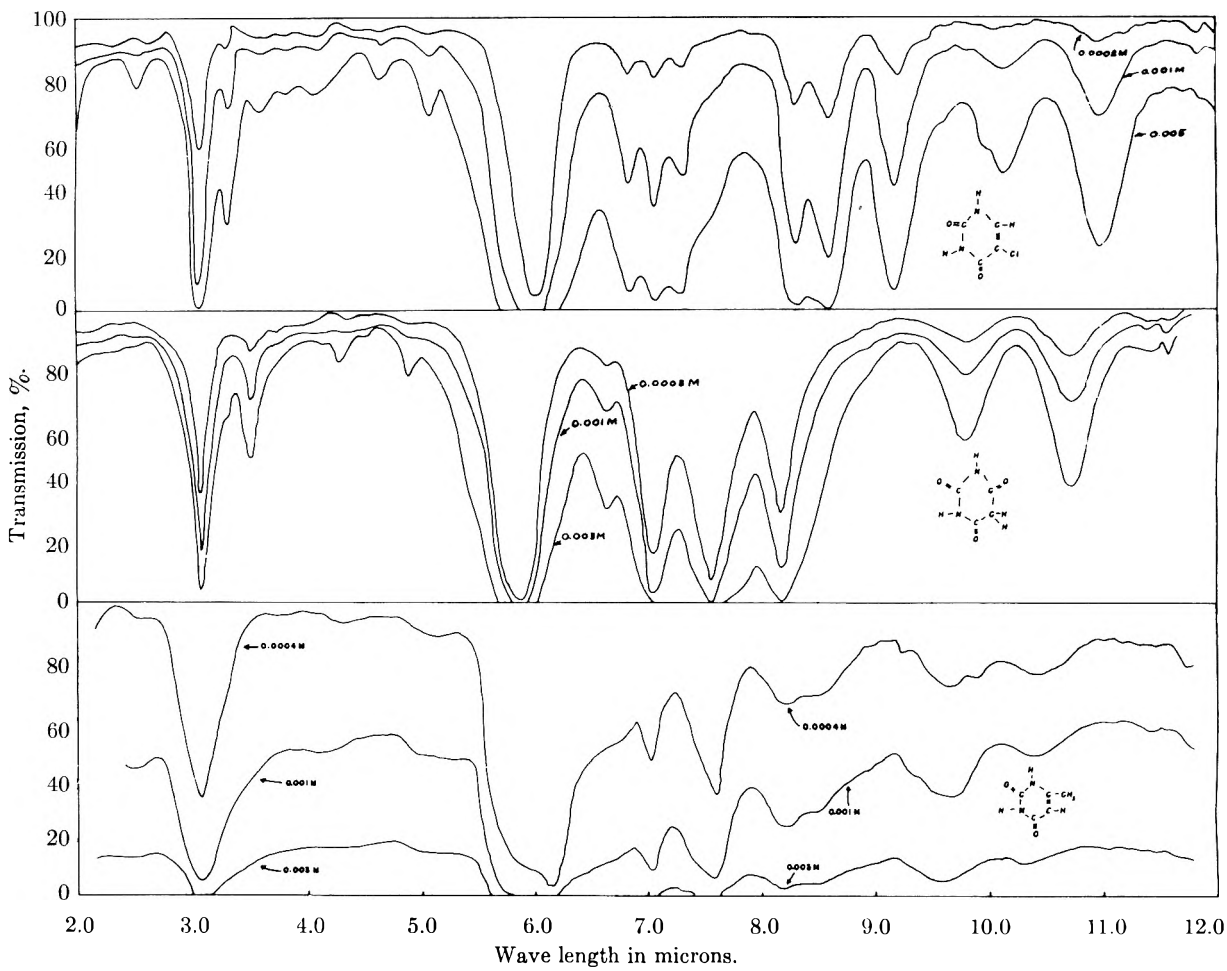

Fig. 4.—Infrared spectra of 5-chlorouracil, barbituric acid and 6-methyluracil in molten antimony trichloride. All spectra in a 5.4 cm. cell with silver chloride windows.

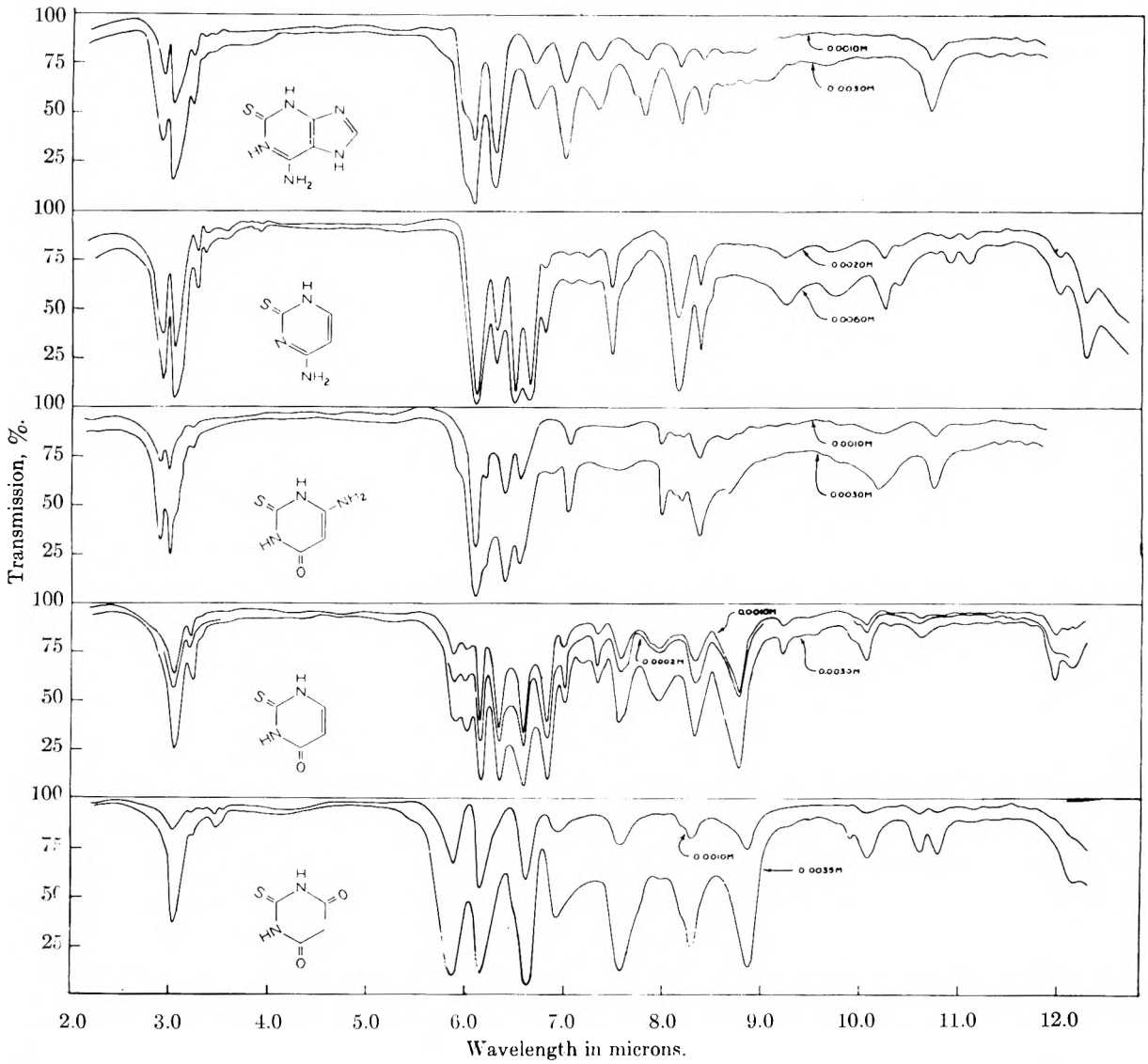

Fig. 5.—Infrared spectra of thioadenine, thiocytosine, 4-amino-2-thiouracil, 2-thiouracil and 2-thiobarbituric acid in molten antimony trichloride. All spectra in 5.5 cm. cell with silver chloride windows.

TABLE II

NaCl REGION

	1ν N–H asym. of NH_2	1ν N–H of N–H	1ν sym. N–H of NH_2	1ν C–H aro-matic	1ν C–H ali-phatic	1ν C=O	1ν C=N	1δ N–H of N–H and NH_2	Thio-ureide ion	C–H of CH_3	1ν C–N	1δ C–H out of plane
Cytosine	...	3.07	...	...	...	5.76	6.01	6.48	...	...	7.25	8.26
Uracil	...	3.05	...	...	...	5.98	...	...	...	...	7.30	8.31
						6.08						
Thymine	...	2.92	...	...	3.33	5.97	...	...	...	6.77	7.36	8.38
						6.08						
6-Methyluracil	...	3.08	...	...	...	6.18	...	...	...	...	...	8.23
Dihydrothymine	...	2.92	...	...	3.47	5.97	...	...	...	6.76	7.33	8.23
5-Chlorouracil	...	3.08	...	...	...	6.00	...	...	...	...	7.33	8.33
6-Ethoxyuracil	...	3.08	...	...	3.44	5.79	...	6.23	...	...	...	8.14
6-Ethoxy-1-methyluracil	...	3.08	...	...	3.50	5.82	...	6.23	...	...	...	8.14
Barbituric acid	...	3.08	...	...	...	5.90	...	...	...	...	...	8.18
Adenine	...	3.09	...	...	...	...	5.97	6.23	...	...	...	8.16
Hypoxanthine	...	3.11	...	...	...	5.88	...	6.37	...	...	7.35	8.19
Guanine	...	3.09	...	...	...	5.91	...	6.18	...	...	...	8.23

TABLE II (*Continued*)

	1ν N–H asym. of NH_2	1ν N–H of N–H	1ν sym. N–H of NH_2	1ν C–H aro-matic	1ν C–H ali-phatic	1ν C=N	1ν C=N	1δ N–H of N–H and NH_2	Thio-ureide ion	C–H of CH_3	1ν C–N	1δ C–H out of plane
Xanthine	...	3.11	...	...	...	5.85	...	6.37	...	...	7.33	8.15
Uric acid	...	2.92	...	...	...	6.03	...	...	...	...	7.40	...
Thioadenine	2.90	3.02	3.02	3.22	...	...	5.96	6.28	6.06	...	...	8.14
Thiocytosine	2.92	3.04	3.04	3.28	...	...	6.09	6.47	6.29	...	...	8.34
2-Thiouracil	...	3.04	...	3.24	...	...	...	...	6.35	...	...	8.33
2-Thiobarbituric acid	...	3.04	...	...	...	5.87	...	...	6.14	...	...	...
4-Amino-2-thiouracil	2.90	3.00	3.05	3.24	...	...	...	6.19	6.39	...	...	8.34
Thiothymine	...	3.04	...	3.24	3.44	...	...	...	6.44	6.86	...	8.35
6-Methyl-2-thiouracil	...	3.06	...	3.23	3.44	...	...	...	6.41	6.83	...	8.48
6-Propyl-2-thiouracil	...	3.05	...	3.23	3.39 3.43 3.50	...	...	...	6.41	6.84	...	8.37
Orotic acid	..	3.03	...	3.24	...	5.88 6.05	...	..	..	...	7.30	8.16
K salt of orotic acid	...	3.01	...	3.22	...	5.89 6.02	...	...	...	...	7.33	8.13

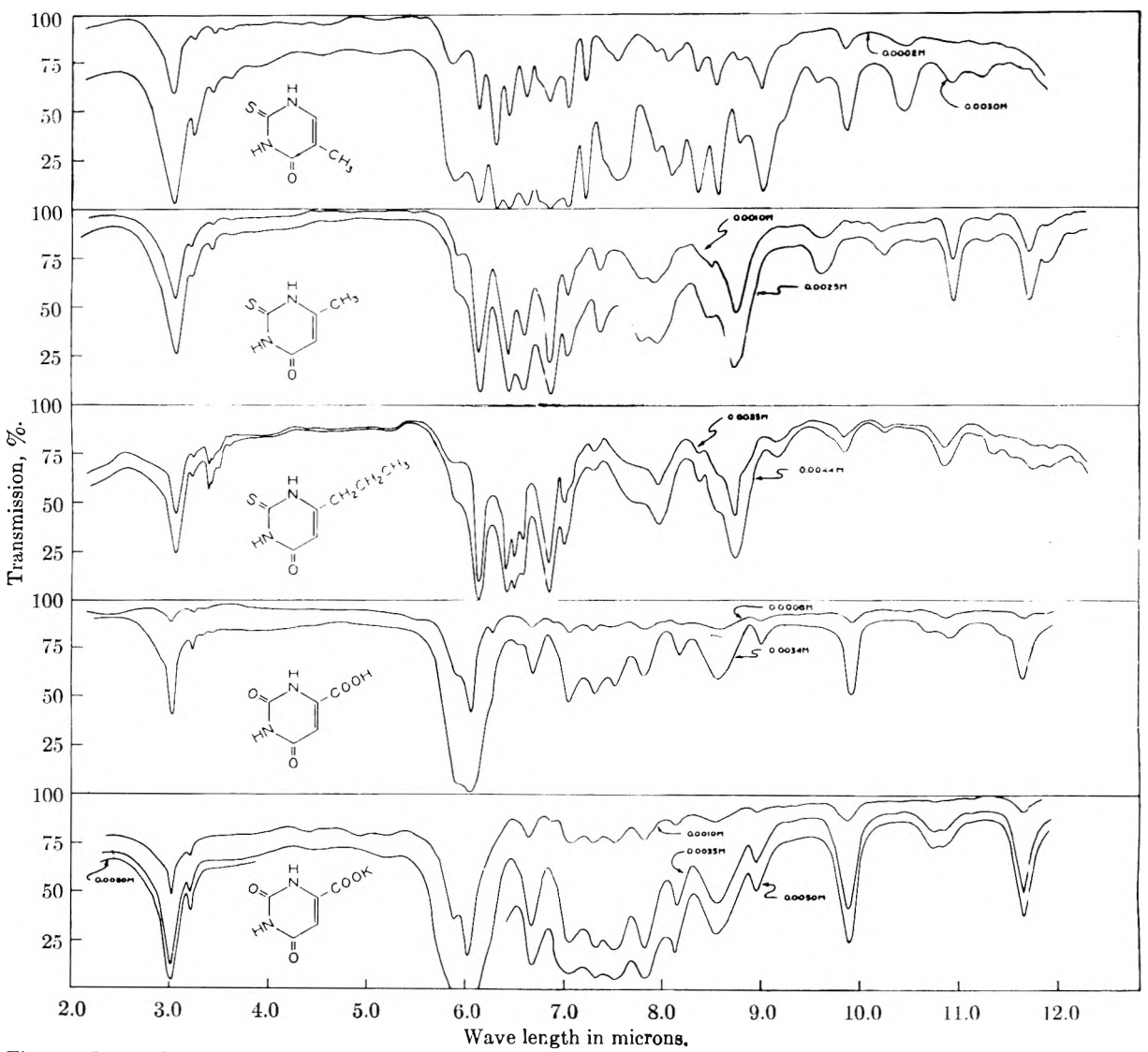

Fig. 6.—Infrared spectra of thiothymine, 6-methyl-2-thiouracil, 6-propyl-2-thiouracil, orotic acid and potassium salt of orotic acid in molten antimony trichloride. All spectra in 5.5 cm. cell with silver chloride windows.

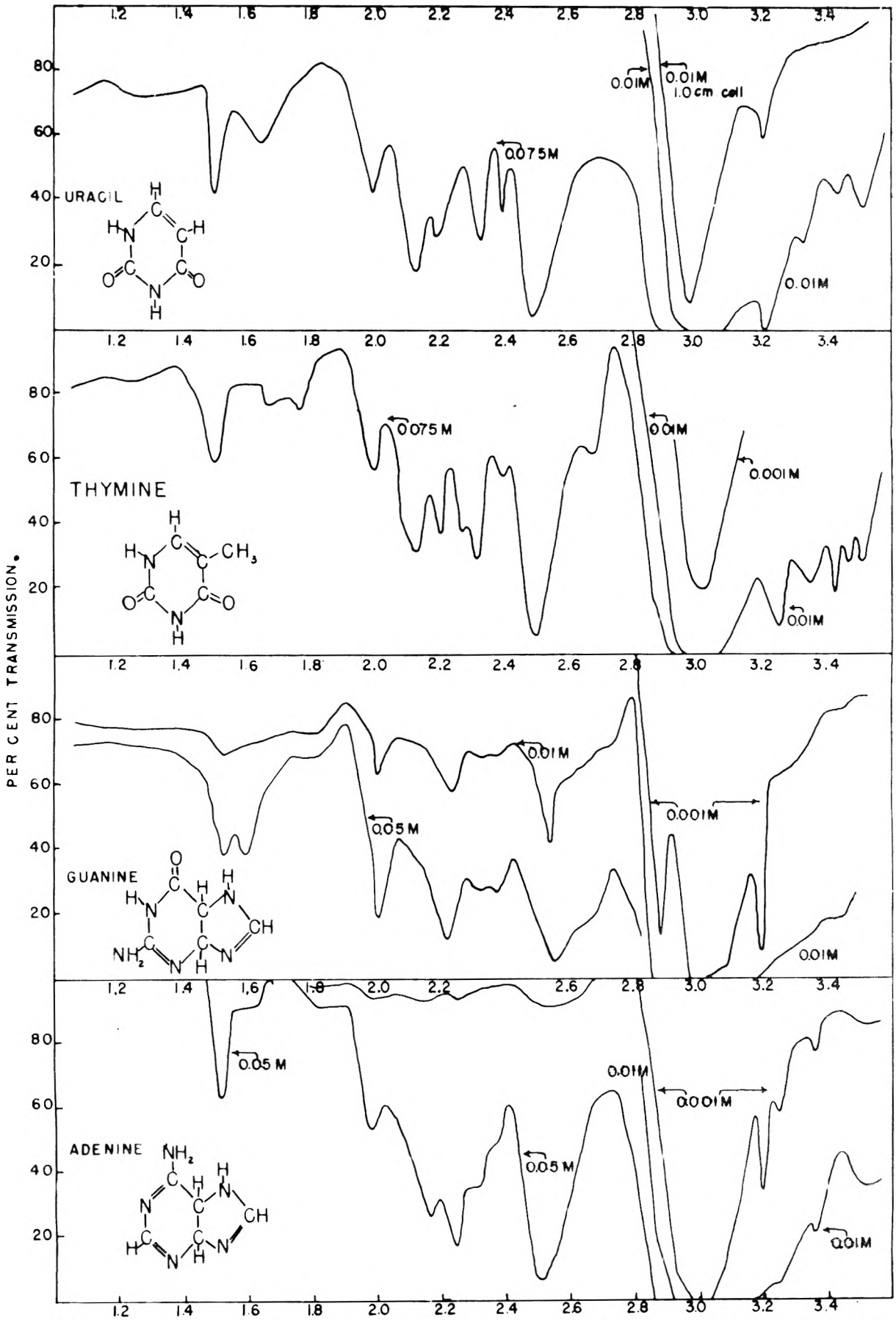

Fig. 7.—Infrared spectra of uracil, thymine, guanine and adenine in molten antimony trichloride. All spectra in 1.0 cm. cell with silver chloride windows.

most stable bands found in the infrared region. All the compounds under consideration contain several of the above groups; for this reason, this region can be very helpful in obtaining information pertaining to the structure of the purines and

Short and Thompson[10] as well as Brownlie[8] have made similar assignments in their work on a number of substituted pyrimidines. In addition to the above workers, several other investigators have also attributed the peaks falling at these positions to

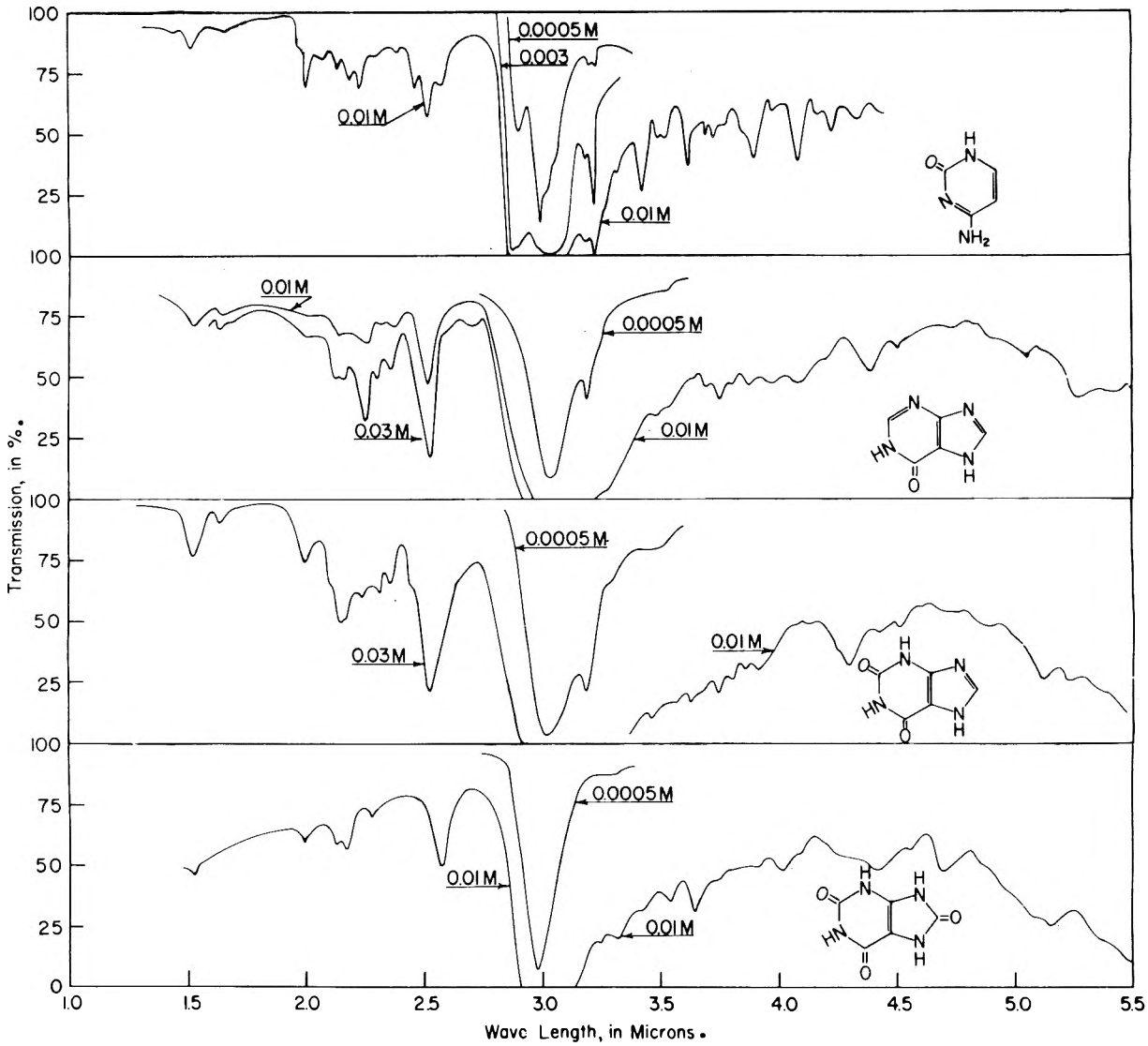

Fig. 8.—Infrared spectra of cytosine, hypoxanthine, xanthine and uric acid in molten antimony chloride. All spectra in 5.4 cm. cell with silver chloride windows.

pyrimidines. A peak or shoulder at approximately 2.9 μ and in several cases a second peak or shoulder at approximately 3.03 μ was observed in the compounds containing an amino group. The peak at 2.9 μ has been assigned to the asymmetrical fundamental stretching frequency of the NH_2 group and the shoulder at 3.03 μ to the symmetrical fundamental stretching frequency of the same group. the NH_2 group.[8,10-12] Each compound studied, including those observed in the NaCl region only, show a strong peak in their spectra at about 3.0 μ. This peak has been assigned to the N–H fundamental stretching frequency of the ring imide

(11) V. D. Croy, Master's Thesis, University of Colorado, 1951.

(12) H. M. Randall, *et al.*, "Infrared Determination of Organic Structures," D. Van Nostrand Co., New York, N. Y., 1949.

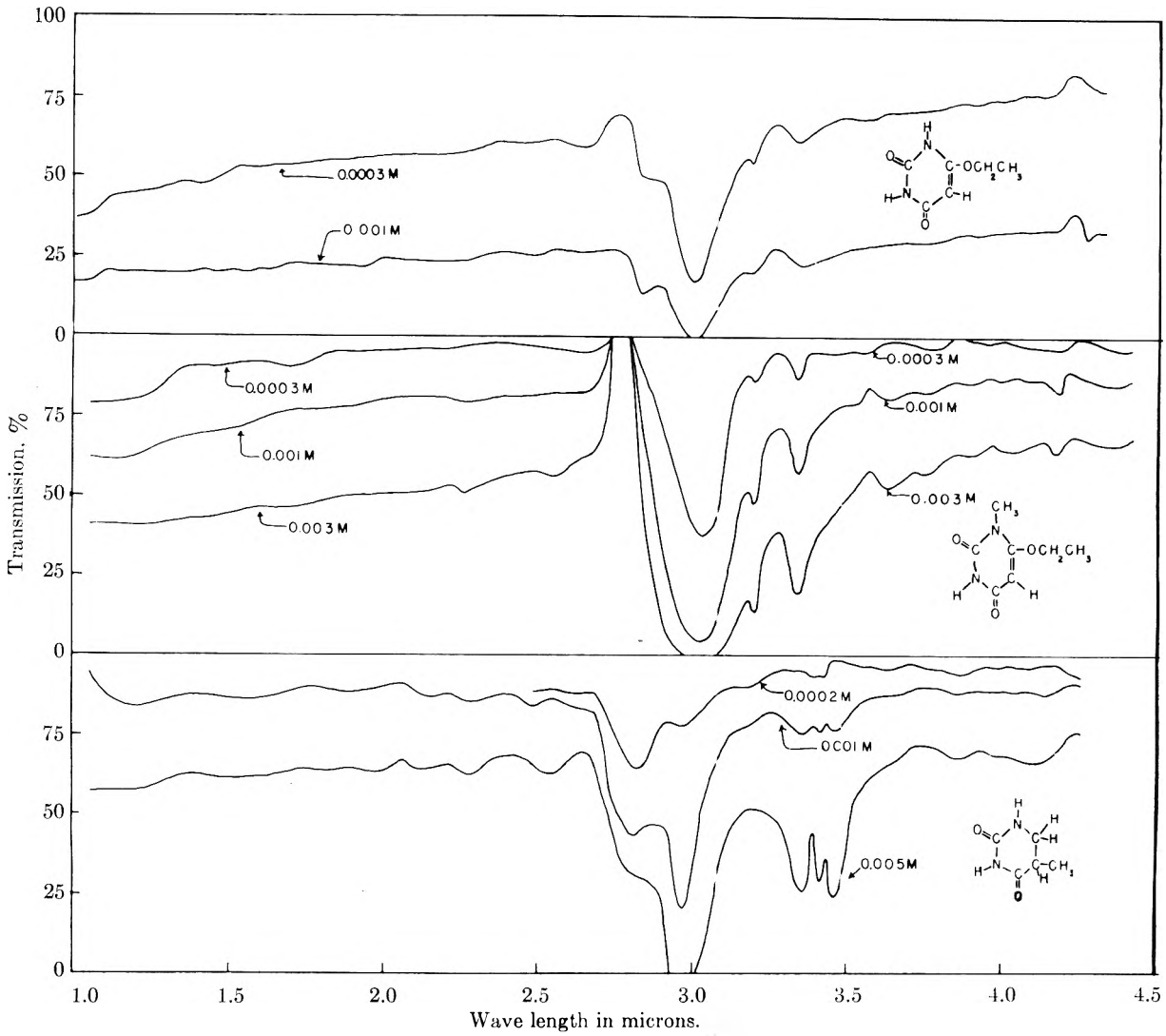

Fig. 9.—Infrared spectra of 6-ethoxyuracil, 6-ethoxy-1-methyl uracil and dihydrothymine in molten antimony trichloride. All spectra in 5.4 cm. cell with silver chloride windows.

group. It may also include the first overtone of several of the bands arising in the double bond region. This would account for the broadening of the band on the long wave length side. In support of this, it may be noted that cytosine, thiocytosine and to a lesser extent some of the other compounds, show several distinct shoulders on the upper wave length side of this band. This band falls in a region attributed to both normal and hydrogen bonded imide and amide groups.[5,8,13–19] No shifting of the N–H band occurs with an increase in concentration. This would indicate that little or no intermolecular hydrogen bonding takes place, since this type of hydrogen bonding is dependent on concentration. The position of the bands attributable to the aromatic and aliphatic C–H groups has been well established.[11,14,20–23] They fall in the 3.2–3.3 μ and 3.4–3.6 μ regions, respectively. The locations of these bands in the various compounds are given in Tables I and II. The presence of little or no absorption in the 2.70–2.85 μ region implies that these compounds exist in the keto form when dissolved in antimony trichloride. In the case of the thiouracils, there is little evidence of the presence of an S–H group vibration in the region generally ascribed to it. In general, the spectra of the thiopyrimidines and thiopurines are similar to those of their oxygen analogs in the LiF region, with the addition, of course, of overtones due to bands arising from the presence of the sulfur atom in the compounds.

The most obvious difference between the spectra of the pyrimidines and thiopyrimidines occurs in the double bond region. A number of intense bands, absent in the pyrimidines, appear in the

(13) R. E. Richards and H. W. Thompson, *J. Chem. Soc.*, 1248 (1947).

(14) A. M. Buswell, W. H. Rodebush and M. F. Roy, *J. Am. Chem. Soc.*, **60**, 2444 (1938).

(15) S. Mizushima, T. Shimanouti, S. Nagakura, K. Kuratani, M. Tsuboi, H. Baba and O. Fuzioka, *ibid.*, **72**, 3490 (1950).

(16) C. S. Marvel and C. H. Young, *ibid.*, **73**, 1066 (1951).

(17) E. E. Magat, *ibid.*, **73**, 1367 (1951).

(18) S. Mizushima, T. Shimanouti, *et al.*, *ibid.*, **73**, 1330 (1951).

(19) H. W. Thompson, *J. Chem. Soc.*, 328 (1948).

(20) J. J. Fox and A. E. Martin, *ibid.*, 318 (1939).

(21) R. B. Barnes, R. C. Gore, U. Liddell and V. Williams, "Infrared Spectroscopy," Reinhold Publ. Corp., New York, N. Y., 1944.

(22) L. Kellner, *Proc. Roy. Soc. (London)*, **A157**, 110 (1936).

(23) F. T. Wall and G. W. McMillan, *J. Am. Chem. Soc.*, **62**, 2225 (1940).

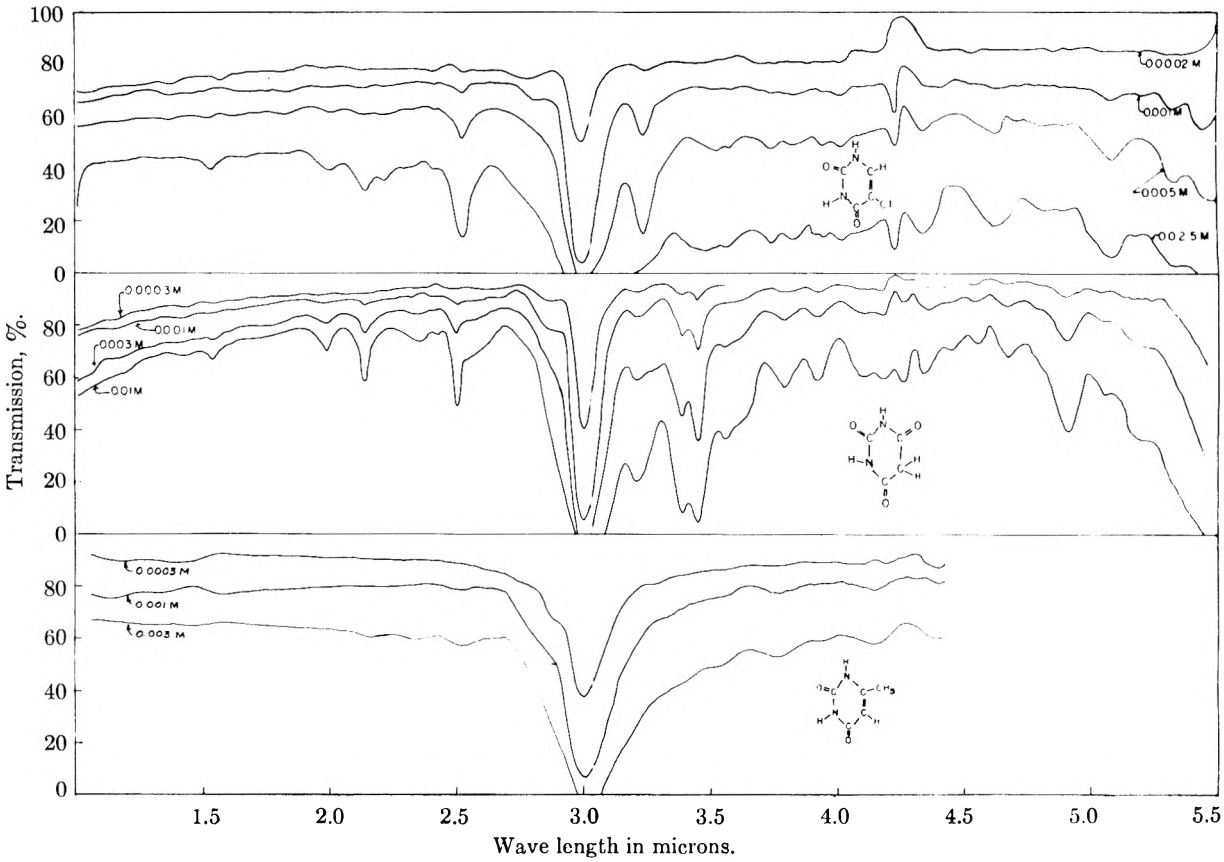

Fig. 10.—Infrared spectra of 5-chlorouracil, barbituric acid and 6-methyluracil in molten antimony trichloride. All spectra in 5.4 cm. cell with silver chloride windows.

spectra of the thiopyrimidines. Randall, *et al.*,[12] attributes these bands to the presence of a thioureide ion in these molecules. One of these new bands is believed to be due to a C–N group which has obtained some double bond character from the positive charge acquired by the carbon in the formation of the thioureide ion. From considerations of several saturated ring compounds, such as thiobarbituric acid, which give rise to only one or two new bands, it appears that the band due to the above group falls in the 6.2–6.4 μ region. The spectra of all the compounds show one or more peaks in the 5.7–6.1 μ region. In general, these peaks have been assigned to carbonyl groups. Two peaks are observed in this region for uracil, thymine, orotic acid and the potassium salt of orotic acid. Randall, *et al.*,[12] attribute the first peak at about 5.9 μ to a carbonyl group in the 4-position and the second peak, about 6.0 μ region, to a 2-positional carbonyl group. Several of the thiopyrimidines give rise to a shoulder of medium intensity rather than to a distinct peak, but it might be noted that this shoulder is not found in the thiopyrimidines which do not contain a carbonyl group.

The peak occurring in cytosine, thiocytosine, adenine and thioadenine at about 6.0 μ has been assigned to C=N[24] group stretching vibrations on the basis of the following observations. There are two ways of assigning the peaks that arise at 5.97 and 6.23 μ in adenine. Number I would be to assign the peak at 5.97 μ to a stretching vibration of the C=C group and the peak at 6.23 μ to the stretching vibration of the C=N group. Number II would require the assigning of the peak at 5.97 μ to the stretching frequency of the C=N and C=C groups and the peak at 6.23 μ to the bending vibration of the N–H group. The second possibility has been given preference over the first, since the C=C stretching motion changes the resultant dipole by relatively small amounts, thus giving rise to a rather weak peak. This does not follow the experimental results, as can be seen from Fig. 2. Also the C=N stretching vibration should give a stronger band and, with the three present in the adenine molecule, it should be very intense. Both of the above observations support the assignment given in II and tend to disprove I. It might also be noted that the relative intensities of these two peaks in thioadenine, Fig. 5, which has fewer C=N groups serves to substantiate the assignment given in II.

A number of the compounds under consideration contain methylene and/or methyl groups. The bending frequencies of these groups fall in the 6.8 μ region.[8,3,12,25] Thus the bands occurring there have been given this assignment whenever it was plausible to do so. The band due to the

(24) H. M. Randall, R. G. Fowler, N. Fuson, and J. R. Dangl, "Infrared Determination of Organic Structures," D. Van Nostrand Co., New York, N. Y., 1949.

(25) G. Herzberg, "Molecular Spectra and Molecular Structures, II. Infrared and Raman Spectra of Polyatomic Molecules," D. Van Nostrand Co., New York, N. Y., 1945.

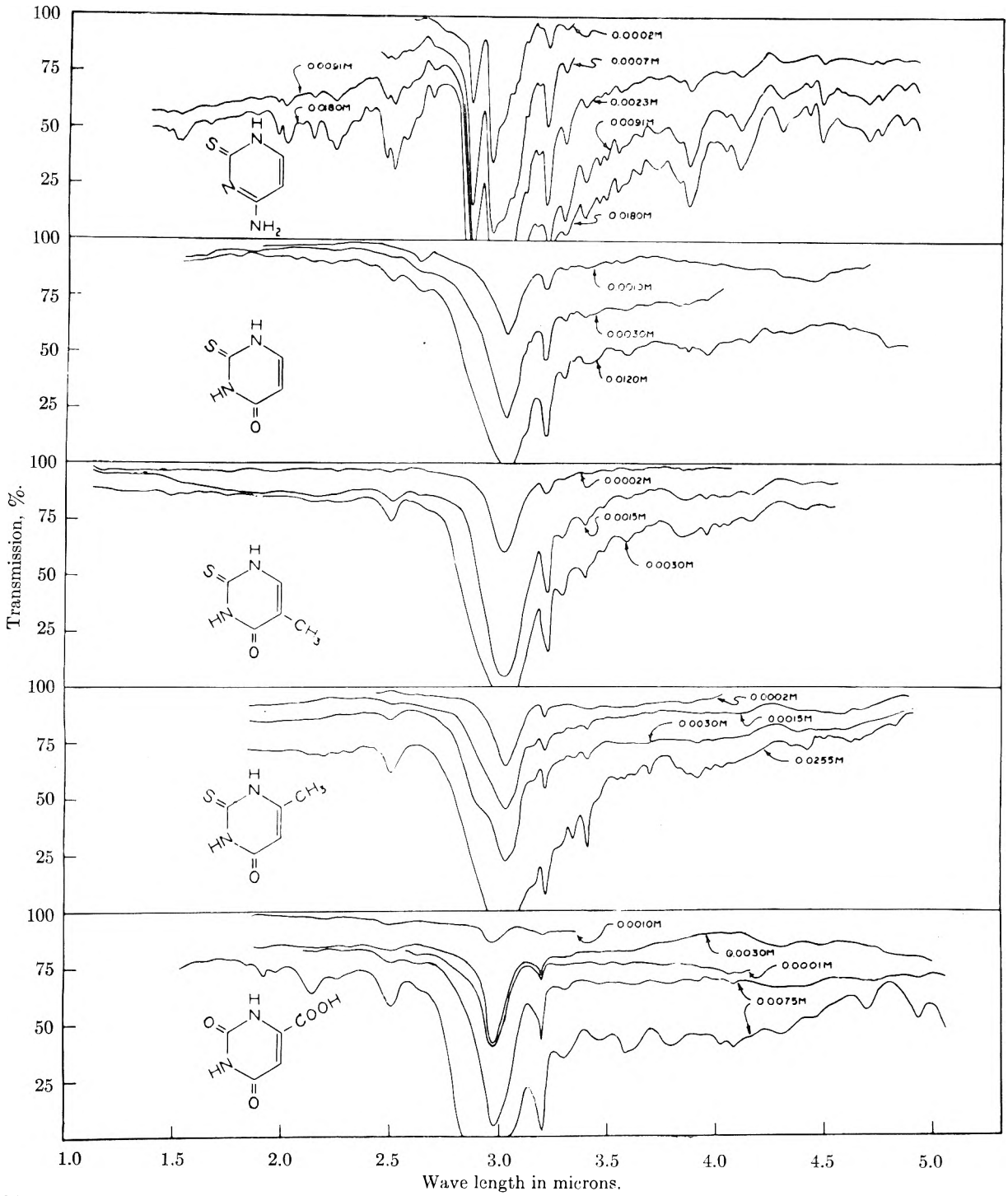

Fig. 11.—Infrared spectra of thiocytosine, 2-thiouracil, thiothymine, 6-methyl-2-thiouracil and orotic acid in molten antimony trichloride. All spectra in 1.0 cm. cell with silver chloride windows.

C–N stretching frequency should be fairly strong in the pyrimidines and purines and weak, on the assumption that the thioureide structure is present, in the thiopyrimidines and thiopurines. Based on the above observations, the peak arising about 7.3 μ has been given this assignment. The specific assignments for the individual compounds are, of course, given in Table II.

A peak appearing in the region from 8.14 μ to 8.48 μ for the pyrimidines and thiopyrimidines and from 8.14 μ to 8.23 μ in the purines and thiopurines has been assigned to the C–H bending out of plane frequency on the basis of the agreement of the number of C–H groups in the molecule to the intensity of the peak. Only uric acid, Fig. 1, failed to show this peak. Other investigators[8,13] have also assigned this peak to the C–H bending frequency out of plane and it is significant that compounds containing no C–H group (tetra-substituted pyrimidines) do not show a peak in this region.

CONDUCTANCE OF MERCAPTANS IN PYRIDINE IN ADDITION OF HEAVY METAL ACETATES

BY DAVID H. ROSENBLATT AND GEORGE N. JEAN

Contribution from the Chemical Corps Medical Laboratories, Army Chemical Center, Md.

Received February 4, 1955

Conductance curves are presented for the addition of mercuric, phenylmercuric, zinc, cadmium, lead and silver acetates to 2,3-dimercapto-1-propanol (BAL), 1,3-dimercapto-2-propanol, 2-mercaptoethanol and *n*-decylmercaptan, dissolved in pyridine. Explanations for some of the results are suggested.

I. Introduction

In the course of investigations on the chemistry of BAL (2,3-dimercapto-1-propanol), we undertook the conductometric study of reactions between heavy metal acetates and mercaptans in pyridine. Our early results indicated no conformance to an easily recognizable pattern that would permit prediction of the nature of interaction of an untested mercaptan–metal combination. The type of survey here described could be extended indefinitely, employing other metal salts and mercaptan types, without leading to the formulation of a general theory. For this reason, detailed study was limited to four mercaptans and six metal salts. A few additional related experiments have also been included.

Pyridine was chosen as a solvent for the following three reasons: (a) it dissolves the mercuric mercaptides of BAL and 1,3-dimercapto-2-propanol,[1] (b) it is a good solvent for many heavy metal salts,[2] and (c) its acetic acid solutions have very low conductances.[2]

II. Experimental

Materials.—BAL and 1,3-dimercapto-2-propanol were purified through the mercury mercaptides[1] and distilled at 2.7 mm. Commercial samples of *n*-decylmercaptan and 2-mercaptoethanol were used without further purification. The *n*-decylmercaptan was only 93% pure, according to the average mole ratios at the titration end-points, and corrections were made accordingly in the data presented here.

The pyridine was of a grade sold for Karl Fischer water analyses.

The heavy metal acetates were all of reagent grade, and their pyridine solutions were 0.200 *M* in the case of the monovalent salts and 0.100 *M* for the divalent salts.

Apparatus.—A Serfass Conductivity Bridge, Model RC M15, made by Industrial Instruments, Inc., was used for conductance measurements with the 60 cycle source.[3] The conductivity cell,[4] of the dip type commonly used for testing distilled water, had smooth platinum electrodes and a cell constant of 0.122 cm.$^{-1}$. Titrations were carried out in a cylindrical vessel 40 mm. in diameter and 110 mm. high, through the outer jacket of which water was circulated at 25°. Water-pumped nitrogen, after passage through Fieser's solution, anhydrous calcium chloride and pyridine, was introduced into the vessel through a tube from above. Solutions of the metal salts in pyridine were added from a 5-ml. microburet, graduated to 0.01 ml. and provided with a reservoir and greaseless Teflon stopcocks. Teflon-covered magnetic bars were used for stirring. After introduction of the mercaptan solution, the top of the vessel was covered with aluminum foil to prevent air from diffusing in.

Procedure.—A sample of mercaptan was weighed into a 25-ml. volumetric flask and diluted to volume with pyridine just prior to use. An aliquot, chosen to contain 0.75 to 0.95 mequiv. of thiol, was added to the amount of pyridine[5] necessary to bring the total volume to 70 ml., and a slow stream of nitrogen was passed into the solution. The conductance was measured before insertion of the buret tip to

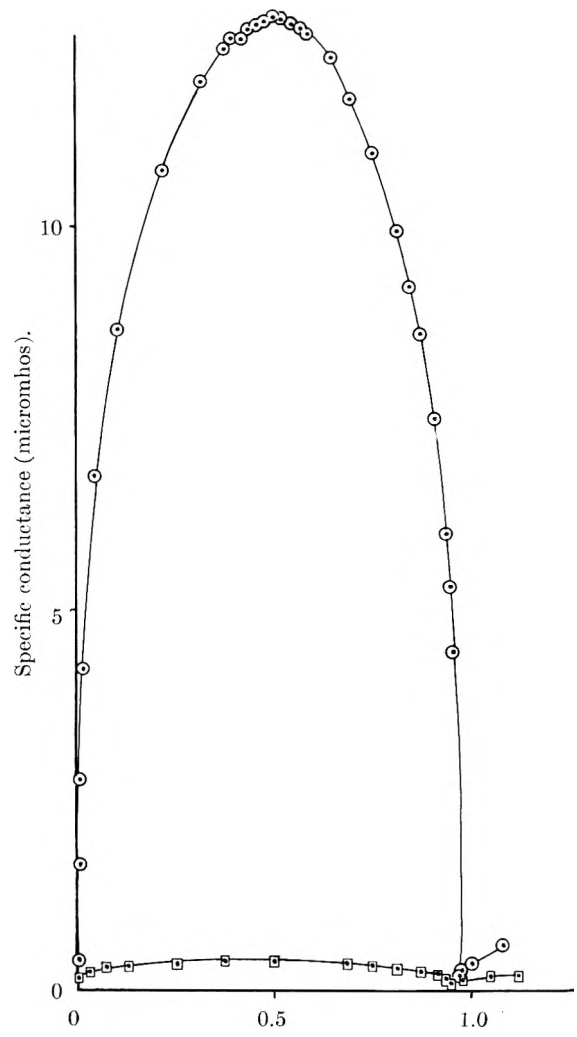

Fig. 1.—Conductance of mercaptans in pyridine on addition of 0.100 *M* mercuric acetate: ⊙, BAL (0.90 meq.); ⊡, 1,3-dimercapto-2-propanol (0.79 meq.) for comparison.

(1) B. Sjöberg, *Ber.*, **75**, 13 (1942).

(2) L. F. Audrieth and J. Kleinberg, "Non-Aqueous Solvents," John Wiley and Sons, Inc., New York, N. Y., 1953, pp. 123–125.

(3) The 60 cycle source permitted more accurate readings, at very low conductances, than did the 1000 cycle source.

(4) When no precipitate was formed during a titration, the cell was cleaned by immersion in methanol, distilled water and methanol again, and air-dried just before use. When a precipitate had formed it was removed with nitric acid followed by thorough water rinsing in which case there often remained, on the electrodes, a conducting contaminant. The latter was best removed by soaking the cell in pyridine; the cell was dried again before use.

(5) The conductance of the pyridine was checked before addition of the mercaptan solution in order to assure that the apparatus was free from conducting impurities. When the conductance was more than 1 micromho the pyridine was replaced by a fresh portion.

avoid effects of diffusion of the titrant. The buret and the aluminum foil were put in place and titration begun. After each addition of heavy metal salt solution, stirring was continued for a few seconds, stopped,[6] and a conductance reading made. Occasionally, after the lapse of a minute, the conductance was remeasured in order to check the constancy of the readings.

III. Results

The results of the conductometric titrations are given in Figs. 1–9. In the absence of a precipitate equilibrium was generally established instantaneously. In regions of precipitate formation, indicated by broken lines on the graphs, the conductance readings usually drifted downward with time. Only the first reading after each increment of metal acetate was graphed.

Mercuric Acetate.—Of the six metal salts for which data are given here, mercuric acetate showed the greatest relative difference between BAL and the other mercaptans. The maximum in the BAL curve (Fig. 1) occurred a little past the mid-point (*i.e.*, equivalents $Hg(OCOCH_3)_2$/equivalents SH = 0.5), corresponding to a ratio of one mercury atom per two BAL molecules, and a minimum, which could be considered the titration end-point, was found at an equivalent ratio of 1:1. Also, with the other mercaptans (Fig. 2) maxima were reached near the mid-points and end-point minima near 1:1 equivalent ratios of mercuric acetate to

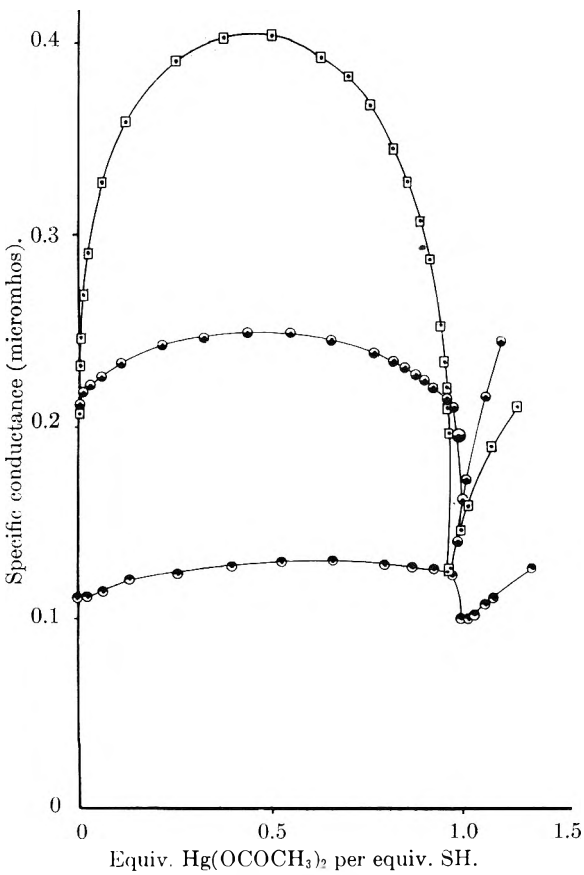

Fig. 2.—Conductance of mercaptans in pyridine on addition of 0.100 *M* $Hg(OCOCH_3)_2$: ⊡, 1,3-dimercapto-2-propanol (0.79 meq.); ◒, 2-mercaptoethanol (0.92 meq.); ◓, *n*-decylmercaptan (0.76 meq.).

(6) Both the magnetic stirrer and the circulating pump interfered and had to be stopped when readings were to be made.

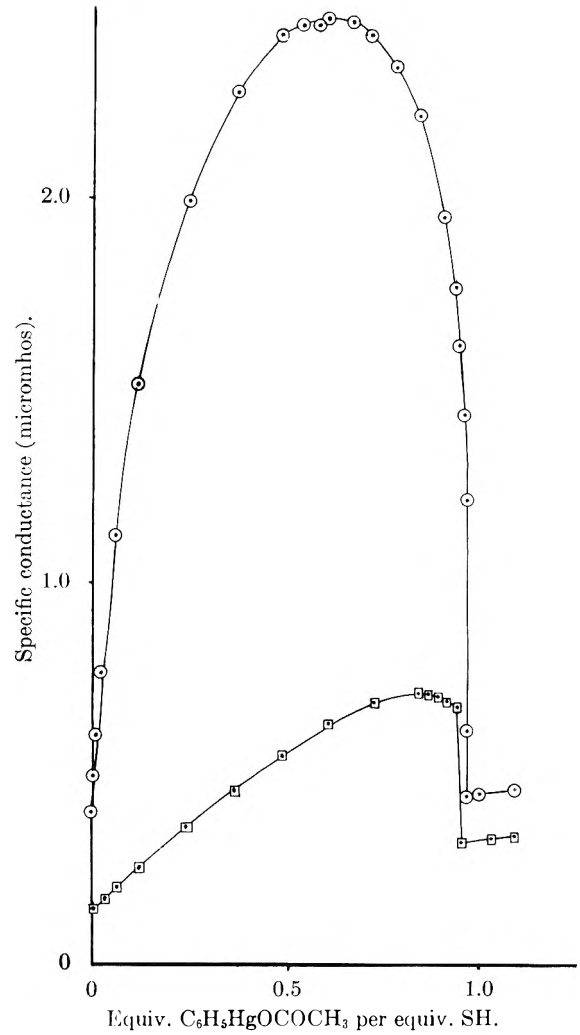

Fig. 3.—Conductance of mercaptans in pyridine on addition of 0.200 *M* $C_6H_5HgOCOCH_3$: ⊙, BAL (0.82 meq.); ⊡, 1,3-dimercapto-2-propanol (0.82 meq.).

mercaptan. With the exception of *n*-decylmercaptan, the end-point conductances were less than the mercaptan conductances before addition of the metal salt. No attempt was made to study the effect of additional mercuric acetate past the 1:1 equivalent ratio, but the possibility of further interactions is not excluded. A mixture of BAL with 2-mercaptoethanol (data not given here) gave a higher conductance maximum than the sum of the maximum values obtained with the individual mercaptans.[7,8]

Phenylmercuric Acetate.—With BAL the conductance maximum on titration with phenylmercuric acetate was one-fifth as large as that obtained with mercuric acetate, whereas with the

(7) When, earlier in the course of this investigation, a sample of 1,3-dimercapto-2-propanol obtained from another laboratory was titrated with mercuric acetate, a much higher conductance maximum was obtained, and the curve was peculiarly flattened. This could best be explained on the basis of a small admixture of BAL.

(8) Ethanedithiol gave a curve, the first part of which showed a high conductance like that of BAL, but a heavy precipitate and an abrupt drop in conductance appeared when about one-third of the stoichiometric quantity of mercuric acetate had been added. It is evident that there was a condition of supersaturation with respect to the non-conducting reaction product, which favored the existence of the conducting species, prior to the precipitation.

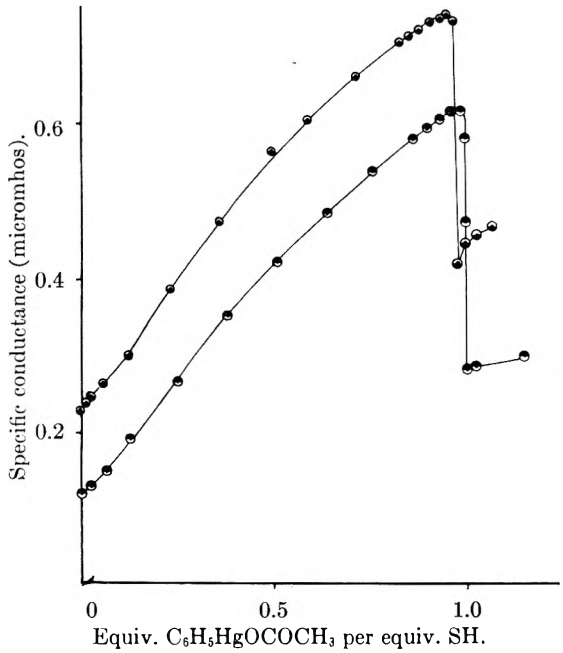

Fig. 4.—Conductance of mercaptans in pyridine on addition of 0.200 *M* $C_6H_5HgOCOCH_3$: ◒, 2-mercaptoethanol (0.84 meq.); ◓, *n*-decylmercaptan (0.78 meq.).

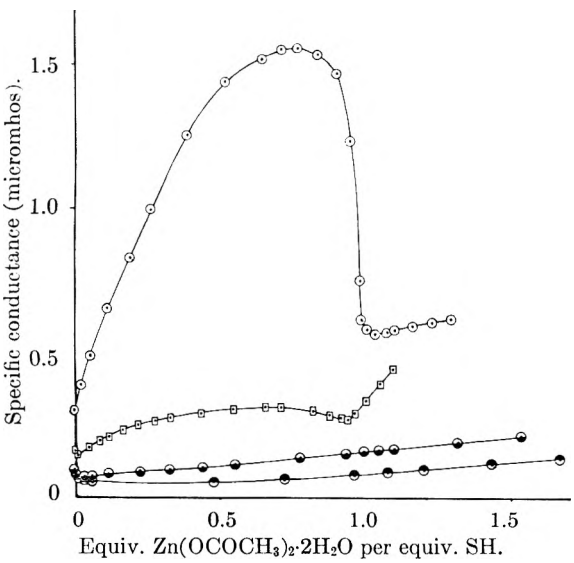

Fig. 5.—Conductance of mercaptans in pyridine on addition of 0.100 *M* $Zn(OCOCH_3)_2 \cdot 2H_2O$: ⊙, BAL (0.77 meq.); ⊡, 1,3-dimercapto-2-propanol (0.91 meq.); ◒, 2-mercaptoethanol (0.91 meq.); ◓, *n*-decylmercaptan (0.83 meq.).

other mercaptans and phenylmercuric acetate the maxima were higher (Figs. 3, 4). The maxima for all four mercaptans occurred closer to the end-points with phenylmercuric acetate than with mercuric acetate. In contrast to the other metal salts discussed herein (excluding cases where precipitation took place) phenylmercuric acetate did not react instantaneously, although the conductances did attain constant values within two or three minutes after each increment of titrant. The end-point conductances were higher than the initial conductances.

Zinc Acetate (Fig. 5).—Both BAL and 1,3-dimercapto-2-propanol gave conductance curves with zinc acetate which showed maxima and end-point

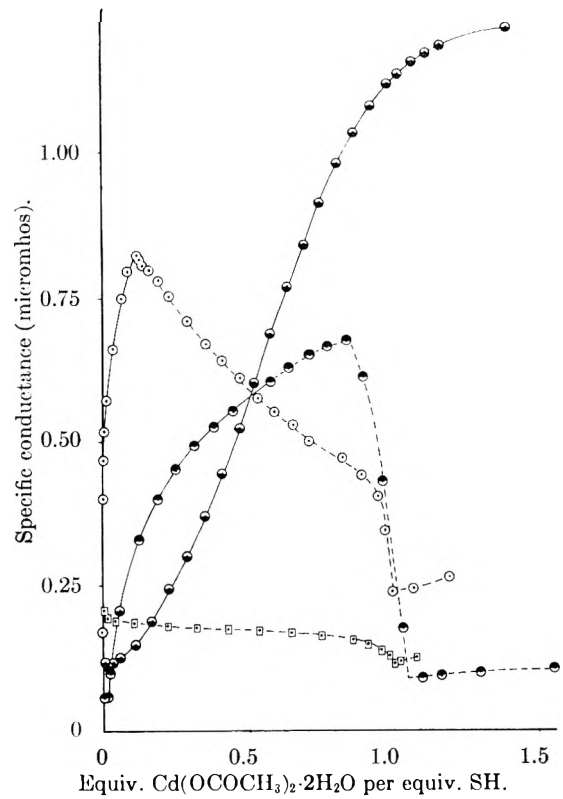

Fig. 6.—Conductance of mercaptans in pyridine on addition of 0.100 *M* $Cd(OCOCH_3)_2 \cdot 2H_2O$: ⊙, BAL (0.84 meq.); ⊡, 1,3-dimercapto-2-propanol (0.93 meq.); ◒, 2-mercaptoethanol (0.85 meq.); ◓, *n*-decylmercaptan (0.77 meq.).

minima, the latter close to 1:1 equivalent ratios. The end-points were not sharp, however, and were significantly higher than the initial conductances. By contrast, in the case of 2-mercaptoethanol and *n*-decylmercaptan no end-point minima appeared; at the beginning of the titrations curious drops to minima occurred for which we can offer no explanation.

Cadmium Acetate (Fig. 6).—BAL and *n*-decylmercaptan gave conductance curves with cadmium acetate which had maxima appearing approximately where precipitation began. Precipitation and decreasing conductances were observed during the entire course of addition of cadmium acetate to 1,3-dimercapto-2-propanol. As with zinc acetate, the 2-mercaptoethanol gave an initial drop in conductance when cadmium acetate was added, but the conductance then increased markedly, and only gave signs of leveling off after the 1:1 ratio of equivalents $Cd(OCOCH_3)_2$/equivalent SH had been exceeded. The end-point conductances for BAL and 1,3-dimercapto-2-propanol were lower than the initial conductances.

Lead Acetate (Fig. 7).—With BAL a very sharp drop in conductance, accompanied by scanty yellow precipitation, followed the appearance of a maximum. The occurrence of a minimum at an equivalent ratio of lead acetate to BAL of about 0.9 (rather than 1.0) was anomalous, but could be demonstrated on repetition of the experiment. In the case of 1,3-dimercapto-2-propanol, a copious yellow precipitate formed immediately after the conductance maximum had been reached. After an initial

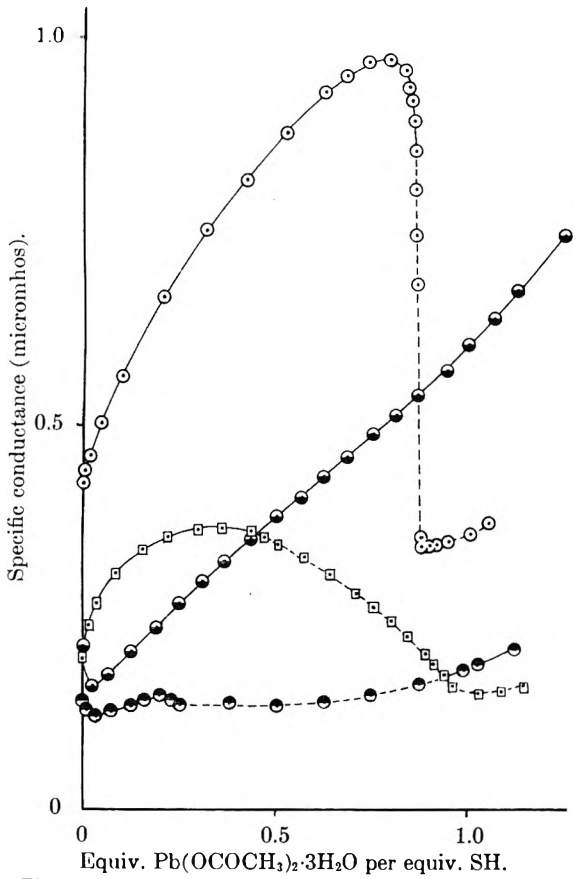

Fig. 7.—Conductance of mercaptans in pyridine on addition of 0.100 *M* $Pb(OCOCH_3)_2 \cdot 3H_2O$: ⊙, BAL (0.95 meq.); ⊡, 1,3-dimercapto-2-propanol (0.87 meq.); ◒, 2-mercaptoethanol (0.80 meq.); ◓, *n*-decylmercaptan (0.80 meq.).

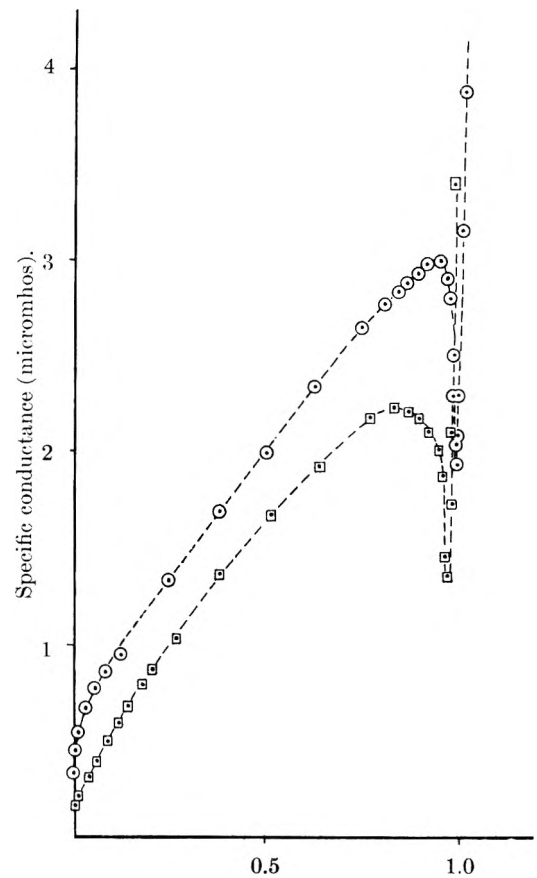

Fig. 8.—Conductance of mercaptans in pyridine on addition of 0.200 *M* $AgOCOCH_3$: ⊙, BAL (0.81 meq.); ⊡, 1,3-dimercapto-2-propanol (0.78 meq.).

drop in conductance, 2-mercaptoethanol gave a curve which showed no sign of leveling off when the stoichiometric amount of lead acetate had been added. The variations in conductance of *n*-decylmercaptan on addition of lead acetate were almost insignificant; as with most known lead mercaptides,[9] the precipitate was yellow. Only 1,3-dimercapto-2-propanol gave an end-point conductance lower than the conductance of the mercaptan before addition of the lead salt.

Silver Acetate.—Silver acetate was the only reagent that precipitated all of the mercaptans studied. Unlike the previously described experiments in which precipitation occurred, the conductances continued to rise on addition of the metal salt past the turbidity point. The early peak and drop exhibited by 2-mercaptoethanol were evidently associated with a temporary condition of supersaturation, which was terminated when precipitation began. The end-points at an equivalent ratio of 1:1 in the titrations of BAL and 1,3-dimercapto-2-propanol (Fig. 8) were indicated by very sharp minima (higher than the initial conductances), but no such minima were observed for *n*-decylmercaptan and 2-mercaptoethanol (Fig. 9).

(9) Addition of lead acetate in pyridine to ethanedithiol in the same solvent gave a yellow precipitate which became white within a few seconds. With methanol as the medium, it took about half an hour for the color transition to occur, while the dry yellow mercaptide was stable for longer periods (*cf.* C. Werner, *Jahresbericht*, **15**, 424 (1862)).

Nevertheless the titration curves for the latter two compounds had sharp break points at an equivalent ratio of 1:1 because of the high conductance of the silver acetate.

Other Heavy Metal Salts.—During preliminary screening, manganous, nickel and cobaltous acetates gave irregular curves with BAL and 1,3-dimercapto-2-propanol, characterized by relatively high specific conductances, by slow attainment of equilibrium at certain points in the titrations, and by no minima or breaks at the calculated end-points (assuming 1:1 reactions). The reactions of manganous acetate have been described elsewhere.[10] Nickel acetate and cobaltous acetate gave dark brown and very dark olive-brown solutions, respectively.

IV. Discussion

The choice of pyridine as the solvent for use in this study proved fortunate in that the reaction products were in most cases soluble. Hence, the removal of conducting intermediates by the formation and precipitation of non-conducting substances was largely prevented. Pyridine also provided an excellent selective medium for the dissociation of the conducting intermediates; it is with the nature of the latter that we are most concerned.

The ratio of reactants at the conductance maxi-

(10) D. H. Rosenblatt and G. N. Jean, *Anal. Chem.*, in press.

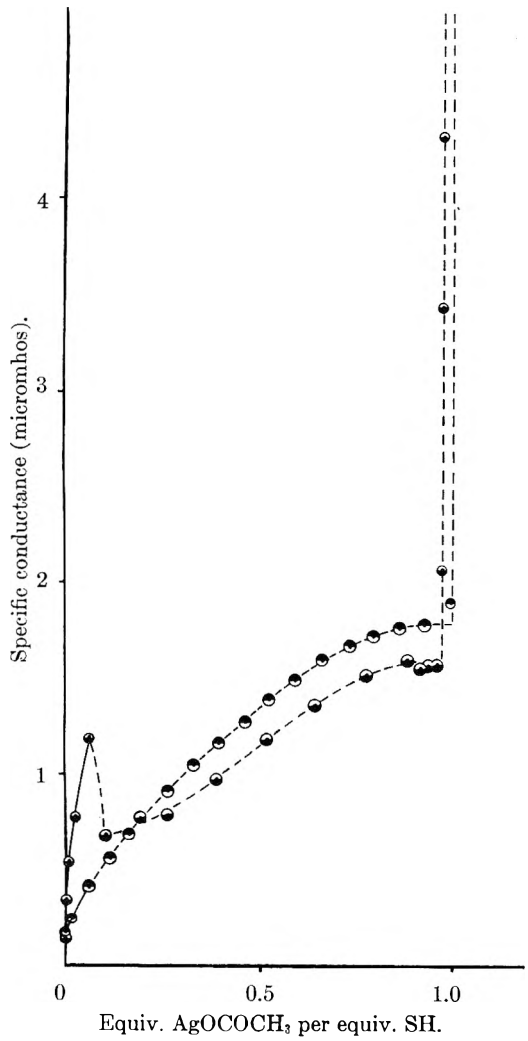

Fig. 9.—Conductance of mercaptans in pyridine on addition of 0.200 *M* $AgOCOCH_3$: ◒, 2-mercaptoethanol (0.77 meq.); ◓, *n*-decylmercaptan (0.75 meq.).

mum for the BAL-mercuric acetate reaction suggests that the reactions of BAL are of the type[11]

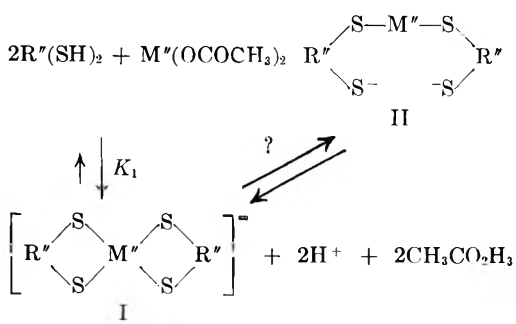

$R''(SH)_2$ = dithiol, such as BAL
M″ = divalent heavy metal ion, such as mercuric

Complexes such as $Hg(SCN)_4^=$, $CdI_4^=$ and $Ag(CN)_2^-$ are well known; however, little information could be found on analogous complex ions in which the ligands were mercapto groups. Gilman and coworkers[12] observed that the mercuric ion is held in aqueous solution (*p*H 7.5) by a twofold excess of BAL even in the presence of sodium sulfide. The same group[13] also reported the solubility of the cadmium ion with BAL in the presence of a basic medium. They formulated[12,13] the structures IV

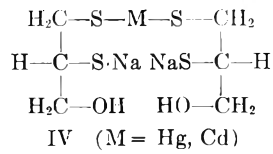

IV (M = Hg, Cd)

which are essentially the same as II. Mills and Clark[14] prepared compounds V

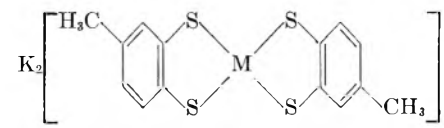

V (M = Hg, Zn or Cd)

and replaced the potassium ion in V to form the corresponding quinine salts. It is interesting to note that the manganous complex of BAL is evidently of another type,[10] and this is most likely true for the nickel and cobalt complexes. The dithiol–heavy metal reactions which are characterized by maxima within regions where the dithiols are in excess and minima at the 1:1 ratio probably can be better explained by structures of type I than by II (or IV), because only chelation can account for the increased acidity of the mercapto groups. Such chelation complexes, especially when the conductances of the metal acetates are relatively small, would be chiefly responsible for the total conductances of the solutions. The concentration–conductance relationships[15] could not be expected to be linear, but the maxima would nevertheless correspond to the highest concentrations reached by the type I species. The exact locations of the maxima would depend on the values of the equilibrium constants K_1 and K_2.[16] Precipitation would shift the reactions to III, causing a decrease in conductance. If we extend the explanation to all mercaptan complexes of this type, the structures for complexes of monovalent metal ions would be of forms VI or VII, and those of divalent ions of forms I or VIII.

These formulations do not explain the behavior of 2-mercaptoethanol with lead and cadmium, neither do they show why, with silver acetate, the conductances of BAL and 1,3-dimercapto-2-propanol continue to increase well past the beginning of precipitation, and then decrease sharply near the end points. Possibly this behavior is related to the ex-

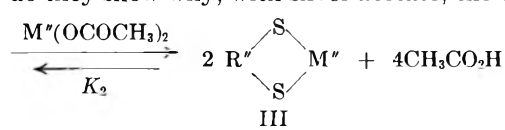

III

(11) H^+ and acetic acid are assumed to be solvated.

(12) A. Gilman, R. P. Allen, F. S. Philips and E. St. John, *J. Clin. Invest.*, **25**, 549 (1946).

(13) A. Gilman, F. S. Philips, R. P. Allen and E. S. Koelle, *J. Pharmacol.*, **87**, Suppl., 85 (1946).

(14) W. H. Mills and R. E. D. Clark, *J. Chem. Soc.*, 175 (1936).

(15) The high conductances of the complexes may be attributed to the relatively great dissociability of ion pairs containing large ions.

(16) Since these are not of the same dimensions, their ratio to each other is not the only determining quantity.

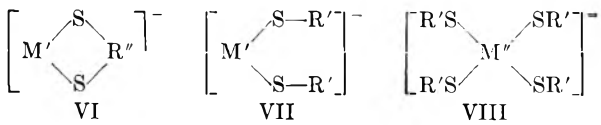

VI VII VIII

M′ = monovalent heavy metal ion, such as phenylmercuric
M″ = divalent heavy metal ion, such as mercuric
R′SH = monothiol, such as 2-mercaptoethanol
R″$(SH)_2$ = dithiol, such as BAL

traordinarily high dissociation constants of silver salts in pyridine.[17]

(17) D. S. Burgess and C. A. Kraus, *J. Am. Chem. Soc.*, **70**, 706 (1948).

A surprising feature of some of the titration curves is the appearance of extremely low end-point conductances. Even if it is supposed that all the current at these end-points was carried by the acetic acid formed in the reactions, the conductance of the acetic acid still was lower than that of the mercaptans initially present. It would be of interest to supplement this observation with measurements of the comparative dissociation constants of mercaptans and carboxylic acids in pyridine. The evidence indicates that mercaptans in pyridine are about as strongly dissociated as carboxylic acids.

THE POLY-COMPONENT AQUEOUS SYSTEMS CONTAINING THE CHLORIDES OF Ca^{2+}, Mg^{2+}, Sr^{2+}, K^+ AND Na^+ BETWEEN 18 AND 93°

BY GUNNAR O. ASSARSSON AND AINO BALDER

Chemical Laboratory of the Geological Survey of Sweden, Stockholm 50, Sweden

Received February 5, 1955

The aqueous four-component system containing the chlorides of calcium, magnesium and potassium was investigated between 18 and 93°. With increasing temperature the existence area of tachydrite grows at the expense of the magnesium chloride hexahydrate and the calcium chloride hydrates; the area of the double salt baeumlerite increases chiefly at the expense of calcium chloride dihydrate and carnallite; and above 92° the double salt dicalcium chloride magnesium chloride hexahydrate grows chiefly at the expense of tachydrite. The system is not changed substantially with additional sodium and strontium chloride. No new compounds occur.

In some earlier papers[1] the present authors have presented their reports on the formation of the solid phases from solutions belonging to the binary, ternary and two of the quaternary aqueous systems containing the chlorides of calcium, magnesium, strontium, potassium and sodium. The temperature range chosen for the experiments lies between 18° and about 100°, because the properties of the solutions within this range are of some importance, in connection with the crystallization of the solid phases as well as the elucidation of the paragenesis of the natural salt deposits. The report is brought to completion in this paper by an account of some of the results from studies of some other quaternary and poly-component systems.

The experimental conditions have been described earlier. Substances present in small quantities, in particular sodium and strontium, were in most cases determined spectrophotometrically. The solid phases formed were determined by graphical extrapolation according to Roozeboom, by calculation according to Igelsrud and Thompson[2] and they were identified microscopically with a heat stage microscope.

The Quaternary Aqueous System of the Chlorides of Ca^{2+}, Mg^{2+} and K^+.—The ternary aqueous systems belonging to this quaternary system have been investigated rather thoroughly. At temperatures higher than 100–200°, however, some completing determinations are desirable. These questions, however, do not lie within the scope of the present investigations. The ternary anhydrous system of the chlorides has been examined quite recently.[3] The aqueous isotherms at 0°,[2] 35°,[4] 75°[4] have been published earlier but of the influence of the components on the formation of the phases and on the change of concentration little is known. From the experimental material, some observations may be given here, chiefly concerning the lowest formation temperatures of the phases and the concentration of the solutions at some isothermally invariant points (Table I). A graphical polythermal representation of the four component system between the lowest temperature (−55°) and the melting point of the anhydrous phases is very difficult to present clearly and intelligibly, owing to the occurrence of the four double salts and the large numbers of hydrates and to the unknown parts of the ternary systems. The principal diagrams are therefore drawn as Jänecke projections on the water-free side of the tetrahedron (Fig. 1), and represent the equilibria between 0 and 93° only, these being the most important for the purposes mentioned above. Only those parts of the diagrams which concern the solutions very rich in calcium chloride are of interest in this connection.

The transformation of calcium chloride hexahydrate into α-tetrahydrate takes place at 24.8°.[5] The change in concentration of the solutions rich in calcium chloride, which takes place with increasing temperature in the invariant and monovariant equilibria, involves mainly an increase in the

(1) G. O. Assarsson, *J. Am. Chem. Soc.*, **72**, 1433 (1950); G. O. Assarsson and Aino Balder, THIS JOURNAL, **57**, 207 (1953); **57**, 717 (1953); **58**, 253 (1954); G. O. Assarsson, Geol. Survey of Sweden, Ser. C, Yearbook 42, No. 10, 1948 (English).

(2) I. Igelsrud and T. G. Thompson, *J. Am. Chem. Soc.*, **58**, 2003 (1936).

(3) A. I. Ivanov, *Doklady Akad. Nauk, S.S.S.R.*, **86**, 539 (1953).

(4) W. L. Lightfoot and E. F. Prutton, *J. Am. Chem. Soc.*, **68**, 1001 (1946); **69**, 2098 (1947); **70**, 4112 (1948); **71**, 1233 (1949).

(5) J. H. van't Hoff, *Z. anorg. Chem.*, **47**, 253 (1905).

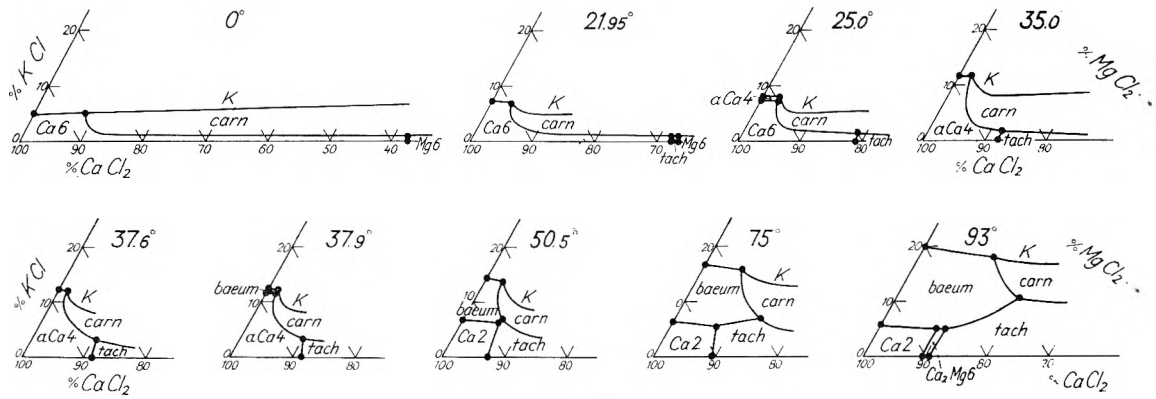

Fig. 1.—The quaternary system $CaCl_2$–$MgCl_2$–KCl–H_2O, Jänecke projection on the water-free side of the tetrahedron: 0.0° according to Igelsrud and Thompson[2]; 25.0°, van't Hoff[5]; 35.0°, Lightfoot and Prutton; 75.0°, the solutions, Lightfoot and Prutton.[4] Concerning the symbols see Table I, concentration weight per cent.

TABLE I

EQUILIBRIA IN THE QUATERNARY SYSTEM $CaCl_2$–$MgCl_2$–KCl–H_2O

Solid phases: Ca6 = $CaCl_2 \cdot 6H_2O$; Ca4 = $\alpha CaCl_2 \cdot 4H_2O$; Ca2 = $CaCl_2 \cdot 2H_2O$; Mg6 = $MgCl_2 \cdot 6H_2O$; carn = carnallite $KMgCl_3 \cdot 6H_2O$; tach = tachydrite $CaMg_2Cl_6 \cdot 12H_2O$; baeum = baeumlerite $KCaCl_3$; Ca_2Mg6 = $Ca_2MgCl_6 \cdot 6H_2O$; K = KCl.

Temp., °C.	Solution, wt. % $CaCl_2$	$MgCl_2$	KCl	Solid phase
21.50	30.9	14.1	0.5	Ca6 + Mg6
	30.8	14.3	0.4	Mg6 + carn
21.95	41.5	1.6	3.3	carn + Ca6 + K
	31.7	13.5	0.3	tach + carn + Ca6
	31.4	14.0	0.3	tach + carn + Mg6
37.6	51.5	0.8	6.7	Ca4 + carn + K
	47.6	5.0	1.6	Ca4 + carn + tach
37.9	50.9	0.6	7.3	carn + baeum + K
	51.3	0.5	7.0	carn + baeum + Ca4
	47.8	5.0	1.7	carn + tach + Ca4
50.5	49.8	1.5	8.5	carn + baeum + K
	50.8	3.9	4.0	carn + baeum + tach
	52.3	3.4	3.7	baeum + tach + Ca2
93.0	41.9	7.7	10.3	baeum + carn + K
	40.9	11.5	6.0	baeum + tach + carn
	51.1	7.1	2.9	baeum + tach + Ca_2Mg6
	53.5	5.9	2.8	baeum + Ca_2Mg6 + Ca2

potassium chloride content and a decrease in the magnesium chloride content, until the formation begins of the double salt potassium calcium chloride. The lowest formation temperature of this double salt, which will here be referred to as baeumlerite,[6] is only some tenths of a degree lower in the present quaternary system than in the ternary aqueous system potassium chloride–calcium chloride. The second double salt tachydrite has its lowest formation temperature at 21.95° in the ternary system; here again the change in lowest formation temperature when potassium chloride is added, is insignificant. As the temperature increases the existence area of tachydrite grows at the cost of the existence areas of calcium chloride and magnesium chloride hydrates. Another phase transformation α-calcium chloride tetrahydrate–dihydrate takes place at 41.5 ± 0.5°. At about 50° the existence area of tachydrite touches that of baeumlerite and very nearly at the same temperature that of calcium chloride dihydrate. This temperature range has not here been examined in more detail, being without greater importance. More interesting is the fact that as the temperature further increases, the existence area of baeumlerite begins to widen at the expense of those of carnallite and tachydrite so that it forms a triangular strip between these two areas. This seems to be the main feature of the crystallization at temperatures higher than 100°. At 92.0 ± 0.5° the double salt dicalcium chloride–magnesium chloride hexahydrate begins to crystallize. At 93.0° the area of this double salt is a narrow ribbon, and at increasing temperature it becomes wider chiefly at the expense of the existence areas of calcium chloride dihydrate and tachydrite.

Compounds other than those earlier known from the ternary systems do not occur within the temperature range investigated.

The Polynary Aqueous Systems Containing the Chlorides of Ca^{2+}, Mg^{2+}, Sr^{2+}, K^+ and Na^+.—The saturated solutions, belonging to those systems and being rich in chlorides of calcium, magnesium and potassium, contain small amounts of strontium and sodium chloride. There are no new phases formed. The small concentration of strontium and sodium chloride influences the lowest formation temperatures of the phases rather insignificantly, in general by only one or two tenths of a degree (sodium chloride) or one to one and a half degrees (strontium chloride). The crystallization of solid solution calcium strontium chloride hexahydrate and the interrupting gap containing strontium chloride dihydrate, described earlier,[1] are influenced by the presence of gradually increasing amounts of magnesium chloride, so that

TABLE II

EQUILIBRIA IN THE HEXANARY SYSTEM $CaCl_2$–$MgCl_2$–$SrCl_2$–KCl–NaCl–H_2O

Solid phases: Sr6 = $SrCl_2 \cdot 6H_2O$; Sr1 = $SrCl_2 \cdot H_2O$; Na = NaCl; see further Table I.

Temp., °C.	Solution, wt. % $CaCl_2$	$MgCl_2$	$SrCl_2$	KCl	NaCl	Solid phase
21.95	40.5	1.4	1.0	3.1	0.4	Ca6 + carn + Sr6 + K + Na
93.0	39.0	9.9	3.0	6.2	0.3	baeum + tach + carn + Sr1 + Na

(6) The reasons for this name will be discussed elsewhere (*cf.* O. Renner, *Cbl. Min.*, 106 (1912)).

the gap disappears from the isotherms at about 25°. There are no other properties of the systems worthy of special mention.

Two analyses of the mother liquor at 21.9 and 93.0 may be given here to illustrate the composition (Table II).

POLYMER CHAIN CONFIGURATION NEAR A BOUNDARY EXERTING FORCES

By H. L. Frisch

Department of Chemistry, University of Southern California, Berkeley, Calif.

Received February 5, 1955

The configuration of a flexible polymer chain, built up by the successive deposition of single segments, near a phase boundary exerting forces on the individual segments is studied. It is shown that the end-to-end distance probability distribution satisfies instead of a simple diffusion equation a Fokker–Planck equation whose convective terms are proportional to the forces exerted by the boundary. When these forces are small, solutions by perturbation series are given, while for large forces an approximate solution is derived in the case of attraction. The effect of the chain configuration on such surface properties as the adsorption of polymer from solution, the stabilization of colloidal suspensions by dissolved macromolecules, the surface tension of polymer solutions, etc., is treated.

I. Introduction

Theoretical studies of the adsorption of flexible macromolecules onto solids from their solution,[1,2] the surface tension of polymer solutions[3] as well as certain other surface properties of polymer solutions[4] show that these may depend strongly on the configuration of the polymer chain near a phase boundary. In the case of adsorption, preliminary experimental investigations show that such is indeed the case and indicate rough qualitative agreement between theory and experiment.[5] In the absence of strong forces exerted by the phase boundary, the configuration of the polymer chain can be assumed to be given by an appropriate solution of the diffusion equation with a boundary condition corresponding to perfect reflection and neglecting disturbing effects arising from excluded volume.[1] In systems without pronounced polar character or polymer–substrate specificity, the forces acting on the polymer are of the order of kT, that is, sufficiently weak to produce at most a small perturbation in the random coil configuration of the polymer. We shall estimate the magnitude of this perturbation.

On the other hand in certain systems strong forces will be acting on the segments of the polymer chain leading to the failure of a simple perturbation treatment. Such an instance could well be expected to occur in biologically important polymer substrate systems, *e.g.*, antigen–antibody reactions, in which mutual specificity plays an important role. We shall present a treatment which applies in first approximation in such cases (strong forces) for sufficiently large polymer chains. The precise specification of a polymer chain of t segments in such a force field would require the introduction of the joint probability distribution of all t segments, specifying the location of each segment. In most applications such detail is unnecessary, interest being centered on the probability distribution of end-to-end distances $w(x, y, z; t)$ where x, y, z are the coördinates in a coördinate system of the t^{th} segment at whose origin the first segment of the polymer chain is located. We shall try to estimate this probability assuming the following.

(1) That $w(x, y, z; t)$ is not affected by the force field in the x and y direction but merely along the z direction (being the vertical distance of the segment from the boundary), so that

$$w(x, y, z; t) = w_0(x; t)\, w_0(y; t)\, w(z; t) \qquad (1)$$

where $w_0(x; t) = (2\pi ft)^{-1/2} \exp(-x^2/4ft)$ and f is the segment diffusion constant, in the "random flight" analogy.

(2) The potential $V(\xi)$, consisting in general of both attractive and repulsive terms, acts on every segment s, $1 \leqslant s \leqslant t$, separated a distance ξ from the phase boundary.

(3) The boundary is impenetrable to all polymer chains.

(4) The deposited polymer chain can be thought to be built up of successive depositions of the polymer segments and for simplicity but without real loss in generality the first segment is assumed to lie at $z = 0$, *i.e.*, on the boundary.

(5) We shall neglect certain complicating effects such as those arising from excluded volume considerations, etc.

Let a segment be placed in a certain configuration at a distance ξ from the boundary. The force acting on this segment is obtained from the gradient of the potential $V(\xi)$ as

$$-\frac{\partial V(\xi)}{\partial \xi} = F(\xi) = \epsilon_0 g(\xi) \qquad (2)$$

The effect of this force will be to disturb the equal likelihood of placing a segment directed either toward or away from the phase boundary. Assumptions (1), (4) and (5) guarantee that the location of the t^{th} segment depends only on the location of the t-1st segment and thus $w(z; t)$ is found as a solution

(1) H. L. Frisch, R. Simha and F. R. Eirich, *J. Chem. Phys.*, **21**, 365 (1953); R. Simha, H. L. Frisch and F. R. Eirich, This Journal, **57**, 584 (1953); H. L. Frisch and R. Simha, *ibid.*, **58**, 507 (1954).

(2) R. Ullman, paper presented at the 124th meeting of the American Chemical Society, September 6–11, 1953, Chicago, Illinois.

(3) Fumio Oasawa and Sho Asakura, *J. Chem. Phys.*, **22**, 1255 (1954).

(4) Such as for instance the stabilization of colloidal suspensions. *Cf.* E. L. Mackor and J. H. van der Waals, *J. Colloid Sci.*, **7**, 535 (1952) as well as reference 3.

(5) W. Heller and T. L. Pugh, *J. Chem. Phys.*, **22**, 1778 (1954), as well as papers quoted in references 1.

of a typical "random flight" integral equation whose kernel function is not isotropic. It can be shown[6] that for sufficiently large t among other conditions this integral equation may in turn be replaced by the Smoluchowski equation.[1,6]

$$\frac{\partial w}{\partial t} = f\frac{\partial^2 w}{\partial z^2} + \frac{\partial}{\partial z}[v(z)w(z;\ t)] \tag{3}$$

where $v(z)$, the "drift velocity," gives the magnitude of the drift of the t^{th} segment located at z, with $v(z)$ positive if the forces exerted by the phase boundary at z are attractive. Then "drift velocity" $v(z)$ satisfies the usual Langevin equation[6] (*cf.* eq. 2)

$$v(z) = \beta F(z) = \lambda f g(z) \tag{4}$$

where β the segment mobility is equal to f/kT and $\epsilon_0/kT = \lambda$. Thus the larger is ϵ_0 the larger will be the deviation of $w(z;\ t)$ from $w_0(z;\ t)$ which is a solution of a simple diffusion equation obtained by setting λ equal to zero in

$$\frac{\partial w}{\partial t} = f\left[\frac{\partial^2 w}{\partial z^2} + \lambda\frac{\partial}{\partial z}(g(z)w)\right] \tag{5}$$

obtained by substituting eq. 4 in eq. 3. The degree of flexibility of the polymer chain also affects the magnitude of the drift term since v is proportional to f and the latter decreases as the flexibility of the chain increases.[1] Equation 5 has to be solved under the initial and boundary conditions (*cf.* assumptions 3 and 4).

$$w \longrightarrow \delta(z) \text{ as } t \longrightarrow 0 \tag{5'}$$

$$\frac{\partial w}{\partial z} + \lambda g w = 0 \text{ at } z = 0 \text{ for } t > 0$$

and

$$w,\ \partial w/\partial z \longrightarrow 0 \text{ as } z \longrightarrow +\infty,\ t > 0$$

Before we can proceed we will have to find a suitable form for $V(\xi)$ the segment potential energy. This energy will itself be given as an integral over the surface of the phase boundary of the intermolecular forces exerted on a segment by each molecule composing the boundary. These forces may contain besides electrostatic, inductive and dispersive force contributions, terms which may arise due to the formation of chemical or quasi-chemical bonds between polymer segments and active sites on the substrate. The form of $g(z)$ to be used in eq. 5 will depend on the polarity, chemical structure, etc., of the molecular species involved[7] but in the absence of strong specificity will generally be represented to a sufficient approximation by the $g(z)$ derived from a square-well potential[8]

$$\begin{aligned} V(z) &= +\infty && \text{for } z < 0 \\ &= -\epsilon_0 && \text{for } 0 \leqslant z \leqslant R \\ &= 0 && \text{for } z > R \end{aligned}$$

i.e.

$$g(z) = \delta(z - R),\ z > 0 \tag{6}$$

In most applications of this theory[1-4] to surface sensitive properties of polymer solutions one requires only the value of $w(z;\ t)$ at $z = 0$ and the first few moments of $w(z;\ t)$, which are incidentally linearly related as can be seen directly from eq. 5 on multiplication by z and integration from zero to infinity, *viz.*

$$\begin{aligned} \frac{d}{dt}\langle z\rangle_t &= \frac{d}{dt}\int_0^\infty zw(z;\ t)\,dz \qquad (7a)\\ &= f[w(0;\ t) - \lambda\int_0^\infty g(z)\,w(z;\ t)\,dt] \\ &= f[w(0;\ t) - \lambda\langle g(z)\rangle_t] \end{aligned}$$

Similarly one finds for the second moment $\langle z^2\rangle_t$

$$\frac{d\langle z^2\rangle_t}{dt} = 2f[1 - \lambda\langle zg(z)\rangle_t] \tag{7b}$$

Both these equations show that as expected attractive forces exerted by the boundary decrease the extension of the chain as measured by the average and average square chain length by changing the functional form of the distribution and secondly by decreasing these by the terms $\langle g(z)\rangle_t$ and $\langle zg(z)\rangle_t$. For at least small values of λ the asymptotic estimate $\langle z\rangle_t g(\langle z\rangle_t)$ for $\langle zg(z)\rangle_t$ should suffice. Since for small λ, $\langle z\rangle_t$ is of the order of $t^{1/2}$ (*cf.* eq. 7a) say $\langle z\rangle_t = at^{1/2}$, this and eq. 7b should allow us to estimate the effect on the polymer chain configuration of the range of the forces exerted by the boundary. Thus if these, *i.e.*, $g(z)$, fall off[7] as $A(z - R)^{-\delta}$ we find

$$\frac{d\langle z^2\rangle}{dt}\,t = 2f\left[1 - \lambda A a^{\delta+1}t^{1/2}\left(t^{1/2} - \frac{R}{a}\right)^{-\delta}\right]$$

showing that the correction term becomes negligible for sufficiently large t and if $\delta > 1$ which will generally be the case; in particular surface dispersion forces have $\delta \simeq 4$.[7]

II. The Weak Field, High Temperature Solution

For arbitrary $g(z)$ no explicit general solution has been found but for the limiting case of small $\lambda = \epsilon_0/kT$ eq. 5 can be solved in terms of a perturbation series in the parameter λ. This case corresponds to either the case where the forces exerted by the boundary are very weak (ϵ_0 very small) or where the temperature of the polymer system is high as for example in a melt. Thus for $\lambda << 1$ we write

$$w(z;\ t) = \sum_{n=0}^{\infty}\lambda^n w_n(z;\ t) \tag{8}$$

where the successive $w_n(z;\ t)$ are found, on substitution of eq. 8 in eq. 5 and 5', to satisfy

$$\frac{\partial w_0}{\partial t} = f\frac{\partial^2 w_0}{\partial z^2};\quad \frac{\partial w_n}{\partial t} = f\left[\frac{\partial^2 w_n}{\partial z^2} + \frac{\partial Q_{n-1}}{\partial z}\right],\ n = 1, 2, \ldots \tag{9}$$

where

$$Q_{n-1} = g(z)\,w_{n-1}(z;\ t) \tag{9'}$$

and

$$\left.\begin{aligned} w_0 &\longrightarrow \delta(z) \\ w_n &\longrightarrow 0 \end{aligned}\right\} \text{ as } t \longrightarrow 0$$

$$\left.\begin{aligned} \frac{\partial w_0}{\partial z} &= 0 \\ \frac{\partial w_n}{\partial z} &= -Q_{n-1} \end{aligned}\right\} \text{ at } z = 0 \text{ for } t > 0$$

and

$$w_0,\ w_n,\ \frac{\partial w_0}{\partial z},\ \frac{\partial w_n}{\partial z} \longrightarrow 0 \text{ as } z \longrightarrow \infty$$

(6) S. Chandrasekhar, *Rev. Modern Phys.*, **15**, 1 (1943).

(7) For a recent review on details of these surface forces see J. H. Honig, *Ann. N. Y. Acad. Sci.*, **58**, 741 (1954).

(8) J. O. Hirschfelder, C. F. Curtiss and R. B. Bird, "Molecular Theory of Gases and Liquids," John Wiley and Sons, Inc., New York, N. Y., 1954, p. 158 ff.

The successive solutions of eq. 9 for w_n can be obtained by inverting the Laplace transforms of $w_0(z;\ t)$ and $w_n(z;\ t)$

$$\bar{w}_0(z;\ p) = \int_0^\infty e^{-pt}\, w_0(z;\ t)\, dt$$

$$\bar{w}_n(z,\ p) = \int_0^\infty e^{-pt}\, w_n(z;\ t)\, dt$$

where

$$\bar{w}_n(z,\ p) = -\int_0^\infty g_{n-1}(z, z_0;\ p)\, \frac{\partial \bar{Q}_{n-1}}{\partial z_0}(z_0;\ p)\, dz_0 \quad (10)$$

$$\bar{w}_0(z;\ p) = 2e^{-qz}/q;\ q = +(p/f)^{1/2}$$

with

$$\bar{Q}_{n-1}(z_0;\ p) = \int_0^\infty e^{-pt} Q_{n-1}(z;\ t)\, dt$$

The Greens' function $g_{n-1}(z, z_0;\ p)$ is found to be

$$-g_{n-1}(z, z_0;\ p) = \frac{e^{-q(z_0+z)}}{2[q + Q_{n-1}(0;\ p)]} + \frac{1}{2q}\{e^{-q(z_0-z)} H(z_0 - z) + e^{-q(z-z_0)} H(z - z_0)\}$$

with $H(x)$ the Heaviside unit function. Equations 8 and 10 specify the desired solution for small λ, for example if $g(z)$ satisfied eq. 6 one finds using the above solution that

$$w(0;\ t) = \frac{2}{(2\pi f t)^{1/2}}[1 + \lambda e^{-R^2/ft}] + O(\lambda^2) \quad (11)$$

$$= w_0(0;\ t)[1 + \lambda e^{-R^2/ft}] + O(\lambda^2)$$

If R is small, $R \approx 2$; then the above result shows that the magnitude of the correction depends primarily on ϵ_0 the depth of the potential well (*cf.* eq. 6). Although ϵ_0 will vary considerably depending on the nature of the substrate–polymer system under consideration a rough idea of the order of magnitude of this entity can be obtained from the comparable ϵ_0 values found for a number of pure vapors from the second virial coefficient.[7] Thus in the absence of specificity and pronounced polar character ϵ_0 in λ could be approximated by the values of simple hydrocarbons, *e.g.*, $\epsilon_0/k \simeq 244°$K. for ethane, etc. In the solution this value should be further reduced in view of the shielding by the solvent molecules. The perturbation procedure is thus justified and the magnitude of the correction which has to be introduced into $w(0;\ t)$ and the moments will not exceed a numerical factor of two at room temperature or above. As polar influences increase the treatment presented above becomes less satisfactory since ϵ_0/k for methyl chloride is about 469°K. while for water vapor in which the possibility of hydrogen bonding exists ϵ_0/k is 1260°K.[7] In such cases the perturbation treatment must fail.

III. The Strong Attractive Field Solution

For large values of ϵ_0/k an alternate approximate solution of eq. 5 will be presented which holds only if the forces exerted by boundary are very strongly attractive. In the absence of external forces one can represent the unperturbed configuration of the polymer chain as resulting from a stationary balance ($\partial w/\partial t = 0$) between the effects of diffusion of the chain ends and a harmonic restoring force (replacing the $\partial w/\partial t$ term) with a force constant proportional to kT and inversely proportional to t. This suggests that even in the presence of forces exerted by the phase boundary a balance between the diffusion "force" with both the harmonic restoring force and the forces exerted by the boundary producing the drift velocity $v(z) = f\lambda g(z)$ must be reached as long as $v(z) > 0$. If these forces are very strong, $\lambda >> 1$, we can neglect the effect of the harmonic restoring force in this balance. Alternatively phrased we can consider this instance as one in which we are justified in neglecting "random flight" correlations in placing successive segments of the chain in comparison with the effect due to the force field of the boundary, *i.e.*, $\partial w/\partial t$ in eq. 5 vanishes and we thus obtain

$$\frac{\partial^2 w}{\partial z^2} = -\lambda \frac{\partial}{\partial z}[g(z)w] \quad (12)$$

An appropriate solution of this equation is

$$w(z;\ t) = Ae^{-\lambda \int_0^z g(\xi)\, d\xi} \quad (13a)$$

since it satisfies the boundary conditions at zero, approximately the one at infinity and can be normalized

$$1 = \int_0^t w(z;\ t)\, dz = A \int_0^t e^{-\lambda \int_0^z g(\xi)\, d\xi dz}$$

so that

$$A = 1 \Big/ \int_0^t e^{-\lambda \int_0^z g(\xi)\, d\xi dz} \quad (13b)$$

Substituting eq. 2 into eq. 13b we find

$$w(z;\ t) = \frac{\exp\left\{\frac{V(z)}{kT}\right\}}{\int_0^t \exp\left\{\frac{V(z)}{kT}\right\} dz} = w(0,\ t) \exp\left\{\frac{V(z) - V(0)}{kT}\right\} \quad (13c)$$

In deriving eq. 13c we have assumed that the strong boundary forces remain strong over the whole range of distances accessible to the t^{th} polymer segment of our chain. Should this not be the case as for example for a very deep but narrow square well potential eq. 13c should be replaced in first approximation by the more general relation

$$w(z;\ t) = \frac{\exp\left\{\frac{V(z) - V(0)}{kT}\right\} H(R - z) + w_0(z;\ t)\, H(z - R)}{\int_0^\infty \left\{\exp\left\{\frac{V(z) - V(0)}{kT}\right\} H(R - z) + w_0(z;\ t)\, H(z - R)\right\} dz} \quad (14)$$

where $w_0(z;\ t)$ is the unperturbed probability distribution which holds outside $z = R$ the range of the forces exerted on the t^{th} segment by the phase boundary.

IV. Applications and Conclusion

The applications of the foregoing theory are diverse and we shall restrict our discussion to those mentioned in the introduction, in particular the adsorption of flexible macromolecules from their solution. As has been previously shown[1] the probability that the τ^{th} segment of the polymer chain adheres to the phase boundary, $p(\tau)$ is given by

$$p(\tau) = \alpha_0(1 - \theta)\int_0^\tau \int_0^{2\pi} w_0(x, y, 0;\ \tau)\rho d\rho d\phi \quad (15a)$$

$$= \alpha_0(1 - \theta)\int_0^\tau \int_0^{2\pi} w_0(x;\ \tau)w_0(y;\ \tau)w(0;\ \tau)\rho d\rho d\phi$$

$$= 2\alpha_0(1 - \theta)\, w(0;\ \tau)[1 - e^{-\tau/4f}];\ 1 \leq \tau \leq t$$

where θ is the fraction of the surface of the phase boundary covered, α_0 is the probability that if a segment touches it adheres, $\rho^2 = x^2 + y^2$ and $\phi = \tan^{-1}(y/x)$. It is by way of this relation that the configuration of the chain influences the adsorption of the chain through the indicated proportionality to $w(0, t)$. For weak boundary forces $w(0, t)$ is independent of the range of these forces ($\delta \simeq 4$) as long as these decrease at least as the inverse square of the distance between the segment and the boundary (*cf.* eq. 7) and for non-polar neutral polymer segments and molecules of the substrate $w(0, t)$ is given by eq. 11 in first approximation. This leads[1] to an average $<p(\tau)>_t = p = [2\alpha_0(1-\theta)/(\pi f t)^{1/2}][1+\lambda]$. The average number of anchors $<\nu> = pt = <\nu>_0[1+\lambda]$ is still $0(t^{1/2})$ and the adsorption isotherm is unchanged in form from that given in reference 1

$$\frac{\theta}{1-\theta} = (KC)^{1<\nu>} = (KC)^{1/<\nu>_0[1+\lambda]} \quad (15b)$$

neglecting activity corrections where C is the concentration of polymer in solution and K is the known affinity constant. The increase in $<\nu>$ is at most by a factor of two ($\lambda < 1$) and can thus be neglected by assuming it to be already incorporated in the term α_0.

On the other hand if $\epsilon_0 >> kT$ it follows from eq. 14 that for moderate R, $w(0; t) \approx 1/R$ and hence $<\nu> = pt =$ constant $(1-\theta)\alpha_0 t/R$ by virtue of eq. 15a. This result means that sufficiently strong attractive forces of moderate range cause the chains to deposit completely onto the substrate surface. In such a case the amount of polymer removed from even very dilute solution almost equals the saturation value. As the range of the boundary forces decreases the result given above must be modified somewhat since $w(0; t)$ is no longer completely independent of t, nonetheless, to a first approximation $<\nu>$ is still proportional to t rather than $t^{1/2}$. The implications of the foregoing both for the mechanism of reinforcement and stabilization of colloid particles follows directly from previous discussions of the increase of the parameter $<\nu>$.[1a,4,5]

The author is indebted to Professor Robert Simha for having suggested this problem and many clarifying discussions.

THE SORPTION OF WATER VAPOR ON MAGNESIUM OXIDE

BY R. I. RAZOUK AND R. SH. MIKHAIL

Chemistry Department, Faculty of Science, Ein-Shams University, Abbassia, Cairo, Egypt

Received February 5, 1955

Sorption–desorption isotherms of water vapor were determined at 35° on seven specimens of magnesium oxide prepared by the dehydration of brucite at 350, 500, 650, 800, 950, 1020 and 1100° with the aid of an electric sorption balance. The sorption isotherms are sigmoid, and definite limiting sorption values are invariably attained at saturation vapor pressure. The oxides prepared at or below 650° are rehydrated stoichiometrically at saturation vapor pressure, but as the temperature of dehydration is raised, the uptake of water at saturation diminishes, and, ultimately, when brucite is dehydrated at 1100°, the oxide obtained is "deadburnt" and does not take up the least amount of water from the vapor phase. In all cases, appreciable hysteresis occurs, and thorough evacuation at room temperature of the rehydrated oxide removes only almost two-thirds of the water content at saturation, while the remaining one-third can only be expelled by outgassing at higher temperatures. Resorption isotherms are also sigmoid but distinct from the initial sorption isotherms though the two curves join together at the saturation point, forming thus a perfectly reproducible desorption–resorption loop. It is suggested that the water uptake is not merely a surface phenomenon, but rather a bulk effect, and that the water molecules are held up in the oxide lattice with binding forces which have two different strengths each of which being characteristic of the orientations in one of the two lattices of magnesium oxide crystallites described by Garrido.

Introduction

The sorption of water vapor on oxides and hydrous oxides has been studied extensively in certain cases especially on oxide gels like silica, alumina and ferric oxide gels. Other metal oxide–water vapor systems have not yet been thoroughly investigated, and the properties of such systems need further systematic study. Moreover, most of the earlier work dealt with amorphous and microcrystalline oxides, the properties of which depend to a great extent on the exact details of preparation, the treatment they have undergone and in particular on the temperature to which they were subjected, and on aging.[1]

The present investigation deals with the sorption of water vapor on magnesium oxide prepared by the dehydration of native brucite under controlled conditions. This system was chosen on the following grounds: (i) brucite occurs in well-defined crystalline form of the hexagonal C 6 system as lamellae which can be readily cleaved and may be obtained in a very pure state; (ii) extensive work has been done on the structural study of the system MgO–H_2O mainly with the aid of X-ray measurements, and, in most cases, it has proved that there exist only two solid phases, *viz.*, brucite $Mg(OH)_2$, and periclase MgO, and no others.[2] (iii) the dehydration of brucite at various temperatures has been thoroughly studied.[3]

The hydration of magnesia prepared from the carbonate or hydroxide has been measured by some authors. Campbell[4] obtained an impure oxide by burning magnesite between 600 and 800° which could be hydrated completely in 3 days. Between 1000 and 1100°, the magnesia suffered a change resulting in a marked decrease in its rate of hydration, and the oxide obtained by decomposition at

(1) S. J. Gregg, "The Surface Chemistry of Solids," London, 1951.

(2) R. Fricke, *et al.*, *Z. anorg. Chem.*, **166**, 244 (1927); G. F. Hüttig and W. Frankenstein, *ibid.*, **185**, 403 (1929); W. Büssem and F. Koberich, *Z. physik. Chem.*, **B17**, 310 (1932).

(3) S. J. Gregg and R. I. Razouk, *J. Chem. Soc.*, **S1**, 36 (1949).

(4) A. J. Campbell, *Ind. Eng. Chem.*, **1**, 665 (1910).

1450° combined with only 60% of the water necessary to form $Mg(OH)_2$, on being immersed in water for 18 months. Opinions differ, however, as to this temperature at which such a change takes place. Thus Le Chatelier[5] gave 1600°, Parravano and Mazzetti[6] 800°, while Mellor[7] pointed out the absence of a definite temperature, and showed that the change proceeds more quickly the higher the temperature of calcination. Recently, Colegrave, Richardson and Rigby[8] observed that a sharp decrease in the hydration tendency of magnesia occurred as the calcination temperature was raised from 1300 to 1400°. It is highly probable that this divergence of results is due in part to the presence of impurities. Indeed, the latter authors showed directly that the hydration tendency is greatly influenced by impurities, while Moteki and Murotani[9] reported that the addition of iron oxide accelerated sintering.

Experiments on the sorption of water vapor by magnesium oxide led Ishikawa and Sano[10] to suggest that the adsorbed water does not cause hydration of the oxide instantaneously, but that it remains for a certain period of time in an adsorbed state. This view was confirmed by Fricke and Buckmann[11] and by Quartaroli and Belfiori.[12] Isikawa and Kanamori,[13] working with light and heavy water on magnesium oxide obtained by the dehydration of the hydroxide, succeeded in relating the adsorption velocities to the diffusion rates of the vapors through the capillary pores of magnesium oxide. Burdese[14] investigated recently the adsorption of water vapor on oxides of magnesium prepared by the calcination of the hydroxide and carbonate. He found that in presence of air the equilibrium of physical adsorption was reached after 2 hours, but that the uptake of water continued for a longer time due to the formation of the hydroxide, which in its turn, would adsorb more water vapor. In absence of air, the author found that equilibrium is practically attained in 30 minutes, and that the adsorption gives rise to an isotherm of type IV in Brunauer's classification,[15] which was accompanied by pronounced hysteresis. However, Burdese confined the latter experiments to one single oxide calcined at 600°, and the measurements did not exceed an equilibrium pressure of 0.75 relative vapor pressure.

Experimental

The determination of the amount of sorbed water vapor was carried out with the aid of an electric sorption balance similar to that described by Gregg.[16] The apparatus used was composed of the electric sorption balance, a manometer, a water supply system, all of which were placed in an air thermostat regulated at 35 ± 0.1°, and an evacuation system consisting of a mercury diffusion pump coupled with a Cenco-Hyvac high vacuum oil pump and a McLeod gage.

The magnesium oxide used in the present investigation was prepared from a piece of brucite kindly offered by Basic Dolomite, Inc., Cleveland, Ohio, part of which was used in studying the kinetics of the thermal decomposition of brucite.[3] It proved to be very pure, and on ignition the loss in weight was 30.90%. Seven specimens of oxide, designated MgO(I)-MgO(VII) were prepared by the dehydration of brucite under vacuum at 350, 500, 650, 800, 950, 1020 and 1100°, respectively. The first two specimens were dehydrated at their respective temperatures of 350 and 500° *in situ* whereas the others were dehydrated outside the balance case in a silica tube at the required temperatures and later evacuated *in situ* at 500° for 3 hours. This procedure was necessary because the balance case was made of Pyrex glass and could not be heated safely to temperatures above 600° under vacuum. Preliminary experiments with water vapor and also with other vapors have proved that 500° is a suitable outgassing temperature for expelling sorbate from magnesium oxide and is as efficient as higher temperatures without the danger of sintering. For the purpose of standardization, care was taken in all cases to ensure that the dehydration temperature was attained in one hour and that the specimen was kept at that temperature for 5 hours. On account of the relatively slow sorption of water vapor on magnesium oxide, an interval of 24 hours was allowed between successive measurements. Repeated experiments have shown that this interval is sufficient to ensure equilibrium conditions from the vapor phase.

Results and Discussion

The sorption of water vapor at 35° on the specimens of magnesium oxide prepared by the dehydration of brucite at various temperatures gives sigmoid isotherms which invariably attain limiting sorption values at saturation vapor pressure. Curves A in Figs. 1–3 illustrate the results of experiment in the case of MgO(II), MgO(IV) and MgO(VI), respectively, and show the relation between the amount of sorbed water vapor s, expressed in moles per mole of oxide, as a function of the equilibrium relative vapor pressure p/p_0.

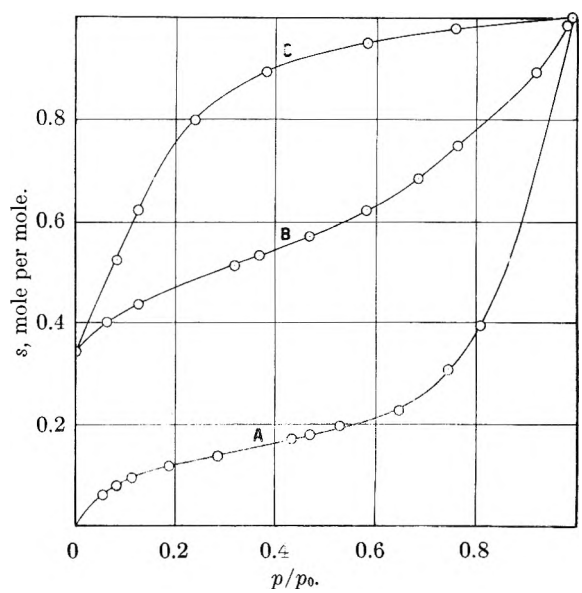

Fig. 1.—Sorption isotherms of water vapor on MgO(II), dehydrated at 500°: A, sorption; C, desorption; B, resorption at 35°.

(5) H. Le Chatelier, *Compt. rend.*, **102**, 1243 (1886).

(6) N. Parravano and C. Mazzetti, *Atti accad. Lincei*, [5] **30**, I, 63 (1921).

(7) J. W. Mellor, *Trans. Ceram. Soc.*, **16**, 85 (1917).

(8) E. B. Colegrave, H. M. Richardson and G. R. Rigby, *Discs. Faraday Soc.*, **5**, 352 (1949).

(9) K. Moteki and T. Murotani, *J. Ceram. Assoc. Japan*, **55**, 426 (1950).

(10) F. Ishikawa and K. Sano, *J. Chem. Soc. Japan*, **53**, 704 (1932).

(11) R. Fricke and H. Buckmann, *Ber.*, **72B**, 1199 (1939).

(12) A. Quartaroli and O. Belfiori, *Ann. Chem. Applicate*, **31**, 61 (1941).

(13) H. Isikawa and I. Kanamori, *Bull. Inst. Phys. Chem. Research (Tokyo)*, **19**, 1213 (1940).

(14) A. Burdese, *Atti. Accad. Sci. Torino, Classa Sci. Fis. Mat. et Nat.*, **86**, 107 (1951–1952).

(15) S. Brunauer, "The Adsorption of Gases and Vapors," Oxford, 1944.

(16) S. J. Gregg, *J. Chem. Soc.*, 561 (1946).

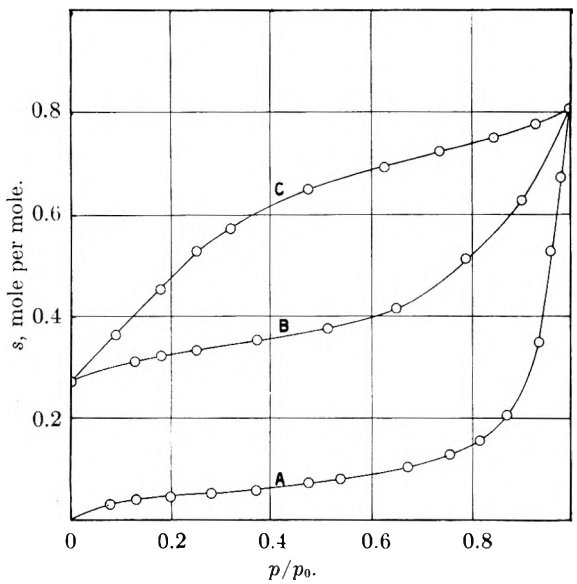

Fig. 2.—Sorption isotherms of water vapor on MgO(IV), dehydrated at 800°: A, sorption; C, desorption; B, resorption, at 35°.

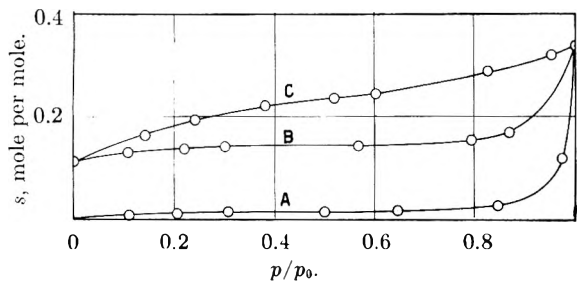

Fig. 3.—Sorption isotherms of water vapor on MgO(VI), dehydrated at 1020°: A, sorption; C, desorption; B, resorption, at 35°.

It has been found that the quantity of water taken up by the oxide at saturation vapor pressure depends very little on the dehydration temperature so long as it is below 650°. In case of MgO(I), the saturation value amounts to 0.9535 mole per mole of oxide, on the assumption of a completely dehydrated brucite, as compared with one mole per mole if complete rehydration of the oxide takes place. The difference between these two values may be accounted for by the incomplete dehydration of brucite at 350°. Indeed, it has been observed that dehydration at 350° does not convert all brucite into periclase but that the reaction comes to a standstill at 3–5% short of completion.[3,17] Heating at 500° for five hours brings about complete dehydration, and the saturation point for MgO(II) thus obtained reveals an uptake of 1.002 moles per mole, indicating complete rehydration with very little extra adsorption. The amount of water sorbed at saturation by MgO(III) is 0.9936 mole per mole, showing also almost complete rehydration.

On the other hand, raising the temperature of dehydration above 650° diminishes the uptake of water considerably. Thus the maximum amount of water taken up by MgO(IV) at saturation is 0.8071 mole per mole, whereas the values for MgO(V) and MgO(VI) are only 0.7037 and 0.3371 mole per mole, respectively. Finally the oxide obtained by the dehydration of brucite at 1100° for five hours seems to be completely inert or "deadburnt" and has no ability to take up even the smallest measurable amount of water. This temperature is well below the corresponding temperatures recorded by most of the earlier investigators, and is probably characteristic of the oxide prepared from native brucite, which is usually formed under severe conditions, and not of the oxide obtained from precipitated hydroxide or from carbonate. Curve A of Fig. 4 shows the relation between the maximum amount of water taken up from the vapor phase by the oxide and the dehydration temperature.

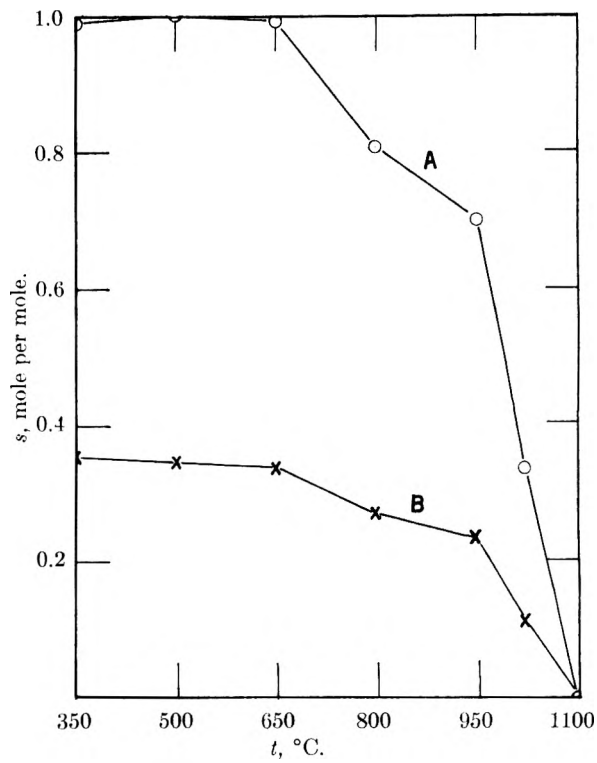

Fig. 4.—Effect of temperature of dehydration on (i) the amount sorbed at saturation vapor pressure (circles), and (ii) the amount retained after outgassing at 35° (crosses).

On following desorption down to thorough evacuation at 35°, a series of graphs illustrated by curves C of Figs. 1–3 is obtained. Appreciable hysteresis takes place and a large proportion of the quantity of water taken up by the oxide is not driven off by outgassing at this temperature. A similar behavior has been observed in other systems such as the silica– and alumina–water systems.[18] The water retained on evacuation at 35° by the various specimens is as follows: MgO(I), 0.3554; MgO(II), 0.3437; MgO(III), 0.3359; MgO(IV), 0.2709; MgO(V), 0.2360; MgO(VI), 0.1124 mole per mole. These values indicate that the amount of water retained by the oxide after outgassing at room temperature is almost the same for oxides prepared at or below 650°, but diminishes regularly with rise

(17) H. Induzuka, *J. Geol. Soc. Japan*, **48**, 244 (1941); W. Eitel and H. Kedesdy, *Abhandl. Preuss. Akad. Wiss.*, **5**, 13 (1943); P. Jolibois and M. Bergès, *Compt. rend.*, **224**, 78 (1947); Th. Duvel and C. Duvel, *Anal. Chim. Acta*, **2**, 45 (1948).

(18) K. S. Rao, THIS JOURNAL, **45**, 513 (1941); D. Papée, *Compt. rend.*, **234**, 952, 2536 (1952).

of temperature when dehydration takes place above 650°. This is made clear from curve B of Fig. 4. It is of interest to note that when the retained water is related to the water taken up at saturation vapor pressure it represents almost the same fraction, *viz.*, 37.3% for MgO(I), 34.4% for MgO(II), 33.8% for MgO(III), 33.6% for MgO(IV), 33.5% for MgO(V) and 33.3% for MgO(VI).

This retained water, however, could be expelled by raising the outgassing temperature. In case of MgO(I), for example, it is found that raising the temperature to 100° does not lead to further loss of water, but outgassing at 200° results in a loss of about 9%, whereas heating to 350° expels almost all the water held by the oxide.

When the magnesium oxide with its retained water is next exposed to the vapor of the latter, resorption takes place giving rise to sigmoid isotherms also as is illustrated by curves B in Figs. 1–3. These resorption isotherms end at saturation vapor pressure with the same sorption values obtained on the originally dehydrated brucite. The desorption–resorption cycle represented by curves B and C in Figs. 1–3 is perfectly reproducible and does not show any drift with time, so that it represents states of real equilibrium.

This definite and reproducible hysteresis appears in contrast with the results of Giauque and Archibald[19] on the decomposition pressure of $Mg(OH)_2$, for they obtained the same pressures when equilibrium was approached by raising or lowering the temperature, and, therefore on dehydration and rehydration. It may be that the system behaves in a different way at the higher temperatures used by those authors. As a matter of fact, some cases are known for which the hysteresis loop diminishes in size with rise of temperature.[20] Attempts are being made at the present to investigate the effect of temperature on the sorption of water vapor by magnesium oxide and on the hysteresis loop.

Unlike most hysteresis cases in sorption phenomena, the desorption isotherms of water vapor on magnesium oxide do not meet the original isotherms at zero pressure, while the reproducible desorption–resorption loop does not close at the lower pressures and even the isotherms approach each other at definite angles when the equilibrium pressure becomes zero. Under these conditions it becomes difficult to explain the hysteresis in terms of the familiar theories based on capillary condensation,[21] and, indeed, rough estimate of the pore size distribution from the desorption isotherms with the aid of Kelvin's equation gives a very small value for the most probable pore size, and indefinitely small values for the pore radii at the lowest pressures. On the other hand, the generalized domain theory of hysteresis developed by Everett[22] may account for the phenomenon. According to Everett, hysteresis is in general due to the existence of a very large number of independent domains at least some of which can exist in metastable states, and to the persistence of these metastable states in the change of either one physical state to the other or in both changes. Such is the state of affairs in the present system when the hydroxide is dehydrated and the oxide rehydrated. It is expected that during the dehydration of brucite, the formation of the periclase lattice results in a high degree of strain. The domains may thus be related to the presence of cracks and faults in the structure of the original solid as well as to the state of strain created by the formation of a new phase possessing a different molar volume and a different crystalline structure. Furthermore, at the lower temperatures of dehydration, the strain is usually the greater, and so would be the extent of hysteresis; but as this temperature is raised, the strain becomes less and so also the hysteresis. Inspection of the hysteresis loops in Figs. 1–3 confirms this view.

The appreciable hysteresis and its persistence down to the lowest equilibrium pressures, together with the stoichiometric uptake of water at saturation vapor pressure by the oxides prepared below 650°, indicate that the process is not a simple surface phenomenon. It seems that the exposure of magnesium oxide to water vapor leads first to the adsorption of water molecules on the external surface of the oxide and then to their penetration into the lattice of the latter. The molecules which penetrate through the solid then get attached in some form of binding, probably to oxygen ions, in a stoichiometric ratio. However, the strength of binding does not seem to be uniform for all molecules, and it appears that a fraction, about one-third, is very firmly held so that it cannot be expelled by evacuation at room temperature. The remaining two-thirds are held up by weaker forces so that extensive outgassing at room temperature results in the removal of this water from the oxide.

This picture seems in harmony with the recent work of Garrido[23] who concluded from his study of the structural changes accompanying the dehydration of brucite by means of X-ray measurements, that dehydration gives rise to crystallites having two different lattices corresponding to two orientations in which two planes are identical and parallel to two planes of brucite, while the third is different in each case. Garrido found further that dehydration at 500° results in about 75% of crystallites possessing orientation I and about 25% possessing orientation II. It is natural that the forces of binding of the water molecules in the crystallites are characteristic of the state of orientation. According to Garrido, the ratio in which crystallites of the two orientations exist is 3:1, a value which approaches the ratio between the amount of water which is loosely held by the oxide and that which is retained, *viz.*, 2:1. This indicates that the water molecules taken up by crystallites possessing orientation II are held in the magnesium oxide lattice by forces which are much stronger than in crystallites of orientation I. The difference between the two ratios is not unexpected in view of the different con-

(19) W. F. Giauque and R. Archibald, *J. Am. Chem. Soc.*, **59**, 561 (1937).

(20) A. G. Foster, THIS JOURNAL, **55**, 638 (1951).

(21) A. G. Foster, *Trans. Faraday Soc.*, **28**, 645 (1932); L. H. Cohan, *J. Am. Chem. Soc.*, **60**, 433 (1938); E. O. Kraemer, "Treatise on Physical Chemistry," John Wiley and Sons, Inc., New York, N. Y., 1931; J. W. McBain, *J. Am. Chem. Soc.*, **57**, 699 (1935); K. S. Rao, THIS JOURNAL, **46**, 500 (1941); S. M. Katz, *ibid.*, **53**, 1166 (1949); etc.

(22) D. H. Everett and W. I. Whitton, *Trans. Faraday Soc.*, **48**, 749 (1952); D. H. Everett and F. W. Smith, *ibid.*, **50**, 187 (1954).

(23) J. Garrido, *Ion*, **11**, 206, 453 (1951).

ditions of dehydration, for it has been found that both the temperature of dehydration and also its duration are effective in determining the properties of active solids.[24]

In case of oxides which are prepared at temperatures above 650°, the amount of water taken up at saturation does not correspond to the stoichiometric requirements for $Mg(OH)_2$, although the ratio between the loosely held water and the retained water still remains about 2:1. It is probable that as a result of dehydration at the higher temperatures only a fraction of the oxide, in its two forms of orientation, remains active and capable of binding with water molecules, the other fraction having lost this ability through sintering. The proportion of active oxide diminishes with rise of temperature until the oxide becomes completely "deadburnt" at 1100°.

(24) S. J. Gregg, *J. Chem. Soc.*, 3940 (1953); also unpublished work from this Laboratory.

A PHYSICOCHEMICAL STUDY OF AQUEOUS CITRIC ACID SOLUTIONS

BY BARBARA J. LEVIEN

Department of Chemistry, University of Western Australia, Nedlands

Received February 9, 1955

The apparent osmotic coefficients of citric acid solutions at 25° have been determined up to saturation by the isopiestic method. By making allowance for the ions present the osmotic and activity coefficients for the citric acid molecule have been determined to 1.1 molal. The degree of dissociation has been found by conductivity measurements which were corrected for viscosity effects, involving density measurements, viscosity measurements and conductivity measurements of hydrochloric acid in varying concentrations of citric acid. The solubility, heat of solution and partial molal volume have been calculated. K_m for the first dissociation has been calculated up to 1.1 M, using the activity coefficients for the citric acid molecule obtained in this work.

Introduction

This work was undertaken at the suggestion of Professor H. A. Krebs to provide thermodynamic data for citric acid solutions. The vapor pressures obtainable by the isopiestic method do not alone provide complete information on the activity coefficients of the undissociated molecule owing to the appreciable ionization of the acid; hence conductivity measurements were also made so that a correction for the ionization could be applied.

Experimental

Preparation of Solutions.—Crude anhydrous citric acid was prepared from the monohydrate by heating at 100–102° in an air oven for several days. Analytical reagent quality citric acid monohydrate was then placed in a vacuum desiccator over the anhydrous acid until the monohydrate attained constant weight. A sample of acid obtained from Professor Krebs was so treated and analyzed for purity by potentiometric titration against carbonate-free sodium hydroxide solution and found to be within 0.1% of the monohydrate composition. Solutions were prepared from the monohydrate by weighing the required quantity and dissolving in doubly distilled water of specific conductivity 1.1×10^{-6} ohm^{-1} cm.$^{-1}$. More dilute solutions were prepared by dilution of a concentrated stock solution. In no case were solutions kept more than two weeks.

TABLE I

ISOPIESTIC SOLUTIONS OF CITRIC ACID AND SODIUM CHLORIDE AT 25°

m_1, molality of anhydrous citric acid, m_2, molality of sodium chloride.

m_1	m_2	m_1	m_2	m_1	m_2
0.2093	0.1209	1.2264	0.7168	5.424	3.565
.2094	.1209	1.697	1.012	5.532	3.641
.2111	.1222	1.751	1.048	5.801	3.824
.3084	.1766	2.359	1.441	6.000	3.956
.3914	.2246	2.651	1.638	6.714	4.445
.5390	.3105	2.667	1.644	6.954	4.597
.5427	.3113	2.721	1.680	7.619	5.034
.6479	.3730	3.154	1.975	8.055	5.308
.7794	.4496	3.855	2.460	8.245	5.433
.8741	.5055	4.486	2.904	8.487[a]	5.588
1.0465	.6088	5.163	3.382	8.560	5.636

[a] Saturated solution.

Isopiestic Measurements.—These were made by the usual method[1] against sodium chloride as reference solute, the experimental results being given in Table I. Points below 0.2 M citric acid were obtained but could not be reproduced with satisfactory accuracy and are therefore not included. The isopiestic sodium chloride solutions in these cases were below 0.1 M which is normally considered the lower limit of the method.

Conductivity Measurements.—These were made with a conventional a.c. bridge circuit, with Wagner earth, at 500,

TABLE II

(a) MOLAR CONDUCTIVITIES OF CITRIC ACID SOLUTIONS AT 25°

c, concn., moles/l.; Λ_{app}, apparent molar conductivity; Λ_{cor}, molar conductivity cor. for the effect of the second dissociation.

c	Λ_{app}	Λ_{cor}
0.01799	72.16	71.81
.04493	47.57	47.43
.06420	40.12	40.02
.1122	30.58	30.53
.1603	25.46	25.43
.2803	18.85	18.84
.4004	15.26	15.25
.7000	10.46	10.451
1.000	7.79	7.788

(b) CONDUCTIVITIES OF 0.1004 N HYDROCHLORIC ACID IN CITRIC ACID

c, concentration of citric acid in moles/l.; κ_{sp}, obsd. specific conductivities; Λ_{HCl}, conductivity of hydrochloric acid, cor. for the presence of the ions from citric acid

c	κ_{sp}	Λ_{cor}
0	0.03928	391.2
0.2	.03765	367.5
.5	.03506	332.3
.7	.03320	308.8
1.0	.03041	274.9

(1) R. A. Robinson and D. A. Sinclair, *J. Am. Chem. Soc.*, **56**, 1830 (1934).

1000 and 2000 c.p.s. The bridge had been calibrated and had a precision of better than 0.05%. The conductance cells were of standard design with cell constants (1) 0.5235 and (2) 6.217 cm.$^{-1}$. They were calibrated with both 0.1 and 0.01 D potassium chloride solutions using the Jones and Bradshaw standards.[2] An oil thermostat controlled to ±0.005° was used for the conductivity work. The observed conductivities are given in Table II. The solvent correction was ignored as is usual for acid solutions.

Density Measurements.—These were made using a simple pyknometer of 20-ml. capacity, the experimental results being given in Table III. The reproducibility was $\pm 5 \times 10^{-5}$ in the density and the equation

$$d^{25}_4 = 0.99707 + 0.07700m - 0.00774m^2 \qquad (1)$$

fits the observed values with a mean deviation of ±0.00004.

TABLE III

DENSITIES OF CITRIC ACID SOLUTIONS AT 25°

m, molality of anhydrous citric acid; w, weight % of anhydrous citric acid; $d_{calc.} - d_{obs.}$, deviation of obsd. value from that calcd. by eq. 1.

m	w	d^{25}_4	$d_{calc.} - d_{obs.}$
0.09931	1.8722	1.00471	−0.00007
.2011	3.7022	1.01222	+ .00006
.2824	5.1469	1.01820	.00000
.4064	7.243	1.02717	+ .00005
.5913	10.202	1.03989	.00000
.8491	14.248	1.05693	− .00006
1.2415	19.258	1.08074	.00000

Viscosity Measurements.—These were made using an Ostwald viscometer calibrated with doubly distilled water and 20% sucrose. The absolute viscosity of water was taken as 0.8937 cp. and that of the sucrose as 1.704 cp.[3] Times of outflow were in the range 620–960 sec. and agreed to ±0.1 sec. Repeated filtration through sintered glass was necessary to obtain this reproducibility. The experimental results are given in Table IV.

TABLE IV

RELATIVE VISCOSITIES OF CITRIC ACID SOLUTIONS AT 25°

m, molality of anhydrous citric acid; η/η°, viscosity relative to water.

m	η/η_0	m	η/η_0
0.12092	1.0539	0.7533	1.3753
.2089	1.0948	.9489	1.4885
.3999	1.1875	1.2602	1.6802

Apparent Osmotic Coefficients.—These have been evaluated from the osmotic coefficients of Robinson for sodium chloride.[4] The values, given in Table V, are computed with disregard for the ionization of the acid.

Osmotic and Activity Coefficients for the Undissociated Citric Acid Molecule.—These are obtained essentially by making allowance for the effect of the ions present, which demands a knowledge of the degree of dissociation, this being obtained from the conductivity data as follows.

(1) A value of Λ^0 for citric acid is assumed. The correctness of this assumption is then tested by calculating the first dissociation constant and comparing with the value obtained thermodynamically by Bates and Pinching.[5]

(2) Values of the degree of dissociation α may then be found from Λ^0 and the conductivity data,

TABLE V

APPARENT OSMOTIC COEFFICIENTS OF CITRIC ACID SOLUTIONS AT 25°

m, molality of anhydrous citric acid; ϕ, apparent osmotic coefficient of citric acid (computed as a non-electrolyte).

m	ϕ	m	ϕ	m	ϕ
0.2	1.077	1.1	1.076	5.0	1.390
.3	1.062	1.5	1.103	5.5	1.431
.4	1.059	2.0	1.137	6.0	1.467
.5	1.057	2.5	1.176	6.5	1.503
.6	1.058	3.0	1.217	7.0	1.537
.7	1.060	3.5	1.260	7.5	1.570
.8	1.062	4.0	1.303	8.0	1.600
.9	1.066	4.5	1.347	8.487[a]	1.629
1.0	1.071				

[a] Saturated solution.

making due allowance for the effect of change in viscosity of the solutions. This effect is determined by separate experiments.

(3) Knowing α, the correction to the apparent osmotic coefficient may be made, giving the osmotic coefficient of the molecule.

(4) The activity coefficient of the molecule may be calculated from the osmotic coefficient of the molecule.

(5) These activity coefficients may be confirmed by the computation of K_m.

(1) λ^0 for the hydrogen ion is known, 349.81[6], and λ^0 for the citrate ion was assumed to be the same as that for the picrate ion, 30.39.[7] This assumption appears not unreasonable, since the ions $C_6H_7O_7^-$ and $C_6H_2N_3O_7^-$, respectively, are of closely comparable size and both present a large number of oxygen atoms in any encounter with other molecules.

If Λ^0 has been chosen correctly then the first ionization constant should extrapolate to the known correct value, since any effects due to increase in viscosity, neglect of molecule activity coefficients and any inadequacies in conductivity theory will be approximately linearly dependent upon concentration. However it is necessary to make allowance for the ions produced by the second dissociation. Since the concentration of products of the second stage of dissociation must be nearly constant at 1.7×10^{-5} molar ($K_2 = 1.73 \times 10^{-5}$)[5] in virtue of the much larger and nearly equal concentrations of H^+ and H_2Cit^- ions arising from the first stage, a constant correction estimated at 7×10^{-6} ohm^{-1} cor.$^{-1}$ was applied to all the measured specific conductivities. This correction was only 0.6% in the most dilute solution studied and was less than 0.2% above 0.1 molar.

Using the corrected values of Λ a crude value for α may be obtained from the conductivity ratio Λ/Λ^0, but it is better, once the first estimate of ionic concentration has been made to compute the equivalent conductivity of the free ions, Λ_i, by means of the equation[8]

$$\Lambda_i = \Lambda^0 - \frac{(B_1\Lambda^0 + B_2)\sqrt{c_i}}{1 + B_a^0\sqrt{c_i}} \qquad (2)$$

(2) G. Jones and B. C. Bradshaw, *J. Am. Chem. Soc.*, **55**, 1780 (1933).

(3) E. C. Bingham and R. F. Jackson, *Bull. Bur. Standards*, **14**, 59 (1918).

(4) R. A. Robinson, *Trans. Roy. Soc. N. Z.*, **75**, 203 (1945); R. H. Stokes and B. J. Levien, *J. Am. Chem. Soc.*, **68**, 333 (1946).

(5) R. G. Bates and G. D. Pinching, *ibid.*, **71**, 1274 (1949).

(6) B. B. Owen and F. H. Sweeton, *ibid.*, **63**, 2811 (1941).

(7) H. M. Daggett, E. J. Bair and C. A. Kraus, *ibid.*, **73**, 799 (1951).

(8) R. A. Robinson and R. H. Stokes, *ibid.*, **76**, 1991 (1954).

TABLE VI

PRELIMINARY CALCULATIONS TO CHECK $\Lambda^0 = 380.2$

c, concn., moles/l.; Λ_{cor}, molar conductivity cor. for the effect of second dissociation; α', α'', first and second approximations to the degree of dissociation; c_i', c_i'', first and second approximations to the concn. of ions present; Λ_i, equiv. conductivity of ions H^+ and H_2Cit^- at the ionic concn., c_i; $y_\pm$, mean ionic activity coefficient calcd. by eq. 3.

c	Λ_{cor}	$\alpha' = \frac{\Lambda_{cor}}{\Lambda^0}$	c_i	Λ_i	$\alpha'' = \frac{\Lambda_{cor}}{\Lambda_i}$	c_i''	$y_\pm^2$	$K' \times 10^4$
0.01799	71.81	0.1890	0.003400	372.16	0.1930	0.003472	0.8828	7.331
.04493	47.43	.1248	.005607	370.18	.1281	.005765	.8537	7.218
.06420	40.02	.1053	.006760	369.33	.1084	.006959	.8420	7.124
.1122	30.53	.08034	.009014	367.91	.08298	.009310	.8225	6.930

where $c_i = \alpha c = (\Lambda/\Lambda_i)c$ and $\mathring{a}$ is taken as 5 Å. This equation is used since it has been shown to give a better representation of the change of Λ^0 with concentration than the Onsager limiting law. By using successive approximations for c_i a final estimate of α is obtained, and using activity coefficients for the ions present, obtained from the Debye–Huckel equation

$$-\log y \approx -\log f = \frac{A\sqrt{c_i}}{1 + B\mathring{a}^0\sqrt{c_i}} \qquad (3)$$

where $A = 0.5091$. K' is obtained.

$c_i = 0.031$ was the maximum value for the ionic concentration encountered and therefore the use of both equations 2 and 3 is perfectly valid. Since the effective size of the H_2Cit^- ion should be greater than that of the chloride ion and since hydrochloric acid requires $\mathring{a} = 4.4$[9] and ion size parameter of $\mathring{a} = 5$ was chosen for citric acid. However the results are not very sensitive to the choice of this parameter.

A plot of log K' against c is shown in Fig. 1. The extrapolated value gives $K_c = 7.41 \times 10^{-4}$ which agrees very well with $K_c = 7.43 \times 10^{-4}$, the value corresponding on the molarity scale to the Bates and Pinching[5] molality scale value of 7.45×10^{-4} obtained from electromotive force measurements. It is also interesting to note that if Λ^0 were assumed to be 382, K' at $c = 0.01799$ would be 7.24×10^{-4} so that the estimated value $\lambda^0 = 30.39$ for the H_2Cit^- ion must be very nearly correct.

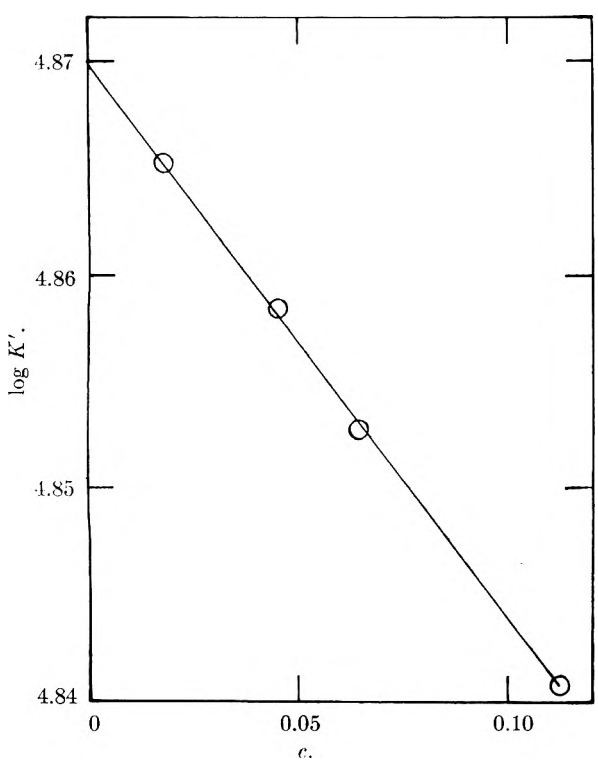

Fig. 1.—Extrapolation for first dissociation constant at 25°.

(9) R. H. Stokes, *J. Am. Chem. Soc.*, **76**, 1988 (1954).

Since the above calculations were made purely as a check of the correctness of $\Lambda^0 = 380.2$, only the data for the four most dilute solutions were used. The calculations for these points are summarized in Table VI.

(2) The values of α obtained in the above calculations are not the true values in any solutions in which the viscosity is different from that of pure water. It is known that viscosity has a marked effect on conductivity but the exact form of the correction necessary is not known. Preliminary calculations in which the molar conductivities were multiplied by the appropriate viscosity ratios led to unsatisfactory values for α. In short it seemed that the relationship of decrease in conductivity to increase in viscosity was not a simple one. Consequently the effects of the presence of undissociated citric acid on the conductivity were determined experimentally as outlined below.

The conductivities of 0.1 N hydrochloric acid in water and in varying concentrations of citric acid were measured, the assumption being that the effect of undissociated citric acid is the same on hydrochloric acid as on the ions of citric acid (H^+ and H_2Cit^-). This assumption should not be far wrong since about 90% of the conductivity is due in each case to the hydrogen ion. One must however allow in the total conductivity for the conductivity due to the H^+ and H_2Cit^- ions from the citric acid.

Taking the case of 0.1004 N hydrochloric acid (hereafter referred to as 0.1 N for brevity) in 0.7 molar citric acid as a concrete example, with $K_1 = 7.43 \times 10^{-4}$ [5] and $y_\pm = 0.80$ (the value for 0.1 N hydrochloric acid in water)[10]

$$\frac{x(0.1004 + x)}{0.7 - x} = \frac{7.43 \times 10^{-4}}{0.64} = 1.16 \times 10^{-3} \qquad (4)$$

where x is the concentration of the ion H_2Cit^-, x is found to be 7.45×10^{-3} moles/l. In the next step, that of finding the equivalent conductivity of the ions arising from the citric acid, the validity of reducing Λ^0 for citric acid in the same ratio as Λ^0 for hydrochloric acid seems justified for the reason mentioned above.

$$(\lambda_{H^+} + \lambda_{H_2Cit^-})_{0.1N\ HCl} = \Lambda^0_{H_3Cit} \times \frac{\Lambda_{0.1N\ HCl}}{\Lambda^0_{HCl}}$$
$$= 380.2 \times 391.2/426.1$$

(10) H. S. Harned and B. B. Owen, "The Physical Chemistry of Electrolytic Solutions," Reinhold Publ. Corp., New York N. Y., 1950, p. 547.

This would hold good in water, but the presence of the undissociated citric acid molecules will reduce the value still further in the same ratio as the conductivity of 0.1 N hydrochloric acid is reduced by the presence of the citric acid. Since at this stage we are concerned only with computing a small correction term, the uncorrected equivalent conductivity of 0.1 N HCl in the 0.7 molar citric acid can be used as an adequate approximation, giving

$$(\lambda_{H^+} + \lambda_{H_2Cit^-})_{0.1N\ HCl} = 380 \times \frac{391}{426} \times \frac{331}{391} = 295$$
$$+0.7\ \text{molar}\ H_3Cit$$

where 331 is the uncorrected Λ value for 0.1 N HCl in 0.7 molar citric acid. In the general case

$$(\lambda_{H^+} + \lambda_{H_2Cit})_{0.1N\ HCl} = \Lambda^0_{H_3Cit} \times \frac{\Lambda_{uncor}}{\Lambda^0_{HCl}} \qquad (5)$$
$$+y\ \text{molar}\ H_3Cit$$

The specific conductivity due to the citric acid ions can then be calculated and leads finally to Λ for the hydrochloric acid, as may be shown by continuing the above example. If $(\Lambda_{H^+} + \lambda_{H_3Cit}) = 295$ and $x = 7.45 \times 10^{-3}$ moles/l. then the contribution of the citric acid ions to the specific conductivity is 0.00220 ohm^{-1} cm.$^{-1}$. But the measured value of κ_{sp} is 0.03320. Hence

$$\kappa_{sp}^{HCl} = 0.03100$$
$$C_{HCl} = 0.1004\ N$$

and

$$\Lambda_{HCl} = 308.8$$

These results are shown in Table IIb. We are now in a position to correct the molar conductivities of pure citric acid for the effect of viscosity. The η/η^0 values corresponding to the required citric acid concentrations were read off from a graph constructed from the values in Table IV and next the $\Lambda_{H_2O}/\Lambda_{H_3Cit}$ ratios at these values from a graph of log η/η^0 against log $\Lambda_{H_2O}/\Lambda_{H_3Cit}$. Once the apparent Λ had been modified by the "Λ factor," α was calculated in the way outlined in section (1). The values of α are given in Table VII.

(3) The next step, to calculate the contribution to the osmotic coefficient due to the ions, necessitates first a knowledge of α at round molalities since the apparent osmotic coefficients were available at molalities and not molarities. These can be obtained by graphical interpolation, invoking the α results in Table VII and the densities in Table III.

TABLE VII

DEGREE OF DISSOCIATION OF CITRIC ACID SOLUTIONS

c, concn., moles/l., α, final value for degree of dissociation.

c	α	c	α
0.01799	0.1940	0.2803	0.05632
.04493	.1299	.4004	.04769
.06420	.1106	.7000	.03653
.1122	.08590	1.000	.03080
.1603	.07310		

The subsequent procedure involves two assumptions (a) that the apparent osmotic coefficients are made up as

$$\phi_{app}\, m = \phi_{molecule}\, m(1 - \alpha) + 2\phi_i m_i \qquad (6)$$

i.e., that the logarithms of the water activities due to the molecule and to the ions are additive and (b) that the osmotic coefficients of the ions are similar to those of any other 1–1 salt at the same *ionic* concentration. Using therefore a plot of ϕ against m_i for sodium chloride,[11] ϕ_i at m_i were read off, and hence from the above equation $\phi_{molecule}$ at $m(1 - \alpha)$, *i.e.*, $m_{molecule}$ were calculated. The results for sodium chloride were taken since they were available at the low concentrations required, but at these low concentrations it would not matter for the purposes of this correction whether sodium chloride or some other 1–1 salt is used. The results are given in Table VIII and plotted in Fig. 2. The lowest point does

TABLE VIII

OSMOTIC AND ACTIVITY COEFFICIENTS OF THE CITRIC ACID MOLECULE. FIRST DISSOCIATION CONSTANT FOR CITRIC ACID

m, molality of anhydrous citric acid; α, degree of dissociation; $m_{mol} = m(1 - \alpha)$, molality of citric acid molecule; ϕ_{mol}, osmotic coefficient of the citric acid molecule; γ_{mol}, activity coefficient of the citric acid molecule; K_m, first dissociation constant (on molality scale) of citric acid.

m	α	m_{mol}	ϕ_{mol}	γ_{mol}	$K_m \times 10^4$
0.2	0.0668	0.1866	1.016	1.014	7.51
.3	.0556	.2833	1.011	1.022	7.51
.4	.0490	.3804	1.015	1.030	7.54
.5	.0442	.4779	1.017	1.038	7.49
.6	.0410	.5754	1.022	1.045	7.57
.7	.0382	.6733	1.026	1.053	7.51
.8	.0359	.7713	1.031	1.062	7.44
.9	.0342	.8692	1.036	1.072	7.45
1.0	.0328	.9672	1.043	1.082	7.48
1.1	.0313	1.0656	1.049	1.095	7.34

not seem satisfactory but in view of the number of isopiestic results obtained in that region one hesitates to ascribe the discrepancy entirely to experimental inadequacy. At the same time it does occur near the lower limit of the isopiestic method.

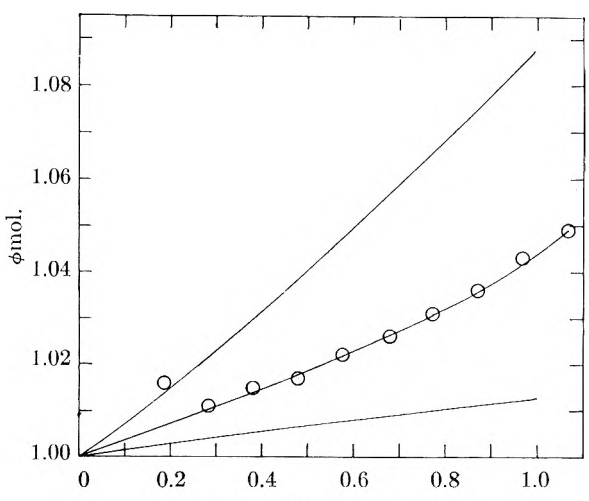

Fig. 2.—Osmotic coefficient of molecular citric acid at 25°: top curve, sucrose; middle curve, citric acid; bottom curve, glycerol.

(4) The activity coefficients of the molecule were calculated from the osmotic coefficients of the molecule, ignoring the lowest point and extrapolating the curve to the theoretical limit of unity at zero

(11) G. J. Janz and A. R. Gordon, *J. Am. Chem. Soc.*, **65**, 218 (1943).

concentration. The results are given in Table VIII.

(5) Every quantity except $\gamma_{\pm}$ necessary for the calculation of K_m has now been obtained, and this at the required m_i was taken from the data for hydrochloric acid.[10]

$$K_m = \frac{\alpha^2 m \gamma_{\pm}^2}{(1 - \alpha)\gamma_{mol}} \quad (7)$$

is given in Table VIII. The mean value is 7.49×10^{-4} which compares very favorably with the value of 7.45×10^{-4} obtained from e.m.f. measurements by Bates and Pinching.[5]

Solubility.—The solubility was calculated from the isopiestic results at saturation by the method of Scatchard, Hamer and Wood.[12] The composition of the saturated solution is 61.99% by weight or 8.487 M. This compares very well with the figure of 62.03% found by Dalman.[13]

Heat of Solution.—Using the equation[14] for a monohydrated non-electrolyte and the temperature coefficient of solubility given by Dalman[13]

$$\Delta H_{sol.} = \left(1 - \frac{m}{55.51}\right) RT^2 \left(\frac{dm}{dT}\right)_{sat} \left[\left(\frac{\phi}{m}\right)_{sat} + \left(\frac{\partial \phi}{\partial m}\right)_T\right] \quad (8)$$

the last heat of solution was found to be 7.12 kcal./mole.

Partial Molal Volume.—Using the equation

$$\bar{V}_2 = \frac{M}{d} - \frac{1000 + mM}{d^2} \frac{\partial d}{\partial m} \quad (9)$$

where $\partial d/\partial m$ was taken as $0.07700 - 0.01548\ m$ from equation 1, the partial molal volume was calculated at several concentrations in the range 0.1 to 1 M, the results varying from 114.8 to 115.7 cc./mole. This may be compared with the value of 124.6[15] for the anhydrous solid.

Discussion

The osmotic coefficients for the undissociated citric acid molecule are compared in Fig. 2 with the values given for glycerol and sucrose by Scatchard, Hamer and Wood.[14] Citric acid lies between glycerol and sucrose as might be expected purely on the grounds of increase in size from $C_3H_8O_3$ to $C_6H_8O_7$ to $C_{12}H_{22}O_{11}$. All three compounds contain large numbers of polar groups with which to interact with water and the number of hydroxyl groups increases from 3, to 4, to 6, which could also affect the osmotic coefficients in the same order.

The correctness and constancy over the concentration range studied of the value derived for K_m for the first dissociation of citric acid is a fair indication of the essential correctness of the method whereby the effects due to the presence of the ions have been eliminated.

Acknowledgments.—The author wishes to thank Professor Krebs for the sample and details of purification of the citric acid provided and Dr. R. H. Stokes for much helpful advice and discussion during the planning and carrying out of this work.

(12) G. Scatchard, W. J. Hamer and S. E. Wood, *J. Am. Chem. Soc.*, **60**, 3061 (1938).

(13) L. H. Dalman, *ibid.*, **59**, 2547 (1937).

(14) A. T. Williamson, *Trans. Faraday Soc.*, **40**, 429 (1944).

(15) "Handbook of Chemistry and Physics," Chemical Rubber Publ. Co., Cleveland, Ohio, 1940, p. 745.

HYBRIDIZATION AND DIPOLE MOMENT[1]

BY JULIAN H. GIBBS

General Electric Research Laboratory, Schenectady, New York

Received February 12, 1955

Orbital hybridization, as determined by bond angle, can account for the major variations in electric dipole moment among the hydrides and organic derivatives of vertical series of non-metallic elements of the periodic system. This is shown by calculation of the moments of purely covalent forms of such compounds.

Introduction and Model

The labor involved in even an approximate quantum-mechanical treatment of but a single property of a single simple molecule has led to the use of empirical schemes, involving concepts such as electronegativity, induction, steric repulsion, etc., for qualitative discussions of properties of large numbers of molecules. Since their relationship to fundamental quantum-mechanical principles is not clear, these treatments are often *ad hoc*, and they seldom permit quantitative calculations. Furthermore they lead to incorrect predictions in many cases.

It is the purpose of this article to show that the quite reasonable assumptions commonly made in both of the more fundamental, quantitative methods of treating valence (valence bond and molecular orbital) alone provide an interpretation of many of the major qualitative variations in electric dipole moment among covalent molecules.

The assumptions are, first, that the molecular wave function may be compounded reasonably well from a small number of low energy atomic orbitals and, second, that the axes of these atomic orbitals are coincident with the axes of the singly-covalent bonds, if any, to which they contribute.[2]

The simplest application of these approximations is to be found among the saturated hydrogen and organic compounds of the covalent-bond forming elements of the IVth, Vth, VIth and VIIth main columns of the periodic system (the non-metals), inasmuch as hydrogen and carbon orbitals may be taken as pure s and pure tetrahedral hybrid, respec-

(1) Presented in part to the Division of Physical and Inorganic Chemistry at the 126th National Meeting of the American Chemical Society, New York, N. Y., September, 1954.

(2) L. Pauling, "The Nature of the Chemical Bond," Cornell Univ. Press, Ithaca, N. Y., 1945, Chapter III.

tively. It is thus only necessary to examine the hybridization of the non-metal in each compound.

Examination of the literature reveals that the bond angles of the hydrogen compounds of the non-metals of groups V and VI (H_3N, H_3P, etc., and H_2O, H_2S, etc.) decrease rapidly with increasing atomic number from a value near the tetrahedral at the second row elements (N, O) to an asymptotic value of 90°, the latter angle being approached as early as the third row elements (P, S). The methyl compounds, on the other hand, exhibit bond angles which decrease much more slowly with increasing atomic number. The available bond angle data for these compounds are shown in Table I.

According to the assumption that the relevant atomic orbitals point in the bond directions it may, therefore, be concluded that the hydrogen compounds lose their hybridization much more rapidly than the methyl (ethyl, phenyl) compounds on increasing atomic number of the non-metal. This hybridization rule will be shown to account for many of the variations in dipole moment among the members of these series.

Although the application of these assumptions to the calculation of dipole moments has been effected in the framework of both of the accepted methods in valency theory, for simplicity only the treatment in (localized) molecular orbitals will be discussed here.

Lennard-Jones[3] recently has shown how an antisymmetrized set of highly localized and "equivalent" orbitals may be obtained from a given set of antisymmetrized non-localized molecular orbitals. This provides theoretical justification for the localized molecular orbital method, which had hitherto enjoyed only the empirical justification involved in the known chemical integrity of chemical bonds.

The LCAO description given by this method for a bond which is assumed to be localized between atoms A and B is

$$\psi_{bdA-B} = a\phi_A + b\phi_B \qquad (1)$$

ϕ_A and ϕ_B may be hybrids of the basic s and p functions of atoms A and B, respectively

$$\phi_A = (\cos \epsilon_{bdA})\,(ns)_A + (\sin \epsilon_{bdA})\,(np)_A \qquad (2)$$

and similarly for ϕ_B.

For lone pair electrons on atom A the orbital description is

$$\psi_{lpA} = (\cos \epsilon_{lpA})\,(ns)_A + (\sin \epsilon_{lpA})\,(np)_A \qquad (3)$$

The parameters a, b, ϵ_{bdA} and ϵ_{lpA} are not all independent. The normalization condition for ψ_{bdA-B} relates a and b so that only the "electronegativity" ratio a/b is arbitrary. Then too, there are orthogonality conditions between orbitals of the type ψ_{bdA-B} and those of the type ψ_{lpA} so that the hybridization parameters ϵ_{bdA} and ϵ_{lpA} are related.

There are, therefore, two types of parameters to be considered, the electronegativity ratios, *e.g.*, a/b, and the hybridization parameters, *e.g.*, ϵ_{bdA} or ϵ_{lpA}.

For the determination of an electronegativity ratio minimization of the molecular energy is impractical because such calculations are very sensitive to the approximations which must be made. Therefore, no such calculations will be performed here. Rather, the approach will be to discuss the properties of purely covalent structures for the molecules in which $a = b$ in all bonds. The results so obtained will then be compared with experiment and the role of electronegativity differences inferred from any systematic discrepancies with experimental results which may appear.

A hybridization parameter, ϵ_{bdA}, is determined by the B–A–B bond angle, designated by α, through the agency of the orthogonality condition between 2 or 3 bond orbitals, ψ_{bdA-B}, emanating from the atom A. In considering this orthogonality condition it is only necessary to orthogonalize the contributions from atom A to the bonds, that is, the various ϕ_A, since the overlap of an orbital ϕ_A pointing in the direction of one bond with an orbital ϕ_B of an atom of type B lying along the axis of another bond will be small.[4]

The parameter ϵ_{lpA} is determined by the conditions of orthogonality between the various ψ_{lpA} and between the ψ_{lpA} and the ψ_{bdA-B}. In the latter condition the various ψ_{bdA-B} may again be approximated by the appropriate ϕ_A, because of the smallness of the overlap between ψ_{lpA} and ϕ_B.

Subject to these approximations, the orthogonality conditions yield quite simple relations between ϵ_{lpA}, ϵ_{bdA} and α

$$2 \cos \epsilon_{lpA} \sin \epsilon_{lpA} = 2 \cos \epsilon_{bdA} \sin \epsilon_{bdA} \sqrt{3(1 + 2\cos\alpha)} = 2\sqrt{\frac{-3\,(1 + 2\cos\alpha)\cos\alpha}{(1 - \cos\alpha)^2}} \equiv F_V(\alpha) \qquad (4)$$

for the case where A is a group V element with three equivalent attached B groups, and

$$4 \cos \epsilon_{lpA} \sin \epsilon_{lpA} \cos [(1/2)\beta] = 4 \cos \epsilon_{bdA} \sin \epsilon_{bdA} \cos [(1/2)\alpha] = 2\sqrt{\frac{-2\,(1 + \cos\alpha)\cos\alpha}{(1 - \cos\alpha)^2}} \equiv F_{VI}(\alpha) \qquad (4a)$$

for the case where A is a group VI element with 2 attached B groups and an angle β between the lone pair orbital axes. These relations will be needed below.

Dipole Moments

The variations in electric dipole moment among the members of the vertical series of compounds in question are displayed graphically in Fig. 1. The moments of the hydrogen compounds decrease monotonically with increasing atomic number of the non-metal in a vertical series (*e.g.*, $\mu_{H_3N} > \mu_{H_3P} > \mu_{H_3As}$). On the other hand the available data on the corresponding methyl, ethyl and phenyl compounds exhibit a maximum at the third row element (*e.g.*, $\mu_{R_2O} < \mu_{R_2S} > \mu_{R_2Se}$).

This difference between the latter variations and those among the hydrogen compounds is difficult to explain on the basis of the usual arguments concerning electronegativity differences and bond moments. That is, the same substitutions (*e.g.*, S for O) cause a decrease in moment in the case of the hydrides and an increase in moment in the case of the organic compounds.

(3) J. E. Lennard-Jones, *Proc. Roy. Soc. (London)*, **A198**, 1 (1949); **198**, 14 (1949).

(4) J. A. Pople, *ibid.*, **A202**, 323 (1950).

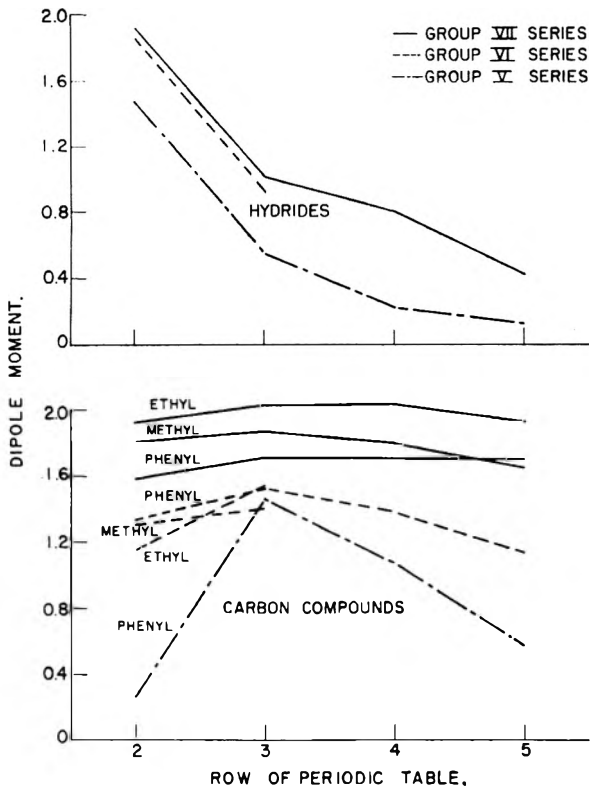

Fig. 1.—Electric dipole moments of the organic derivatives and hydrides of the elements of the Vth and VIth main groups of the periodic system ($\times 10^{18}$ e.g.s.).

However, it has recently been emphasized in both the localized MO[5,6] and valence bond[5,7] methods that the unshared or lone pair electrons of the nonmetal may make the major contribution to the over-all molecular moment. That is, if the orbitals of a lone pair bearing atom are largely hybridized, the lone pair electrons are not symmetrically disposed about the nucleus as in pure s or p orbitals but are oriented outward on the side of the atom opposite to that containing the bonded substituents. This is the key to an explanation already suggested[8] for the variations in dipole moment and basicity among these compounds. In what follows this explanation for the dipole moments, which is based on the assumptions mentioned in the introduction, is given in full and illustrated with calculations.

The molecular dipole moment may be taken as the vector sum of lone pair moments and bond moments the magnitudes of which are defined as follows.

A lone pair moment, μ_{1pA}, including the contribution from 2 protons on the nucleus A as well as that of the unshared electron pair, is given by

$$\mu_{1pA} = 2e\int x_A\psi^2_{1pA}\,d\nu \qquad (5)$$

where x_A is the coördinate lying along the symmetry axis of the lone pair orbital, ψ_{1pA}, and is measured from the nucleus A. Substitution of the expression (3) for ψ_{1pA} into (5) gives

$$\mu_{1pA} = 4e\cos\epsilon_{1pA}\sin\epsilon_{1pA}\int x_A(ns)_A(np)_A d\nu \qquad (6)$$

a moment which is only non-zero if $\psi_{1p\ A}$ is a hybrid (both $\cos\epsilon_{1pA}$ and $\sin\epsilon_{1pA} \neq 0$).

A bond moment $\mu_{bd\ A-B}$, including the contribution from one proton on each of the bonded nuclei, A and B, as well as that of the shared electron pair, is given by

$$\mu_{bdA-B} = 2e\int x_{A-B}\psi^2_{bdA-B}d\nu \qquad (7)$$

where x_{A-B} is the coördinate lying along the axis of the bond A–B and is measured from the bond midpoint. Substitution of the expression (1) for ψ_{bdA-B}, with the approximation $a = b$, into (7) gives, after translation of the origins of the coördinates appearing in the 1st 2 terms[9]

$$\mu_{bdA-B} = 2ea^2(-\int x_A\phi_A^2\,d\nu + \int x_B\phi_B^2\,d\nu + 2\int x\phi_A\phi_B\,d\nu) \qquad (8)$$

x_A now being measured from A toward B, x_B from B, and x from the midpoint of the A–B bond. Substitution of the expression (2) for ϕ_A into the 1st term gives an expression which, like the expression for a lone pair moment, is zero unless ϕ_A is a hybrid. The third term, the "homopolar bond moment,"[10] will be discussed below.

In the case where A is a group V element substitution of (4) into (6) gives for the lone pair moment

$$\mu_{1pAV} = 2eF_V(\alpha)G(A) \qquad (9)$$

where $G(A)$ has been written for the integral in (6).

Similarly in the group VI case the resultant of 2 lone pair moment vectors, with an angle β between their symmetry axes, is given by

$$\mu_{1pAVI} = 8e\cos[(1/2)\beta]\cos\epsilon_{1pA}\sin\epsilon_{1pA}\,G(A) = 2eF_{VI}(\alpha)G(A) \qquad (9a)$$

Now the first term in the expression (8) for the bond moment, μ_{bdA-B}, may be added vectorially to its 2 counterparts from the other 2 bonds emanating from A in the case where A is a group V element to give, again with the invocation of (4)

$$-2ea^2F_V(\alpha)G(A) \qquad (10)$$

a term which arises from the hybridization of A. This term may be added to that due to the hybridization of the lone pairs to give for the "hybridization moment" or "polarization" of A

$$\mu_{hAV} = 2e(1-a^2)F_V(\alpha)G(A) \qquad (11)$$

and for the group VI case

$$\mu_{hAVI} = 2e(1-a^2)F_{VI}(\alpha)G(A) \qquad (11a)$$

Now, as the existence of the 2nd term in equation 8 shows, there will be terms similar to (10) [or (11) for the lone pair bearing atoms] for every atom in a molecule. However, matters are simplified by consideration of hydrogen and carbon compounds. The hydrogen atoms contribute no non-zero terms of the form (10) since the H_{1s} orbital is not a hybrid and the integral, $\int x_H\phi_H^2\,d\nu$, is zero. In the case of the carbon atoms the expressions similar to (10) are very nearly zero because of the approximate[11]

(5) D. Z. Robinson, *J. Chem. Phys.*, **17**, 11, 1022 (1949).

(6) A. B. F. Duncan and J. A. Pople, *Trans. Faraday Soc.*, **49**, 3, 217 (1953).

(7) E. Warhurst and E. Whittle, *Nature*, **167**, 767 (1951).

(8) J. H. Gibbs, *J. Chem. Phys.*, **22**, 8, 1460 (1954).

(9) C. A. Coulson, *Trans. Faraday Soc.*, **38**, 433 (1942).

(10) R. S. Mulliken, *J. Chem. Phys.*, **3**, 573 (1935).

(11) This is not exactly true even for purely covalent bonds since the values of a are not quite the same for non-equivalent C bonds. There are small variations in the overlap integrals which arise in the normalization of the bond orbitals,

cancellation of the tetrahedrally (or trigonally, in the case of the phenyl compounds) oriented carbon orbital moments.

Thus, aside from the "homopolar bond moments" only the "hybridization moments" of the lone pair bearing elements need be considered. The orbital moments of a lone pair bearing element do not cancel one another because the lone pair orbitals have a full $2e$ of electronic charge associated with them whereas the bond forming orbitals of such an element carry only the share a^2 of the full $2e$ of charge in a bond.

The functions $F_V(\alpha)$ and $F_{VI}(\alpha)$ are shown in Fig. 2. They start at zero for $\alpha = 90°$, the condition of pure p bonding for which in the group V case the lone pair is a pure s function. As the bond angle α increases, $F_V(\alpha)$ and $F_{VI}(\alpha)$ increase sharply. $F_V(\alpha)$ has its maximum at $\alpha = 101° 52'$, corresponding to sp hybridization of the lone pair orbital and sp^5 hybridization in the orbitals contributing to the 3 bonds. $F_{VI}(\alpha)$, on the other hand, has its maximum at 109° 28′, corresponding to tetrahedral or sp^3 hybridization of all the atomic orbitals. The reason for this difference lies in the differing geometry of the 2 cases. The lone pair orbital in the group V case always lies along the axis of the resultant moment, the latter having its maximum when the lone pair orbital moment has its maximum. In the group VI case, however, there is a geometric factor, $\cos[(1/2)\beta]$, for the projection of the two lone pair moments onto the axis of the resultant moment. This factor is zero for sp hybrids, since the two point in opposite directions normal to the BAB plane. This is actually the equivalent orbital description of the case of no hybridization (maximum s character in the lone pair) since the sp hybrids are formed by simple linear combinations of the s and p orbitals left over when pure p orbitals are used for the bonding. It occurs, of course, when $\alpha = 90°$. The most favorable compromise, for largeness of resultant moment, between the magnitude of the orbital moments and the geometric factor projecting them onto the resultant axis occurs at the tetrahedral angle in this case.

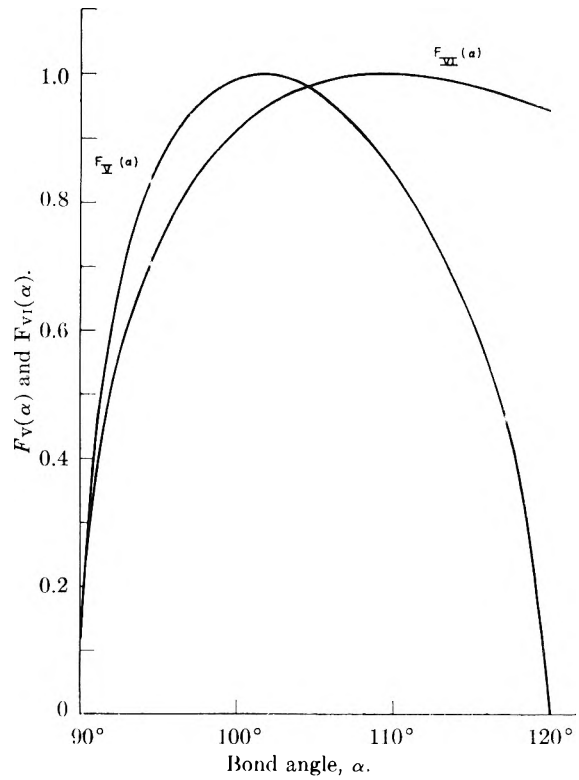

Fig. 2.—The functions $F_V(\alpha)$ and $F_{VI}(\alpha)$.

TABLE I

BOND ANGLES

Group V series			
H Compounds		CH_3 Compounds	
H_3N	107° ± 2°	$(CH_3)_2N$	108° ± 4°
H_3P	93.5°	$(CH_3)_3P$	100° ± 4°
H_3As	92.0°	$(CH_3)_3As$	96° ± 5°
H_3Sb	91.5°	$(CH_3)_3Sb$	

Group VI series			
H Compounds		CH_3 Compounds	
H_2O	104° ± .5°	$(CH_3)_2O$	110° ± 5°
H_2S	92.33°	$(CH_3)_2S$	105° ± 5°
H_2Se		$(CH_3)_2Se$	
H_2Te		$(CH_4)_2Te$	

TABLE II

THE INTEGRALS $G(A)$ FOR VARIOUS ATOMS, A

(Atomic Units)

Atom	$G(A)$	Atom	$G(A)$	Atom	$G(A)$
N	0.740	O	0.634	F	0.555
P	1.263	S	1.112	Cl	0.994
As	1.396	Se	1.266	Br	1.158

The integrals, $G(A)$, are given for the atoms in question in Table II. Slater functions[12] have been adopted for the radial parts of the basic s and p atomic orbitals in calculating these quantities. It will be seen that they increase with atomic number in a vertical series in much the same fashion as atomic radii, that is, rapidly at first and then more slowly.

This shows that a given degree of asymmetry of an orbital, described by the appropriate hybridization parameter, ϵ, will produce a greater polarity in that orbital if the orbital is large than if it is small. Thus, as shown by equations 11 for the atom as a whole, the hybridization moment is governed by a size effect, expressed by $G(A)$, as well as a hybridization effect manifest in $F_V(\alpha)$ or $F_{VI}(\alpha)$.

The "hybridization moments," calculated from equations 11 are given in Table III.[13] It will be noted that the hydrogen compounds do not exhibit the very large initial increase in hybridization moment that the carbon compounds do on increasing atomic number in a vertical series. The reason for this is as follows. The large decrease in the hybridization effect, $F_V(\alpha)$ or $F_{VI}(\alpha)$, which accompanies the large decrease in bond angle in these hydrides, tends to offset the increase in the orbital size effect, $G(A)$. On the other hand, in the case of the organic compounds, the decrease in $F_V(\alpha)$ or $F_{VI}(\alpha)$

(12) J. C. Slater, *Phys. Rev.*, **36**, 57 (1930).

(13) The values given were calculated on the basis of the central values for the bond angles in the cases where Table I shows a significant experimental error. Fortunately, the larger uncertainties in bond angle occur in the regions of the flat maxima for $F_V(\alpha)$ and $F_{VI}(\alpha)$. The same bond angles were used for H_2Se and $(CH_3)_2Se$ as for H_3As and $(CH_3)_3As$, respectively.

indicated by the bond angles is too small to offset the initially large increase in $G(A)$, but is adequate to offset the subsequent small increase in $G(A)$. This is the origin of the maximum moment observed at the second row element.

TABLE III

HYBRIDIZATION MOMENTS

($\times 10^{18}$ c.g.s.)

H_3N	3.50	$(CH_3)_3N$	3.41	H_2O	3.14	$(CH_3)_2O$	3.22
H_3P	4.86	$(CH_3)_3P$	6.37	H_2S	3.03	$(CH_3)_2S$	5.56
H_3As	4.36	$(CH_3)_3As$	6.53	H_2Se	2.39	$(CH_3)_2Se$	5.14

The "homopolar bond moments" must now be considered. Those integrals involved in their calculation which could not be found in the literature have been evaluated[14] in prolate spheroidal ("football") coördinates, again using Slater-type atomic orbitals. The values of the homopolar bond moments thus obtained are given in Table IV. The values for bonds involving carbon have been calculated for the case of tetrahedral carbon orbitals only. The values for trigonal carbon would not be very different from these.

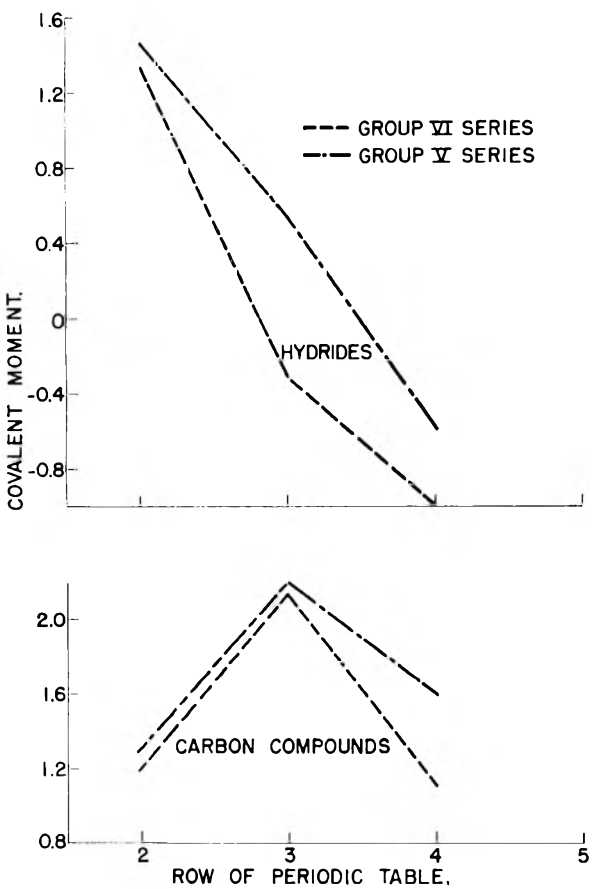

Fig. 3.—Dipole moments of covalent forms calculated from localized MO for the organic derivatives and hydrides of the elements of the Vth and VIth main groups of the periodic system($\times 10^{18}$ c.g.s.).

(14) In the cases of bonds involving row 4 elements, for which the "effective" principal quantum number in the atomic orbitals is the non-integral value 3.7, the approximation $r_A^{3.7} = r_A^4/r_{0A}^{0.3}$, where r_{0A} is the covalent radius of A, has been used to facilitate the integrations involved. Inasmuch as the homopolar dipole integrals only have non-zero contributions from the regions of overlap of the atomic orbitals, which regions are roughly centered around r_{0A}, this should not be a serious approximation.

TABLE IV

HOMOPOLAR BOND MOMENTS

($\times 10^{18}$ c.g.s.)

H–N	−0.85	C–N	+0.15	H–O	−0.65	C–O	+0.27
H–P	−1.75	C–P	− .44	H–S	−1.52	C–S	− .26
H–As	−2.16	C–As	− .75	H–Se	−1.88	C–Se	− .67

As Table IV shows, the homopolar moments for the bonds to the lone pair bearing atoms, A, vary monotonically with increasing atomic number of A in ever increasing opposition to the hybridization moment of A, the sign of which was taken as positive. This variation is greater for the hydrogen compounds than for the carbon compounds. Thus these terms contribute to the downward trend of the moments of the hydrides and, to a lesser extent, to the ultimate downward trend of the moments of the carbon compounds.

The reason for this variation in these homopolar moments lies in the fact that these are principally dependent upon the size difference between the bonded atoms,[10] since they are essentially a measure of the deviations of the centroids of the "overlap charges" from the bond midpoints.

The homopolar moments of the C–H bonds merely contribute an essentially constant amount to the moments of all the members of an organic series.

The resultant moments obtained for the covalent forms when these homopolar dipole terms are added vectorially to each other and to the hybridization moments are plotted in Fig. 3. As should be expected for such crude calculations, the absolute values of the results are not in very good agreement with the experimental values. However, the variations among the members of the vertical series do show the correct qualitative behavior.

There are two outstanding discrepancies between the values obtained for the hydrides and their experimental values.

First, these "covalent moments" show the wrong variation among the members of the horizontal series H_3N, H_2O; H_3P, H_2S; and, for that matter, $(CH_3)_3N$, $(CH_3)_2O$; and probably $(CH_3)_3P$, $(CH_3)_2S$. This situation would almost certainly be corrected by inclusion of contributions from partial ionic character of the bonds.

Second, the values decrease so rapidly in the vertical series that they actually go negative[15] for some of the heavier hydrides. This is partially, at least, a consequence of the over-estimation of homopolar bond moments in the localized molecular orbital method. The results of calculations[16] on these compounds by the valence bond method, which under-estimates these terms, do not go negative in this fashion.

Another possible source of the latter difficulty may be seen in the following consideration. These heavy hydrides with the too-small or negative moments all have bond angles close to 90°. Inspec-

(15) The possibility that the experimental values for these should be taken as negative may be ruled out by the following consideration. If the moments were positive for the lighter hydrides and negative for the heavier ones, the absolute values measured experimentally would show a minimum at one of the intermediate compounds in a vertical series. No such minimum is observed in either Group V or Group VII for which complete sets of experimental values are available.

(16) J. H. Gibbs, unpublished results.

tion of the curves for $F_V(\alpha)$ and $F_{VI}(\alpha)$ shows that these quantities are very sensitive functions of α in this region. Furthermore these compounds have large values of $G(A)$ into which the values for $F_V(\alpha)$ and $F_{VI}(\alpha)$ are multiplied. Thus any small error in the value of α or in the assumption of coincidence of orbital axes and bond axes will lead to large errors in the calculated covalent moments for these compounds.

The curves labeled "carbon compounds" apply not only to methyl but also to ethyl compounds, providing that they have the same bond angles, α, around the lone pair bearing atom, since, to the degree of accuracy implied in the approximations made in these calculations, the moments of ethyl and methyl compounds are identical. That is, inductive effects[17] are automatically neglected in the approximations that $a = b$ for all bonds, that all overlap integrals involving orbitals not bonded to one another are zero, and that the orbitals are completely localized. In the absence of inductive effects, the moment of an ethyl group is, of course, the same as that of a methyl group which in turn is equivalent to a single C–H bond moment.

Furthermore, these curves also apply approximately to the phenyl compounds, again providing that the bond angles around the lone pair bearing atoms are the same as in the corresponding methyl cases, since the homopolar dipole terms in the *para* C–H bonds and in the bonds between the carbon atoms and the lone pair bearing atoms will be approximately the same as in the analogous aliphatic bonds. The moments of the *ortho* and *meta* C–H bonds cancel by symmetry of course. Electromeric effects are neglected in the assumption of complete localization of the localized MO for the bonds to the phenyl rings.[18]

The principal discrepancy with experiment to be noted in these curves is the overemphasis of the maximum at the 3rd row element. The only experimental curve which shows such a sharp maximum is the one for the phenyl derivatives of the Vth group elements, and the closeness of the similarity between this curve shape and the calculated one is probably spurious for the following reason. The smallness of the experimental moment exhibited by triphenylamine is almost certainly due to phenomena not allowed for in the calculations. Both steric hindrance and the possibility of resonance between the 3 phenyl groups should tend to open the central valence angle, α, out well beyond the tetrahedral value used in the calculation. Inspection of the curve for $F_V(\alpha)$ shows what this would do to the dipole moment. In this connection the only slightly larger moment of trimethylamine, 0.65 D (not plotted in Fig. 1 because of the unavailability of the moments of the rest of this methyl series), is of interest in view of the strain which has been postulated for this molecule as well.[19] Furthermore, the moments of pyrrolidine and piperidine, whose C–N–C valence angles can hardly be much greater than tetrahedral because of the geometric requirements of the saturated 5- and 6-membered rings, are much larger, 1.57 and 1.17 D, respectively.

Any further discussion of the discrepancies between calculated and experimental values seems futile in view of the approximations, such as the use of Slater-type atomic orbitals with screening constants only known to be appropriate for isolated atoms, which are necessary in the calculations. For this reason the significance of the calculations must be considered as largely limited to the qualitative conclusions which may be drawn from them. They do show that the usual assumptions of valency theory lead to factors and terms in the moments of purely covalent forms which are of the correct relative orders of magnitude for the competition between them to yield the rather surprising qualitative variations in dipole moment which are observed experimentally in the vertical series discussed.

So far, nothing has been said concerning the possible origin of the phenomenon of greater hybridization in the organic derivatives than in the hydrides of the non-metals particularly of the 3rd and 4th rows of the periodic table. There is one observation which can be made on this point, however. The halogen compounds exhibit the same qualitative dipole moment behavior as the Group V and Group VI series. This suggests that the qualitative variations in hybridization among the members of the halogen series are the same as those among the members of the Group V and Group VI series. This in turn suggests that steric hindrance between the organic substituents is not primarily responsible for the large degree of hybridization retained by the organic derivatives of the 3rd (and 4th) row elements. Evidently the origin of this difference in hybridization between the organic derivatives and the hydrides lies primarily in the fundamental energetics of the process of hybridization and bond formation in the bonded atoms themselves.

Acknowledgment.—The author wishes to acknowledge his indebtedness to the late Sir John Lennard-Jones and his colleagues, Dr. George Hall and Dr. John Pople, for helpful discussion in the formulative stages of this work. The author also wishes to thank Dr. Bruno Zimm and Dr. Heinz Pfeiffer for helpful discussions in the later stages and Miss Virginia Thomas for the performance of many numerical computations.

(17) See, for example, C. P. Smyth, *J. Am. Chem. Soc.*, **63**, 57 (1941).

(18) It has not been necessary to assume localization of the orbitals inside the ring since the moment due to all of these must be zero by symmetry. Such an assumption would not, of course, be acceptable.

(19) H. C. Brown, H. Bartholomay and M. D. Taylor, *J. Am. Chem. Soc.*, **66**, 435 (1944).

RAMAN SPECTRA OF SOME ETHER-BORINE ADDITION COMPLEXES

BY BERNARD RICE AND HENRY S. UCHIDA[1]

Contribution from the Department of Chemistry, St. Louis University, St. Louis, Missouri

Received February 14, 1955

Raman spectra were obtained for the liquid systems, diborane–tetrahydrofuran, diborane–dimethyl ether and diborane–diethyl ether. The results were in accord with the formation of an $R_2O:BH_3$ addition complex in each system. Tetrahydrofuran–borine was the most stable and diethyl ether–borine the least stable of these complexes. The Raman frequencies were assigned to the BH_3X skeletal model, where X represented an ether. Potential constants were calculated for this model of tetrahydrofuran–borine.

Introduction

The present Raman spectroscopic investigation is a study of the addition complex formed when diborane is dissolved in tetrahydrofuran, dimethyl ether or diethyl ether. Evidence for complex formation in these systems has appeared in the literature.[2] The previous investigators demonstrated, at best, that the complex is formed in a ratio of one mole diborane to two moles of ether. However, from a knowledge of the chemistry of the reactants it seemed reasonable to most investigators to imply that the reaction can be represented by the general equation

$$2R_2O + B_2H_6 \rightleftarrows 2R_2O:BH_3$$

Our Raman spectral measurements justify this assumption. The spectral data permit a comparison of the stability of the three ether–borine addition complexes and the determination of force constants for tetrahydrofuran–borine.

Experimental

Apparatus and Method.—A three prism spectrograph (manufactured by Lane-Wells), with an average dispersion of 22 Å./mm. in the range from 4358 to 4916 Å., was used. The diborane–ether solutions were maintained in a closed system and low temperature Raman exposures were obtained by the method described by Lord and Nielsen.[3]

Chemicals.—The diborane was prepared by the reaction of lithium borohydride with boron trifluoride. The sample, purified by repeated fractionation, had a vapor pressure of 225 mm. at −112° in agreement with the literature value.

The tetrahydrofuran, diethyl ether and dimethyl ether were dried and distilled *in vacuo*. The vapor pressure of the purified ethers agreed with the literature values.

Solutions.—The Raman spectrum of the diborane–dimethyl ether solution was observed at two temperatures. The diborane–diethyl ether system was treated in a similar fashion. On the other hand, Raman spectra were obtained at the same temperature for two diborane–tetrahydrofuran solutions which differed in concentration. The concentrations of the solutions and the temperatures at which they were studied are listed in Table I.

TABLE I

SOLUTIONS, CONCENTRATIONS AND TEMPERATURES OF RAMAN DETERMINATIONS

Soln.	Concn. B_2H_6/R_2O (mole ratio)	Temp., °C.
B_2H_6–C_4H_8O	1/4	−25
	1/8	−25
B_2H_6–$(CH_3)_2O$	1/6	−70
	1/6	−40
B_2H_6–$(C_2H_5)_2O$	1/10	−75
	1/10	0

Data.—In Table II, the Raman frequencies of the most concentrated of the two diborane–tetrahydrofuran solutions studied are listed. For purposes of comparison, the Raman frequencies of pure tetrahydrofuran are also included in the table. The spectrum of the more dilute diborane–tetrahydrofuran solution differs only in the relative intensity of some of the Raman lines.

TABLE II

RAMAN FREQUENCIES OF A DIBORANE–TETRAHYDROFURAN SOLUTION AND PURE TETRAHYDROFURAN

Diborane–Tetrahydrofuran Frequency (cm.$^{-1}$)	Intensity	Tetrahydrofuran Frequency (cm.$^{-1}$)	Intensity
472	3		
859	7d		
917	8	911	10
976	2	1028	3
1049	5d	1068	1
1173	5	1170	0
1236	4d	1232	8
1364		1364	
1450	6	1445	7
1487	5d	1487	7
2097[a]	2	2261	0
2284	8		
2398	9		
2523[a]	1	2717	0
2874	8d	2860	8d
2908	9	2909	9
2948	9d	2954	9d
2994	10d		

[a] Raman lines assigned to unreacted diborane.

The Raman frequencies of the solution of diborane in dimethyl ether at the lower temperature (−70°) are reported in Table III, along with the frequencies of the pure ether. The effect of an increase in temperature on the spectrum was again a change in the relative intensities of some of the Raman lines.

Raman exposures were taken of the diborane–diethyl ether solutions, maintained at −75°, until the background on the photographic film became too intense to permit the observation of any more Raman lines. The spectrum contained two weak frequencies, one at *2289* and the other at *2410* cm.$^{-1}$ which are not observable in the spectra of the pure components. On the other hand, the spectrum of the diborane–diethyl ether solution maintained at 0° contained only frequencies characteristic of the pure components.

Discussion

Raman Frequencies of the Borine Complexes.—The spectral data were analyzed and found to be consistent with the assumption that ether–borine complexes are formed. The Raman lines which cannot be ascribed to the spectra of the pure components have been abstracted from the solution

(1) Taken in part from a thesis submitted by Henry S. Uchida in partial fulfillment of the requirements for the degree of Doctor of Philosophy, June, 1954.

(2) H. I. Schlesinger and A. B. Burg, *J. Am. Chem. Soc.*, **60**, 290 (1938); J. R. Elliott, W. L. Roth, G. F. Roedel and I. M. Boldebuck, *ibid.*, **74**, 5211 (1952).

(3) R. C. Lord and E. Nielsen, *J. Opt. Soc. Am.*, **40**, 655 (1950).

TABLE III

RAMAN FREQUENCIES OF A DIBORANE–DIMETHYL ETHER SOLUTION AND PURE DIMETHYL ETHER

Diborane–dimethyl ether		Dimethyl ether[4]	
Frequency (cm.$^{-1}$)	Intensity	Frequency (cm.$^{-1}$)	Intensity
387	0	330 (?)	
560	0	412	1
791[a]	0		
878	4		
921	6	920	5
1044	1		
1092	1	1100	0
1144	1	1150	4
1171	2		
1450	7	1448	6b
2104[a]	1		
2115	?		
2290	4		
2401	4		
2525[a]	1		
2812	10	2810	10
2863	6	2863	6
2921	3	2916	5
2951	6	2951	4
2992	6	2986	6

[a] Raman lines assigned to unreacted diborane.

spectra and are listed in Table IV. There appears to be a shift in the positions of some of the non-abstracted frequencies from their positions in the spectra of the pure ethers. However, the diffuse nature of these Raman lines limited the precision with which their positions could be measured and therefore it was not possible to ascribe any significance to these differences. The 1173 cm.$^{-1}$ frequency of the tetrahydrofuran solution is listed in our table of abstracted frequencies even though it is coincident with a frequency in the spectrum of the pure ether. This was done because there is a marked increase in the relative intensity of this frequency in the spectrum of the solution as compared to its relative intensity in the spectrum of the pure ether.

TABLE IV

RAMAN FREQUENCIES OF COMPLEXES ABSTRACTED FROM SPECTRA OF SOLUTIONS

Diborane–tetrahydrofuran Frequencies (cm.$^{-1}$)	Diborane–dimethyl ether Frequencies (cm.$^{-1}$)	Diborane–diethyl ether Frequencies (cm.$^{-1}$)
472	387	
859	560	
976	878	
1049	1044	
1173	1171	
2284	1476	
2398	2290	2289
2994	2401	2410

It should be emphasized that the abstracted frequencies do not represent all the observed Raman frequencies of the addition complexes. The ether parts of the complexes give rise to frequencies so similar to those of the unreacted ethers that these frequencies cannot be abstracted from the spectra of the solutions. One may have anticipated that the carbon–oxygen bonds of an ether would differ appreciably from the corresponding bonds in a complex in which a borine group also is bonded to the oxygen. However, the solution spectra do not warrant such a conclusion.

There are noticeable similarities between the frequencies abstracted for the different complexes. Where differences are observed, reasonable explanations may be advanced for their occurrence. For example, the arithmetic mean of the 387 and 560 cm.$^{-1}$ frequencies, which occur in the diborane–dimethyl ether spectrum, is 473 cm.$^{-1}$. This is almost identical with the 472 cm.$^{-1}$ frequency of the diborane–tetrahydrofuran spectrum. Later, in the section on assignments of frequencies, this correspondence is made significant when a possibility for Fermi resonance in the diborane–dimethyl ether complex is proposed.

There are no frequencies in the diborane–dimethyl ether spectrum similar to the two that occur at 976 and 2944 cm.$^{-1}$ in the diborane–tetrahydrofuran spectrum. The absence of the first line may be simply a question of intensity. The diborane–dimethyl ether spectrum had an intense continuous background which made the detection of weaker lines more difficult. The second frequency corresponds to an absorption band of the same magnitude in the infrared spectrum of tetrahydrofuran and therefore it may arise in the Raman spectrum of the complex. A similar conclusion may be reached for the 1476 cm.$^{-1}$ frequency of the diborane–dimethyl ether spectrum which corresponds to strong absorption band in the infrared spectrum of the pure ether.

Although only two weak lines were abstracted from the diborane–diethyl ether spectrum, they also fit into the trend and correspond to the most intense abstracted frequencies in the Raman spectra of the two other ether solutions.

Assignment of Frequencies.—The Raman frequencies listed in Table IV are most easily discussed in terms of a postulated molecular model for the $R_2O:BH_3$ complex. Consider the ether group as a point particle, X, attached to one of the terminal positions of a tetrahedral boron atom. This postulated model for the H_3BX molecule would belong to point group C_{3v}. All six normal modes of vibration of this model give rise to Raman active fundamental frequencies. Most of the abstracted frequencies (Table V) are assigned to normal modes of vibration of this postulated molecular model of the ether–borine complexes.

TABLE V

ASSIGNMENT OF FREQUENCIES TO THE H_3BX MOLECULAR MODEL

Designation	Description	$C_4H_8O:BH_3$	$(CH_3)_2O:BH_3$	$(C_2H_5)_2O:BH_3$
ν_1	B–H stretching (in phase)	2284	2290	2289
ν_2	H–B–H deformation (in phase)	1049	1044	
ν_3	B–O stretching	859	878	
ν_4	B–H stretching (out-of-phase)	2398	2401	2410
ν_5	H–B–H deformation (out-of-phase)	1173	1171	
ν_6	$H_3{\equiv}B{-}O$ bending	976		

(4) B. L. Crawford, Jr., and L. Joyce, *J. Chem. Phys.*, **7**, 307 (1939).

There appears to be very little question about the assignment of the boron–hydrogen stretching frequencies, ν_1 and ν_4. The magnitudes of the frequencies assigned to ν_1 are in good agreement with a frequency of 2290 cm.$^{-1}$ observed in the Raman spectrum of an aqueous solution of sodium borohydride[5] and assigned to the symmetrical boron–hydrogen stretching mode of vibration of the borohydride ion. These frequencies are considerably lower than those characteristic of terminal hydrogen stretching in diborane and aluminum borohydride (2500 to 2600 cm.$^{-1}$). In the latter two cases the terminal boron–hydrogen bonds are most likely of the sp^2 type while in the ether–borine complexes and the borohydride ion they are probably sp^3 type bonds.

The intense Raman lines at 859 and 878 cm.$^{-1}$ of tetrahydrofuran–borine and dimethyl ether–borine, respectively, were assigned to boron–oxygen stretching on the basis of the expected magnitude of the frequencies characteristic of bonds between atoms of such mass. The spectral data available for comparison with our boron–oxygen stretching frequency are limited; however, comparable assignments at 754 and 947 cm.$^{-1}$ have been made for symmetrical and antisymmetrical boron–oxygen stretching, respectively, of the aqueous borate ion,[6] $B(OH)_4$.

Our assignment of frequencies to the BH_3 deformation modes of vibration is consistent with similar assignments in sodium borohydride[7] and borine carbonyl.[8] The weak Raman line that occurs at 976 cm.$^{-1}$ in the tetrahydrofuran–borine spectrum was assigned to H–B–O bending; however, we do not have similar frequencies of other compounds for comparison.

The 472 cm.$^{-1}$ frequency abstracted from the tetrahydrofuran–borine spectrum was not assigned to the H_3BX skeletal model but could be characteristic of B–O–C bending, while the 387 and 560 cm.$^{-1}$ frequencies abstracted from the dimethyl ether–borine spectrum may arise from a Fermi resonance between B–O–C and a C–O–C bending modes of vibration. As mentioned in the previous section, the 2994 cm.$^{-1}$ frequency of tetrahydrofuran–borine and the 1476 cm.$^{-1}$ frequency of dimethyl ether–borine may arise from the ether parts of the complexes. Thus we account for all the abstracted frequencies. Of course, the possibility exists that reasonable assignments could be made for an entirely different molecular model. However, we were not able to find another model for which the frequencies could be assigned in a reasonable fashion.

Potential Constants of Tetrahydofuran–Borine

A normal coördinate treatment, based on the H_3BX skeletal model, was carried out for tetrahydrofuran–borine. A similar treatment was not made for dimethyl ether–borine, since one of the anticipated frequencies (ν_6) was missing.

(5) W. J. Lehmann, Ph.D. Thesis, Saint Louis University, 1954.

(6) J. O. Edwards, G. C. Morrison, V. F. Ross and J. W. Schultz, *J. Am. Chem. Soc.*, **77**, 266 (1955).

(7) W. C. Price, H. C. Longuet-Higgins, B. Rice and T. F. Young, *J. Chem. Phys.*, **17**, 217 (1949).

(8) R. D. Cowan, *ibid.*, **18**, 1101 (1950).

The valence force potential function used (similar to one proposed by Cleveland and Meister for methyl chloride[9]) was

$$2V = f_d\Sigma(\Delta d_i)^2 + f_D(\Delta D)^2 + f_\alpha\Sigma(d\Delta\alpha_i)^2 + f_\beta\Sigma(d\Delta B_i)^2 + 2f_{\alpha\beta}[(d\Delta B_1)(d\Delta\alpha_{12} + d\Delta\alpha_{23}) + (d\Delta\beta_2)(d\Delta\alpha_{12} + d\Delta\alpha_{23}) + (d\Delta\beta_3)(d\Delta\alpha_{13} + d\Delta\alpha_{13})] + 2f_D\Sigma(d\Delta D\Delta\alpha_i) + 2f_{D\beta}\Sigma(d\Delta D\Delta\beta_i)$$

In this equation d and D represent the boron–hydrogen and boron–oxygen distances, respectively, while α and β designate the hydrogen–boron–hydrogen– and hydrogen–boron–oxygen angles, respectively. The significance of the potential constants, the f's in the equation, can be determined from the subscripts used.

The values chosen for the bond distances were: $d = 1.31 \times 10^{-8}$ cm. and $D = 1.52 \times 10^{-8}$ cm. These values were supplied to us by Dr. George W. Schaeffer of St. Louis University, who calculated them from covalent bond radii corrected for the difference in electronegativity of the bonded atoms. The angles α and β were assumed to be tetrahedral for lack of more precise information. A problem was presented in the choice of mass for the group represented by the symbol X. The value obtained for the force constant f_D, characteristic of the boron–oxygen bond, is very sensitive to the mass assigned. A minimum value for f_D would perhaps be obtained if the mass of an oxygen atom was used for X, while the result obtained if the entire tetrahydrofuran mass was used could be considered a maximum. Both masses were tried in separate calculations. Clearly, calculations of this type would be improved if it were possible to select, "*a priori*," an effective mass for a group treated as a point particle.

The six frequency equations were solved by a method of approximation, whereby the force constants were adjusted until the left-hand and right-hand sides of each equation differed by only a few tenths of a per cent. The results of our calculations are listed in Table VI. As can be observed, the magnitude of the boron–oxygen stretching potential constant f_D is very sensitive to the choice of mass of X. The only other term which differs appreciably in the two sets of values is $(f_{D\alpha} - f_{D\beta})$. However, the significance of this "correction" term is not too apparent. Our lower value of 3.29×10^5 dyne cm.$^{-1}$ for f_D appears to be closest to the "best" value. This can be seen by application of Gordy's rule,[10] which relates force constants to the bond distance and electronegativity of the bonded atoms. On the basis of this rule, a value of 3.74×10^5 dynes cm.$^{-1}$ is obtained for this force constant. We may consider this value as the magnitude of the force constant for a normal covalent boron–oxygen bond. Since our skeletal treatment of tetrahydrofuran–borine left us with a choice somewhere between 3.3 and 5.4×10^5 dynes cm.$^{-1}$ for the boron–oxygen force constant, we can speculate that the donor–acceptor boron–oxygen bond in this molecule is comparable in strength to a normal covalent boron–oxygen bond.

(9) F. F. Cleveland and A. G. Meister, "Molecular Spectra II," Illinois Institute of Technology, 1948.

(10) W. Gordy, *J. Chem. Phys.*, **14**, 305 (1946).

TABLE VI

POTENTIAL CONSTANTS OF BH_3X MODEL OF TETRAHYDROFURAN–BORINE, $\times 10^5$ DYNES CM.$^{-1}$

Mass of X	f_D	f_d	$f\alpha$	$f\beta$	$f\alpha\beta$	$f_{D\alpha} - f_{D\beta}$
$X = 16.00$	3.29	3.01	0.300	0.474	0.0415	−0.320
$X = 72.10$	5.40	3.01	.306	.488	.0406	− .502

Relative Stabilities of Ether–Borine Complexes

A quantitative measure of the apparent equilibrium constants was not attempted, but an estimate can be made of the relative stabilities of the ether–borines. The intensity, I, of a Raman line characteristic of a particular substance is proportional to the concentration of that substance, hence

$$\frac{[R_2OBH_3]}{[B_2H_6]} = \frac{k_1 I_{R_2OBH_3}}{k_2 I_{B_2H_6}}$$

The ratio of the proportionality constants, k_1/k_2, should depend primarily on the nature of the two species in solution. The intensities of the lines at 2524, 2284, 2290 and 2289 cm.$^{-1}$ were chosen as indicative of the concentration of diborane, tetrahydrofuran–borine, dimethyl ether–borine and diethyl ether–borine, respectively.

If we assume that the ratios k_1/k_2 are almost the same for all the diborane–ether systems investigated, a comparison of the stabilities of the complexes can be obtained. The above assumption appears to be reasonable, since the magnitude of the boron–hydrogen stretching frequency, whose intensity we have chosen to be indicative of the concentration of the complex, remains almost unchanged in the three ether–borines. Thus this bond is only slightly affected by the nature of the ether parts of the complexes and similarly the intensities of vibrations characteristic of this bond may be only slightly affected.

The solutions for which we were able to calculate "intensity ratios" are listed in Table VII. Calculations were not made for the diborane–diethyl ether system, since the observed lines characteristic of the complex in this system were too weak. We can conclude, therefore, that diethyl ether–borine is the least stable of the complexes.

TABLE VII

"INTENSITY RATIOS" OF DIBORANE–ETHER SOLUTIONS

Solution	Initial mole ratio B_2H_6/R_2O	Temp., °C.	$I_{R_2OBH_3}/I_{B_2H_6}$
B_2H_6–C_4H_8O	1/4	−25	8
B_2H_6–$(CH_3)_2O$	1/6	−40	2
B_2H_6–$(CH_3)_2O$	1/6	−70	4

The "intensity ratio" of dimethyl ether–borine at −70° is twice as large as its value at −40°. As anticipated, complex formation is favored by a drop in temperature. Even at −25° the "intensity ratio" of the diborane–tetrahydrofuran system is four times as great as the value for the diborane–dimethyl ether system at −40°. It would be best to compare "intensity ratios" of both solutions at the same temperature and concentration of diborane. However, if the initial mole ratio of diborane to tetrahydrofuran was reduced from 1/4 to 1/6 and the temperature decreased from −25 to −40°, the "intensity ratio" for the diborane–tetrahydrofuran system should be still greater than 8. Therefore, we can conclude that the tetrahydrofuran–borine complex is the most stable of the ether–borines.

Thus the order of stabilities of the ether–borines is: $C_4H_8OBH_3 > (CH_3)_2OBH_3 > (C_2H_5)_2OBH_3$. This is the same order observed[11] for the analogous ether–boron trifluoride complexes in the vapor phase. This order emphasizes the predominance of steric to inductive effects.

(11) H. C. Brown and R. M. Adams, *J. Am. Chem. Soc.*, **64**, 2557 (1942).

THERMODYNAMICS OF SODIUM CARBONATE IN SOLUTION[1]

BY C. EDWARD TAYLOR

Contribution from The Institute of Paper Chemistry, Appleton, Wisconsin

Received February 14, 1955

The thermodynamics of sodium carbonate in aqueous solution has been studied from 15 to 95°. From electromotive force measurements of the concentration cells $Ag–Ag_2CO_3$ $Na_2CO_3(0.1)$ NaHg $Na_2CO_3(m_2)$ $Ag_2CO_3–Ag$ and determinations of solution vapor pressures, the activity coefficients have been calculated over a concentration range of 0.1 to 1.5 m below 65° and 0.1 to 2.5 m at 65° and above. The relative partial molal enthalpies have been calculated between 25 and 80°.

Experimental

Concentration Cell Measurements.—The equilibrium e.m.f.s of the concentration cells were measured at 15, 25, 37.5, 50 and 65°. The reference solution was 0.1 m and drawn from a large reservoir of constant composition. The value of m_2 was varied from 0.2 to 1.5 m. The solutions were prepared using weighed amounts of reagent grade sodium carbonate and twice-distilled water. The sodium carbonate analyzed 99.8 to 99.9% using constant-boiling hydrochloric acid diluted to 0.5 N after heating at 140° for an hour. The dissolved oxygen in the solutions was removed by stripping with nitrogen at reduced pressure, and the solutions were stored under a positive nitrogen pressure. The reference solution was stored in an 18-liter bottle lined with a plastic bag to eliminate attack on the glass by the solution. Analyses of each solution were run in triplicate using weighed samples and standard hydrochloric acid.

The silver–silver carbonate electrodes were similar to the type 2 electrodes of Harned.[2] Due to the higher solubility of silver carbonate, the electrodes were electrolyzed in 0.5 m sodium bicarbonate at 200 ma./cm.^{2} for two hours. It was necessary to form very fine porosity silver on the platinum spirals to obtain equilibrium potentials. These electrodes are apparently less stable than other silver electrodes, but with care in preparation they were usually reproducible to 0.1 mv.

(1) This communication contains material from a dissertation presented to The Institute of Paper Chemistry in partial fulfillment of the requirements for the degree of Doctor of Philosophy from Lawrence College, June, 1954. The work was done under the direction of Roy P. Whitney.

(2) H. S. Harned, *J. Am. Chem. Soc.*, **51**, 416 (1929).

The 0.2% sodium amalgam was prepared by electrolysis of sodium hydroxide in contact with reagent grade mercury. The prepared amalgam was washed successively with water and acetone and dried by vacuum in the reservoir.

The apparatus was adapted with a few modifications from previous studies and is shown in Fig. 1. All stopcocks were out of the bath for ease in operation at high temperatures. The amalgam lines leading from the reservoir to the cells dipped into the bath for about six inches to permit temperature control of the amalgam entering the cells. The water bath was covered by a film of oil to prevent evaporation. By means of a series of mercury-to-platinum thermoregulators, the thermostat was controlled to 0.02° of the desired temperature.

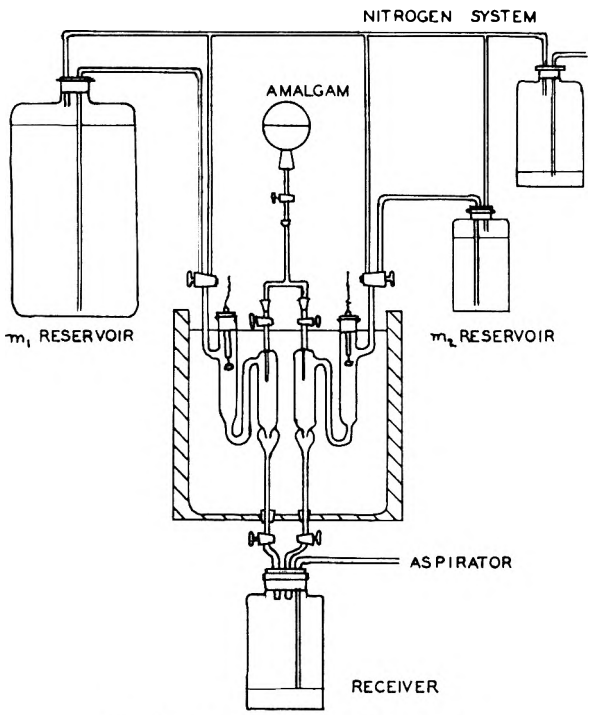

Fig. 1.—Concentration cell apparatus.

In the operation of the cells, a pair of freshly prepared electrodes were put in the apparatus at 25°, the cell units were filled, and the e.m.f. was measured periodically until the equilibrium value was attained. During the equilibration period, the solutions flowed through the cell units at a rate of 0.5 to 1.0 ml./min. The temperature was changed to 15° and the procedure was repeated. Subsequently the equilibrium values were determined again at 25° and then at 37.5, 50 and 65°. Once the electrodes came to equilibrium at 25°, equilibrium was quickly attained when the bath temperature was changed. The silver–silver carbonate electrodes were somewhat unstable at the highest concentrations at 50 and 65°, but the values determined after the cells reached temperature equilibrium were reproducible.

The results are listed in Table I. For each concentration cell, two or three pairs of electrodes were used to measure the e.m.f. over the entire temperature range. The data were averaged by cross-plotting e.m.f. *versus* concentration at constant temperature and e.m.f. *versus* temperature at constant concentration. The most reliable data were taken from the smooth curves.

TABLE I

EQUILIBRIUM ELECTROMOTIVE FORCES OF CONCENTRATION CELLS AT 15 TO 65°

Molality	E.m.f. in mv. 15°	25°	37.5°	50°	65°
0.1005	Ref. soln.		0.0	0.0	0.0
.2008	−18.7	−20.2	−22.4	−24.2	−25.1
.4009	−37.3	−40.2	−44.4	−47.0	−48.8
.6014	−48.2	−52.1	−57.1	−59.8	−61.9
.8470	−57.5	−62.0	−67.5	−70.2	−71.8
1.0047	−62.0	−66.8	−72.1	−75.0	−76.2
1.5355	−73.3	−78.8	−84.1	−86.8	−88.6

Vapor Pressure Determinations.—The vapor pressures of solutions were determined by the dynamic or gas saturation method of comparing the vapor pressure of the solution with that of water at the same temperature. It was assumed that Dalton's law of partial pressures was applicable for the mixture of nitrogen and water vapor between 65 and 95° at one atmosphere.

The apparatus is shown in Fig. 2. The gas saturation cells were similar to those used by Pearce and Snow.[3] The presaturators were 3-neck flasks with mercury seal stirrers which were designed to form many small bubbles and splash the liquid high in the flasks. The presaturators were very effective and caused only a small pressure drop. Anhydrous magnesium perchlorate was used as a desiccant in the absorption tubes. Ethylene glycol was used in the bath to reduce heat loss due to evaporation and simplify cleaning of the cells for changes of solution. The thermostat was operated at 65, 80 and 95° and was controlled by mercury-to-platinum thermoregulators to 0.02°.

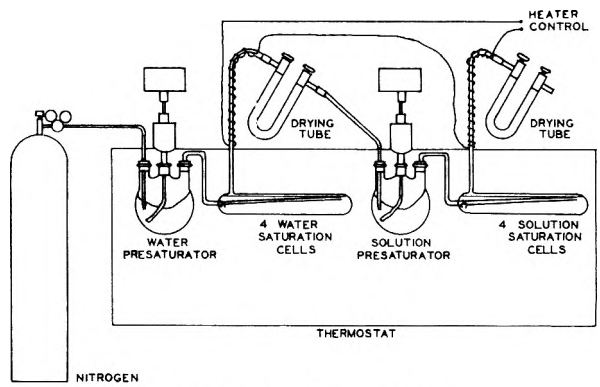

Fig. 2.—Vapor pressure apparatus.

For each of the 14 solutions between 0.1 and 2.5 m, four determinations were made at 65, 80 and 95°. The results were plotted as a function of concentration, and the values from the smooth curves are shown in Table II. The estimated accuracy of the data was 0.2 to 0.5%.

TABLE II

VAPOR PRESSURES OF SODIUM CARBONATE SOLUTIONS FROM 65 TO 95°

Molality	Vapor pressure in mm. 65°	80°	95°
(Water)	187.6	355.3	634.3
0.1009	186.8	353.5	631.4
.1507	186.4	352.6	629.9
.1999	185.9	351.9	628.7
.4013	184.4	349.2	623.8
.5017	183.6	347.9	...
.5994	182.9	346.6	619.0
.6934	182.2	...	...
.8046	181.5	344.3	614.3
1.001	180.2	342.1	610.2
1.146	179.3	340.5	607.4
1.444	177.3	337.4	601.8
1.519	176.7	336.7	600.4
2.011	173.7	330.8	589.8
2.520	169.8	324.1	578.2

Derived Thermodynamic Data

Activity Coefficients from Concentration Cell Data.—From the thermodynamic equation for the concentration cells

$$E = -\frac{3}{2}\frac{RT}{\mathfrak{F}} \ln \frac{m_{\pm 2}\,\gamma_{\pm 2}}{m_{\pm 1}\,\gamma_{\pm 1}} \qquad (1)$$

(3) J. N. Pearce and R. D. Snow, THIS JOURNAL, **31**, 231 (1927).

and the Debye–Hückel equation

$$\log \gamma_{\pm} = \frac{-S_f\sqrt{\Gamma}}{1 + A\sqrt{\Gamma}} + Bc - \log(1 + 0.054m) \quad (2)$$

the activity coefficient data were evaluated. For preliminary calculation the effects of hydrolysis on $m_{\pm}$, $\gamma_{\pm}$ and Γ were neglected. Rather than solving for factors A and B by simultaneous equations from the e.m.f. of two concentration cells, the method of Jones and Dole[4] was used to average all the experimental data between 0.1 and 1.0 m. It should be noted that equation 12 of Jones and Dole should be

$$\Delta E = \frac{-(2.303)(3)RT}{2\mathfrak{F}}\left[\left(\frac{S_f\Gamma_2}{(1 + A\sqrt{\Gamma_2})^2} - \frac{S_f\Gamma_r}{(1 + A\sqrt{\Gamma_r})^2}\right)\Delta A + (c_2 - c_r)\Delta B\right] \quad (3)$$

From the values of A and B at each temperature, the activity coefficient of the reference solution was calculated from equation 2. The values of $\gamma_{\pm 2}$ at all other concentrations were calculated using equation 1.

It is not possible to determine the exact errors in the results due to the hydrolysis of the salt because the activity coefficients of the individual ions are not known. However, by assuming that at any concentration

$$\gamma_{Na^+} \cong \gamma_{HCO_3^-} \cong \gamma_{OH^-} \quad (4)$$

and

$$\gamma_{CO_3^=} \cong \gamma_{\pm}^2 \quad (5)$$

the errors may be estimated from the equation for the hydrolysis constant

$$K_H = \frac{K_w}{K_{2A}} = \frac{mx^2}{(1 - x)}\left(\frac{\gamma_{HCO_3^-}\,\gamma_{OH^-}}{\gamma_{CO_3^=}}\right) \quad (6)$$

where x is the fraction of the carbonate ion concentration hydrolyzed. The second ionization constant of carbonic acid is known only up to 50°.[5] From 15 to 50° the change in the degree of hydrolysis from 0.1 to 1.5 m was small, and the maximum error in $m_{\pm 2}/m_{\pm r}$ was 0.7% at 50°. Since the errors were significantly smaller at lower values of $m_{\pm 2}$ and lower temperatures, corrections for hydrolysis were unnecessary.

The results of the calculations are shown in Table III. The Debye–Hückel equation represented the activity coefficients with a high degree of accuracy from 0.1 to 1.0 m over the entire temperature range. The maximum difference in the values listed in Table III and those calculated by equation 2 was only 0.002.

TABLE III

ACTIVITY COEFFICIENTS AT 15 TO 65°

Molality		15°	25°	37.5°	50°	65°
0.1005	$\gamma_{\pm}$	(0.448)	(0.465)	(0.504)	(0.524)	(0.529)
.2008	$\gamma_{\pm}$	.371	.393	.441	.466	.471
.4009	$\gamma_{\pm}$	.306	.331	.382	.405	.405
.6012	$\gamma_{\pm}$	.273	.300	.349	.367	.365
.8470	$\gamma_{\pm}$	.249	.276	.321	.334	.325
1.0047	$\gamma_{\pm}$	.237	.263	.303	.316	.303
1.5355	$\gamma_{\pm}$	.210	.230	.268	.274	.263

(4) G. Jones and M. Dole, *J. Am. Chem. Soc.*, **51**, 1084 (1929).
(5) H. S. Harned and S. R. Scholes, Jr., *ibid.*, **63**, 1706 (1940).

Activity coefficient data have been reported previously only at 25° by Lortie and Demers[6] and Saegusa.[7] Lortie and Demers determined their data from freezing point depression measurements and vapor pressure determinations. They estimated that their data were 2.6 to 3.1% high because of the effect of hydrolysis at 0.005 m. Saegusa measured the e.m.f. of galvanic cells and graphically extrapolated the data from 0.001 m to infinite dilution. The extrapolation depended primarily upon the e.m.f. between 0.001 and 0.05 m where the errors due to the flowing sodium amalgam electrode and the solubility of silver carbonate may be appreciable. The results of the different studies are shown in Fig. 3. It appears that the difference in the results is due to the methods of extrapolation rather than any errors in the measurement of the change in free energy with dilution.

Activity Coefficients from Vapor Pressures.—From the equation

$$\log \frac{\gamma_{\pm 2}}{\gamma_{\pm r}} = -\int_{a,\text{ at } m_r}^{a,\text{ at } m_2} \frac{1000}{mM\nu}\, d\log a_1 - \log \frac{m_2}{m_r} \quad (7)$$

the logarithmic ratios of the activity coefficients were calculated from the vapor pressure data.

TABLE IV

EVALUATION OF EQUATION 7 BY GRAPHICAL INTEGRATION

Molal concn.	65° p (mm.)	65° $\log \frac{\gamma_{\pm 2}}{\gamma_{\pm 0.2}}$	80° p (mm.)	80° $\log \frac{\gamma_{\pm 2}}{\gamma_{\pm 0.4}}$	95° p (mm.)	95° $\log \frac{\gamma_{\pm 2}}{\gamma_{\pm 0.4}}$
0.0000	187.65	.....	355.30	.....	634.30	.....
.1000	186.78	+0.1153	353.45	+0.1406	631.40	+0.1471
.2000	185.95	+ .0623	351.95	+ .0770	628.75	+ .0778
.3000	185.14	+ .0278	350.50	+ .0357	626.20	+ .0345
.4000	184.38	Ref.	349.15	Ref.	623.80	Ref.
0.5000	183.62	−0.0238	347.85	−0.0303	621.45	−0.0262
.6000	182.90	− .0452	346.65	− .0574	619.00	− .0502
.7000	182.21	− .0651	345.45	− .0829	616.70	− .0708
.8000	181.53	− .0828	344.35	− .1056	614.40	− .0896
.9000	180.86	− .0990	343.20	− .1262	612.25	− .1075
1.0000	180.21	−0.1138	342.10	−0.1446	610.20	−0.1238
1.2500	180.56	− .1452	339.50	− .1856	605.50	− .1612
1.5000	176.86	− .1682	336.90	− .2198	600.75	− .1963
2.0000	173.72	− .2038	330.95	− .2624	590.10	− .2384
2.5000	169.98	− .2274	324.40	− .2871	578.70	− .2654

TABLE V

ACTIVITY COEFFICIENTS FROM VAPOR PRESSURE MEASUREMENTS

Molality	65° $\gamma_{\pm}$	80° $\gamma_{\pm}$	95° $\gamma_{\pm}$
0.1000	0.522	0.489	0.448
.2000	.462	.423	.382
.3000	.426	.384	.345
.4000	(.400)	(.354)	(.319)
.5000	.379	.330	.300
.6000	.361	.310	.284
.7000	.345	.293	.271
.8000	.330	.278	.260
.9000	.318	.264	.249
1.0000	.308	.254	.240
1.2500	.286	.231	.220
1.5000	.272	.213	.203
2.0000	.250	.193	.184
2.5000	.237	.183	.173

(6) L. Lortie and P. Demers, *Can. J. Research*, **18B**, 373 (1940).
(7) F. Saegusa, *Science Repts. Tôhoku Univ. First Ser.*, **34**, 147 (1950).

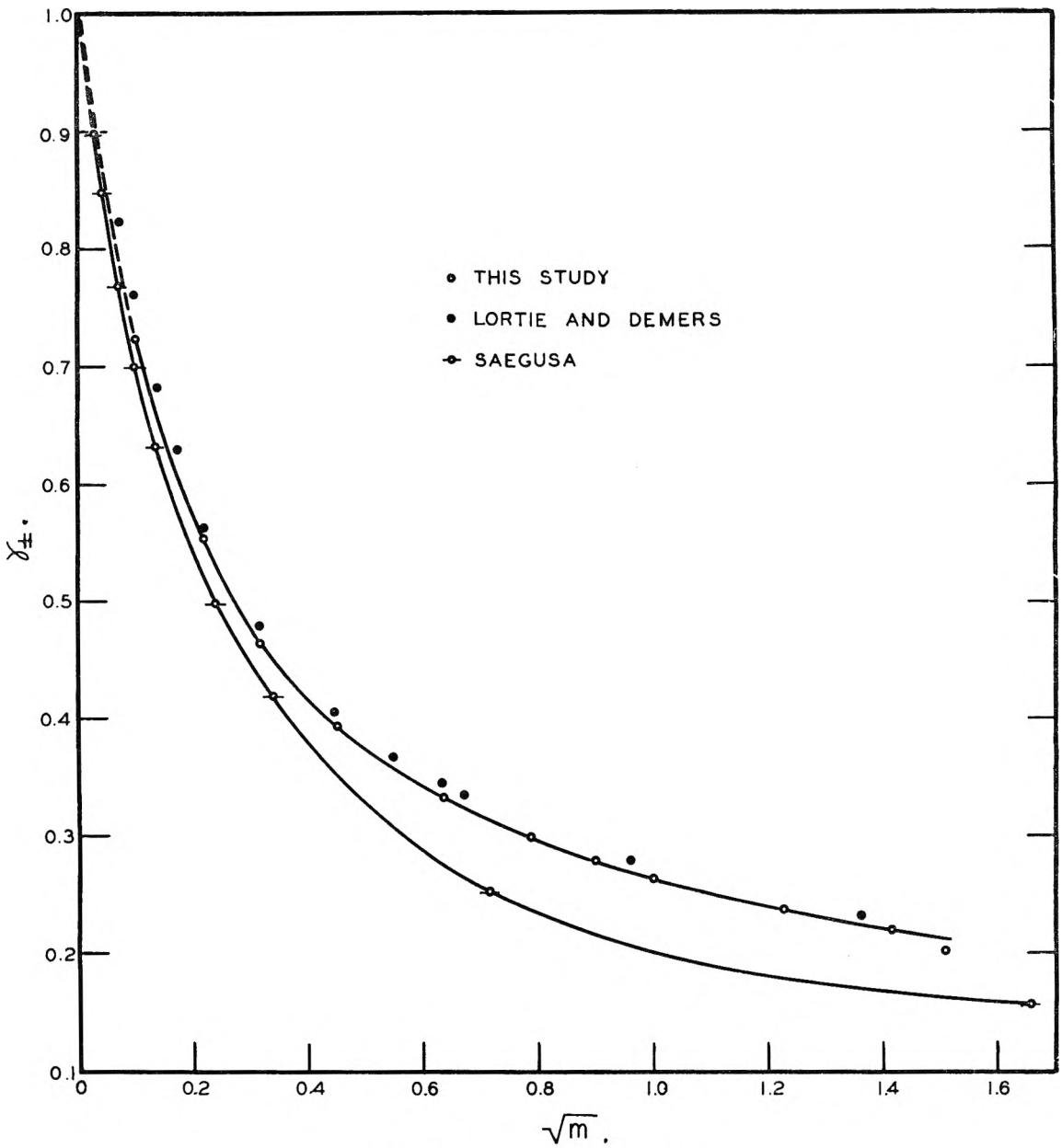

Fig. 3.—Activity coefficient data at 25°.

For calculation purposes a reference solution of 0.4000 *m* was chosen. Because of the sensitivity of the factor log a_1, it was necessary to determine the vapor pressures of the solutions from smooth curves of the data as a function of concentration and then average the calculations by an intermediate graph of log a_1 *versus* *m*. The results of the evaluation of equation 7 are shown in Table IV.

For the extrapolation of the data to infinite dilution the Debye–Hückel equation 2 was used. A method similar to that for the concentration cell data was developed to evaluate *A* and *B* from all the values of log $\gamma_{\pm 2}/\gamma_{\pm 1}$ from 0.1 to 1.0 *m*. The activity coefficients of the reference solution were calculated from equation 2 and the values of $\gamma_{\pm 2}$ were calculated from the data in Table IV. The results are shown in Table V. The maximum difference between the values listed in the table and those calculated by the Debye–Hückel equation was 0.001 between 0.1 and 1.0 *m*.

The activity coefficient data from 15 to 95° are represented in Fig. 4. The results appear to be internally consistent over the entire temperature range. The agreement between the results at 65° from the two experimental methods of determination is good. At 0.1 *m* the difference is 1.3%; at 1.0 *m* the difference is about 1.5%. The results appear to be reasonably accurate over the entire temperature range.

Relative Partial Molal Enthalpies.—The evaluation of $\bar{L}_2$ was carried out using the fundamental equation

$$\bar{L}_2 = -3RT^2\left(\frac{\partial \ln \gamma_{\pm}}{\partial T}\right)_{T,P} \qquad (8)$$

The slopes of the curves in Fig. 4 were determined by the front face mirror technique at 25 through 80°

and listed in Table VI. The values of $\bar{L}_2$ are not highly accurate. Values of $\bar{L}_2$ may be calculated from the enthalpies of solution estimated by Bichowsky and Rossini.[8] At 18°, the values of $\bar{L}_2$ are nearly four times as great as $\bar{L}_2$ calculated at 25° in this study. It is believed that the values of $\bar{L}_2$ from this study are more reliable.

TABLE VI

RELATIVE PARTIAL MOLAL ENTHALPIES OF SODIUM CARBONATE IN SOLUTION

Molality	$\bar{L}_2$ in cal./mole 25°	37.5°	50°	65°	80°
0.10	−291	−335	−122	+172	+386
.20	−413	−425	−160	+223	+504
.40	−501	−438	−166	+332	+662
.60	−622	−405	−118	+414	+705
.80	−624	−436	− 66	+520	+639
1.00	−631	−447	− 31	+675	+460
1.50	−642	−332	− 14	+616	+351

NOMENCLATURE

A	Constant in the Debye-Hückel equation
a	Activity
B	Constant in the Debye-Hückel equation
c	Molarity in moles per 1000 ml. of solution
d	Prefix, indicating differential
E	Electromotive force
K	Ionization constant; K_w —for water
K_{2A}	Second constant at H_2CO_3
K_H	Hydrolysis constant
L	Relative partial molal enthalpy
M	Molecular weight
m	Molality in moles per 1000 g. of solvent
$m_\pm$	Mean ionic molality
N	Normality in g. equivalents per liter
P	Total pressure
p	Vapor pressure
R	Ideal gas constant
S_f	Limiting slope of the Debye-Hückel equation
T	Absolute temperature
x	Degree of hydrolysis (fraction of ion concn. hydrolyzed)
Γ	Ional concentration
γ	Molal activity coefficient
$\gamma_\pm$	Mean ionic molal activity coefficient
Δ	Prefix, indicating finite difference
ν	Number of ions of an electrolyte
1	Referring to solvent
2	Referring to solute
r	Referring to reference solution
∂	Prefix, indicating partial differential
e.m.f.	Electromotive force
$\mathfrak{F}$	Faraday charge
ln	Natural logarithm to the base e
log	Common logarithm to the base 10

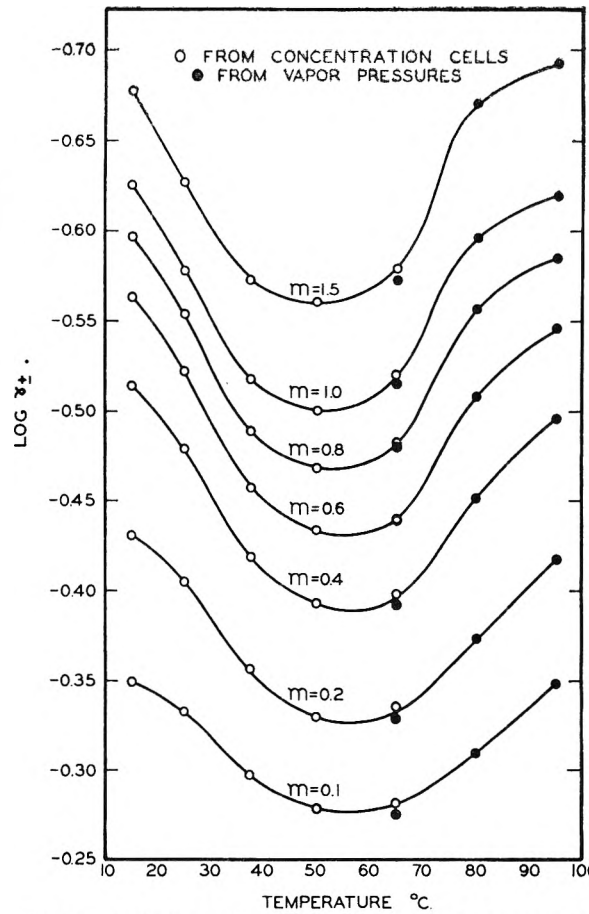

Fig. 4.—Activity coefficient variation with temperature.

(8) F. R. Bichowsky and F. D. Rossini, "The Thermochemistry of the Chemical Substances," Reinhold Publ. Corp., New York, N. Y., 1936, p. 144.

DYNAMIC MECHANICAL PROPERTIES OF THE SYSTEM CELLULOSE TRIBUTYRATE–TRICHLOROPROPANE[1]

BY ROBERT F. LANDEL AND JOHN D. FERRY

Contribution from the Department of Chemistry, University of Wisconsin, Madison, Wis.

Received February 15, 1955

Dynamic mechanical properties of concentrated solutions of three fractions of cellulose tributyrate in 1,2,3-trichloropropane have been studied by the wave propagation and single transducer methods. Concentration ranges were about 5 to 25% for fractions H ($M\eta$ = 300,000) and R2b (152,000), and 28 to 45% for fraction L (55,000). H was also studied by stress relaxation at 25.6%. The real parts of the complex dynamic rigidity and viscosity, reduced to unit concentration and viscosity at 25° by the usual method of reduced variables, superposed for each fraction at all temperatures (−5 to 35°) and concentrations. The relaxation distribution functions calculated from dynamic rigidity, dynamic viscosity and stress relaxation were in good agreement for each fraction. Each relaxation spectrum consisted of a horizontal plateau with a terminal zone at long times very close to the location predicted by the Rouse theory. The plateaus were flatter and longer than those observed for solutions of vinyl polymers of comparable molecular weight, indicating that the tendency to mechanical coupling of neighboring molecules is much stronger in the case of the cellulose ester.

Introduction

With the exception of Philippoff's work[2] on cellulose acetate in 1934, almost all investigations of the dynamic mechanical properties of concentrated polymer solutions have been concerned with vinyl polymers—in particular, polyisobutylene, polyvinyl acetate and polystyrene. The results of these studies are remarkably similar for different polymers of comparable molecular weight. The temperature and concentration dependence of dynamic properties can be described (provided the molecular weight is not too high[3,4]) by a simple scheme of reduced variables,[5] and all data can be combined in a distribution function of relaxation times reduced to a standard reference state of unit concentration and viscosity. This function, in its intermediate or plateau zone, is practically identical[6] for samples of the three polymers mentioned above with weight-average molecular weights near 400,000. Since the nature of the monomer unit plays such a minor role, the relaxation distribution function is evidently determined primarily by the flexible carbon–carbon backbone which is common to all vinyl polymers.

It is therefore of interest to make a detailed study of a polymer with a very different backbone structure, to see in the first place whether the method of reduced variables will still be applicable to describe the temperature and concentration dependence of mechanical properties, and in the second place whether the relaxation distribution function will reveal differences which can be correlated with chain architecture. Cellulose derivatives are admirably suited to this purpose, for their oxygen-linked anhydroglucose rings contrast sharply with the carbon–carbon linkages of vinyl polymers and lead to far more extended molecular chains.[7,8]

We have chosen the tributyrate ester as a derivative which has a uniform chemical composition, lacks polar groups which could lead to specific association, is readily soluble in suitable solvents, does not undergo excessive crystallization, and has been subjected to careful thermodynamic study in solution.[7] Fractions have been used to determine the molecular weight dependence of dynamic mechanical properties while avoiding effects of extreme molecular weight heterogeneity. The solvent chosen for all dynamic measurements reported here is 1,2,3-trichloropropane,[9] which is sufficiently powerful so that no crystallization or gelation is detected except at very high concentrations for polymer of relatively low molecular weight. Investigations of *o*-dimethyl phthalate solutions, which form gels through partial crystallization, will be reported subsequently.[11]

Materials

The 1,2,3-trichloropropane (TClP) was obtained from the Shell Chemical Corp.[12] and the Matheson Co.[13] The straw-colored Shell product was distilled through a 30-plate Oldershaw bubble cap column at atmospheric pressure (cor. b.p. 157.4–157.9°, literature 158°). The colorless Matheson product was vacuum distilled using a water aspirator. The former distillate was used in preparing the solutions of fraction R2b; the latter, for fractions H and L. The TClP and all solutions were stored in the dark to minimize solvent decomposition.

Acetone was obtained in several grades from several sources. All was distilled through the Oldershaw column to remove any traces of metallic salts which might be present.

Two samples of cellulose tributyrate (CTB) were obtained from the Eastman Kodak Co. through the courtesy of Dr. C. J. Malm, No. 103,278 (Stock I) and No. 103,371 (Stock II). Since polyvalent cations could cross-link the polymer if any free carboxyl groups were present, the polymer was not allowed to come into contact with metallic surfaces and a painstaking effort was made to exclude cations from all solutions. These precautions could not be maintained once dynamic measurements were begun, since the solutions unavoidably came into contact with aluminum and stainless steel surfaces.

Fractionation of Polymer.—The precipitant, conductivity water, was added with vigorous stirring to an approximately 1% solution (by weight) of the polymer in acetone. When a sufficient amount of precipitate had formed it was dissolved by heating the solution to 35° in a large water-bath and then reprecipitated by slowly lowering the temperature

(1) Part XVIII of a series on Mechanical Properties of Substances of High Molecular Weight.

(2) W. Philippoff, *Physik. Z.*, **35**, 900 (1934).

(3) J. D. Ferry, I. Jordan, W. W. Evans and M. F. Johnson, *J. Polymer Sci.*, **14**, 261 (1954).

(4) T. W. DeWitt, H. Markovitz, F. J. Padden, Jr., and L. J. Zapas, *J. Colloid Sci.*, in press.

(5) J. D. Ferry, *J. Am. Chem. Soc.*, **72**, 3746 (1950).

(6) L. D. Grandine, Jr., and J. D. Ferry, *J. Appl. Phys.*, **24**, 679 (1953).

(7) L. Mandelkern and P. J. Flory, *J. Am. Chem. Soc.*, **73**, 3206 (1951); **74**, 2517 (1952).

(8) A. M. Holtzer, H. Benoit and P. Doty, THIS JOURNAL, **58**, 624 (1954).

(9) This solvent had also been used in earlier studies of polyvinyl acetate.[10]

(10) J. D. Ferry, W. M. Sawyer, G. V. Browning and A. H. Groth, Jr., *J. Appl. Phys.*, **21**, 513 (1950).

(11) R. F. Landel and J. D. Ferry, unpublished work.

(12) Shell Chemical Corp., 500 Fifth Ave., N. Y. 18, N. Y.

(13) The Matheson Co., Inc., Joliet, Illinois.

to 25 ± 0.1°. After settling, the precipitate was usually separated by decantation.

Both stocks contained some insoluble debris and a brown impurity which was initially soluble with the whole polymer in acetone. The debris and most of the impurity could be separated in the first precipitate; with care, the remainder of the latter could be precipitated in the second cut and both of these initial fractions then had to be refractionated to remove it entirely. Since the fractionation scheme was complicated by the presence of this material, the details of the separations leading to the various fractions are omitted here but are given elsewhere.[14]

Three fractionations were made. The first involved 160 g. of stock I; it yielded fraction R2b and a set of fractions used in osmometry and in the determinations of the sulfur content and degree of esterification. Subsequently, fractions H and L were prepared from stock I and II, respectively, by making rough separations of two 160-g. portions of stock and then combining and refractionating the appropriate crude cuts.

The final fractions obtained were precipitated in a fluffy fibrous form suitable for direct drying by pouring aliquots of 5 to 10% solutions into a large excess of conductivity water with vigorous stirring. Each precipitate was removed to a wash bath of fresh water before adding the next aliquot. After each fraction had been completely precipitated it was washed several times with water and then dried for several days in a vacuum oven at about 1 mm. mercury and room temperature.

Chemical Characterization.—Stock I and the fractions from the first large scale fractionation were tested for variations in the sulfur content and in the degree of esterification, to make sure that fractionation was not taking place on the basis of chemical composition as well as on the basis of molecular weight.[15,16] The total amount of sulfur present as both inorganic sulfates and bound sulfur was determined by the method of Malm and Tanghe,[17] while the method of Malm, Genung and Williams[18] was used to analyze for the presence of free hydroxyl groups. The results indicated that the polymer was fully esterified and essentially sulfur-free, and had not been fractionated on the basis of chemical composition.

Osmotic Pressure and Intrinsic Viscosity.—Osmotic pressure measurements[19] at 25.00 ± 0.01° were made on methyl ethyl ketone solutions of six fractions. The osmometer and its operation have been described elsewhere.[20] Solution densities were calculated on the assumption of additive volumes of polymer and solvent. Molecular weights were calculated on the basis of the Berglund extrapolation[21] of the square root of the reduced osmotic pressure (π/c) to zero concentration.[22]

The specific viscosities (η_{sp}) of the same fractions in acetone at 25.0 ± 0.1° were measured in Ubbelohde viscometers having negligible kinetic energy corrections. The intrinsic viscosities ($[\eta]$, in dl./g.) were obtained from the double extrapolation of the reduced specific viscosity (η_{sp}/c) and the inherent viscosity ($\ln \eta_r/c$) to zero concentration The relation between intrinsic viscosity and molecular weight (M) was found to be $[\eta] = 4.80 \times 10^{-5} M^{0.88}$. The molecular weights of fractions H and L were calculated by this equation.

Table I gives the number-average molecular weight, the second virial coefficient A_2, $[\eta]$ and the Huggins[23] constant k' for the fractions whose osmotic pressures were measured. The values of k' are somewhat higher than those found by Mandelkern and Flory[7] for cellulose tributyrate in methyl ethyl ketone, but are similar to those of Badgley and Mark[24] for cellulose acetate in acetone.

TABLE I

RESULTS OF OSMOTIC PRESSURE AND VISCOSITY MEASUREMENTS

Fraction	$\bar{M}n \times 10^{-3}$	$A_2 \times 10^4$, mole cm.³/g.²	$[\eta]$, dl./g.	k'
IB_1	360 ± 25	5.0	3.82 ± 0.03	[b]
R1b	296 ± 30	5.2	3.12 ± .05	0.59
IIIA	218 ± 8	6.3	2.20 ± .05	.67
R2a	170 ± 10	6.1	1.88 ± .03	.68
R2b	152 ± 10	6.4	.....	..
IVB	77 ± 2	6.2	1.00 ± .03	.61
H	300[a]	..	3.15 ± .02	.65
L	55[a]	..	0.70 ± .02	.51

[a] Molecular weight calculated from intrinsic viscosity ($= \bar{M}\eta$). [b] Non-linear extrapolation.

Methods

The solutions were made up by weight and usually mixed at room temperature, although occasionally a temperature of 40° was employed. The initial solution of fraction L (55.3%) had to be heated to 60° before mixing was complete because it formed a chromatic gel at lower temperatures owing to crystallite growth. More dilute solutions became thixotropic and then gelled with decreasing temperature. The chromatic sheen evident in the gels persisted in such solutions and this fact was used as an indication of the presence of crystallites at low temperatures. Since the crystallites are randomly oriented and birefringent, the depolarization of light serves as a more sensitive test for their presence. These crystallite phenomena were found only with the solutions of fraction L.

The dynamic rigidities, G', and dynamic viscosities, η', were measured for all three fractions with the single transducer Model 2 of Smith, Ferry and Schremp[25] over a temperature and frequency range of 15° (approximately) to 35° and 160 to 400 c.p.s., respectively. Concentrations ranged from about 5 to 10% for fractions R2b and H and 28 to 34% for fraction L. The same quantities were measured at higher concentrations by the method of transverse wave propagation[26,27] over temperature and frequency ranges of −5 to 40° and about 200 to 6,000 c.p.s., respectively; the concentration range was about 8 to 25% for R2b and H and 34 to 45% for L. Solutions of the first two fractions gave unusually clear wave patterns with only moderate damping; useful patterns were obtained over a wider frequency range than is customarily observed, of the order of 1 to 1.5 decades of logarithmic frequency.

In addition, measurements of non-Newtonian viscosity and of stress relaxation following the cessation of a constant rate of strain were made on a single solution of fraction H (25.6% by weight) at four temperatures from 5 to 30° using the coaxial cylinder apparatus of Schremp, Ferry and Evans.[28] To minimize evaporation of the solvent at the highest temperature, the surface of the solution was covered with 0.5 cm. of glycerol.

The steady flow viscosities of all solutions were measured over approximately the same temperature range noted above, using the falling ball method with the Faxén correction for wall effects.[29] The solution densities were measured explicitly at different temperatures with a calibrated pycnometer, using freshly boiled distilled water as the containing fluid.

(14) R. F. Landel, Ph.D. Thesis, University of Wisconsin, 1954.

(15) R. Signer and J. Liechti, *Helv. Chim. Acta*, **21**, 530 (1938).

(16) S. Rogovin and S. Glassman, *Kolloid Z.*, **76**, 210 (1936).

(17) C. J. Malm and L. J. Tanghe, *Ind. Eng. Chem., Anal. Ed.*, **14**, 940 (1942).

(18) C. J. Malm, L. B. Genung and R. F. Williams, *ibid.*, **14**, 935 (1942).

(19) We wish to thank Dr. Ignacio Tinoco for making these measurements.

(20) G. V. Browning and J. D. Ferry, *J. Chem. Phys.*, **17**, 1107 (1949).

(21) P. J. Flory, "Principles of Polymer Chemistry," Cornell Univ. Press, Ithaca, N. Y., 1953, p. 280.

(22) A reasonable linear extrapolation could also be made by plotting π/c against c. Molecular weights obtained in this manner were related to intrinsic viscosity by the equation $[\eta] = 2.9 \times 10^{-4} M^{0.72}$.

(23) M. L. Huggins, *J. Am. Chem. Soc.*, **64**, 2716 (1942).

(24) W. J. Badgley and H. Mark, *J. Phys. Colloid Chem.*, **51**, 58 (1947).

(25) T. L. Smith, J. D. Ferry and F. W. Schremp, *J. Appl. Phys.*, **20**, 144 (1949).

(26) J. N. Ashworth and J. D. Ferry, *J. Am. Chem. Soc.*, **71**, 622 (1949).

(27) W. M. Sawyer and J. D. Ferry, *ibid.*, **72**, 5030 (1950).

(28) F. W. Schremp, J. D. Ferry and W. W. Evans, *J. Appl. Phys.*, **22**, 711 (1951).

(29) The results of the viscosity measurements will be discussed in a forthcoming communication.

Results

The values of G' and η' were reduced to a standard state by the method of reduced variables.[5] Figure 1 shows the wave propagation data from the

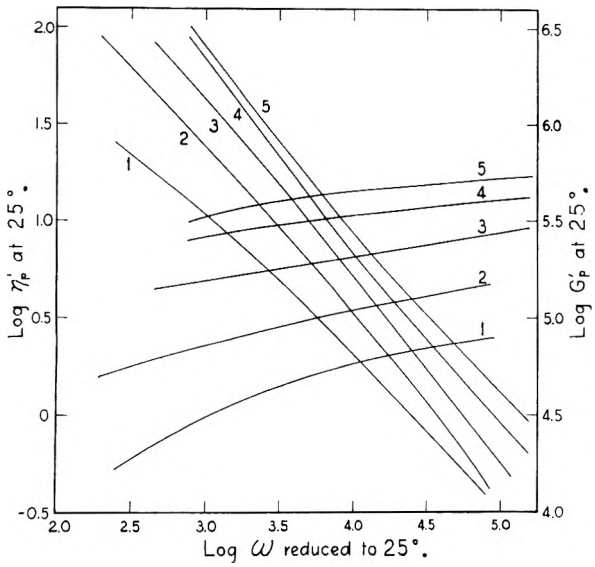

Fig. 1.—Dynamic rigidity G' (ascending curves) and dynamic viscosity η' (descending curves), plotted logarithmically against frequency, all reduced to 25° for sample H at various concentrations (weight fraction polymer): 1, 0.072; 2, 0.104; 3, 0.156; 4, 0.210; 5, 0.256 (wave propagation measurements).

solutions of fraction H partially reduced for temperature only, to 25°, on the assumption that all relaxation times depend identically on T. The reduced variables here are $G'_p = G'T_0c_0/Tc$ and $\eta'_p = \eta'\eta_0cT/\eta c_0T_0$, where $T_0 = 298°K.$; c, c_0, η and η_0 are the concentrations (g./cc.) and steady flow viscosities at the temperatures T and T_0, respectively. The reduced frequency is $\omega\eta T_0c_0/\eta_0Tc$, where ω is the circular frequency in radians/sec. The individual points are not shown; they fell on the composite curves within experimental error. At a given frequency, both G' and η' increase with concentration.

The dashed lines of Fig. 2 show the same data for fraction H further reduced to eliminate the effects of concentration, assuming that all relaxation times depend identically on c. The standard state in this case is that of unit concentration and unit viscosity at 298°K. so that $G'_r = G'T_0/Tc$, $\eta'_r = \eta'/\eta$, and $\omega_r = \omega\eta T_0/Tc$. The single transducer data reduced to the same reference state are included as individual points. The agreement between the data obtained from the two independent methods is quite good. Similar plots illustrate the results on fraction R2b (Fig. 3) and L (Fig. 4). In each case the heavy curve drawn through all the data represents the reduced variable over the appropriate concentration range. Thus in solutions of this cellulose derivative, just as in those of vinyl polymers, all relaxation times within the ranges covered here depend identically on temperature and concentration.

For brevity the results of the stress relaxation and non-Newtonian viscosity studies on fraction H

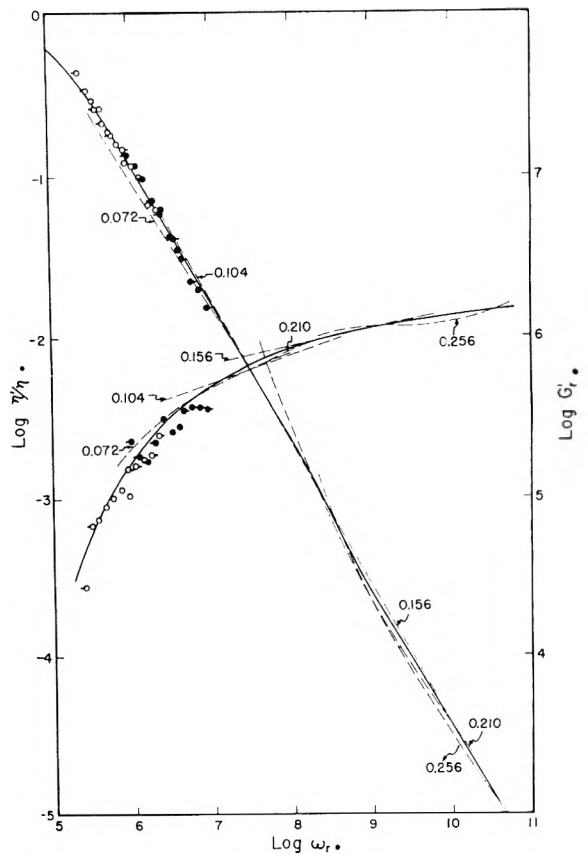

Fig. 2.—Data of Fig. 1 reduced to unit viscosity and unit concentration at 25°, together with single transducer data at weight fractions of 0.072 (black circles) and 0.045 (open circles). Tag right, 10°; no tag, 25°; tag left, 35°. Numerals denote weight fraction of polymer corresponding to dashed lines reproduced from Fig. 1.

are presented only in terms of the reduced distribution function.

To make the calculation from stress relaxation, the dependence of the steady flow rate of strain ($\dot{\gamma}$) on stress ($\mathfrak{T}$) was first fitted to the empirical equation $\dot{\gamma} = k_1 \sinh k_2\mathfrak{T}$, to determine the parameters[30] k_1 and k_2. The distribution function was then obtained from the slopes of stress–log time plots at various rates of shear preceding relaxation by the formula[28]

$$\Phi = -(d\mathfrak{T}/d \log t)/4.606\, tk_1 \tanh^{-1}\{(\dot{\gamma}/k_1)/(1 + [1 + (\dot{\gamma}/k_1)^2]^{1/2})\}$$

Values of Φ thus calculated superposed for various rates of shear preceding relaxation; moreover, on converting the average of these values to Φ_r and plotting log Φ_r *vs.* log τ_r ($= \tau Tc/\eta T_0$), the reduced values superposed for all temperatures (Fig. 5).

The function Φ can also be obtained from the dependence of apparent viscosity, $\eta_a = \mathfrak{T}/\dot{\gamma}$, on $\dot{\gamma}$. The functions $\eta_a(\dot{\gamma})$ and $\eta'(\omega)$ are closely simi-

(30) In this calculation, the average rate of strain within the annular gap was taken as usual as the geometric mean of the values at the inner and outer surfaces. The parameters k_1 and k_2 can be determined somewhat more accurately by a more elaborate procedure of Tillmann[31] which takes into account varying rate of strain within the gap. However, this was not considered necessary for present purposes, especially since Φ_r is not too sensitive to k_1 and k_2.

(31) W. Tillmann, *Kolloid-Z.*, **131**, 66 (1953).

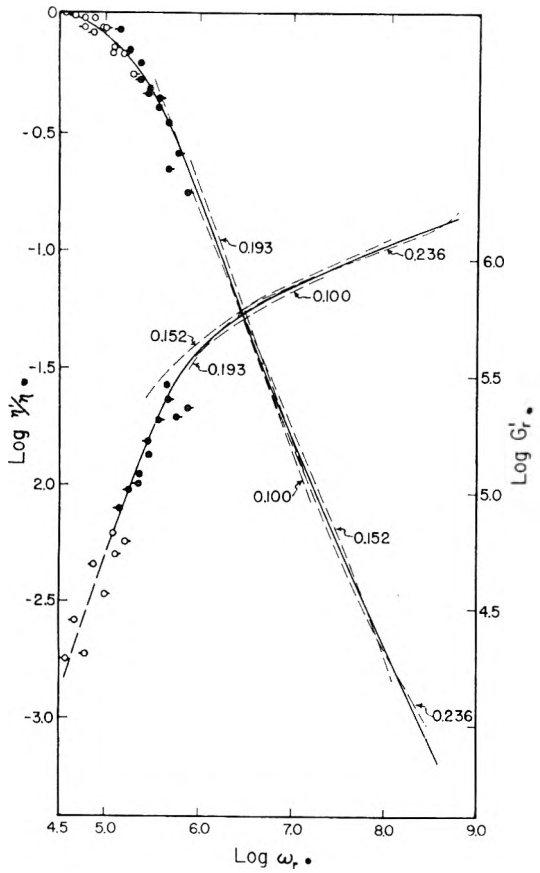

Fig. 3.—Dynamic rigidity and viscosity for sample R2b reduced to unit viscosity and unit concentration at 25°, from wave propagation measurements (dashed lines) and single transducer (points). Key same as in Fig. 2 except that open circles are 0.068 and black circles 0.100 weight fraction, and tag right indicates 15°.

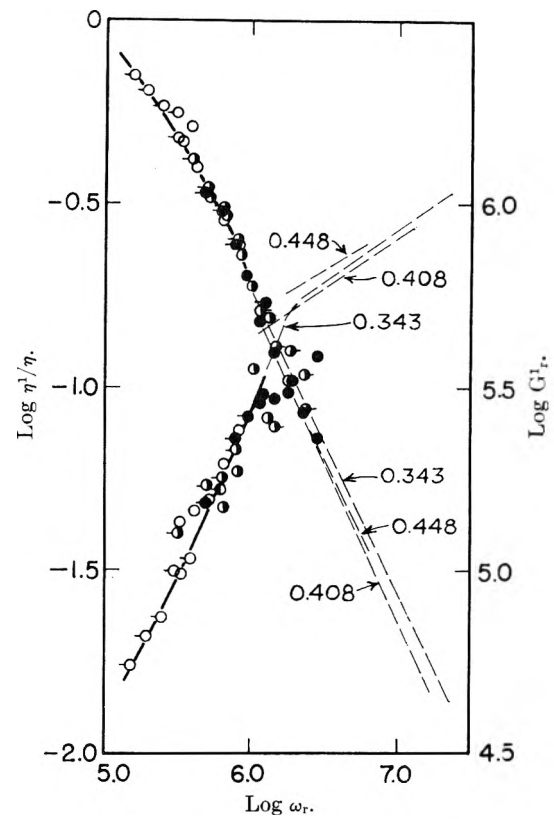

Fig. 4.—Dynamic rigidity and viscosity for sample L reduced to unit viscosity and unit concentration at 25°, from wave propagation measurements (dashed lines) and single transducer (points). Weight fractions for latter: open, 0.280; half black, 0.312; black, 0.345. Temperatures: tag right, 12°; no tag, 20°; tag left, 30°.

lar,[32–34] from which it follows,[32] approximately, that $\Phi_r = -\dot{\gamma}_r \eta_{ar} d \log \eta_{ar}/d \log \dot{\gamma}_r$. Here $\eta_{ar} = \eta_a/\eta$ and $\dot{\gamma}_r = \dot{\gamma}\eta T_0/Tc$. Values for the distribution function obtained in this way for fraction H are also plotted in Fig. 5, and agree quite well with those from stress relaxation. The close coincidence is probably fortuitous, since more precise measurements on other systems have shown a small deviation.[4]

Distribution Functions.—The relaxation distribution function Φ_r, reduced to unit viscosity and concentration, was also calculated from the dynamic data of Figs. 2, 3 and 4 by the usual second approximation formulas.[35] The results are presented in Fig. 6. The values of Φ calculated from G' and from η' are independent and therefore serve as a test of the internal consistency of the results. They should be and are the same within experimental error. (The experimental uncertainty in wave propagation measurements is somewhat greater for η' than for G', and the latter is considered a more reliable source for Φ in sample L, where some divergence appears.) Moreover, the curve for fraction H includes the terminal zone of the spectrum as determined from the heavy line through the stress relaxation points of Fig. 5. In this case a satisfactory correlation between the results of three dif-

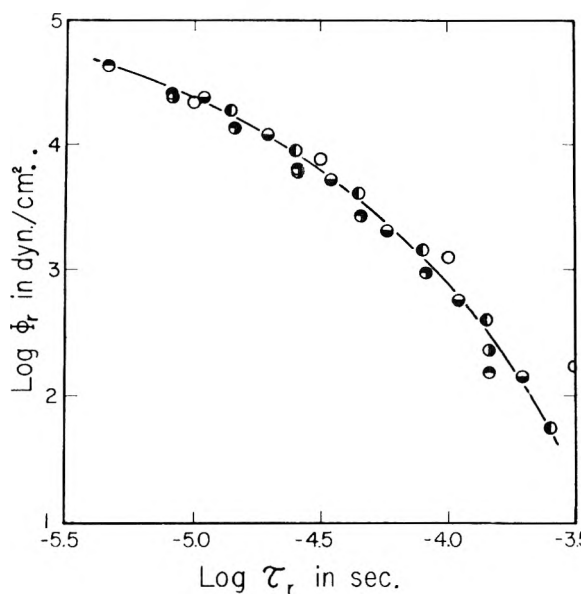

Fig. 5.—Relaxation distribution function for sample H, weight fraction 0.256, calculated from non-Newtonian flow (open circles) and from stress relaxation measurements at 5° (top black), 15° (right black), 25° (bottom black), and 35° (left black).

(32) T. W. DeWitt, reported at the Society of Rheology, October, 1953.

(33) F. Bueche, *J. Chem. Phys.*, **22**, 1570 (1954).

(34) J. D. Ferry, M. L. Williams and D. M. Stern, THIS JOURNAL, **58**, 987 (1954).

(35) J. D. Ferry and M. L. Williams, *J. Colloid Sci.*, **7**, 347 (1952).

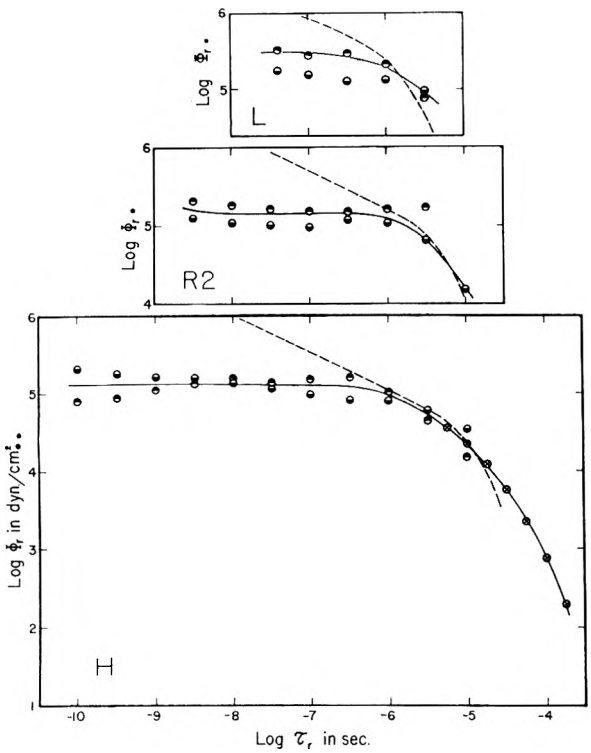

Fig. 6.—Relaxation distribution functions for the three samples, calculated from dynamic rigidity (top black), dynamic viscosity(bottom black), and stress relaxation (crosses); all reduced to unit viscosity and concentration. Dashed curves are calculated from the Rouse theory.

ferent types of measurement is observed in that they all fall on a smooth curve. The agreement between stress relaxation data on the 25.6% solution and single transducer data on the 4.8 and 7.2% solutions is especially noteworthy in that it confirms the assumptions involved in the concentration reduction treatment over this range. Similar correlations have previously been found for polystyrene[6] and polyvinyl acetate.[36]

There is evidently no difference in behavior between the complex, more extended backbone of cellulose tributyrate and the simple carbon chain of vinyl polymers insofar as the applicability of reduced variables is concerned. However, the shapes of the relaxation distribution functions for the two backbone types, compared for similar molecular weights, are quite different. The relaxation spectrum of fraction H is reproduced in Fig. 7 together with those of several vinyl polymers of roughly equal weight-average molecular weight. The region of time scale portrayed here is the intermediate or plateau zone, between the terminal zone on the right and the transition zone on the left where at shorter times the transition to glass-like consistency begins. The vinyl polymers exhibit slopes with a minimum numerical value of 0.25, the central zone being only partially flattened rather than forming a level plateau. The CTB, by contrast, presents a perfectly flat plateau over 4 decades of logarithmic time. All three of the CTB fractions exhibit this plateau—even L, whose molecular weight is only 55,000. It is also evident in the data of Philippoff[2,37] on cellulose acetate and in measurements of this Laboratory on cellulose trinitrate[38] which will be reported subsequently.

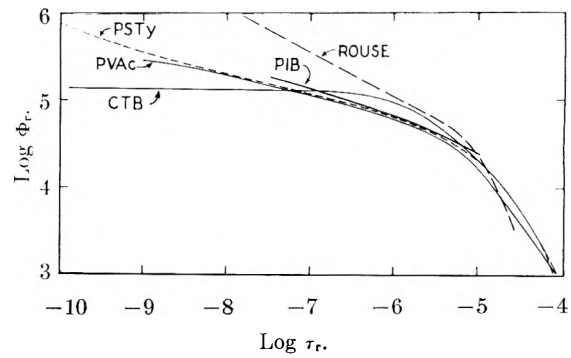

Fig. 7.—Relaxation distribution functions for concentrated solutions of the following polymers: CTB, cellulose tributyrate, fraction H (Fig. 6); PVAc, polyvinyl acetate[10] in 1,2,3-trichloropropane, M_w = 420,000; PSty, polystyrene[6] in Decalin, M_w = 370,000; PIB, polyisobutylene[3] in Decalin, M_η = 320,000; ROUSE, Rouse theory for molecular weight of 340,000.

In vinyl polymers, a flat plateau extending over several decades appears in concentrated solutions when the molecular weight is sufficiently high—for polyisobutylene,[3] for example, when $M_\eta > 10^6$. Thus the primary manifestation of the cellulose backbone in viscoelastic properties is the presence of a flat plateau in the relaxation spectrum at an unusually low molecular weight.

Discussion

According to the theory of Rouse,[39] the form of the relaxation spectrum depends on cooperative modes of Brownian motion of the polymer chain and (except at very short times) not at all on details of chemical structure. As modified slightly for concentrated solutions and expressed in terms of reduced variables,[5,40] the theory requires only the polymer molecular weight for an explicit calculation of the distribution function. Theoretical Rouse curves are shown in Figs. 6 and 7; they reproduce the terminal zones of the three cellulose tributyrate spectra with remarkable success.[41]

However, the Rouse theory predicts no plateau—only a linear distribution function with a slope of $-1/2$ on a double logarithmic scale as shown. The existence of the plateau has been attributed to the coupling of neighboring molecules by entanglement with a resultant abnormal prolongation of the longest relaxation times.[3,42,43] Clearly, the coupling effect is much stronger in cellulose tributyrate than in vinyl polymers (Fig. 7). This may mean either

(36) M. L. Williams and J. D. Ferry, *J. Colloid Sci.*, **10**, 1 (1955).

(37) T. L. Smith, *J. Polymer Sci.*, **14**, 37 (1954).

(38) D. J. Plazek and J. D. Ferry, unpublished work.

(39) P. E. Rouse, Jr., *J. Chem. Phys.*, **21**, 1272 (1953).

(40) J. D. Ferry, in H. A. Stuart, "Die Physik der Hochpolymeren," Vol. IV, Springer, Heidelberg, in press.

(41) The theory actually predicts a discrete terminal relaxation time. The tail shown is a fictitious continuous curve which would be calculated by our approximation methods[35] from stress relaxation measurements on a Rouse polymer.[3]

(42) F. Bueche, *J. Appl. Phys.*, in press.

(43) J. D. Ferry, R. F. Landel and M. L. Williams, *ibid.*, **26**, 359 (1955).

that the points of entanglement are more closely spaced (as they appear to be in polymethyl methacrylate[42] compared with polystyrene) or that each coupling point is more effective in reducing the mobility of the chain and hence increasing the average friction coefficient in long-range coöperative motions. In the latter case, the dependence of steady flow viscosity on molecular weight should involve an exponent higher than the 3.4 which appears to be characteristic of vinyl polymers.[42,44,45] Preliminary data[29] do indicate that this is so.

The significance of the height of the plateau in Φ remains uncertain. It decreases slightly with increasing molecular weight, being 3.0, 1.4 and 1.3 $\times$ 10^5 dyne/cm.^{2}, respectively, for fractions L, R2b and H. In concentrated solutions of high molecular weight polyisobutylenes[3] the plateau heights range from 0.6 to 1.0 $\times$ 10^5 dyne/cm.^{2}. The plateaus found in relaxation spectra of undiluted unvulcanized rubbers of high molecular weight[46,47] range from 1.4 to 4 $\times$ 10^5 dyne/cm.^{2}. We suspect that this rather general level is determined by the nature of the random distribution of entanglement points and not on the structure of either backbone or side chains.

Acknowledgments.—This work was part of a program of research on the physical structure and properties of cellulose derivatives and other polymers supported by the Allegany Ballistics Laboratory, Cumberland, Maryland, an establishment owned by the United States Navy and operated by the Hercules Powder Company under Contract NOrd 10431. It was also supported in part by a grant from Research Corporation and by the Research Committee of the Graduate School of the University of Wisconsin from funds supplied by the Wisconsin Alumni Research Foundation.

(44) M. F. Johnson, W. W. Evans, I. Jordan and J. D. Ferry, *J. Colloid Sci.*, **7**, 498 (1952).

(45) F. Bueche, *J. Appl. Phys.*, **24**, 423 (1953).

(46) W. Kuhn, O. Künzle and A. Preissmann, *Helv. Chim. Acta*, **30**, 307 (1947).

(47) L. J. Zapas, S. L. Shufler and T. W. DeWitt, *J. Polymer Sci.*, in press.

THE ANOMALOUS MONOLAYER ADSORPTION OF HELIUM[1]

BY RUDRA PAL SINGH[2] AND WILLIAM BAND

Department of Physics, The State College of Washington, Pullman, Washington

Received February 17, 1955

Lennard-Jones developed a quantum mechanical theory of physical adsorption on the hypothesis that adsorption energy is due to induced dipole–dipole interaction between the adsorbed atom and the adsorbing surface, the latter being treated as a conducting plane without structure. The present paper reports an attempt to understand the anomalously high density in the first monolayer of helium adsorbed on solid surfaces in terms of this Lennard-Jones model, by taking into account the fact that the forces causing adsorption perturb the helium atom wave function and so modify the interaction between neighboring helium atoms. The minimum strength of the forces needed to cause anomalous adsorption is found to be much too large to be explained in terms of induced dipole–dipole effects, and it is suggested that the anomaly may be more profitably discussed in terms of relatively strong permanent (non-uniform) local crystal fields in the adsorbing surface.

Introduction

The anomalously high density of helium adsorbed in the first monolayer on solids was first reported by Schaeffer, Smith and Wendell[3] using carbon adsorbents. The surface area was measured by analyzing nitrogen isotherms. The volume of helium adsorbed in the first layer was found to be several times greater than expected. A similar anomaly was found by Long and Meyer[4] to occur with Fe_2O_3 adsorbers, and by Mastrangelo and Aston[5] with TiO_2. Frederikse and Gorter[6] confirmed the results with Fe_2O_3. Helium is apparently the only substance exhibiting this effect.

When the anomaly was first discovered, there was considerable doubt about its reality: the B.E.T. theory[7] of adsorption, by means of which the volume in the first layer is calculated, might be inapplicable. The fact that it yields the anomaly might itself invalidate the theory: according to the B.E.T. model, each adsorbed atom becomes a possible site for another adsorbed atom in the next monolayer, but with an anomalously dense first layer, this cannot be true. Band[8] modified the B.E.T. model to include this possibility explicitly at the outset, recalculated the volume in the first layer, and obtained essentially the same effect. There seems no reasonable doubt that the interatomic distance in the helium monolayer is no greater than 2.0 $\times$ 10^{-8} cm., compared with approximately twice this distance in liquid helium.

Several qualitative explanations of the anomalous packing in the first monolayer have been suggested. The most promising was in terms of zero-point energy. The interatomic distance in helium for a minimum van der Waals potential is about 2.8 $\times$ 10^{-8} cm.; but by increasing the interatomic distance to about 4 $\times$ 10^{-8} cm. as observed in liquid helium, the zero-point energy is so greatly reduced that stability is gained in spite of the increase in van der Waals potential. The liquid is "blown up" by its zero-point energy, and the adsorption mechanism is supposed to collapse this pressure. In one sense this explanation leads to more trouble than it resolves. Solid helium under 35 atm. or

(1) Supported in part by ONR.

(2) On leave of absence from the University of Allahabad.

(3) W. D. Schaeffer, W. R. Smith and C. B. Wendell, *J. Am. Chem. Soc.*, **71**, 863 (1949).

(4) E. Long and L. Meyer, *Phys. Rev.*, **76**, 440 (1949); **84**, 551 (1952); **85**, 1035 (1952).

(5) S. V. R. Mastrangelo and J. G. Aston, *J. Chem. Phys.*, **19**, 1370 (1951).

(6) H. P. R. Frederikse and C. J. Gorter, *Physica*, **16**, 403 (1950).

(7) S. Brunauer, P. H. Emmet and E. Teller, *J. Am. Chem. Soc.*, **60**, 309 (1938).

(8) W. Band, *Phys. Rev.*, **76**, 441 (1949).

more pressure has a greater zero-point energy than the liquid phase, although it is still quite small—about 73 cal./mole as determined from the Debye temperature 32.5°K. The interatomic distance in the anomalous monolayer is much less than that in solid helium, and so implies an even larger zero-point energy in the monolayer. A crude estimate in terms of the Heisenberg uncertainty relation suggests that the zero-point energy is inversely proportional to the square of the interatomic spacing, and this yields an estimated zero-point energy in the monolayer of the order of 350 cal./mole. The observed energy of adsorption is about 50 cal./mole at high percentage coverage, so the potential responsible for adsorption must have a net depth not less than 400 cal./mole. At the interatomic distance 2×10^{-8} cm. in the monolayer, the interatomic potential of two unperturbed helium atoms, using Lennard-Jones[9] potential turns out[10] to be about 1200 cal./mole repulsive. To explain the required net negative 400 cal./mole we therefore have to find an adsorption mechanism capable of producing a total negative potential of some 1600 cal./mole. The straightforward induced dipole–dipole interaction between a helium atom and a conducting plane, the Lennard-Jones model,[11] is inadequate by a factor of about one hundred to provide so great an energy. The field intensity needed can be estimated as follows: The energy of an atom having polarizability α in a field of intensity F is $^1/_2\alpha F^2$. Taking the polarizability of helium atom[12] as 0.206×10^{-24} cm.,[3] the field intensity required to induce an energy equivalent of 1600 cal./mole works out as $F = 10^6$ dynes/e.s.u., or 0.058 atomic unit. Such fields may be large enough to perturb significantly the van der Waals attraction between two adsorbed helium atoms. Thus, the dipole moment of one helium atom, induced by adsorption, could be opposite in sign to that induced in any neighboring atom, thus adding a direct dipole-dipole attraction between neighboring adsorbed helium atoms. The more strongly polarized the helium atoms are by adsorption, the greater the effect. It was hoped that possibly this increased attraction would permit a smaller adsorption field intensity to produce the required adsorption potential, and so allow the Lennard-Jones picture to be retained. However, the correction turns out to be less than 6% of the energy of adsorption, and no appreciable change in the field intensity results. The perturbation calculations are outlined in the next section.

Perturbation Calculations

Hassé[13] has given the wave function of a helium atom in a perturbing electric field F in the form

$$u = e^{-n(r_1 + r_2)}(1 + cr_{12})\{1 + A(x_1 + x_2) + B(r_1x_1 + r_2x_2)\} \quad (1)$$

where r_1, r_2 are the distances of the two electrons from the nucleus, r_{12} the inter-electron distance; x_1, x_2 the electron coördinates in the direction of the field F; $c = 0.364$, $n = 1.849$, $A = 0.3844F$, $B = 0.3845F$; all the quantities are expressed in Hartree atomic units. We use this function in the more approximate form

$$u_1 = e^{-n(r_1 + r_2)}(1 + cr_{12})\{1 + A(x_1 + x_2 + r_1x_1 + r_2x_2)\} \quad (2)$$

with $A = 0.3845F$. The adsorbing surface is the y–z plane, and the z-axis joins two neighboring nuclei. The neighboring helium atom, polarized in the opposite sense, is represented by the wave function

$$u_2 = e^{-n(r_3 + r_4)}(1 + cr_{34})\{1 - A(x_3 + x_4 + r_3x_3 + r_4x_4)\} \quad (3)$$

where the coördinates are relative to the second nucleus.

The coulomb interaction between these two atoms expressed in atomic units is

$$V = (1/R^3)(x_1x_3 + y_1y_3 - 2z_1z_3 + x_1x_4 + y_1y_4 - 2z_1z_4 + x_2x_3 + y_2y_3 - 2z_2z_3 + x_2x_4 + y_2y_4 - 2z_2z_4) \quad (4)$$

where R is the distance between the two nuclei. The first- and second-order perturbation energies due to this interaction are formally

$$\Delta E_1 = (1/N) \int\cdots\int u_1^2 V u_2^2 \, d\tau_1 d\tau_2 d\tau_3 d\tau_4 \quad (5a)$$

$$\Delta E_2 = (1/N) \int\cdots\int u_1^2 V^2 u_2^2 \, d\tau_1 \, d\tau_2 \, d\tau_3 \, d\tau_4 / (E_{11} + E_{21} - E_{12} - E_{22}) \quad (5b)$$

where $N = \int\cdots\int u_1^2 u_2^2 \, d\tau_1 \, d\tau_2 \, d\tau_3 \, d\tau_4$; E_{11}, E_{21} are the negative energies of the two atoms in their unperturbed ground states, and E_{12}, E_{22} are the negative energies of the two atoms in their first excited states. Numerically these energies are $E_{11} + E_{21} = 2.75$ atomic units, $E_{12} + E_{22} = 0.70$ atomic unit. All the integrals involved in evaluating eq. 5 have been computed[14] and we find

$$\Delta E_1 = -0.4128 F^2/NR^3$$
$$\Delta E_2 = -(0.08256 + 2.8110F^2 + 2.2181F^4)/(2.05NR^6) \quad (6)$$
$$N = 0.2671 + 0.3606F^2 + 0.1216F^4$$

In the absence of polarization, $F = 0$, the second order perturbation becomes $E_{20} = -65.8 \times 10^{-12}(a_0/R)^6$ erg, which compares favorably with the value given by Slater,[15] namely, $-68 \times 10^{-12}(a_0/R)^6$ erg. Taking $R = 2 \times 10^{-8}$ cm., or about 3.8 atomic units, and assuming the estimated value of F as 0.058 atomic unit, as discussed in the previous section, the first-order dipole–dipole term in eq. 6 turns out to be -2.67×10^{-5} atomic unit, while the second order, van der Waals term, is about -50.5×10^{-5} atomic unit. The increased attraction due to the field F is thus only about 6%, and amounts in effect to no more than 18.6 cal./mole.

The possible effect of polarization on the repulsive term in the Lennard-Jones potential, due to overlap, can hardly be estimated with any degree of precision. Some idea of the effect however may be obtained by evaluating the first order dipole–

(9) J. E. Lennard-Jones, *Proc. Phys. Soc.*, **43**, 471 (1931).

(10) Using the more recent values of the Lennard-Jones constants given by D. ter Haar, "Elements of Statistical Mechanics," Rinehart & Company, Inc., New York, N. Y., 1954, p. 179.

(11) J. E. Lennard-Jones, *Trans. Faraday Soc.*, **28**, 333 (1932); *Proc. Roy. Soc. (London)*, **156A**, 6, 29 (1936).

(12) W. H. Keesom, "Helium," Elsevier Publishing Co., New York, N. Y., 1942.

(13) H. R. Hassé, *Proc. Camb. Phil. Soc.*, **26**, 542 (1930).

(14) R. P. Singh, ONR technical report project NR 010-603, June 24, 1954.

(15) K. C. Slater, *Phys. Rev.*, **32**, 355 (1928).

dipole term ΔE_1 in terms of the symmetrized wave function

$$u_S = u_1(1,2)u_2(3,4) - u_1(1,4)u_2(2,3) - u_1(2,3)u_2(1,4) + u_1(3,4)u_2(1,2)$$

The resulting value of ΔE_1 with $F = 0.058$ turns out to be[14] positive 2.16×10^5 atomic units.

Discussion

We have shown that the possible increase in mutual attraction between neighboring adsorbed helium atoms due to their polarization in the adsorbing field is no more than 6%; a very rough indication also has been given that the overlap repulsive component in the interaction between them is increased by an amount that may just about cancel the increased attraction. In any case it is quite clear that the perturbations in question are far too small to alter the problematic situation appreciably: namely, that it is still necessary to postulate an adsorbing field intensity of roughly 0.058 atomic unit in order to bind the adsorbed atoms against their mutual repulsion, against their high zero-point energy, and still retain 50 cal./mole energy of adsorption. The major difficulty therefore remains: if the adsorbing mechanism is capable of holding helium atoms against their mutual repulsion of 1200 cal./mole at full coverage, plus about 350 cal./mole zero-point energy, plus 50 cal./mole energy of adsorption, why does the energy of adsorption increase to no more than about 100 cal./mole at 10% coverage, when presumably the repulsive 1200 cal./mole has practically disappeared?

There seems no escape from the conclusion that the adsorbing mechanism does not merely *balance* the mutual repulsion by means of a compensating negative energy, but that the mechanism is such as actually to *remove* the repulsion almost completely at all coverages of the monolayer. It is however clear that the present perturbation theory based on the Lennard-Jones model is quite inadequate to achieve this. It is suggested that the adsorbed monolayer may be regarded as a two-dimensional alloy with the adsorbing surface, the helium atoms entering the surface structure of the adsorbing solid. The forces involved are the local crystalline fields leaking out through irregularities in the surface. Such irregularities are presumably of molecular dimensions, and the fields of a higher order of intensity than those existing between polarized helium atoms. Each adsorbed helium atom may be completely immersed in such a local field, and so become essentially a part of the lattice structure of the adsorbing surface, interactions between neighboring helium atoms being completely swamped by the perturbing effects of such a process. This picture has the merit that it would explain why only the smallest of atoms exhibit the effect; others like nitrogen are too large to be submerged in the surface irregularities.

A MINIMUM-PRINCIPLE FOR NON-EQUILIBRIUM STEADY STATES

By Thor A. Bak

Contribution from The Departments of Chemistry, The University of Copenhagen, Copenhagen, Denmark, and Columbia University, New York, New York

Received April 13, 1955

It is shown that a non-equilibrium steady state is accompanied by a minimum in a characteristic function which may be described as the sum of resistances times fluxes squared. For a steady state near equilibrium the function is, except for a constant factor, identical with the entropy production. This minimum principle provides the basis for an extension of Le Chatelier's principle.

Introduction

Prigogine[1] has shown that for an open system in which two irreversible processes take place, the steady state is characterized by the minimum rate of entropy-production consistent with the external constraints which prevent the system from reaching equilibrium. The theorem has been generalized by de Groot[2] to systems with an arbitrary number of reactions. The proofs given by both authors are based on the Onsager[3] relations, and the nature of the processes is therefore immaterial. Recently Klein and Meijer[4] have derived the theorem by the methods of statistical mechanics for a particular irreversible process—the flow of matter and energy through a small capillary connecting two containers of an ideal gas maintained at slightly different temperatures by two heat baths. Although the general use of the principle of minimum entropy production was initiated by Prigogine's paper, it is worth mentioning that a special case was proved almost a century ago in a nowadays rather unknown paper by Helmholtz.[5]

It is a necessary condition for all the proofs given for the theorem that there be linear relations between the forces and fluxes.[6,7] This means that if we want to apply the theorem to a system in which heat conduction, diffusion or chemical reactions take place, we can only use it for steady states which are near true thermostatic equilibrium. It can be proven for the steady states which are characterized by this minimum in the rate of entropy production that they are stabilized in the sense that Le Chatelier's principle is valid.

It would be interesting to apply this theorem to

(1) J. Prigogine, "Etude Thermodynamique des Phénomènes irréversibles," Editions Desoer Liège, 1947, Chap. V.

(2) S. R. de Groot, "Thermodynamics of Irreversible Processes," North-Holland Publ. Co., Amsterdam, 1951, Chap. X.

(3) L. Onsager, *Phys. Rev.*, **37**, 405 (1931); **38**, 2265 (1931).

(4) M. J. Klein and P. H. E. Meijer, *ibid.*, **96**, 250 (1954).

(5) H. Helmholtz, "Wissenschaftliche Abhandlungen von H. Helmholtz," Leipzig, 1882, I, 223.

(6) K. G. Denbigh, *Trans. Faraday Soc.*, **48**, 389 (1952).

(7) A. E. Nielsen, *Bull. classe sci., Acad. roy. Belg.*, **40**, 539 (1954).

systems in which chemical reactions approach a time-independent state but this is, as mentioned above, only possible for very special cases. On the other hand it is well known that a chemical reaction in a steady state is stabilized by a "moderation theorem," *i.e.*, if one perturbs the system by adding to it small amounts of a component which is in a steady state, the system will tend to re-establish its original unperturbed state.

As all steady states in chemical kinetics are stabilized in this way, it is tempting to try to establish a more general minimum principle which characterizes any time-independent state. This can be done for processes that are described by a diffusion equation (or the corresponding difference equation) by comparison with the variational solution of the problem of Plateau[8] as recently pointed out by Müller[9] and by Prigogine.[10] It is the purpose of this investigation to use this method on a specific example.

Description of the System.—We will consider a system, the particles or sub-systems of which can exist in N different states. The set of states is for convenience taken to be the integers $1, 2, \ldots N$.

A particle in state i has a certain probability w_i for transition to state $i + 1$ and a probability w_{-i} for transition to state $i - 1$. We shall call this System I.

It is intuitively clear that this system will approach an equilibrium as the time goes to infinity. From the fact that the system is an irreducible Markov chain with ergodic states, it follows that this equilibrium is independent of the initial states of the system.

In order to get a system which approaches a steady state different from equilibrium we add a constant flux J into state 1 from the left and introduce a probability w_N of leaving the system from state N. We shall call this System II.

The change of the system with time is now described by the set of differential equations

$$\begin{aligned}
\dot{X}_1 &= J - w_1X_1 + w_{-2}X_2 \\
\dot{X}_2 &= w_1X_1 - (w_2 + w_{-2})X_2 + w_{-3}X_3 \\
&\vdots \\
\dot{X}_N &= w_{N-1}X_{N-1} - (w_N + w_{-N})X_N
\end{aligned}$$

in which $X_i = X_i(t)$ is the number of particles in state i or the probability that the system is in state i. For System I, J and w_N equal zero, whereas they are both greater than zero in System II.

Later we shall need the time-independent solutions to the two sets of differential equations. They can easily be formed by putting $\dot{X}_i = 0$ and solving the linear equations. They are, of course, well known.[11] We shall here briefly outline a more powerful method of solving the equations in which the time-dependent solutions are formed first.

In System I let us use the boundary condition $X_i(0) = \delta_{1i}$. We then use the Laplace transformation

$$x_i(s) = \int_0^\infty e^{-st}X_i(t)\,dt$$

and get the following system of equations

$$\begin{aligned}
-1 &= -(w_1 + s)x_1 + w_{-2}x_2 \\
0 &= w_1x_1 - (w_2 + w_{-2} + s)x_2 + w_{-3}x_3 \\
&\vdots \\
0 &= w_{i-1}x_{i-1} - (w_i + w_{-i} + s)x_i + w_{-i-1}x_{i+1} \\
&\vdots \\
0 &= w_{N-1}x_{N-1} - (w_N + s)x_N
\end{aligned}$$

It is seen that it is easy to find relations between the fractions x_i/x_{i-1}. They can be expressed as

$$\frac{x_i}{x_{i-1}} = \frac{w_{i-1}}{w_i + w_{-i} + s - w_{-i-1}x_{i+1}/x_i}$$

and as we have $x_N/x_{N-1} = w_{N-1}/(w_{-N} + s)$ we can express x_i/x_{i-1} as a finite continued fraction. From the first equation we then get

$$x_1 = \cfrac{1}{s + w_1 - \cfrac{w_1w_{-2}}{s + w_2 + w_{-2} - \cfrac{w_2w_{-3}}{s + w_3 + w_{-3} - \ddots - \cfrac{w_{N-1}w_{-N}}{s + w_{-N}}}}}$$

and from the expression for x_2/x_1 we then get x_2, etc.

In principle it is now possible to apply the inversion formula to x_i and get X_i. Even without doing so we can, however, infer the properties of $X_i(t)$ for $t \to \infty$ from the properties of $x_i(s)$ for $s \to 0+$.

By calculation it is seen that the expression for x_1 can be written as

$$x_1 = f_1(s)/(sf_2(s))$$

in which $f_1(s)$ and $f_2(s)$ are polynominals of the $(N - 1)^{\text{th}}$ degree, which include a constant term. That is, for $s \to 0+$

$$x_1 \sim A_I\frac{1}{s}$$

in which $A_I = f_1(0)/f_2(0)$. By virtue of one of the Tauberian theorems[12] we then have for $t \to \infty$

$$X_1 \sim \frac{d}{dt}(A_It/\Gamma(2)) = A_I$$

By simple algebra we get the familar expression

$$X_1^{-1} = A_I^{-1} = 1 + \frac{w_1}{w_{-2}} + \frac{w_1w_2}{w_{-2}w_{-3}} + \ldots + \frac{w_1 \ldots w_{N-1}}{w_{-2} \ldots w_{-N}}$$

When we apply the Laplace transformation to the differential equations for System II we get for the boundary conditions $X_i(0) = 0$

$$\begin{aligned}
0 &= Js^{-1} - (w_1 + s)x_1 + w_{-2}x_2 \\
0 &= w_1x_1 - (w_2 + w_{-2} + s)x_2 + w_{-3}w_3 \\
&\vdots \\
0 &= w_{i-1}x_{i-1} - (w_i + w_{-i} + s)x_i + w_{-i-1}x_{i-1} \\
&\vdots \\
0 &= w_{N-1}x_{N-1} - (w_N + w_{-N} + s)x_N
\end{aligned}$$

(8) R. Courant and D. Hilbert, "Methoden der Mathematischen Physik," II, Verlag von Julius Springer, Berlin, 1937, p. 535.

(9) H. Müller, *Ann. Physik*, 6 Folge, **7**, 73 (1950).

(10) J. Prigogine, *Bull. classe sci., Acad. roy. Belg.*, **40**, 471 (1954).

(11) J. A. Christiansen, "Advances in Catalysis," Vol. V, Academic Press, Inc., New York, N. Y., 1953, 311.

(12) D. V. Widder, "The Laplace Transform," Princeton Univ. Press, Princeton, N. J., 1946, 182.

Proceeding as before, we get $x_1(s)$ as a continued fraction

$$x_1 = \cfrac{Js^{-1}}{s + w_1 - \cfrac{w_1 w_{-2}}{s + w_2 + w_{-2} - \cfrac{w_2 w_{-3}}{s + w_3 + w_{-3} - \ddots - \cfrac{w_{N-1} w_N}{s + w_N + w_{-N}}}}}$$

which we can write as

$$x_1 = Js^{-1} f_3(s)/f_4(s)$$

where $f_3(s)$ and $f_4(s)$ are polynominals of the $(N-1)^{\text{th}}$ and N^{th} degree, respectively, both containing a constant term. Denoting $f_3(0)/f_4(0)$ by A_{II} we have for $t \to \infty$

$$X_1 \sim \frac{d}{dt}(JA_{II}t/\Gamma(2)) = A_{II}J$$

and by simple algebra we get

$$X_1 = JA_{II} = J\left(\frac{1}{w_1} + \frac{1}{w_1}\frac{w_{-2}}{w_2} + \frac{1}{w_1}\frac{w_{-2}}{w_2}\frac{w_{-3}}{w_3} + \ldots + \frac{w_{-2}\ldots w_{-N}}{w_1 \ldots w_N}\right)$$

which is identical with the expression for steady-stage kinetics given by Christiansen.

The Entropy Production.—Let us consider the above-mentioned System II as a system of chemical reactions in an open system. We then have that the rate of entropy production at constant temperature is

$$\sigma = \frac{dS}{dt} = \frac{1}{T}\sum_{i=1}^{N-1} \mu_i J_i$$

in which μ_i is the chemical potential between state i and $i-1$ and J_i the flux.

Using the relation between rate constants and the equilibrium constant, we can rewrite this as

$$\sigma = \sum_{i=1}^{N-1} \left(\log \frac{w_i X_i}{w_{-i-1}x_{i+1}}\right)(w_i X_i - w_{-i-1}X_{i+1})$$

in which S is measured in units of R.

An expression of this kind has been given by Hearon.[13]

We will show that if the system is near real thermostatic equilibrium, *e.g.*, the kind of time-independent state we have in System I, σ has a minimum in the steady state. We have

$$\frac{\partial \sigma}{\partial X_i} = \frac{1}{X_i}(w_i X_i - w_{-i-1}X_{i+1}) - w_i \log \frac{w_i X_i}{w_{-i-1}X_{i+1}} - \frac{1}{X_i}(w_{i-1}X_{i-1} - w_{-i}X_i) - w_{-i}\log \frac{w_{i-1}X_{i-}}{w_{-i}X_i}$$

We then use the abbreviation $J_i = w_i X_i - w_{-i-1}X_{i+1}$ and, remembering that near equilibrium we can expand the logarithms

$$\log \frac{w_i X_i}{w_{-i-1}X_{i+1}} = \log\left(1 + \frac{J_i}{w_{-i-1}X_{i+1}}\right) \sim \frac{J_i}{w_{-i-1}X_{i+1}}$$

in which $\bar{X}_{i+1}$ is the equilibrium value of X_{i+1}, we get

$$\frac{\partial \sigma}{\partial X_i} = 0 \text{ implies } J_i - J_{i-1} = 0$$

from which we see that all $\partial\sigma/\partial X_i$ equal zero in the steady state. That the corresponding stationary value of σ is actually a minimum can be proven by computing the second derivatives. We shall, however, give a simpler proof later.

If we introduce the expansion of the logarithm directly in the expression for σ, we get

$$\sigma = \sum_{i=1}^{N-1} \frac{1}{w_{-i-1}\bar{X}_{i+1}} J_i^2$$

We shall call $\bar{X}_1/(w_{-i-1}\bar{X}_{i+1})$ the i'th resistance R_i. By computation we get

$$R_i = \frac{w_{-2}w_{-3}\ldots w_{-i}}{w_1 w_2 \ldots w_i}$$

The name resistance is fairly obvious when we consider, for instance, a discontinuous heat conduction between N metal spheres connected by thin conducting lines.[14] If we imagine that all the thermal conductivity is in the lines and all the heat capacity is in the spheres, the evolution in time of the system will be governed by a set of equations like I or II. If in this system we compute the reciprocal of the i'th heat conductivity, we get the above-written R_i.

The Minimum Principle.—We want to describe the time-independent state of System II as the minimum of some characteristic function. To do so we remember that in the limiting continuous case the stochastic process can be described by a one-dimensional diffusion equation such as

$$\frac{\partial c}{\partial t} = \frac{\partial}{\partial x}\left[D(x)\frac{\partial c}{\partial x}\right]$$

in which $c = c(xt)$ is the concentration, and $D(x)$ is the diffusion constant. We also have the relation

$$J = -D(x)\frac{\partial c}{\partial x}$$

The time-independent state is apparently described by

$$\frac{\partial}{\partial x}\left[D(x)\frac{\partial c}{\partial x}\right] = 0$$

and it is well known that this is the Euler Lagrange equation corresponding to

$$\delta \int_{x_1}^{x_2} D\left(\frac{\partial c}{\partial x}\right)^2 dx = 0$$

As we know the time-independent solution of the diffusion equation exists, we also know that it minimizes this integral. This integral can also be written

$$\delta \int_{x_1}^{x_2} D^{-1}J^2(x,t)\,dx = 0$$

from which we see that the stationary state is characterized by a minimum of an integral that closely resembles the sum

$$\sum_i R_i J_i^2$$

in the previous section.

It is also easy here to see the relation between this integral and the entropy production. We have

$$\sigma = \frac{1}{T}\int_{x_1}^{x_2} J(xt)\,d\mu(xt)$$

and, as $\mu = \mu_0 + RT\log c$

$$\sigma = \frac{1}{T}\int_{x_1}^{x_2} \frac{1}{Dc} J^2\,dx$$

(13) J. Z. Hearon, *Bull. Math. Biophys.*, **12**, 85 (1950).

(14) B. O. Koopman, *J. Operations. Res. Soc. Amer.*, **1**, 3 (1952).

S again being measured in units of R. It is seen that if c can be considered constant, the condition σ = min. is equivalent with the above-stated variational principle.

We now want to find the coefficients r_i which give us a sum

$$\sum_i r_i J_i^2$$

which has a minimum for $J_i = J$, the steady state flux.

The necessary condition is

$$\frac{\partial}{\partial X_i} \sum_i r_i J_i^2 = 2r_i J_i w_i - 2r_{i-1} J_{i-1} w_{-i} = 0$$

For $J_i = J_{i-1} = J$, we get the following recursion formula for r_i

$$r_i = \frac{w_{-i}}{w_i} r_{i-1}$$

which, aside from a constant factor, determines r_i as being identical with the resistance R_i.

The Principle of Le Chatelier.—We are now in a position to discuss the principle of Le Chatelier which states that if we disturb a system which is in equilibrium, the system will tend to re-establish the original state. It has been proven that the principle is also valid if the system is originally in a steady state near equilibrium. We shall here prove that it is valid for any steady state.

We consider System II in a state where $\Sigma R_i J_i^2$ has a minimum. Let the perturbation be an introduction of a small amount of compound i, Δx_i. We then have

$$\Sigma' R_i J_i^2 - \Sigma R_i J_i^2 > 0$$

in which Σ is the sum before the perturbation, Σ' the sum after the perturbation. This gives

$$2[R_i J_i w_i + R_{i-1} J_{i-1} w_{-i}] \Delta X_i > 0$$

neglecting squares in ΔX_i. Remembering that $R_i = w_{-2} w_{-3} \ldots . w_{-i} / w_1 w_2 \ldots . w_i$, we have

$$R_i w_i = R_{i-1} w_{-i}$$

and therefore

$$2R_i w_i (J_i - J_{i-1}) \Delta X_i > 0$$

As $2R_i w_i > 0$, we have

$$(J_i - J_{i-1}) \Delta X_i > 0$$

When $\Delta_i J = (J_i - J_{i-1}) > 0$, X_i is decreasing, and when it is less than zero, X_i is increasing. Therefore

$$\Delta_i J \Delta X_i > 0$$

which is an immediate consequence of the minimum principle, is an expression for Le Chatelier's principle.

Acknowledgments.—The author's thanks are due to Professor J. A. Christiansen, University of Copenhagen, who suggested this problem to him, and to Dr. Hans Brøns, University of Copenhagen, with whom he has discussed various parts of this paper. This work was finished at Columbia University, while the author was holding a fellowship from the Foreign Operations Administration to work with Professor V. K. La Mer, and he would like to express his sincere gratitude for this aid.

NOTES

THE VAPOR PRESSURE OF METHANOL[1]

By David F. Dever, Arthur Finch and Ernest Grunwald

Contribution from the Chemistry Department of Florida State University, Tallahassee, Fla.

Received January 17, 1955

In view of current interest in the thermodynamic properties of methanol,[2,3] we report an accurate redetermination of the orthobaric vapor pressure in the temperature range 14–34°.

Experimental

Materials.—Commercial methanol was dried[4] and fractionated through a 30-plate column. The following constants are reported for the fraction used in the vapor pressure measurements: b.p. 64.7°; $n^{25}D$ 1.3267; water content (by Karl Fischer titration) < 0.03%.

Method of Measurement.—The static method was used. Pressure was measured on a differential mercury manometer whose internal diameter was 1.2 cm. Pressure differences were read to ±0.03 mm. with a Gaertner cathetometer. The liquid was contained in a 10-ml. bulb attached to the main apparatus *via* a 14/36 ground joint, and its temperature was controlled to ±0.005°. The high-vacuum side of the mercury manometer was evacuated to 10^{-5} mm. by means of a single-stage mercury diffusion pump, backed by a Cenco-Hyvac pump. The three main sources of error in static vapor pressure measurements, (1) premature condensation of vapor, (2) gas dissolved in sample, and (3) contamination by grease from stopcocks, etc., were treated as follows.

(1) The connecting tube from the sample in the thermostat to the manometer was kept at 40° by means of a nichrome wire lagged with asbestos. The manometer itself was surrounded by a Pyrex tube in which refluxing ether maintained the temperature above 35°, the highest temperature used in the vapor pressure measurements.

(2) Before introduction into the vapor pressure apparatus, the sample was outgassed in an auxiliary apparatus. The sample was then transferred to the main apparatus, and a series of runs, each at varying temperatures, made. Between runs the vapor was condensed back into the sample bulb and pumped overnight at Dry Ice temperatures with the high-vacuum system. It was found that in any series of runs on one sample, the first and sometimes the second run yielded values slightly higher than the reproducible values obtained with succeeding runs. This was attributed to the completion of the out-gassing process, and consequently only the later runs were accepted. Finally, to ensure that no contamination resulted from small

(1) This work was supported by contract Nonr-988(02) between the Office of Naval Research and Florida State University.

(2) C. B. Kretschmer and R. Wiebe, *J. Am. Chem. Soc.*, **76**, 2579 (1954).

(3) W. Weltner and K. Pitzer, *ibid.*, **73**, 2606 (1951).

(4) N. Bjerrum and L. Zechmeister, *Ber.*, **56**, 894 (1923).

quantities of liquid trapped between the mercury in the walls of the manometer, the mercury was removed, cleaned and dried at 60° under vacuum between each series of runs.

(3) After preliminary experiments, Dow silicone grease was used in minimum quantities as lubricant for the stopcock and ground glass joint in the vapor system. As far as could be judged, no contamination resulted.

Pressure readings were corrected to standard gravity, and temperatures were read to ±0.01° on a thermometer recently calibrated by the National Bureau of Standards. To check the accuracy of the apparatus, the vapor pressure of pure water was measured in the range 25–35°. The mean deviation of eight experimental values from accepted values[5] was 0.17%. The accuracy of the data for methanol is estimated to be 0.25%.

Results

The results of thirty-nine measurements made on two samples are presented in Table I along with vapor pressure values computed by equation 3, derived below. A large scale graph of the data defines a smooth curve and shows no anomalous trends.

TABLE I

ORTHOBARIC VAPOR PRESSURES OF MeOH

t, °C.	p (atm.) Exptl.	Eq. 3	t, °C.	p (atm.) Exptl.	Eq. 3
13.88	0.0920	0.919	24.84	0.1659	0.1660
14.60	.09580	.09577	25.13	.1683	.1685
15.37	.09975	.09991	25.54	.1718	.1721
15.70	.1017	.1017	26.11	.1770	.1772
16.34	.1056	.1054	26.34	.1789	.1793
16.73	.1077	.1077	27.09	.1864	.1863
17.27	.1110	.1109	27.27	.1882	.1880
17.78	.1140	.1141	28.22	.1979	.1973
18.28	.1171	.1171	28.52	.2001	.1999
18.83	.1207	.1208	29.07	.2061	.2059
19.41	.1245	.1246	29.84	.2142	.2140
19.83	.1273	.1274	30.57	.2224	.2218
20.34	.1310	.1311	30.77	.2238	.2241
20.91	.1351	.1351	31.32	.2306	.2303
21.41	.1385	.1387	31.64	.2342	.2339
21.84	.1417	.1419	32.09	.2396	.2392
22.36	.1458	.1459	32.61	.2456	.2453
22.75	.1486	.1489	33.45	.2561	.2556
23.84	.1576	.1576	34.11	.2644	.2639
24.14	.1599	.1601			

In order to show the consistency of these results with existing thermodynamic data,[2,6] we have computed values of

$$-\mathrm{d}\ln p/\mathrm{d}(1/T) = T\Delta H_v/p\Delta V_v \qquad (1)$$

where ΔH_v, the molar heat of vaporization, was computed from the empirical equation of Fiock, Ginnings and Holton,[6] and ΔV_v, the molar volume change of vaporization, was computed using recent values for the virial coefficients of MeOH vapor[2] and accepted values for the density of liquid MeOH.[7]

In the temperature range 15–65°, the calculated values of $\mathrm{d}\ln p/\mathrm{d}(1/T)$ are represented to better than 0.02% by the empirical equation

$$-\mathrm{d}\ln p/\mathrm{d}(1/T) = 5472 - 2.944_6T \qquad (2)$$

as shown in Table II.

(5) F. G. Keyes, *J. Chem. Phys.*, **15**, 611 (1947).

(6) E. F. Fiock, D. C. Ginnings and W. B. Holton, *J. Research Natl. Bur. Standards*, **6**, 881 (1931).

(7) "International Critical Tables," Vol. III, McGraw-Hill Book Co., New York, N. Y., 1928, p. 27.

TABLE II

VALUES OF THE DERIVATIVE, $-\mathrm{d}\ln p/\mathrm{d}(1/T)$

t, °C.	Exptl.	Eq. 2	t, °C.	Exptl.	Eq. 2
15	4624	4624	30	4580	4580
20	4608	4608	34	4568	4568
25	4593	4594	64.65	4478	4478

Upon integration of equation 2 we obtain

$$\log p(\mathrm{atm.}) = 14.47865 - 2376.4/T - 2.9440 \log T \qquad (3)$$

where the constant term 14.47865 is computed from the thirty-nine P–T measurements and has a standard error of the mean of 0.00010. As shown in Table I, the fit is satisfactory. Extrapolation of the data to 1 atmosphere pressure gives a boiling point of 64.67°, which is in fair agreement with the accurate observed value of 64.65°.[8]

Our new results are generally 2–4% higher than previously reported values.[9] For example, at 25.00°, the previous values range from 0.160 to 0.165 atm. as opposed to our equation which gives 0.1673 atm.

(8) J. Timmermans and M. Henneaut-Roland, *J. chim. phys.*, **27**, 401 (1930).

(9) (a) Dittmar and Fawsett, *Trans. Roy. Soc. Edin.*, **33**, [II] 509 (1886–7); (b) Ramsay and Young, *Phil. Trans.*, **177**, 1, 123 (1886); *ibid.*, **178A**, 57 (1887); (c) W. G. Beare, G. A. McVicar and J. B. Ferguson, THIS JOURNAL, **35**, 1068 (1931); (d) D. Radulescu and M. Alexa, *Bull. soc. chim. Romania*, **20A**, 89 (1938); (e) B. Pesce and V. Evdokimoff, *Gazz. chim. ital.*, **70**, 712 (1940).

X-RAY DIFFRACTION STUDY OF THE ABSORPTION OF WATER BY POROUS VITREOUS SILICA

BY JOSEPH S. LUKESH

General Electric Company, The Knolls Atomic Power Laboratory,[1] Schenectady, N. Y.

Received March 1, 1955

A porous form of vitreous silica is produced as an intermediate stage in the preparation of 96% SiO_2, known as "Vycor," manufactured by the Corning Glass Works. The properties of this material have been described by Nordberg.[2] It contains about 35% by volume of void space, with the individual voids being about 10 to 50 μ in diameter. The glass is highly absorbent of gases and liquids. Water, for instance, is absorbed by a specimen approximately one inch square by one-eighth inch thick to the extent of approximately 19% by weight (a figure consistent with 35% by volume of void space) within 20 minutes or less.

There is no physical or chemical evidence to indicate that the water absorbed by the porous vitreous silica is present in any form other than as liquid water. Dehydration, for instance, seems to be a continuous process whose rate depends on temperature. Experimental evidence is superficial, but no discontinuous changes with temperature in the rate of dehydration appear to exist; such would be expected if chemical combination occurred.

Although observations suggest that water is present in the liquid state, no direct evidence has been presented heretofore. In this paper are presented confirming results of an X-ray diffraction study.

(1) The Knolls Atomic Power Laboratory is operated by the General Electric Company for the U. S. Atomic Energy Commission under Contract No. W-31-109 Eng-52.

(2) M. E. Nordberg, *J. Am. Cer. Soc.*, **27**, 299 (1944).

Experimental

Specimens of leached but un-fired vitreous silica ("Vycor") one inch square and one-eighth inch thick were examined by X-ray diffraction both in the equilibrium condition and when saturated with water. Filtered copper Kα radiation was used. By equilibrium condition is meant equilibrium with normal atmospheric temperature, pressure and humidity. The water-saturated specimens were allowed to soak in water under atmospheric pressure until constant weight was achieved. It was found that a period of 20 minutes was sufficient to reach saturation with an increase in weight of about 19%. Surface water was removed by wiping with paper tissue.

Diffraction patterns were obtained by Geiger counter methods. Counts were taken at every degree 2θ from sin $\theta/\lambda = 0.057$ to 0.459. Further extension of the curve was unnecessary for the purposes of the present investigation. In the case of the water saturated sample, the specimen was re-soaked before each measurement to compensate for evaporation.

Results and Discussion

The X-ray diffraction intensity data are plotted as a function of sin θ/λ in Fig. 1. Curve (b) represents the porous glass under equilibrium conditions and (a) the water-saturated material. (It is of interest to note that the intensity curve of the equilibrium sample is identical, within experimental error, with that of high purity vitreous silica[3]).

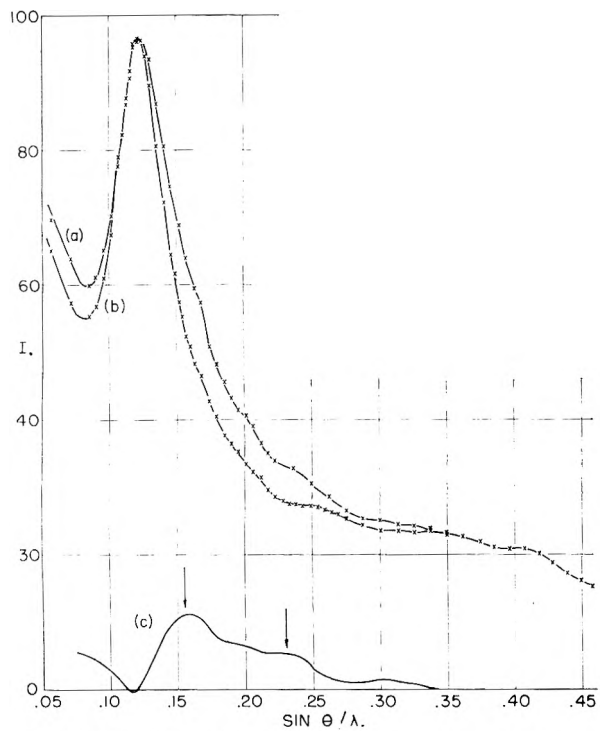

Fig. 1.—X-Ray diffraction intensity curves for porous vitreous silica: (a) water-impregnated; (b) equilibrium; (c) difference between (a) and (b.)

The bottom curve (c) of Fig. 1 represents the difference between (a) and (b). That this is due to liquid water is shown in Fig. 2 where the corrected data (solid curve) of (c) are plotted to a scale comparable with that of the curve of water at 30° reported by Morgan and Warren[4] (dashed curve). The slight shift of the small peak is probably due to the somewhat lower ambient temperature, *ca.* 18°, of the present experiment.

(3) J. S. Lukesh, *Phys. Rev.*, **97**, 345 (1955).

(4) J. Morgan and B. E. Warren, *J. Chem. Phys.*, **6**, 666 (1938).

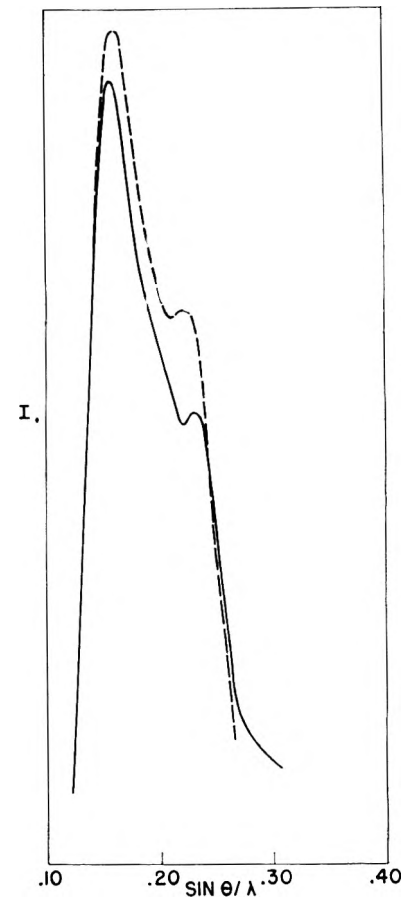

Fig. 2.—X-Ray diffraction curves for difference between water-impregnated and equilibrium porous vitreous silica (solid curve) and liquid water at 30° (dashed curve, adapted from Morgan and Warren.)

Conclusions

X-Ray diffraction analysis has demonstrated that water absorbed by porous vitreous silica exists in the liquid state, except possibly for a monomolecular layer on the surfaces of the voids. While in the present case, physical and chemical evidence are consistent with this view, it is believed that the experimental technique may be of interest in more equivocal systems.

Acknowledgments.—The samples of porous vitreous silica were kindly supplied by Dr. M. E. Nordberg of the Corning Glass Works.

THE IONIZATION CONSTANTS OF THE PYRIDINE MONOCARBOXYLIC ACIDS; A REINTERPRETATION

BY MARTIN L. BLACK

The Research Laboratories, Parke, Davis & Company, Detroit 32, Michigan

Received March 22, 1955

Jellinek and Urwin[1] have recently supplemented and summarized the existing ionization data for the pyridine monocarboxylic acids. Although the raw data generally agree well, all of the work reported and cited by these authors is marked by the same basic error of interpretation which it is the purpose

(1) H. H. G. Jellinek and J. R. Urwin, THIS JOURNAL, **58**, 548 (1954).

of this note to correct. This will be done with reference to the previously unreported ionization constant of isonicotinic acid methyl betaine (I).

Reported[1] ionization data for isonicotinic acid (II) agree upon $(pK_a)_1 \sim 1.70$ and $(pK_a)_2 \sim 4.95$; however, $(pK_a)_1$ is erroneously associated, in these reports, with ionization of the $=\overset{+}{N}H-$ center and $(pK_a)_2$ with $-CO_2H$ ionization.

Presumably, these incorrect assignments are based, in part, upon determinations of the ionization constants of the $=\overset{+}{N}H-$ centers in the pyridine carboxamides; *e.g.*, $pK_a \sim 3.61$ for isonicotinamide.[1] However, when it is possible for the parent acid to ionize in a zwitterionic manner, as in the present case, the amide ionization constants may be misleading. For example, in the present case one might argue that the undissociated $-CONH_2$ and $-CO_2H$ groups should have nearly equal effects on the acid strength of the $=\overset{+}{N}H-$ center, and, therefore, that the pK_a values of 3.61 and 4.95 should refer to the $=\overset{+}{N}H-$ centers since their difference is less than the difference between pK_a's of 3.61 and 1.70. Since this is contrary to the previous consensus,[1] the amide data offers, at best, a rather unsatisfying basis for either view. This suggests that the amide actually has no electrical counterpart among the possible ionic species of II and, therefore, that II ionizes in the zwitterionic manner.

This zwitterionic formulation is consistent with the ionization data for II in the following respects; (1) that the acidity of the $-CO_2H$ group should be increased, relative to that of benzoic acid, by the electron withdrawing effect of the $=\overset{+}{N}H-$ center,[2] and that (2) the acidity of the $=\overset{+}{N}H-$ center should be decreased, relative to that of the same group in the isonicotinamide cation, by the electron contributing effect of the $-CO_2^-$ group.[2] These electrical effects parallel those which obtain[2] among the aliphatic amino acids.

In complete conformity with the zwitterion hypothesis, I has been found to have an "apparent" ionization constant (pK_a') of 1.72 at 26°. Since I can ionize only in the manner

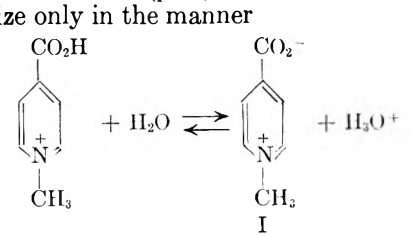

I

and since this corresponds to one step in the zwitterionic formulation

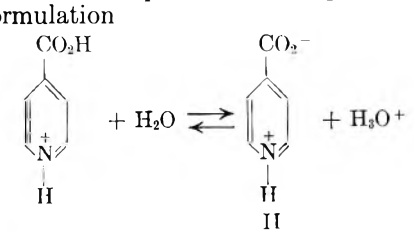

II

(2) E. J. Cohn and J. T. Edsall, "Proteins, Amino Acids, and Peptides," Reinhold Publ. Corp., New York, N. Y., 1943, Chapter 4.

it is clear, by analogy, that the pK_a of 1.70 for II must refer to $-CO_2H$ ionization.

The electrical analogy which must hold between the above equilibria at *p*H's below which the $=\overset{+}{N}H-$ center ionizes (*p*H $\sim$ 4.9)[1] is demonstrated by the ultraviolet spectra of I and II (Figs. 1 and 2).

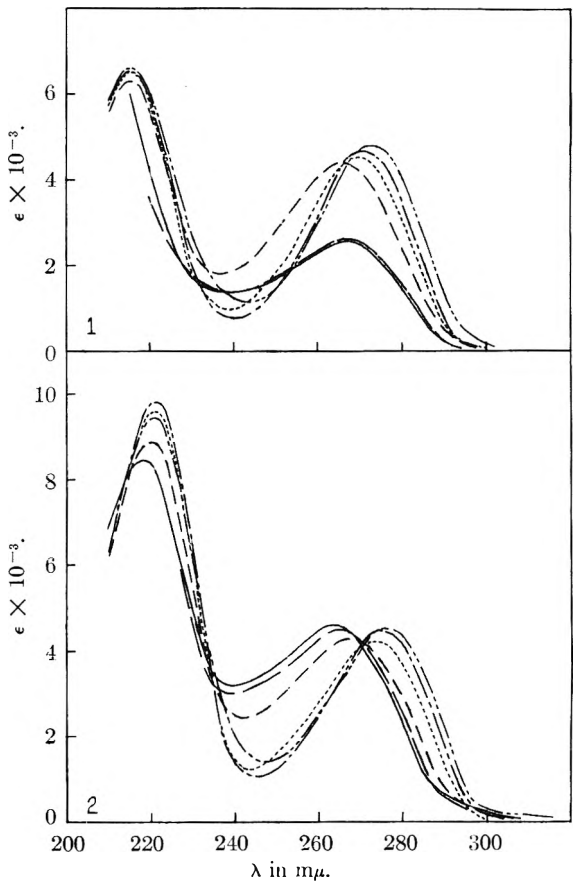

Fig. 1.—(Top curve) ultraviolet absorption spectrum of isonicotinic acid methyl betaine: ——, *p*H 7 buffer; — — —, 0.1 *N* NaOH; — — — —, 0.01 *N* HCl; – – – – –, 0.1 *N* HCl; — — — — —, 1.0 *N* HCl; — — — — — — —, 5.0 *N* HCl.

Fig. 2.—(Bottom curve) ultraviolet absorption spectrum of isonicotinic acid: ——, *p*H 7 buffer; — — —, 0.1 *N* NaOH; — — — — —, 0.01 *N* HCl; – – – – –, 0.1 *N* HCl; — — — — —, 1.0 *N* HCl; — — — — — — —, 5.0 *N* HCl.

For reasons similar to the above, picolinic and nicotinic acids would also presumably behave as zwitterions in solution.[3]

Acknowledgments.—I am indebted to Mr. Leonard Doub of these laboratories for his suggestions on several points of interpretation and to Dr. J. M. Vandenbelt of these laboratories for providing the instrumentation services of his staff.

Experimental

Preparation of Isonicotinic Acid Methyl Betaine (I).—Pyrolysis of methyl isonicotinate[4] gave 42.4% yield of pure product. Purification consisted of four recrystallizations from ethanol–acetone ($\sim$ 4:1), the first two including activated charcoal treatment of the solutions. After drying to constant weight *in vacuo* over P_2O_5 at 100°, the white crystalline product melted sharply with effervescence at 262°

(3) *Cf.* E. B. Hughes, *et al.*, THIS JOURNAL, **53**, 414 (1949), to the contrary.

(uncor.) in a sealed capillary to a brown liquid; Kirpal[4] reports m.p. 264°.

Purification of Isonicotinic Acid (II).—This consisted of four recrystallizations from water and drying *in vacuo* at 110° to constant weight.

Ultraviolet Spectra.—The spectra of Figs. 1 and 2 were determined with the Cary recording spectrophotometer.

Determinations of the Ionization Constant of I. Spectrophotometric Method.—The "apparent" ionization constant (pK_a') of 1.72 for I was determined in aqueous solution at 26° with the Beckman Model DU spectrophotometer by published methods.[5] No corrections have been made for salt effects or non-ideality of solutions.

(4) A. Kirpal, *Monatsh.*, **24**, 525 (1903).

(5) J. M. Vandenbelt, *et al.*, *Anal. Chem.*, **26**, 726 (1954).

Titrimetric Method.—The pK_a' of I in water at 26° was found to lie between 1.5 and 2.0 in duplicate determinations at initial concentrations of 0.0894 and 0.0896% by use of the Beckman Model G *p*H meter according to published methods.[5,6] A range of $pK_a' = 1.5$–2.0 is reported for each determination because of lack of precision, relative to the spectroscopic method, in the highly acid solutions.[6,7] The $pK_a' = 1.75$ mid-point of this range compares excellently with the spectroscopic value of $pK_a' = 1.72$. No correction has been made for salt effects or non-ideality of the solutions.

(6) T. V. Parke and W. W. Davis, *Anal. Chem.*, **26**, 642 (1954).

(7) G. M. Bennett, *et al.*, *J. Chem. Soc.*, 1821, 1823 (1935).

COMMUNICATION TO THE EDITOR

COMMENTS ON SURFACE TEMPERATURES OF BURNING LIQUID NITRATE ESTERS

Sir:

In a recent paper dealing with the measurement of surface temperatures of burning liquid nitrate esters, Steinberger and Carder[1] have discussed the significance of their results with respect to several mechanisms which can be postulated for the combustion process. They conclude that an evaporation type mechanism is incompatible with their data. It is the purpose of this note to point out an error in the calculations and reasoning leading to this conclusion and to comment on what appears to be a misunderstanding regarding a thermal model for the combustion process.

In Section I of their conclusions Steinberger and Carder state that the observed temperature gradients are too low to account for vaporization at the required rates. To illustrate this point, they attempt to calculate the rate of heat transfer to the liquid and in so doing state that ". . . dT/dx is the temperature gradient in the gas just outside the surface, °C./cm., assumed to be equal to the temperature gradient in the liquid at the surface." This cannot be true for the following reason. In the steady flow of heat across the boundary between two media of different thermal conductivities (as a liquid and a gas) with evaporation occurring at the interface, the following relation must be satisfied

$$K_{gas}\left(\frac{dT}{dx}\right)_{gas} = K_{liq}\left(\frac{dT}{dx}\right)_{liq} + H$$

where the K's are thermal conductivities, the temperature gradients are those at the boundary and H is the heat absorbed per unit time by the evaporating species. The gas and liquid gradients cannot be equal unless $H = 0$ and $K_{gas} = K_{liq}$, and such is not the case. Thus the calculation of S. and C. involving a liquid temperature gradient and a gas conductivity has no meaning. To calculate H, then, one must know the gradients at the surface in both liquid and gas as well as the thermal conductivities. One cannot, therefore, rule out an evaporation type mechanism on the basis of the available data.

Moreover, in considering the temperature distribution to be expected for a thermal model for the combustion process, it is stated: "In a purely thermal model the temperature would be expected to rise to a surface temperature of about 500° over a distance of 10 microns, . . .," referring to the work of Olds and Shook[2] for this information. The thermal model should not be restricted to this temperature gradient because of the strong dependence of preheat zone thickness on burning rate. A gradient of 50 deg./micron would be expected only at a burning rate of 1.0 cm./sec., the value used by Olds and Shook in their calculations. Critical examination of the heat flow equation shows that to a first approximation the preheat zone thickness, or distance from surface to any point in the condensed phase at temperature T, is inversely proportional to burning rate. An Olds and Shook type calculation reveals, for example, that the distance from surface to the point at which $T = 100°$ varies from 12 microns at a rate of 1.0 cm./sec. to 418 microns at 0.03 cm./sec. Thus the gradients would not be as steep as anticipated for the range of burning rates used by S. and C. and would, indeed, be quite gradual for the profiles obtained at atmospheric pressure. It might also be pointed out that a calculated surface temperature of 500°, as obtained by Olds and Shook, is not unique but depends principally upon the value of the chemical activation energy employed in solving the differential equation.[3] Under the conditions used in the calculations of Olds and Shook, a 20% change in activation energy effected a 170° change in surface temperature.

Work similar to that of S. and C.[1] has been continued in this laboratory.[4]

CHEMISTRY DIVISION
RESEARCH DEPARTMENT D. L. HILDENBRAND
U. S. NAVAL ORDNANCE TEST STATION
CHINA LAKE, CALIFORNIA

RECEIVED APRIL 18, 1955

(1) Steinberger and K. E. Carder, *J. Phys. Chem.*, **59**, 255 (1955).

(2) R. H. Olds and G. B. Shook, U. S. Naval Ordnance Test Station Technical Memorandum 917, 1952.

(3) R. H. Olds and G. B. Shook, private communication.

(4) D. L. Hildenbrand, A. G. Whittaker and C. B. Euston, THIS JOURNAL, **58**, 1130 (1954)

ORDER THESE SPECIAL PUBLICATIONS FOR YOUR PERMANENT RECORDS

Selected For Reprinting Solely On The Basis Of Their Importance To You

UNIT OPERATIONS REVIEWS

1st Annual Review	$0.50
2nd Annual Review	0.50
4th Annual Review	0.50
5th Annual Review	0.50
6th Annual Review	0.50
7th Annual Review	0.75
8th Annual Review	0.75
9th Annual Review	0.75

FUNDAMENTALS REVIEWS

1st Annual Review	0.75
2nd Annual Review	0.75

UNIT PROCESSES REVIEWS

1st Annual Review	0.50
2nd Annual Review	0.50
5th Annual Review	0.75
6th Annual Review	0.75
7th Annual Review	1.50

MATERIALS OF CONSTRUCTION REVIEWS

2nd Annual Review	0.75
3rd Annual Review	0.50
4th Annual Review	0.75
5th Annual Review	0.75
6th Annual Review	0.75
7th Annual Review	0.75

ANALYTICAL CHEMISTRY REVIEWS

2nd Annual Review	1.50
3rd Annual Review	1.50
5th Annual Review	0.75

RESOURCES SYMPOSIA

Southwest	0.50
Far West	0.50
New England	0.75
Mid Atlantic	0.75
Rocky Mountain—Part 1	0.75
East North Central States	0.75

MISCELLANEOUS REPRINTS

Raman Spectra	0.35
Corrosion Testing in Pilot Plants	0.25
Atmospheric Contamination and Purification Symposium	0.75
Titanium Symposium	0.50
Absorption and Extraction Symposium	0.75
Adsorption Symposium	0.50
Careers in Chemistry & Chemical Engineering	1.00
Information Please Symposium	0.50
Dispersion in Gases	0.50
Statistical Methods in Chemical Production	0.50
Liquid Industrial Wastes Symposium	0.75
Nucleation Phenomena	0.75
Chemical Facts and Figures—1952	1.00
Corrosion Data Charts	0.75
Synthetic Fibers	1.00
Chemical Progress in 1952	0.75
Chemical Facts and Figures	1.50
Process Kinetics Symposium	0.75
X-Ray Symposium	0.75
Emulsion Paints	0.75
Industrial Process Water Symposium	0.75
Symposium on Pilot Plants	0.75
Symposium on Boiler Water Chemistry	0.75
Flow through Porous Media	0.75
Process Instrumentation Symposium	0.75
First Air Pollution Review	0.50
Synthetic Detergents Symposium	0.75

ADVANCES IN CHEMISTRY SERIES

No. 4, Searching the Chemical Literature	2.00
No. 5, Progress in Petroleum Technology	4.00
No. 6, Azeotropic Data	4.00
No. 7, Agricultural Applications of Petroleum Products	1.50
No. 8, Chemical Nomenclature	2.50
No. 9, Fire Retardant Paints	2.50
No. 10, Literature Resources for Chemical Process Industries	6.50
No. 11, Natural Plant Hydrocolloids	2.50

MISCELLANEOUS

Seventy-Five Eventful Years (History of the ACS)	5.00
Chemistry—Key to Better Living	4.00
Combination of Seventy-Five Eventful Years and Chemistry—Key to Better Living	7.50
List of Periodicals Abstracted by Chem. Abs.	3.00
Faculties, Publications, and Doctoral Theses in Chemistry and Chemical Engineering at U. S. Universities	2.00
10 Years Numerical Patent Index (1937–1946)	6.50
27 Year Collective Formula Index	80.00
2nd Decennial Index to Chemical Abstracts	100.00
3rd Decennial Index to Chemical Abstracts	150.60
4th Decennial Index to Chemical Abstracts	120.60

Supply of the above items is limited, and each will be sold only until present stock is exhausted.

Order from: Special Publications Department, American Chemical Society
1155 Sixteenth Street, N.W., Washington 6, D. C.